

ALCONPAT International

Founders members:

Liana Arrieta de Bustillos – **Venezuela**
Antonio Carmona Filho - **Brazil**
Dante Domene – **Argentina**
Manuel Fernández Cánovas – **Spain**
José Calavera Ruiz – **Spain**
Paulo Helene, **Brazil**

Board of Directors International:

President of Honor

Angélica Ayala Piola, **Paraguay**

President

Carmen Andrade Perdrix, **Spain**

General Director

Pedro Castro Borges, **Mexico**

Executive Secretary

José Iván Escalante García, **Mexico**

Technical Vice President

Enio Pazini Figueiredo, **Brazil**

Administrative Vice President

Luis Álvarez Valencia, **Guatemala**

Manager

Paulo Helene, **Brazil**

Revista ALCONPAT

Editor in Chief:

Dr. Pedro Castro Borges
Centro de Investigación y de Estudios Avanzados del Instituto
Politécnico Nacional, Unidad Mérida (CINVESTAV IPN –
Mérida)
Merida, Yucatan, **Mexico**

Co-Editor en Jefe:

Arq. Margita Kliewer
Universidad Católica “Nuestra Señora de la Asunción”
Asuncion, **Paraguay**

Executive Editor:

Dr. José Manuel Mendoza Rangel
Universidad Autónoma de Nuevo León, Facultad de Ingeniería
Civil
Monterrey, Nuevo Leon, **Mexico**

Associate Editors:

Dr. Manuel Fernandez Canovas Universidad
Politécnica de Madrid. Madrid, **Spain**

Ing. Raúl Husni

Facultad de Ingeniería Universidad de Buenos Aires. Buenos
Aires, **Argentina**

Dr. Paulo Roberto do Lago Helene

Universidade de São Paulo.

São Paulo, **Brazil**

Dr. José Iván Escalante García

Centro de Investigación y de Estudios Avanzados del
Instituto Politécnico Nacional (Unidad Saltillo) Saltillo,
Coahuila, **Mexico**.

Dr. Mauricio López.

Departamento de Ingeniería y Gestión de la Construcción,
Escuela de Ingeniería,
Pontificia Universidad Católica de Chile
Santiago de Chile, **Chile**

Dra. Oladis Troconis de Rincón Centro de Estudios de

Corrosión Universidad de Zulia

Maracaibo, **Venezuela**

Dr. Fernando Branco Universidad

Técnica de Lisboa

Lisboa, **Portugal**

Dr. Pedro Garcés Terradillos

Universidad de Alicante

San Vicente, **Spain**

Dr. Andrés Antonio Torres Acosta

Instituto Mexicano del Transporte / Universidad Marista de

Querétaro

Querétaro, **Mexico**

Dr. Luiz Fernández Luco

Universidad de Buenos Aires – Facultad de Ingeniería –
INTECIN

Buenos Aires, **Argentina**

RAV9N2, may – august, 2019

Message from the Editor in Chief

**JOURNAL OF THE LATIN-AMERICAN ASSOCIATION
OF QUALITY CONTROL, PATHOLOGY AND RECOVERY
OF CONSTRUCTION**

<http://www.revistaalconpat.org>

With great satisfaction, we present the second issue of the ninth year of the ALCONPAT journal.

The aim of the journal is to publish case studies within the scope of the Association, namely quality control, pathology and recovery of constructions, including basic and applied research, reviews and documentary research.

This V9N2 issue begins with a work from **Brazil**, where Graziela Pereira da Silva and colleagues present a review about the influence of infrared thermography on masonry walls to detect pathological manifestations. A systematic review was carried out through research with automatic search and snowballing, selection and sifting of articles to restrict them to the desired theme. After that, infrared thermography in the pathological manifestations was studied along with the thermal properties and their behavior, thermal bridges, temperature difference and air infiltrations. Some care must be taken during the execution of experiments and measurements. It has also been shown that infrared thermography is a complex technique.

In the second work, from **Mexico**, Pedro Jesús Poot Cauich et. al. present a review that addresses the mechanics of adhesion, strengthening effect and durability issues of applications of carbon fiber reinforced polymer (CFRP) composite materials in beams. The application of CFRP materials has been widely described, but the focus has been on overall failure parameters. The first issue is strengthening capability of CFRP reinforcement for concrete beams. The second is the local interface bond stress-slip relationship, that is, the local slip. The last issue is the durability of the CFRP sheet/plate, when exposed to a hydro-thermal environment. The role of adhesion and the mechanics of concrete-CFRP adhesion and a sound understanding of the interface between the CFRP and concrete behavior is the key factor for controlling debonding failures in CFRP-strengthened RC beams.

The third work of this issue is from **Brazil**, where Ronaldo Medeiros-Junior and colleagues confront the following concrete properties: water absorptions (by immersion and capillarity), electrical resistivity and compressive strength. Results showed that concretes with higher content of pozzolan had higher resistivity and greater absorption by capillarity, for water-cement ratios lower than 0.60. This behavior is attributed to reduced pore diameters and microstructure densification. However, for water/cement ratio of 0.60, concrete with lower content of pozzolan presented higher absorption by capillarity. It was observed that the compressive strength and the electrical resistivity behaved inversely proportional to the water/cement ratio, and the absorption by

immersion and capillarity are directly proportional to the water/cement ratio. Correlations with high determination coefficients were found between tests.

In the fourth article, from **Mexico**, José Trinidad Pérez-Quiroz et. al. discuss the corrosion performance of dissimilar welded joints between ASTM A615 and AISI 304 stainless steel with and without buttering using Inconel 182. In both cases, the filler metal was ER-309L and the base metals were prepared with a 45° single bevel. One half of the specimens were welded with “buttering” using Inconel 182. The electrochemical results showed that despite welding defects, the welded specimens formed a passive layer in alkaline environments. The specimens welded with buttering exhibited the best corrosion resistance and mechanical properties.

The fifth work, by Daniel V. Ribeiro y Rafaela Oliveira Rey, from **Brazil** evaluated the aggregate alkali reactivity (AAR) of the aggregates used in the metropolitan region of Salvador and the use of mineral additions in order to mitigate this reaction. The accelerated test method using mortar bars, recommended by NBR 15577-4: 2008, was used. The results indicate that the sands of the metropolitan area of Salvador have low reactivity, however, the gravels presented high reactivity and that mineral additions with pozzolanic characteristics can mitigate the AAR. This study, although limited to the conditions used, is unprecedented in the State of Bahia and presents a high index of originality, since it uses higher contents of mineral additions than conventional use. It was concluded that micro silica, if used at very high contents, can even accelerate the AAR.

The sixth work in this issue is written by M. Rendón Belmonte and colleagues from **Mexico**. They describe properties related to the durability of five different mixtures of concrete with different contents of activated fly ash (AFA) and Portland cement (CPC 40). The measurements carried out were apparent speed of ultrasonic pulse, electrical resistivity, fast ion permeability of chloride and mechanical resistance to compression. The performance of all mixtures proved to be durable, and the development of the electrical resistivity and the decrease in the level of the chloride ion permeability were enhanced by the contents of AFA, although the resistance to compression at higher contents of AFA was minor. The maximum percentage of AFA to comply with the current criteria of durability was 65%.

In the seventh work, from **Brazil**, Denis Cardoso Parente et. al. evaluate the use of reuse water from sewage treatment plants in the manufacture of simple concrete casting blocks. The use of these blocks has been adopted as a rationalization option in the structural masonry composition and sealing, by allowing reduction in the losses of materials and coating layers. The study includes the analysis of the physical and mechanical properties of the blocks dosed with effluent and the results show that these properties remain unchanged, which can make feasible the use of the effluent.

In the eighth work, from **Cuba**, Jennifer Lopez Guevara and colleagues report that Santa Clara de

Asis Convent High Choir timber truss has been the victim of humidity and the attack of abiotic and biotic agents which have caused its gradual degradation. For the identification of pathological processes associated with these agents and because of its patrimonial character, a diagnosis study based on an organoleptic inspection and superficial tests was carried out with the available instruments, which allowed identifying the causes. By modeling the structure on SAP 2000 program, they obtained the results that were used to calculate the solutions proposed for the identified pathologies, mainly for the loss of connection between the wall plate and the tie rod beam.

The article that closes this edition is written by Henrique Jorge Nery Lima y et. al. from **Brazil**, who present the case study of pathological manifestations in concrete structures, located in the Northern Road Hub of Brasília, using the GDE / UnB methodology, which qualifies and quantifies the degradation of structural damages. The general state of the structure was characterized in order to serve as a subsidy for decision making regarding routine interventions, in order to extend the useful life of the structure. The methodological routine consists of conducting field inspections; catalog of structural pathologies with photographic survey; characterization of pathologies and classification according to the weighting factors and damage intensity factors of the structure according to the GDE / UnB methodology for special works of art; calculation and overall classification of the structure damage.

We are confident that the articles in this issue will constitute an important reference for those readers involved with questions of evaluations and characterizations of materials, elements and structures. We thank the authors participating in this issue for their willingness and effort to present quality articles and meet the established times.

On behalf of the Editorial Board

A handwritten signature in black ink, appearing to read 'Pedro Castro Borges', written over a circular stamp or seal.

Pedro Castro Borges
Editor in Chief



CONTENT



REVIEW

G. P. Silva, P. I. B. Batista, Y. V. Povóas: The usage of infrared thermography to study thermal performance of walls: a bibliographic review. 117 - 129

P. J. Poot Cauich, R. Martínez-Molina, J. L. Gamboa Marrufo, P. J. Herrera Franco: Adhesion, strengthening and durability issues in the retrofitting of Reinforced Concrete (RC) beams using Carbon Fiber Reinforced Polymer (CFRP) – A Review. 130 – 151

BASIC RESEARCH

R. A. Medeiros-Junior, G. S. Munhoz, M. H. F. Medeiros: Correlations between water absorption, electrical resistivity and compressive strength of concrete with different contents of pozzolan. 152 - 166

J. C. I Ramirez –Soto, J. T. Pérez-Quiroz, J. M. Salgado-López, M. Martínez-Madrid, T. Pérez-López, M. Rendón-Belmonte, E. Alvarez-Alfaro: Electrochemical behavior of dissimilar welded joints between ASTM A615 and AISI 304 with and without buttering using Inconel 182. 167 - 184

D. V. Ribeiro, R. O. Rey: Evaluation of the aggregates used in the metropolitan region of Salvador regarding the occurrence of alkali-aggregate reactions (AAR). 185 - 199

M. Rendón Belmonte, M. Martínez Madrid, R. V. Martínez Pérez, J. T. Pérez Quiroz: Durability of concrete mixtures with different contents of activated fly ash. 200 - 214

A. Plaza Meurer, R. Alves Amorim, L. Carvalho Quintanilha, D. Cardoso Parente: Effluent reuse in the manufacture of concrete blocks for sealing masonry. 215 - 227

STUDY CASES

J. L. Guevara, Y. A. Toirac, C. M. C. Marisy: An approach to the convent of Santa Clara de Asís in Havana. Study of its conservation status and intervention proposals. 228 – 246

H. J. N. Lima, R. S. Ribeiro, R. A. Palhares, G. S. S. A. Melo: Analysis of pathological manifestations of concrete in urban overpasses. 247 - 259

The usage of infrared thermography to study thermal performance of walls: a bibliographic review

G. P. Silva^{1*} , P. I. B. Batista¹ , Y. V. Povóas¹ 

*Contact author: graziela.ps04@gmail.com

DOI: <http://dx.doi.org/10.21041/ra.v9i2.341>

Reception: 04/09/2018 | Acceptance: 18/02/2019 | Publication: 30/04/2019

Responsible Associate Editor: Dr. Paulo Helene

ABSTRACT

This article aims to present the influence of infrared thermography on masonry walls to detect pathological manifestations. A systematic review was carried out through research with automatic search and snow-balling, selection and sifting of articles to restrict them to the desired theme. After that, infrared thermography in the pathological manifestations was studied along with the thermal properties and their behavior, thermal bridges, temperature difference and air infiltrations. In general, some care must be taken during the execution of experiments and measurements. It has also been shown that infrared thermography is a complex technique and should be used.

Keywords: infrared thermography; thermal performance; pathological manifestations; thermal properties; air leakage.

Cite as: Silva, G. P., Batista, P. I. B., Povóas, Y. V. (2019), "*The usage of infrared thermography to study thermal performance of walls: a bibliographic review*", Revista ALCONPAT, 9 (2), pp. 117 – 129, DOI: <http://dx.doi.org/10.21041/ra.v9i2.341>

¹ Universidade de Pernambuco, Brasil.

Legal Information

Revista ALCONPAT is a quarterly publication by the Asociación Latinoamericana de Control de Calidad, Patología y Recuperación de la Construcción, Internacional, A.C., Km. 6 antigua carretera a Progreso, Mérida, Yucatán, 97310, Tel.5219997385893, alconpat.int@gmail.com, Website: www.alconpat.org

Responsible editor: Pedro Castro Borges, Ph.D. Reservation of rights for exclusive use No.04-2013-011717330300-203, and ISSN 2007-6835, both granted by the Instituto Nacional de Derecho de Autor. Responsible for the last update of this issue, Informatics Unit ALCONPAT, Elizabeth Sabido Maldonado, Km. 6, antigua carretera a Progreso, Mérida, Yucatán, C.P. 97310.

The views of the authors do not necessarily reflect the position of the editor.

The total or partial reproduction of the contents and images of the publication is strictly prohibited without the previous authorization of ALCONPAT Internacional A.C.

Any dispute, including the replies of the authors, will be published in the first issue of 2020 provided that the information is received before the closing of the third issue of 2019.

O uso da termografia infravermelha para o estudo do desempenho térmico de paredes: revisão bibliográfica

RESUMO

Este artigo tem por objetivo apresentar a utilização da termografia infravermelha em paredes de alvenaria no auxílio do desempenho térmico. Foi realizado uma revisão sistemática através de pesquisa com busca automática e snow-balling, seleção e peneiramento dos artigos para restringir os artigos ao tema desejado. Após isto, foi estudado sobre a termografia infravermelha nas manifestações patológicas, as propriedades térmicas e seu comportamento, pontes térmicas, diferença de temperatura e infiltrações de ar. De uma forma geral é necessário ter alguns cuidados durante a execução dos experimentos e medições. Ademais foi mostrado que a termografia infravermelha é uma técnica complexa e precisa de ser utilizada.

Palavras-chave: termografia infravermelha; desempenho térmico; manifestações patológicas; propriedades térmicas; vazamentos de ar

Uso de termografía infrarroja para estudiar el desempeño térmico de paredes: una revisión bibliográfica

RESUMEN

Este artículo tiene por objetivo presentar la influencia de la termografía infrarroja en paredes de albañilería para detectar manifestaciones patológicas. Se realizó una revisión sistemática a través de investigación con búsqueda automática y snow-balling, selección y cribado de los artículos para restringir los artículos al tema deseado. Después de esto, fue estudiado sobre la termografía infrarroja en las manifestaciones patológicas, las propiedades térmicas y su comportamiento, puentes térmicos, diferencia de temperatura e infiltraciones de aire. En general es necesario tener algunos cuidados durante la ejecución de los experimentos y mediciones. Además, se ha demostrado que la termografía infrarroja es una técnica compleja y precisa de ser utilizada.

Palabras clave: termografía infrarroja; rendimiento térmico; manifestaciones patológicas; propiedades térmicas; fugas de aire

1. INTRODUCTION

Walls can be evaluated in order to verify better quality for thermal performance. There are several forms of measurements according to the functionality or parameter to be observed, such as mechanical resistance, water absorption, capillarity, thermal performance, geometric characteristics. Those are some aspects that can be evaluated to obtain a satisfactory performance of the walls in a building.

The Brazilian performance standard NBR 15575 (ABNT, 2013) and the base standard on Thermal Performance, NBR 15220 (ABNT, 2005), complement each other: the first defines performance as "behavior in use of a building and its systems" while the second approaches the thermal concepts, properties and their calculations.

Infrared thermography is a non-invasive and non-destructive survey technique. Its capture is done through devices that show infrared radiation, through mechanisms of easy and fast use, though in a complex way. The use of the technique has become more frequent given its fast, precise and non-contact nature which makes possible for it to be used in a wide range of cases (Kylili et al., 2014). Infrared thermography uses a camera to measure the emitted infrared radiation of an object and

convert it into a thermal radiation pattern, which is invisible to the human eye, in a visible image (Clark et al., 2003).

Several researchers have applied infrared thermography techniques for various uses (Bagavathiappan et al., 2013) such as emissivity measurement and determination of global heat transfer coefficient, thus demonstrating a positive potential (Porrás-Amores et al., 2013). O'Grady (2017a) brings important information in his research: about 40% of the energy consumed in Europe comes from buildings. The previous study on thermal behavior of walls avoids errors in the construction phase. Once built, its on-site verification enables to find possible pathologies and/or design deficiencies that lead to a reduction in its thermal performance.

In Argentina, about one third of the energy produced is for the management of buildings, half of which is directed to heating and cooling. In addition, more than 30% is lost due to insufficient thermal insulation or even roofs and walls that are likely to overheat in summer and presenting heat leaks in winter (Marino et al., 2016).

According to the Green Building Council Brazil (2015), based on the national energy balance of 2015, about 50% of all the demanded electricity was for buildings. The consumption of electricity in Brazil, excluding losses, reaches 516.6 TWh: 258 TWh of the total, or the equivalent of BRL 60 billion, are consumed only by buildings. According to the EIA (2018), in the year of 2017 in the United States, about 39% of total energy produced was consumed by households and commercial sectors. In the European Union countries, the tertiary and residential sectors consume about 41% of all energy produced, 55% of which is heat. Similarly, in Serbia, where about 50% of the total energy consumed goes to the buildings, 60% of it is heat (Tanic et al., 2015). In view of this information, it is important to study the thermal behavior of walls.

Rural buildings in China consume a lot of energy and have poor thermal performance due to the type and situation of building materials (Diao et al., 2018). Thus, the detection and quantification of heat losses through buildings become relevant given their extreme importance for society.

There is still a lack of studies on the subject, making it difficult to research and obtain a better understanding of the scope regarding infrared thermography. As a subject that has more than 25 years of relevant studies, researchers are investing in this topic intentionally to explore the full extent of the usage of infrared thermography. In the light of foregoing, this work aims to perform a systematic review of the existing research on the usage of infrared thermography in order to study the parameters, their properties, and influence on the thermal performance of walls.

2. LITERATURE REVIEW

2.1 History of infrared thermography

Infrared thermography was first used for purposes other than civil construction. Its principles were discovered by accident while scientist William Herchel was trying to solve an astronomical problem, in the 1800's (Barr, 1961). Over the years, the technique was improved for use in several sectors (Lucchi, 2018). In 1830, Melloni, an Italian investigator, discovered that NaCl, in natural crystals large enough to be transformed into lenses and prisms, became the main infrared until the 1930's, the era of synthetic crystal (Flir, 2017). The first quantum detector was developed between 1870 and 1920 based on the interactions between the radiations, increasing the precision and considerably reducing the response time (Smith et al., 1958). The thermography was greatly improved during World War II, showing the importance of the technology especially at night. The propagation of the infrared images in the construction sector occurred in the 2000's, with the use of barium-strontium titanate and microbolometer (Lucchi, 2018). In the last years, its use has increased dramatically, mainly in restoration, building construction, and survey works (Kylili et al., 2014; Bianchi et al., 2014). In addition, it is important to note that the use of this technique has been associated with a reduction in size equipment, cost reduction and resolution improvements,

sensitivity and accuracy, operability and portability (Meola, 2012). The use has grown considerably over the last 15 years, mainly for civil engineering and restoration of historic buildings, thus facilitating a diffusion of European legislation not only for energy efficiency but also for energy auditing of buildings (Lucchi, 2018). However, even after 30 years since the beginning of its use, it has not yet been extensively exploited (Grinzato et al., 2002; Albatici and Tonelli, 2010).

2. 2 Standardization of infrared thermography in Brazil and worldwide

Around the world, the use of infrared thermography has been diffused for some years. There are standards regarding the subject such as those of ASTM, ISO and the European Union, which regulate the use of infrared thermography in buildings and their properties. Their use is widely recommended (ASTM, 2013a, ASTM, 2015a, ASTM, 2013b, ASTM, 2015b ISO, 2008, ISO, 2015, EN, 1999).

In Brazil, there is no standard for the topic, and it is often necessary to resort to international standards or adaptations of uses in other areas.

The Brazilian standard that has some aspect regarding the use of the infrared thermography is the NBR 15575 (ABNT, 2013a), which is divided into 6 parts and approaches aspects for a good building performance, including the thermal conditions. However, it does not refer to any field tests to verify this performance. Some Brazilian standards that refer to infrared thermography include NBR 15572 (ABNT, 2013b), NBR 15763 (ABNT, 2009) and NBR 15866 (ABNT, 2010), which cover techniques for its use.

According to Marques and Chavatal (2013) the thermal behavior of a house depends substantially on the interactive activity between the external walls, ceiling and floor. Nowadays, around the world, the walls are constructed with numerous materials in several layers (Robinson et al., 2017). In Brazil, most of the buildings still use traditional materials such as concrete, ceramic blocks and plaster. However, researchers are exploring other materials such as EVA (Silva et al., 2012) and vegetable fibers (Savastano Junior and Pimentel, 2000), in different percentages inserted in traditional materials, to aid in their behavior without removing their characteristics.

2. 3 Methodology

According to Maldague (2001), infrared thermography is divided into two main techniques: active and passive. Lerma et al. (2018) say that the techniques do not meet the substrate in order to avoid damage or future recoveries.

The passive technique is one in which the temperature measurement is done under normal conditions, in objects that have their own thermal energy or somehow store energy by a natural source of heat, with temperature difference between the object studied and the environment (Kylili et al., 2014, Viégas, 2015). In the technique of active infrared thermography, an external source of artificial energy is required, generating a temperature variation over the object (Viégas, 2015). The use of passive thermography will depend on the energy available in nature, and can often suffer from wind, shade, weather and environmental conditions. As the principle of active thermography is the use of artificial heat sources, the use of lamps in the environment can be considered an alternative.

In the active thermography there are some techniques that are differentiated by the nature of the applied stimuli: heating lamps or ultrasound (Kylili et al., 2014). They are named as *Pulsed*, *Lock-in*, *Pulsed-Phase* (Maldague, 2001 apud Rocha, Póvoas, 2017), *Laser Spot Array Thermography* (Pei et al., 2016), *Principal Component Thermography* (Milovanovic et al., 2016; Rajic, 2002), among others.

Since infrared thermography began to be applied in civil construction, it has been used in the monitoring of buildings both quantitatively and qualitatively (Grinzato et al., 2002). The qualitative analysis is considered a technique of infrared thermography that provides instantaneous reports,

since the focus is the profile and not the values (ITC, 2014 apud Viégas, 2015), comparing the value relative to local access in relation to a point (Bagavathiappan et al., 2013).

In the quantitative thermography it is possible to define the severity of the situation for the studied object. The first analysis to be done must be the qualitative, since the quantitative one allows the numerical quantification of the evaluated parameters. If this order is not followed, the procedure is characterized only as a comparative analysis (ITC, 2014 apud Viégas, 2015). The data quantitative analysis allows a precise determination of the temperature in a point or a region (Bagavathiappan et al., 2013).

In order to measure the thermal performance of buildings, there are methods such as the laser spot thermography (LST) (Pei et al., 2016), heat flux meters (HFM) (Danielsky and Fröling, 2015) infrared thermovision (Albatici and Tonelli, 2010), among others.

These techniques are used for the measurement of thermal bridges (O'Grady, 2017a; Bianchi et al., 2014; BRÁS et al., 2014), air infiltration (Lerma et al., 2018), thermal transmittance (Simões et al., 2014; Donatelli et al. 2016), thermal emissivity (Abatici et al., 2013; Ciocia e Marinetti, 2012) and other properties.

The difference between the materials and their humidity, the emissivity to be analyzed, the noise caused by the reflective temperature readings are some of the factors that interfere in the analysis of the infrared thermography.

3. THERMAL PERFORMANCE OF WALLS

Global warming has brought increase in temperature. In this respect, the construction sector seeks improvements in energy efficiency through alternatives that avoid the thermal discomfort of buildings (Cani et al., 2012). The European Directive 2010/31/EU (European Parliament and ff The Council, 2010) provides a description of how energy efficiency of buildings has a role in achieving near zero consumption. Aversa et al. (2017) state that "for this to occur, energy analysis or auditing is an effective and rapid tool for new constructions, projects and in decision-making on the energy renovation of existing buildings often characterized by inefficiencies that lead to waste of energy". Due to the launching of the Performance Standard in Brazil, the NBR 15575 (ABNT, 2013), thermal comfort is presented in discussions. Thermal comfort is defined as the mind condition that expresses the user's satisfaction with an environment (Ghahramani et al., 2018).

3.1 Air leaks

Lerma et al. (2018) worked on a paper to promote a discussion on the opportunities and constraints of using active infrared thermography to detect air leaks. The potential is evaluated in a qualitative approach, comparing the thermograms of passive and active infrared thermography. In addition, there is a quantitative approach, testing methods for numerically interpreting thermograms. An experiment was carried out in a room of a 1980 construction, in the Northwest of Portugal. The experiment was performed in 8 days with different climatic conditions and the measurement was done both on the internal and external side. In the qualitative analysis it was detected, in the active approach, that air infiltrations begin to be visible when the pressure difference is 25Pa. As for the passive approach, the pressure difference must be greater for leaks. In the quantitative analysis, two different positions of the camera were used to detect air leaks: the perpendicular camera (PP) and the parallel camera (PL) to the hand shutter roller. The first technique detected air leaks through the pressure difference and the second detected the colder locations as air leakage points. The results showed that in the quantitative analysis the PP scenario allowed for a more detailed discussion. In the qualitative analysis, the active thermography showed the results clearly.

Grinzato et al. (1998) employed a methodology that resulted in a discussion on the detection and evaluation of imperfections in buildings. In order to detect air leaks, quantitative infrared

thermography was applied on a solid wall with a crack in plaster, producing images before and after leaks for verification. It has been found that a thermal stimulus would be useful in detecting defects, be it solar irradiation, airflow, or radiant flux from an artificial source. The main disadvantage of the transient analysis is the considerable increase in processing time, hardly achieved without exclusive equipment.

3. 2 Thermal bridges

Thermal bridges are defined as "any and all building envelope in which the thermal resistance is significantly altered relative to the current envelope zone" (ISO, 2008 apud Castro, 2010). Changes in thermal resistance can be caused by full or partial penetration of the building envelope by materials with a different thermal conductivity, by varying their thickness and/or by a difference between internal and external areas, which occurs at wall/floor/ceiling junctions (Castro, 2010).

Asdrubali et al. (2012) performed a quantitative analysis, using infrared thermography, with a comparative experiment between an isolated and a non-isolated thermal bridge. The article proposes a methodology to perform a quantitative analysis of some types of thermal bridges, through simple thermographic surveys and subsequent analytical processing. The selected thermal bridge was given by the difference of the structure and the window glass. This wall was placed between 2 rooms, with temperature difference of 20°C. Two analyzes were considered. The difference between the incidence factor of thermal bridges in relation to the two comparisons is 1.606 for the isolate, and 2.000 for the non-isolate. The influence factor calculated in situ is equal to 2.111 and the incidence factor of the thermal bridges calculated by the FLUENT program is equal to 1.262. Therefore, there is a reduction in thermal loss of the thermal bridge by about 40%. For a better performance, simulations were performed for a global heat loss in the winter. A heat loss of 4684W was found, 13.4% of which due to the thermal bridge. The correction of this thermal bridge would reduce the loss of heat to a value of 4307W and the incidence to 8.8%.

Bianchi et al. (2014) used a quantitative analysis of the infrared thermography in the field measurement with the objective of evaluating the energy losses through a 10m² building. The external walls, ceiling and floor were evaluated. For this, a comparison was made between 9 incident factors of calculated and identified thermal bridges. Overall the analysis shows that thermal bridges increase heat loss through building by 9%. The main results show that the procedure is a reliable tool to quantify the incidence of thermal bridges. O'Grady et al. (2017a and 2017b) applied a quantitative approach and showed the loss of heat by the thermal bridges through the temperature difference and the thermal transmittance. Grinzato et al. (1998) performed in their research experiments on three different types of walls: concrete, rock wool and concrete sandwich panel with a rod crossing the insulation layer. The purpose was to verify the behavior of the thermal bridge in the use of quantitative infrared thermography. See table 1 for more information.

Table 1. Summary of studies on thermal bridges

Author	Methodology	Main conclusions
Asdrubali, Baldinelli, Bianchi (2012)	Comparison of the results from quantitative infrared thermography with data obtained by heat flow meters and the results from a finite volume analysis.	The incidence factor of the thermal bridge correctly describes the dispersion degree of the singularity, quantifying the result of the thermal bridging correction.
Bianchi et al. (2014)	Use of quantitative infrared thermography to monitor the area to be studied.	Increased heat losses by approximately 9%.
O’Grady, Lechowska, Harte (2017a)	Use of quantitative infrared thermography on the study of thermal bridges through temperature difference and thermal transmission; experimental methodology proposed by the authors.	Wind impacts the loss of heat by the thermal bridge on the flat side. For thermal bridges with wind speeds between 0.5 m/s and 4 m/s, the relative deviation varied between + 5% and -9%.
O’Grady Lechowska, Harte (2017b)	Use of quantitative infrared thermography on the study of thermal bridges through temperature difference and thermal transmission; experimental methodology proposed by the author.	It works well in the laboratory. After being tested under real conditions, the methodology can be applied to any thermal bridge.

3.3 Thermal properties

Jorge (2011) shows that the walls are elements constructed to separate the environments. When the thermal energy is considered, it can be observed and quantified through the thermal properties. As any object, the walls have mechanical, chemical, and thermal properties. Among the thermal properties, the thermal transmittance, thermal diffusivity, thermal resistance, thermal capacity, heat transfer coefficient, and conductivity stand out.

Aversa et al. (2017) proposes the experimental study on the thermal behavior of opaque walls. They used active thermography stimulated with the objective of evaluating the effectiveness in a dynamic behavior for walls prototypes as well as verifying its success for application in situ. The authors compare a brick wall with a prototype wall with hemp fibers. It was clearly noted that hemp fibers contribute with the decrease factor (ratio between periodic thermal transmittance and thermal transmittance) from 0.87 to 0.92 for the walls with the fibers. In addition, the fibers increased the estimated time difference. It is concluded that different results were found. The next step should be measurement in situ.

Grinzato et al. (2002) used infrared thermography and calculated the thermal diffusivity of a brick sample from an old building in massive masonry, located in the Historical Arsenal of Venice. The authors performed six tests to aid in the mapping of humidity. First, a quantitative analysis was carried out with continuous monitoring and then a qualitative analysis mapped the moisture distribution due to the evaporation water cooling effect. The highest thermal diffusivity found was 5.2800×10^7 m²/s and the lowest was 5.1288×10^7 m²/s. The results showed a successful application to the mapping of moisture for the connection between the walls and the knowledge of the thermal diffusivity in bricks and plaster.

Robinson et al. (2017) aimed to study a simple and low-cost method to estimate the effective thermal diffusivity in structural walls of buildings. For this, they used infrared thermography as an experimental and low-cost method to calculate the thermal diffusivity of the concrete wall under

controlled conditions. The greatest difficulty found in this work was the control of heat loss through the lateral limits of the section, being calculated in situ, since in controlled environment, the lateral limits were isolated. This inexpensive experiment combined with a mathematical model resulted in a concrete diffusivity of $7.2 \text{ m}^2/\text{s} \pm 0.27 \text{ m}^2/\text{s}$, which is sufficiently precise. For this experiment the lateral limits were isolated, but it was concluded that there is a great loss of heat for these limits. Danielsky and Fröling (2015) investigated a quantitative methodology to analyze the thermal performance of building envelope in a non-stationary state condition, including two phases. They did experiments with wood wall exposed to external conditions to calculate the coefficient of heat transfer by convection; the value of $2.63 \text{ W}/(\text{m}^2\text{K})$ was found. The external parameters used were wind speed, humidity, and snowfall. In addition, the heat flow through the wall was assumed to obtain stable state condition only sparsely and for short periods. HFM and infrared thermography were used for the calculation of both the heat transfer coefficient and conductivity. The results of 4% and 3%, respectively for the conductivity and the global transfer coefficient, were found compatible with differences between the methods, suggesting that the thermography method is more accurate.

Donatelli et al. (2016) used active thermography for two prototype walls under controlled environmental conditions and calculated the thermal transmittance in situ, comparing with the thermal transmittance calculated by a computer program. The results showed that the temperature measurements on software (FEA) are identical to those of a real wall, and that the procedure allows the measurement of temperature in prototype walls throughout the year without climatic interference.

O'Grady et al. (2017a) elaborated a study with an efficient, non-destructive method, based on an outside infrared thermographic survey, to determine the performance of the thermal bridge. For this, they compared the values of the thermal properties, mainly of the thermal transmittance, obtained by the quantitative infrared thermography, with the values of a hot box. A computer program was used to adjust the results. The thermal transmittance of these 2 methods with 3 different wind speeds was calculated and compared. For the thermal transmittance, the external convective coefficient was determined using the Jürges approximation and the Nusselt number. The results of this study demonstrated the suitability of both approaches for calculating the value of thermal transmittance; however, the Jürges approach is less time consuming. Infrared thermography is an effective tool for the determination of thermal transmittance.

O'Grady et al. (2017b) propose the use of a non-invasive and easy-to-use method to provide quantitative measurements of the actual thermal performance in the thermal bridge. They studied thermal properties and used quantitative infrared thermography in addition to an experimental program designed to quantify the thermal bridges and tested in a calibrated and controlled hot box. They used the calculation of the thermal transmittance and the temperature variation. Three samples were taken, sample 1 had the highest value found: $0.441 \text{ W}/(\text{mK})$ by hot box and $0.436 \text{ W}/(\text{mK})$ by thermography. It can be concluded that after being tested in the laboratory and presenting excellent results for the external conditions, the observations will be a challenge for the precision of the measurements by the infrared thermography.

3.4 Temperature measurement

Datcu et al. (2005) used quantitative infrared thermography to measure walls in order to improve the measurement of ambient temperature, both internal and external. The authors used an infrared mirror, which allows large measurements of surface temperature by infrared thermography under near-ambient conditions with greater accuracy. To validate the method, an experimental study was performed on a multilayer wall, which simulated an isolation pattern. The methodology addressed in the work allowed to quantify the average radiation around the object using a highly reflective and diffusive aluminum mirror. Then, two heat sources were used: one with $24 \text{ W}/\text{m}^2$ and the other

with 48 W/m^2 . The results were compared to the results of the FLUENT program for the internal environment; as for the external environment, the wall temperature was compared with the window and the heat sink.

Lai et al. (2015) used quantitative passive infrared thermography to analyze the external wall of a skyscraper. Four concrete walls with different coatings were tested. The methodology was used when there were changes of heat flux and solar intensity. They used thermographic cameras and a computer program for analysis. Porras-Amores et al. (2013) used wall and surface measurements to locate the air temperature inside the building. The study focuses on the design of the system, its characterization, and quantification of its accuracy in different configurations. They applied a quantitative thermography to develop a precise measurement technique. An experiment was done in the garage and underground. Small variations in temperature were observed longitudinally.

4. CONCLUSION

As previously shown, infrared thermography may be used in combination with other methods for comparison of values and structures.

The method has a great applicability in the identification of air leak points. The use of active or passive thermography will generate different results. The active technique shows air leaks clearly. External stimuli aid in detection of air leaks, which may be highlighted as advantageous in the use of infrared thermography. Among the uncertainties identified were (1) the difficulties in the longer processing time of the transient analysis, which requires a unique equipment, and (2) the interpretation of the graph data and pressure versus temperature histograms. For future research, the comparison between the thermal images of passive infrared thermography and the active one in a quantitative approach would be very useful.

The advantages found in thermal bridges are simple and effective evaluations of their effect in the thermal energy behavior. Simplicity in the geometry of the building contributes to measured and calculated values. Given the uncertainty of energy consumption in the configuration with thermal bridges, the singular error due to the analysis of each thermal bridge must be taken into account. The incidence factor of the thermal bridge, analytically defined, depends on the internal temperature of both the air and the wall for the infrared thermographic camera to read. Among the applications on thermal bridges identified through the measurements, it should be highlighted the possibility of making interventions to improve the insulation. In addition, it is a useful method to analyze, refine and validate specially designed 3D simulation tools for the evaluation of energy performance in buildings, since they can evaluate thermal fields of internal and external walls.

Regarding the thermal properties, the thermal transmittance calculation was the most discussed topic, approaching several methods to calculate and compare the results. However, there are significant differences between the calculated thermal transmittance and the in-situ measurement. Moreover, some studies have emphasized that in situ measurement of thermal properties would be best performed in winter. A laboratory study indicates that the procedure implemented is aimed at measuring prototype walls throughout the year, without concern for climate change. The advantages of infrared thermography are the multidisciplinary and integration of the results. Among the uncertainty, which was repeated in some studies, one may cite the way the applied methodology would behave or its result in normal conditions, that is, without laboratory control. The difficulties were quite specific, both regarding the use of infrared thermography in historical buildings due to several environmental factors, as well as the heat losses not controlled by the lateral limits of the section under test. there were no restrictions on applicability for this topic.

The approach of infrared thermography for temperature measurement was also used, which succeed as a comparative method. Infrared thermography has the advantage of displaying images with different identifications, to measure the surface temperature in a large area of an element under

construction. Thus, it provides more representative data in relation to point measurements. The difficulties were in the quantitative monitoring through conventional thermography. It presents problems in the measurement of surface temperature and air conditions inside the building. In addition, it can be applied to various surfaces.

In general, most of the work on infrared thermography approached quantitative analysis. The active approach is also widely explored. It was noticed that there is a multidisciplinary between the topics covered, since some authors used infrared thermography to talk about more than one subject, enriching and complementing their studies.

Some authors used computer programs, mainly for the measurement of thermal properties, when there were experimental studies facilitating the comparison between experimental and theoretical values. The researches that used successful experiments with prototypes and controlled conditions contribute with important considerations that the next step would be the measurement in situ. Then, it is expected that infrared thermography will be increasingly exploited and bring better performances and energy savings in buildings.

5. REFERENCES

- ABNT - Associação brasileira de normas técnicas. (2013a). “*NBR 15575: Edificações habitacionais – Desempenho Parte 1 – 6*”. Rio de Janeiro.
- ABNT - Associação brasileira de normas técnicas. (2013b). “*NBR 15572: Ensaio não destrutivos – Termografia Infravermelha – Guia para inspeção de equipamentos elétricos e mecânicos*”. Rio de Janeiro.
- ABNT - Associação brasileira de normas técnicas. (2005). “*NBR 15220: Desempenho térmico das edificações Parte 1 – 5*”. Rio de Janeiro.
- ABNT - Associação brasileira de normas técnicas. (2010). “*NBR 15866: Ensaio não destrutivos – Termografia - Metodologia de avaliação de temperatura de trabalho de equipamentos em sistemas elétricos*”. Rio de Janeiro.
- ABNT - Associação brasileira de normas técnicas. (2009). “*NBR 15763: Ensaio não destrutivos – Termografia – Critérios de definição de periodicidade de inspeção em sistemas elétricos de potencia*”. Rio de Janeiro.
- Albatici, R., Passerini, F., Tonelli, A. M., Gialanella, S. (2013), “*Assessment of the thermal emissivity value of building materials using an infrared thermovision technique emissometer*”, Energy and buildings, V.66, p.33-40. <https://doi.org/10.1016/j.enbuild.2013.07.004>
- Albatici, R., Tonelli, A. M. (2010), “*Infrared thermovision technique for the assessment of thermal transmittance value of opaque building elements on site*”, Energy and Buildings, V.42, No.11, p.2177-2183. <https://doi.org/10.1016/j.enbuild.2010.07.010>
- Asdrubali, F., Baldinelli, G., Bianchi, G. (2012), “*A quantitative methodology to evaluate thermal bridges in buildings*”, Applied Energy, V.97, p.365-373. <https://doi.org/10.1016/j.apenergy.2011.12.054>
- ASTM. (2013a). “*C1046-95: Standard practice for in-situ measurement of heat flux and temperature on building envelope components*”, (West Conshohocken, United States: ASTM International), p. 10. <http://dx.doi.org/10.1520/C1046>
- ASTM. (2013b). “*C1155-95: Standard practice for determining thermal resistance of building envelope components from the in-situ data*”, (West Conshohocken, United States: ASTM International), p. 8. <http://dx.doi.org/10.1520/C1155-95R13>
- ASTM. (2015a). “*C1060-11a: Standard practice for thermographic inspection of insulation installations in envelope cavities of frame buildings*”, (West Conshohocken, United States: ASTM International), p. 7. <http://dx.doi.org/10.1520/C1060-11AR15>
- ASTM. (2015b). “*C1153-10: Standard practice for location of wet insulation in roofing systems*”

using infrared imaging”, (West Conshohocken, United States: ASTM International), p. 6.

<http://dx.doi.org/10.1520/C1153-10R15>

Aversa, P., Palumbo, D., Donatelli, A., Tamborrino, R., Ancona, F., Galietti, U., Luprano, V. A. M. (2017), “*Infrared thermography for the investigation of dynamic thermal behaviour of opaque building elements: Comparison between empty and filled with hemp fibres prototype walls*”, *Energy and Buildings*, V.152, p.264-272. <https://doi.org/10.1016/j.enbuild.2017.07.055>

Bagavathiappan, S., Lahiri, B. B., Saravanan, T., Philip, J., Jayakumar, T. (2013), “*Infrared thermography for condition monitoring – A review*”, *Infrared Physics & Technology*, V.60, p.35-55. <https://doi.org/10.1016/j.infrared.2013.03.006>

Barr, E. S. (1961), “*The infrared pioneers—I. Sir William Herschel*”. *Infrared Physics*, v. 1, p. 1-2.

Bianchi, F., Pisello, A. L., Baldinelli, G., Asdrubali, F. (2014), “*Infrared Thermography Assessment of Thermal Bridges in Building Envelope: Experimental Validation in a Test Room Setup*”, *Sustainability*, V. 10, No. 6, p.7107-7120. <https://doi.org/10.3390/su6107107>

Brás, A., Gonçalves, F., Faustino, P. (2014), “*Cork-based mortars for thermal bridges correction in a dwelling: Thermal performance and cost evaluation*”, *Energy and Buildings*, V.72, p.296–308. <https://doi.org/10.1016/j.enbuild.2013.12.022>

Cani, B. F., Marinoski, D. L., Lamberts, R. (2012), “*Aplicação da termografia infravermelha para verificação da temperatura em telhas cerâmicas com diferentes teores de umidade e condições de limpeza da superfície*” in: XIV Encontro Nacional de Tecnologia do Ambiente Construído - XIV ENTAC, Juíz de Fora: MG (BR).

Castro, J. L. B. B. (2010), “*Quantificação dos coeficientes de transmissão térmica lineares - pontes térmicas*”, Dissertação de Mestrado – Faculdade de Engenharia da Universidade do Porto, Portugal, p.314.

Ciocia, C., Marinetti, S. (2012). “*In-situ emissivity measurement of construction materials*”, in: 11th International Conference on Quantitative InfraRed Thermography, Napoly: Italy.

Clark, M., McCann, D., Forde, M. (2003), “*Application of infrared thermography to the nondestructive testing of concrete and masonry bridges*”. *NDT&E International*, V.36, No. 4, pp. 265- 275.

Danielski, I., Fröling, M. (2015). “*Diagnosis of buildings’ thermal performance - a quantitative method using thermography under non-steady state heat flow*”, *Energy Procedia*, V.83, p.320-329. <https://doi.org/10.1016/j.egypro.2015.12.186>

Datcu, S., Ibos, L., Candau, Y., Mattei, S. (2005), “*Improvement of building wall surface temperature measurements by infrared thermography*”, *Infrared Physics & Technology*, V. 46, p. 451-467. <https://doi.org/10.1016/j.infrared.2005.01.001>

Decreto-Lei Nº 80/2006. (4 de abril de 2006). Regulamento das características do Comportamento Térmico dos Edifícios (RCCTE).

Diao, R., Sun, L., Yang, F. (2018), “*Thermal performance of building wall materials in villages and towns in hot summer and cold winter zone in China*”, *Applied Thermal Engineering*, V. 128, p. 517-530. <https://doi.org/10.1016/j.applthermaleng.2017.08.159>

Directive 2010/31/EU of the European Parliament and of the Council. (2010). Disponível em: <<https://eur-lex.europa.eu/legal-content/EN/TXT/HTML/?uri=CELEX:32010L0031&from=IT>> Acessado em: 13 de Junho de 2018.

Donatelli, A., Aversa, P., Luprano, V. A. M. (2016), “*Set-up of an experimental procedure for the measurement of thermal transmittances via infrared thermography on lab-made prototype walls*”, *Infrared Physics & Technology*, V. 79, p. 135-143. <https://doi.org/10.1016/j.infrared.2016.10.005>

EIA. U.S. Energy information administration. (2018). Disponível em: <https://www.eia.gov/tools/faqs/faq.php?id=86&t=1>. Acessado em: 15 de Junho de 2018.

- EN. (1999), “13187: Thermal performance of buildings. Qualitative detection of thermal irregularities in building envelopes. Infrared method”, (London, United Kingdom: British Standards Institution), p. 16. <https://doi.org/10.3403/01569434U>
- FLIR-Forward Looking Infrared. (2017). “User’s manual FLIR Cx Series” (Wilsonville, United States: FLIR), p. 67.
- Ghahramani, A., Castro, G., Karvigh, S. A., Becerik-Gerber, B. (2018), “Towards unsupervised learning of thermal comfort using infrared thermography”, Applied Energy, V. 211, p. 41-49. <https://doi.org/10.1016/j.apenergy.2017.11.021>
- Green Building Council Brasil. (2015), “O consumo de energia nas edificações do Brasil”. Disponível em: <http://www.gbcbrazil.org.br/detalhe-noticia.php?cod=119>. Acesso em: 03 de julho de 2018.
- Grinzato, E., Bison, P.G., Marinetti, S. (2002). “Monitoring of ancient buildings by the thermal method”, Journal of Cultural Heritage, V.3, p. 21–29. [https://doi.org/10.1016/S1296-2074\(02\)01159-7](https://doi.org/10.1016/S1296-2074(02)01159-7)
- Grinzato, E., Vavilov, V., Kauppinen, T. (1998). “Quantitative infrared thermography in buildings”, Energy and Buildings, V.29, No.1, p. 1-9. [https://doi.org/10.1016/S0378-7788\(97\)00039-X](https://doi.org/10.1016/S0378-7788(97)00039-X)
- ISO (2015), “6781-3: Performance of buildings -- Detection of heat, air and moisture irregularities in buildings by infrared methods -- Part 3: Qualifications of equipment operators, data analysts and report writers”, (Geneva, Suíça: International Organization for Standardization), p. 18.
- ISO (2008), “13790: Energy performance of buildings -- Calculation of energy use for space heating and cooling”, (Geneva, Suíça: International Organization for Standardization), p. 167.
- Jorge, L. F. A. (2011). “Determinação do coeficiente de transmissão térmica em paredes de edifícios”, Dissertação de Mestrado, Universidade da Beira Interior, Portugal, p. 112.
- Kylili, A., Fokaides, P. A., Christou, P., Kalogirou, S. A. (2014). “Infrared thermography (IRT) applications for building diagnostics: A review”, Applied Energy, V.134, p.531-549. <https://doi.org/10.1016/j.apenergy.2014.08.005>
- Lai, W. W., Lee, K., Poon, C. (2015). “Validation of size estimation of debonds in external wall’s composite finishes via passive Infrared thermography and a gradient algorithm”, Construction and Building Materials, V. 87, p. 113-124. <https://doi.org/10.1016/j.conbuildmat.2015.03.032>
- Lerma, C., Barreira, E., Almeida, R. M. S. F. (2018). “A discussion concerning active infrared thermography in the evaluation of buildings air infiltration”, Energy and Buildings, V. 168, p. 56-66. <https://doi.org/10.1016/j.enbuild.2018.02.050>
- Lucchi, E. (2018). “Applications of the infrared thermography in the energy audit of buildings: A review”, Renewable and Sustainable Energy Reviews. v. 82, parte 3, p. 3077-3090. <https://doi.org/10.1016/j.rser.2017.10.031>
- Maldague, X. (2001). “Infrared and Thermal testing: Nondestructive testing handbook. 3th ed, Columbus, OH: Patrick O. Moore, 2001.
- Marino, B. M., Muñoz, N., Thomas, L. P. (2016). “Estimation of the surface thermal resistances and heat loss by conduction using thermography”, Applied Thermal Engineering, V. 114, p. 1213-1221. <https://doi.org/10.1016/j.applthermaleng.2016.12.033>
- Marinoski, D. L., Souza, G. T., Sangoi, J. M., Lamberts, R. (2010). “Utilização de imagens em infravermelho para análise térmica de componentes construtivos”, in: XIII Encontro Nacional de Tecnologia do Ambiente Construído, Canela: Rio Grande do Sul (BR).
- Marques, T. H.T., Chavatal, K. M. S. (2013). “A Review of the Brazilian NBR 15575 standard: applying the simulation and simplified methods for evaluating a social house thermal performance”, in: Symposium on Simulation for Architecture and Urban Design, San Diego: Califórnia (EUA).

- Meola, C. (2012), *Infrared thermography: recent advances and future trends*. Bentham Books, Italy, p.24-26. eISBN: 978-1-60805-143-4.
- Milovanović, B., Pečur, I. B., Štirmer, N. (2016). “*The methodology for defect quantification in concrete using ir thermography*”, *Journal of civil engineering and management*, V. 23, p. 573-582. <https://doi.org/10.3846/13923730.2016.1210220>
- O’Grady, M., Lechowska, A. A., Harte, A. M. (2017b). “*Infrared thermography technique as an in-situ method of assessing heat loss through thermal bridging*”, *Energy and building*, V.135, p. 20-32. <https://doi.org/10.1016/j.enbuild.2016.11.039>
- O’Grady, M., Lechowska, A. A., Harte, A. M. (2017a). “*Quantification of heat losses through building envelope thermal bridges influenced by wind velocity using the outdoor infrared thermography Technique*”, *Applied Energy*, V.208, p. 1038-1052. <https://doi.org/10.1016/j.apenergy.2017.09.047>
- Pei, C., Qiu, J., Liu, H., Chen, Z. (2016). “*Simulation of surface cracks measurement in first walls by laser spot array thermography*”, *Fusion Engineering and Desing*, V.109-111, parte B, p. 1237-1241. <https://doi.org/10.1016/j.fusengdes.2015.11.055>
- Porras-Amores, C, Mazzarrón, F. R., Canas, I. (2013), “*Using quantitative infrared thermography to determine indoor air temperature*”, *Energy and Building*, V.65, p.292-298. <https://doi.org/10.1016/j.enbuild.2013.06.022>
- Rajic, N. (2002), “*Principal component thermography for flaw contrast enhancement and flaw depth characterisation in composite structures*”, *Composite Structures*, V. 58, p. 521-528. [https://doi.org/10.1016/S0263-8223\(02\)00161-7](https://doi.org/10.1016/S0263-8223(02)00161-7)
- Robinson, A. J., Lesage, A. F. J., Reilly, A., Mcgranaghan, G., Byrne, G., O’hegarty, R., Kinnane, O. (2017), “*A New Transient Method for Determining Thermal Properties of Wall Sections*”, *Energy and Buildings*, V. 142, p. 139-146. <https://doi.org/10.1016/j.enbuild.2017.02.029>
- Rocha, J. H. A., Póvoas, Y. V. (2017). “*A termografia infravermelha como um ensaio não destrutivo para a inspeção de pontes de concreto armado: Revisão do estado da arte*”, *Revista ALCONPAT*, V. 7, nº 3. <http://dx.doi.org/10.21041/ra.v7i3.223>
- Savastano Junior, H., Pimentel, L. L. (2000). “*Viabilidade do aproveitamento de resíduos de fibras vegetais para fins de obtenção de material de construção*”, *Revista Brasileira de Engenharia Agrícola e Ambiental - Agriambi*, V. 4, n. 1, p. 103-110. <http://dx.doi.org/10.1590/S1415-43662000000100019>
- Silva, E. P., Cahino, J. E. M., Melo, A. B. (2012), “*Avaliação do desempenho térmico de blocos EVA*”, in: XIV Encontro Nacional de Tecnologia do Ambiente Construído, Juíz de Fora: Minas Gerais (BR).
- Simões, I., Simões, N, Tadeu, A., Riachos, J. (2014), “*Laboratory assessment of thermal transmittance of homogeneous building elements using infrared thermography*”, in: 12th International Conference on Quantitative InfraRed Thermography, Bordeaux: France.
- Smith, R. A., Jones, F. E., Chasmar, R. P. (1958), *The Detection and Measurement of Infrared Radiation*, Oxford University Press.
- Tanic, M., Stankovic, D., Nikolic, V., Nikolic, M., Kostic, D., Milojkovic, A., Spasic, S., Vatin, N. (2015). “*Reducing Energy Consumption by Optimizing Thermal Losses and Measures of Energy Recovery in Preschools*”, *Procedia Engineering*, v. 117, p. 919 – 932. <https://doi.org/10.1016/j.proeng.2015.08.179>
- Viégas, D. J. A. (2015). “*Utilização de termografia infravermelha em fachadas para verificação de descolamento de revestimentos*”, *Dissertação de Mestrado – Escola Politécnica da Universidade de Pernambuco, Recife*, p. 164.

Adhesion, strengthening and durability issues in the retrofitting of Reinforced Concrete (RC) beams using Carbon Fiber Reinforced Polymer (CFRP) – A Review

P. J. Poot Cauch¹ , R. Martínez-Molina¹ , J. L. Gamboa Marrufo¹ , P. J. Herrera Franco^{1*} 

*Contact author: pherrera@cicy.mx

DOI: <http://dx.doi.org/10.21041/ra.v9i2.401>

Reception: 30/03/2019 | Acceptance: 22/04/2019 | Publication: 30/04/2019

ABSTRACT

This paper addresses the mechanics of adhesion, strengthening effect and durability issues of applications of CFRP composite materials in beams. The application of CFRP materials has been widely described, but the main focus has been on overall failure parameters. The first issue is strengthening capability of CFRP reinforcement for concrete beams. The second is the local interface bond stress-slip relationship, that is, the local τ -slip. The last issue is the durability of the CFRP sheet/plate, when exposed to a hydro-thermal environment. The role of adhesion and the mechanics of concrete-CFRP adhesion and a sound understanding of the interface between the CFRP and concrete behavior is the key factor for controlling debonding failures in CFRP-strengthened RC beams.

Keywords: carbon fiber composites; resin-concrete interphase; fiber-matrix interphase; retrofitting; adhesion.

Cite as: Poot Cauch, P. J., Martínez-Molina, R., Gamboa Marrufo, J. L., Herrera Franco, P. J. (2019), "Adhesion, strengthening and durability issues in the retrofitting of Reinforced Concrete (RC) beams using Carbon Fiber Reinforced Polymer (CFRP) – A Review", Revista ALCONPAT, 9 (2), pp. 130 – 151, DOI: <http://dx.doi.org/10.21041/ra.v9i2.401>

¹ Universidad Marista, Mérida, Yucatán, México.

Legal Information

Revista ALCONPAT is a quarterly publication by the Asociación Latinoamericana de Control de Calidad, Patología y Recuperación de la Construcción, Internacional, A.C., Km. 6 antigua carretera a Progreso, Mérida, Yucatán, 97310, Tel.5219997385893, alconpat.int@gmail.com, Website: www.alconpat.org

Responsible editor: Pedro Castro Borges, Ph.D. Reservation of rights for exclusive use No.04-2013-011717330300-203, and ISSN 2007-6835, both granted by the Instituto Nacional de Derecho de Autor. Responsible for the last update of this issue, Informatics Unit ALCONPAT, Elizabeth Sabido Maldonado, Km. 6, antigua carretera a Progreso, Mérida, Yucatán, C.P. 97310.

The views of the authors do not necessarily reflect the position of the editor.

The total or partial reproduction of the contents and images of the publication is strictly prohibited without the previous authorization of ALCONPAT Internacional A.C.

Any dispute, including the replies of the authors, will be published in the first issue of 2020 provided that the information is received before the closing of the third issue of 2019.

Adhesión, reforzamiento y problemas de durabilidad en la restitución de vigas de Concreto Reforzado (CR) usando Polímero Reforzado con Fibra de Carbono (CFRP) - Una revisión

RESUMEN

Este documento aborda la mecánica de la adhesión, el efecto de reforzamiento y la durabilidad de las aplicaciones de materiales compuestos de CFRP en vigas. La aplicación de los materiales de CFRP se ha descrito ampliamente, pero el enfoque principal se ha centrado en los parámetros generales de falla. El primer problema es el fortalecimiento de la capacidad del refuerzo de CFRP para vigas de concreto. El segundo es la relación local tensión-deslizamiento del enlace de la interfaz, es decir, el deslizamiento τ local. El último problema es la durabilidad de la hoja/placa de CFRP, cuando se expone a un ambiente hidro-térmico. El papel de la adhesión y la mecánica de la adhesión de concreto-CFRP y una buena comprensión de la interfaz entre el CFRP y el comportamiento del concreto es el factor clave para controlar las fallas de desunión en vigas de CR reforzadas con CFRP.

Palabras clave: compuestos de fibra de carbono; interfase resina-hormigón; interfase de matriz de fibra; reequipamiento, adhesión.

Adesão, fortalecimento e problemas de durabilidade na restauração de varredura Concreto Reforçado (CR) usando o Polímero Reforçado com Fibra de Carbono (CFRP) - Uma revisão

RESUMO

Este artigo aborda a mecânica de aderência, o efeito de fortalecimento e a durabilidade de aplicações compostas de composto de CFRP em vigas. A aplicação de materiais CFRP foi descrita extensivamente, mas o foco principal tem sido nos parâmetros gerais de falha. O primeiro problema é fortalecer a capacidade de reforço do CFRP para vigas de concreto. O segundo é o relacionamento local tensão-escorregamento do link de interface, isto é, o escorregamento local deslizamento local τ . O último problema é a durabilidade da chapa / chapa CFRP, quando exposta a um ambiente hidrotermal. O papel da adesão e a mecânica da aderência do concreto CFRP e uma boa compreensão da interface entre o CFRP e o comportamento do concreto é o fator chave no controle de falhas de desunião em feixes CR reforçados com CFRP.

Palavras-chave: compósitos de fibra de carbono; interface resina-concreto; interface de matriz de fibra; reequipamento, adesão.

NOMENCLATURE

a – shear span	β_1 – coefficient that determines the approximation of the resultant
b_f – width of the layer of CFRP	compression curve of the concrete to a
b_w – width of the beam	rectangle according to the
b_p – width of bonded CFRP plate	recommendations of ACI 440-2R (2008)
b_c – width of concrete in pull-out experiment	ε_{bi} – strain found in the covering of the
L_b – Length of bonded CFRP	tensile reinforcement in the beam before
L_e – Effective length of CFRP	the strengthen
T_p . thickness of bonded CFRP plate	ε_c – concrete strain
c – height of the block of rectangular	ε_{cu} – concrete ultimate strain
compression equivalent of the concrete	

c_1 – factor obtained by calibration of results (equal to 0.64 for CFRP)	ε_f – carbon fiber strain
d – effective beam height	ε_{fd} – limit value of fiber strain to be adopted in the sizing and verification of reinforcement
d' – centroid position of the compressed reinforcement	ε_{fe} – effective strain in the FRP
f_c – concrete compression strength	ε_{fu} – ultimate strain observed in the polymer at the moment of failure
f_{ctm} – average tensile strength of concrete	ε_s – strain in the tensile reinforcement
f_{fe} – effective strength of the CFRP	ε_s' – strain in the compressed reinforcement
f_s – strength of steel	ε_{ys} – yield strain of the flexural reinforcement
A_f – area of reinforcement applied to the beam	G_f – Interfacial fracture energy
A_s – steel area of the tensile reinforcement	s – local slip;
A_s' – steel area of compressed reinforcement	s_e – elastic component of local slip;
E_f – modulus of elasticity of the CFRP	s_f – local slip when bond stress τ reduces to zero;
E_s – modulus of elasticity of steel	s_0 – local slip at τ_{max} ;
F_{cc} – compression resulting	B_l – bond length factor;
L – total beam length	B_w – width ratio factor;
P – applied load in the experimental test	τ – local bond stress;
T_s – tensile component due to the tensile reinforcement	τ_{max} – maximal local bond stress;
α – reduction coefficient due to the propagation of inclined cracks	τ_u – average bond stress.

1. INTRODUCTION

During the last four decades, the development of materials from the theoretical and technological points of view of advanced composite materials have resulted in an expanded use. Their outstanding engineering properties such as high specific strength and stiffness, lower density, high fatigue endurance, high damping and low thermal coefficient (in fiber direction), etc., have resulted in a constant use in the aerospace, marine and automobile industries.

Reinforced concrete structures may be damaged after a few years in service or exposure to aggressive environments, such as marine and/or industrial environments, and are therefore in need of repair. Then, to allow for a load carrying capacity higher than the original design value, the structural members need to be retrofitted. Corrosion is a major cause of deterioration in civil infrastructure, especially steel bridges, with consequences ranging from the progressive weakening of the structural elements due to cracking and loss of cross-section, to sudden collapse. The high strength-to-weight and stiffness-to-weight ratios of composites make them attractive for use in infrastructure rehabilitation. A common repair/retrofitting technique for concrete beams, is to bond a plate to the soffit of the beam. Initially, steel plates were employed and more recently, attention has been directed towards the use of carbon fiber reinforced plastic composites (CFRP) plates, which offer higher strength/weight, and several attractive attributes mentioned before and an improved durability over their steel counterparts. Furthermore, these advanced composites are being considered as a replacement to the conventional steel in reinforced concrete structures due to a continuing decrease of the cost of CFRP materials and the development of synthetic adhesives based on epoxy resins, (C.K.Y. Leung, (2001), Swamy R.N. et al, (1987), Hamoush S.A. (1990), Norris, (1997), Karbhari, et al, (1995), Saadatmanesh, (1995)).

The performance of the CFRP as a reinforcement agent for concrete elements has been studied, from the structural, material, and application method. The flexural strengthening of RC beams using composites can be provided by epoxy bonding of CFRP plate to the portion of the elements subjected to tensile stresses, with fibers parallel to the principal stress direction. If the composite material fibers are placed perpendicular to the cracks, a large increase in strength and stiffness is achieved as compared to situation where fibers are placed oblique to the cracks. Also, strength enhancement for RC beams of approximately 200% is achieved with carbon fiber reinforced polymer composites (CFRP). The flexural performance of strengthened RC beams is affected by several factors such as modulus of elasticity of CFRP and its center of gravity location relative to the neutral axis, width of laminate, length of laminate, amount of main and shear reinforcement, number of CFRP plies, level of loading, lamination configuration, concrete strength and cover, damage and loading condition, etc. (Sandeep S. et al, 2008).

Adhesion of the external CFRP to the concrete substrate is of critical importance for the effectiveness of the reinforcing mechanism, because it means the transfer of stresses between concrete and the FRPC in order to develop a composite action. Several reports can be found in the technical literature studying different aspects that affect the efficiency of the reinforcing of CFRP. The main objective of this paper is to review the literature (analytical/experimental) of the different parameters that affect the load-transfer mechanisms from the RC element to the CFRP and to discuss the effects of various parameters that affect the durability, especially, parameters related to the adhesive-concrete interface as well as the composite material laminate performance when exposed to hygro-thermal environments. The discussion is kept on a descriptive level and the reader is advised to refer to the cited references for details of parameters and mathematical models.

Parameters such as strength on the average bond strength and the force transfer from the composite plates to the concrete were studied by Chajes, M.J. et al, (1996). They observed two failure mechanisms direct concrete shearing beneath the concrete surface and cohesive-type failure, depending on the type of adhesive and concrete. They also showed that the surface preparation of the concrete can influence the bond strength. Similar studies were conducted by Yoshizawa et al, (1996) who reported that the roughness of the concrete face had an effect on the load bearing capacity of the specimen. Also, when the failure mode of the joint was governed by shearing of the concrete, the ultimate bond strength was proportional to the square root of the concrete strength f'_c . They also found that there is an effective bond length for a joint beyond which no further increase in failure load can be achieved.

2. THE MECHANICS OF CONCRETE-CFRP ADHESION

2.1 Linear analysis of the bonded Concrete-CFRP joint

Debonding between concrete and the externally bonded CFRP sheets/strips externally in flexural and shear strengthening cases decreases the strength efficiency of the CFRP materials or causes a deficiency in member ductility (Dai, et al, 2005). The interface bond strength or local stress-slip property has been shown to influence the peak flexural or shear strength of RC members retrofitted using CFRP by means of analytical models (Buyukozturk and Hearing 1998, fib 2001) giving birth to various bond strength, anchorage length and local bond stress-slip models (Chen and Teng 2001). As stated by Lu, et al (2005), an accurate bond-slip model is of fundamental importance in the modeling of FRP-strengthened RC structure. A sound understanding of the behavior of the interface between the CFRP and concrete is the key factor controlling debonding failures in CFRP-strengthened RC structures. Therefore, for the safe and economic design of externally bonded CFRP systems, in this paper we make reference to the analysis presented by De Lorenzis, L. 2001, and mention other models available in technical literature (see Figure 1), (Taljsten B. 1997, Bizindavyi L. 1999, Mander J. B. 1998, Jeffries, J. M. 2001).

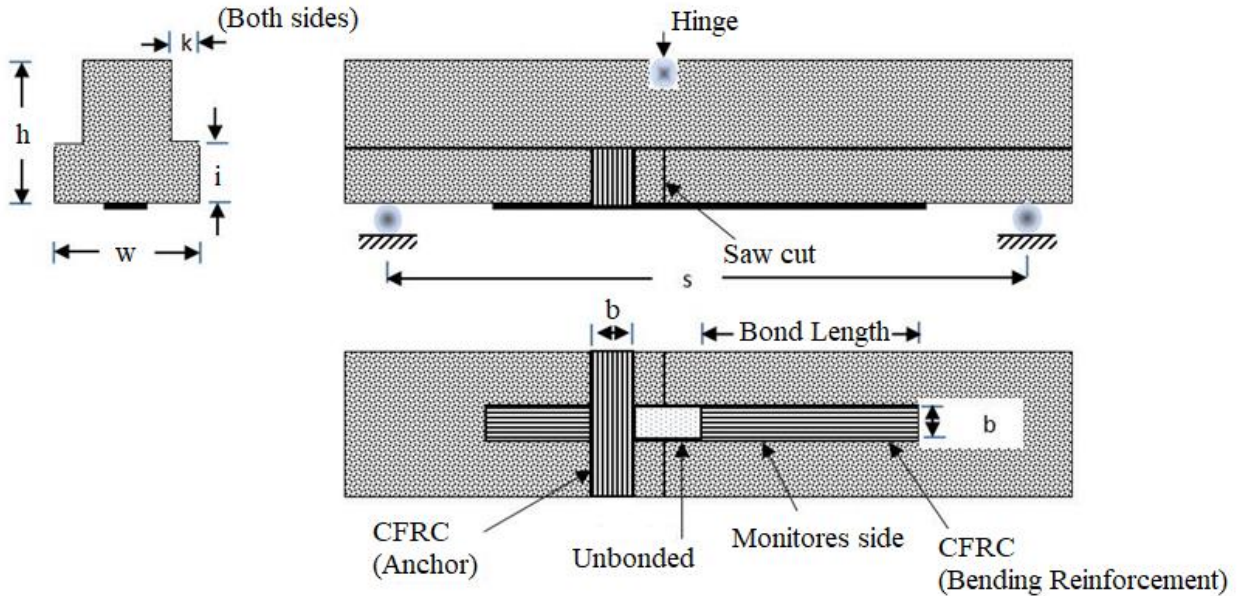


Figure 1. Test specimen showing dimensions of the concrete beam and the position and dimensions of the CFRC bending reinforcing as well as the CFRP anchor. (After De Lorenzis, L. 2001)

Considering static equilibrium and compatibility relations of a differential element of sheet of length dx , and assuming a linear elastic behavior of the CFRP sheet and that the stiffness of the concrete is much higher than the stiffness of the composite, that is, negligible strain in the concrete and that the adhesive is subjected to shear forces only, the following differential equation results. At moderate load levels, a linear bond stress-slip behavior can be adopted:

$$\frac{d^2s}{dx^2} - \frac{1}{tE} \tau[s(x)] = 0 \quad (1)$$

Where s is the slip, τ is the bond stress, x the coordinate along the bonded length of the laminate, t the thickness and E the elastic modulus of the CFRP. At moderate load levels, a linear bond stress-slip behavior can be adopted. A solution of the equation 1 is

$$s(x) = C_1 \text{Sinh } \alpha x + C_2 \text{Cosh } \alpha x \quad (2a)$$

$$\varepsilon(x) = \alpha C_1 \text{Cosh } \alpha x + \alpha C_2 \text{Sinh } \alpha x \quad (2b)$$

$$\tau(x) = Ks(x) \quad (2c)$$

Where:

$$\alpha = \sqrt{\frac{K}{tE}} \quad (3)$$

The constants C_1 and C_2 can be determined from the boundary conditions. If the origin of the coordinate x corresponds to the free end of the sheet ($x = 0$), where no strain exists, and $x = l$ (being l the bonded length) corresponds to the end of the CFRP sheet where the external load is directly applied, the boundary conditions are:

$$\varepsilon(0) = 0 \tag{4a}$$

$$\varepsilon(l) = \frac{\sigma_0}{E} \tag{4b}$$

And equations 2a-c become

$$s(x) = \left(\frac{\sigma_0}{\alpha E} \right) \frac{\text{Cosh } \alpha x}{\text{Sinh } \alpha l} \tag{5a}$$

$$\varepsilon(x) = \left(\frac{\sigma_0}{E} \right) \frac{\text{Sinh } \alpha x}{\text{Sinh } \alpha l} \tag{5b}$$

$$\tau(x) = Ks(x) \tag{5c}$$

The slip modulus K can be estimated using a simple shear model as the ratio of the shear modulus of the adhesive and the thickness of the adhesive layer. Also, when CFRP based on sheets instead of plates are used, the slip modulus $K = G_{int}/t_{int}$ that is, the ratio of the shear modulus of the FRPC, G_{int} and the thickness of the interface t_{int} where G_{int} is the shear modulus of the FRPC sheet-concrete interface and t_{int} is thickness of the interface, can be evaluated as follows: when the composite material is formed *in situ*, using the wet lay-up technique, the resin system intrinsically serves both as the matrix for the composite and the interlayer between the concrete and the composite, i.e., as the adhesive layer. This layer then is the main medium for the transfer of shear stresses between the composite and the concrete. For the estimation of G_{int} , the layer of primer must be also considered. Therefore, G_{int} and t_{int} can be computed from the thicknesses obtained from scanning electron microscopy and the elastic properties of resin and primer the rule of mixture for the shear modulus:

$$G_{int} = \frac{G_{resin} G_{primer}}{t_{resin} G_{primer} + t_{primer} G_{resin}} \tag{6}$$

Where:

$$G_{resin} = \frac{E_{resin}}{2(1+\nu_{resin})} \tag{7}$$

Equation 7 can also be used to estimate the shear modulus of the primer. The local τ -slip curves can be obtained from experimental data as follows. The bond stress, τ , can be found by equilibrium of forces, considering also the linear elasticity of the FRPC.

$$\tau(x) = tE \frac{d\varepsilon_r(x)}{dx} \quad (8)$$

Where ε_r is the CFRP strain to failure, therefore, the $\tau(x)$ diagram can be obtained from the first derivative of the strain vs location diagram multiplied by the elastic modulus E and the thickness.

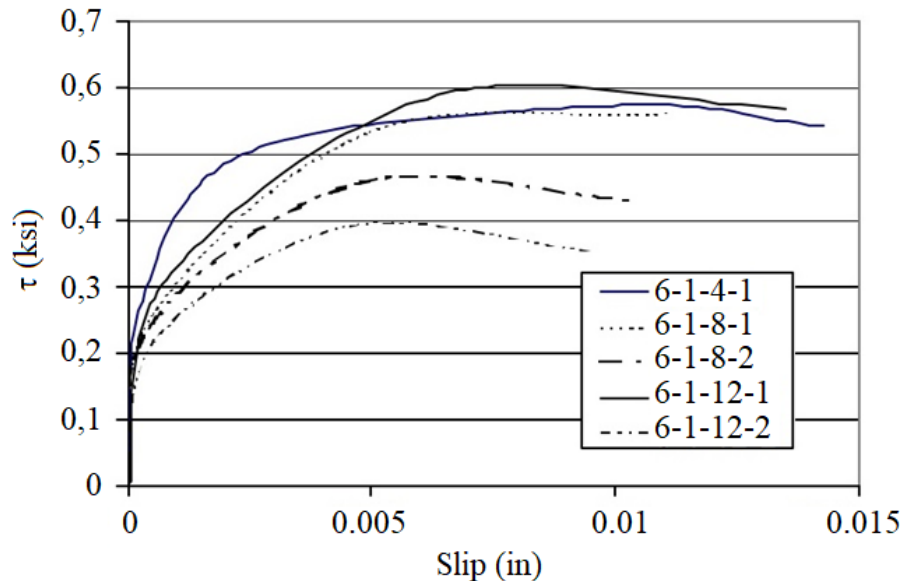


Figure 2. Local τ -slip relationships for specimens with different CFRP bond lengths (4, 8 and 12 in) bonded on the tension side of a concrete beam. Note: 1 in= 25.4 mm; 1 psi= 7.03 kPa (De Lorenzis et al (2001)).

Figure 2 illustrates some bond stress τ - slip curves obtained from tested specimens at a load level corresponding to imminent peeling. This was identified as the load level at which the strain distribution becomes linear. Typical bond τ -slip curves should consist of an ascending branch with continuous stiffness degradation to the maximum bond stress and a curved descending branch reaching a zero-bond stress at a finite value of slip. While a precise bond-slip model should consist of a curved ascending branch and a curved descending branch, other shapes such as a bilinear model can be used as a good approximation. An accurate bond-slip model should provide close predictions of both the shape and fracture energy (area under the bond-slip curve) of the bond-slip curve. None of the existing bond-slip models provides accurate predictions of both the shape and the interfacial fracture energy as found from tests. The area underneath the τ - slip curve, indicated as G_f , is the fracture energy per unit area of the bonded joint (Lu X.Z. 2005).

In a recent paper, Hamze-Ziabari and Yasalovi, (2017), made a summary of existing equations for the prediction of load transfer between concrete and the effective load transfer length of the CFRP. These equations were derived from either fracture mechanics theoretical considerations or from empirical equations calibrated with experimental datasets or combinations of the two. However, the accuracy of these models seemed to be limited. For the sake of completeness, some of these equations are also reproduced in this review (see table 1):

Table 1. Equations to estimate the maximum transferable load P_{max} as well as the effective length of the FRPC.

Reference	Equation maximum transferable load P_{max}	Effective length and considerations
Chen, F.J., Teng, G.J. (2001)	$P_{max} = 0.315\beta_p\beta_L b_p L_e \sqrt{f_c}$	$L_e = \sqrt{\frac{E_p t_p}{f_c}}$ $\beta_p = \sqrt{\frac{2 - \frac{b_p}{b}}{1 + \frac{b_p}{b}}}$ $\beta_L = \begin{cases} 1 & \text{if } L_b \geq L_e \\ \text{Sin } \frac{\pi L_b}{2L_e} & \text{if } L_b \leq L_e \end{cases}$
De Lorenzis <i>et al</i> (2001)	$P_{max} = b_p \sqrt{2E_f t_p G_f}$	G_f is the fracture energy per unit area of the joint, assumed to be equal to 1.06 N-mm/mm ²
Teck-Yong <i>et al</i> (1987)	$P_{max} = \left(0.5 + 0.08\sqrt{\frac{E_f t_p}{1000}}\right) \frac{b L_e f_c}{2}$	
Van Gemert (1980)	$P_{max} = \frac{b_p L f_c}{2}$	
Tanaka (1996)	$P_{max} = (6.13 - \text{Ln}(L_b)) b_p L_b$	
Maeda <i>et al</i> (1997)	$P_{max} = 110.2(10^{-6}) E_f t_p b_p L_e$	$L_e = e^{6.15 - 0.58 \text{Ln}(E_f t_p)}$
Yuan, Wu and Yoshizawa, (2001)	$P_{max} = b_p \sqrt{\frac{2G_f}{\frac{1}{E_p t_p} + \frac{b_p}{b_c E_c t_c}}}$	
Neubauer and Rostasy (1997)	$P_{max} = 0.64 K_p b_p \sqrt{f_c E_p t_p} \text{ if } L_b \geq L_e$ $P_{max} = 0.64 K_p b_p \sqrt{f_c E_p t_p} \frac{L_b}{L_e} \left(2 - \frac{L_b}{L_e}\right) \text{ if } L_b \leq L_e$	$K_p = \sqrt{\frac{2 - \frac{b_p}{b_e}}{1 + \frac{b_p}{400}}}$
Khalifa <i>et al</i> (1998)	$P_{max} = 110.2(10^{-6}) E_p t_p b_p L_e \left(\frac{f_c}{42}\right)^{2/3}$	$L_e = e^{6.13 - 0.58 \text{Ln} E_p t_p}$
Adhikary and Mutsuyoshi (2001)	$P_{max} = b_p L_b (0.25 f_c)$	
Dai <i>et al</i> (2006)	$P_{max} = (b_p + 7.4) \sqrt{2G_f E_p t_p}$	$G_f = 0.514 f_c^{0.236}$
Lu <i>et al</i> 2005	$P_{max} = b_p B_1 \sqrt{2G_f E_p t_p}$	$L_e = a + \frac{1}{2\lambda_1} \text{Ln} \left(\frac{\lambda_1 + \lambda_2 \tan(\lambda_2 a)}{\lambda_1 - \lambda_2 \tan(\lambda_2 a)} \right)$ $\lambda_1 = \sqrt{\frac{\tau_{max}}{s_0 E_p t_p}} \quad \lambda_2 = \sqrt{\frac{\tau_{max}}{(s_f - s_0) E_p t_p}}$

		$a = \frac{1}{\lambda_2} \arcsin \left[0.99 \sqrt{\frac{s_f - s_0}{s_f}} \right]$ $\tau_{\max} = \alpha_1 B_w f_t \quad \alpha_1 = 0.15$ $G_f = 0.308 B_w^2 \sqrt{f_t}$ $s_0 = 0.0195 B_w f_t$ $B_w = \sqrt{\frac{2.25 - \frac{b_p}{b}}{1.25 + \frac{b_p}{b}}}$ $B_1 = \sin \left[\frac{\pi L_b}{2L_e} \right]$
Camli and Binici (2007)	$P_{\max} = \sqrt{\tau_f \sigma_f} \sqrt{E_f t_p b_p} \tanh \left(\frac{\theta L_b}{L_e} \right)$	$L_e = \sqrt{\frac{E_p t_p}{f_c^{1/2}}} \quad \theta = \sqrt{\frac{\tau_f}{\sigma_u f_c^{1/2}}}$ $\tau_f = 3.5 f_c^{0.19}$ $\sigma_u = f_c^\alpha \left(\frac{L_b}{L_e} \right)^\beta \left(\frac{b_b}{b} \right)^\gamma$ $\alpha = -0.4 \quad \beta = 0.8 \quad \gamma = 0.4$
FIB model (2001)	$P_{\max} = 0.64 k_c K_p b_p \sqrt{f_c E_p t_p} \quad \text{if } L_b \geq L_e$ $P_{\max} = 0.64 \alpha k_c K_p b_p \sqrt{f_c E_p t_p} \left(\frac{L_b}{L_e} \right) \left(2 - \frac{L_b}{L_e} \right) \quad \text{if } L_b \leq L_e$	$K_p = \sqrt{\frac{1.125 \left(2 - \frac{b_p}{b_e} \right)}{1 + \frac{b_p}{400}}}$ $\alpha = 1 \quad k_c = 1$
CNR-DT200/2004 2004	$P_{\max} = b_p \sqrt{2 E_p t_p K_G K_p K_1 (f_t f_c)^{1/2}}$	$K_G = 0.03$ $K_1 = \begin{cases} 1 & \text{if } L \geq L_e \\ \frac{L_b}{L_e} \left(2 - \frac{L_b}{L_e} \right) & \text{if } L \leq L_e \end{cases}$ $L_e = \sqrt{\frac{E_p t_p}{2 f_t}}$

		$K_b = \begin{cases} \sqrt{\frac{2-0.33}{1+\frac{b_p}{400}}} & \text{if } \frac{b_p}{b_c} \leq 0.33 \\ \sqrt{\frac{2-\frac{b_p}{b_c}}{1+\frac{b_p}{400}}} & \text{if } \frac{b_p}{b_c} \geq 0.33 \end{cases}$
--	--	---

2.2 CFRP strengthening of beams

The observed failure modes of concrete beams reinforced with CFRP sheets have been reported by Teng *et al* (2003) and further analyzed by Ferreira *et al* (2018). They reported three typical failure modes: (1) tensile failure of the CFRP when its tensile strength is lower than the applied load; (2) debonding of the reinforcement at the laminate-concrete interphase; and (3) a cohesive failure of the concrete and there is separation of the reinforcement together with a layer of concrete.

The first failure mode is attributed to a brittle mode of failure, but it is evident that the CFRP-concrete bond strength is higher. The second mode of failure is attributed to a lack of anchorage of reinforcement, excessive cracking of the beam or faults in the bonding. Again here, failure of the adhesive bond strength may be caused by normal stresses at the end of the CFRP strip, where a stress singularity is known to exist [Leung, 2001, A.R. Khan et al 2014 and R.A. Hawileh et al 2015].

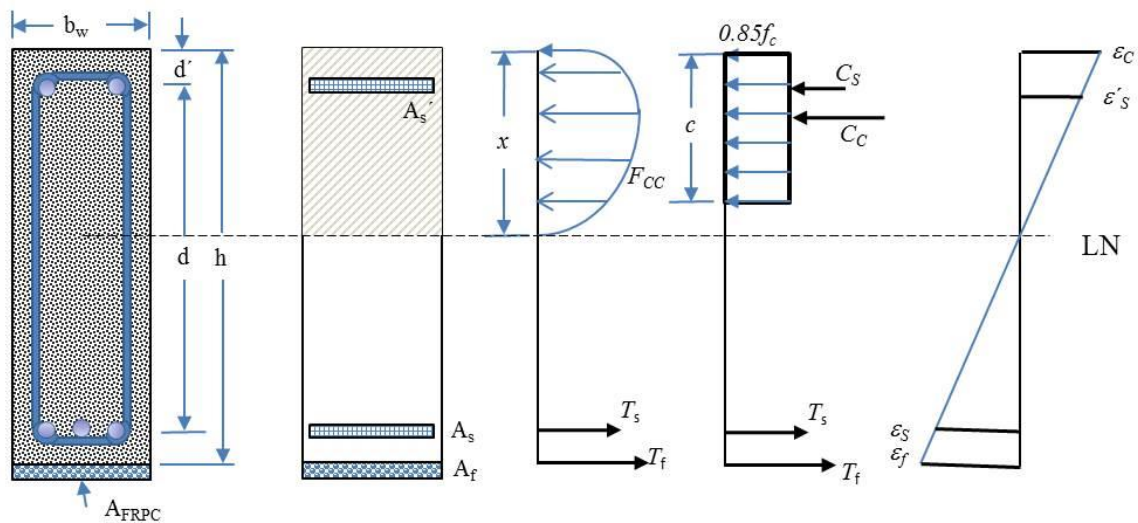


Figure 3. Stress-strain diagram of a steel-reinforced concrete beam strengthened with CFRP (After Ferreira et al 2018)

The analysis of the strengthening of a concrete beam with a CFRP layer loaded in bending presented by Ferreira *et al* (2018) considered that the ratio of the reinforced beam framework is equivalent to the addition on the initial reinforcement ratio with the contribution from the reinforcement (see figure 3).

$$\rho_r = \rho + \frac{A_f E_f}{b_w h E_s} \tag{10}$$

Where ρ is the ratio of the reinforcement of the beam before strengthening, A_f is the area of reinforcement applied to the beam, E_f is the modulus of elasticity of the CFRP, E_s is the modulus of elasticity of steel, b_w and h are the width and height of the beam respectively. The recommendations for the sizing of the CFRP reinforcement according to the American code ACI 440-2R are as follows: The limit value of the fiber strain to be adopted in the sizing and verification of the reinforcement is expressed in terms of the modulus of elasticity of the CFRP, and ε_{fu} , the ultimate strain observed in the polymer at the moment of failure and n , the number of layers of CFRP.

$$\varepsilon_{fd} = 0.41 \sqrt{\frac{f_c}{nE_f t_f}} < 0.9\varepsilon_{fu} \quad (11)$$

The effective strain in the CFRP composite ε_{fe} is expressed as a function of the concrete ultimate strain ε_{cu} and the strain in the covering of the tensile reinforcement in the beam before the strengthening, ε_{bi} and x , the position of the neutral axis.

$$\varepsilon_{fe} = \varepsilon_{cu} \left(\frac{h-x}{x} \right) - \varepsilon_{bi} \leq \varepsilon_{fd} \quad (12)$$

f_{fe} is the effective strength of the CFRP;

$$f_{fe} = E_f \varepsilon_{fe} \quad (13)$$

ε_s' is the strain in the compressed reinforcement and, d' is the centroid position of the compressed reinforcement.

$$\varepsilon_s' = \varepsilon_{cu} \left(\frac{x-d'}{x} \right) \quad (14)$$

The strain in the tensile reinforcement, ε_s , is expressed by:

$$\varepsilon_s = \varepsilon_{fe} \left(\frac{d-x}{h-x} \right) \quad (15)$$

f_s' , the strength in the steel of the compressed reinforcement is given as a function of the strain in the compressed reinforcement ε_s' and the elastic modulus in the steel;

$$f_s' = E_s \varepsilon_s' \leq f_{ys}' \quad (16)$$

The strength in the steel of the tensile reinforcement f_s is given by

$$f_s = E_s \varepsilon_s \leq f_{ys} \quad (17)$$

The position of the neutral axis is calculated as follows:

$$x = \frac{(A_s f_s) + (A_f f_{fe}) - (A_s' f_s')}{\beta_1 (0.85 f_c) b_w} \quad (18)$$

A_s is the steel area of the tensile reinforcement; A_s' is the steel area of the compressed reinforcement; β_1 is a coefficient that determines the approximation of the resultant compression curve of the concrete to a rectangle, being 0.85 for concrete with f_c values lower than 28 MPa, which decreases linearly by 0.05 for each 7 MPa above that limit of tensile strength. The minimum value for such a coefficient, according to ACI 318 (2014), is 0.65.

The conditions at the interface between the composite and concrete require a full understanding from the mechanics point of view. Different epoxy resin formulations or any other adhesive used will result in completely different behavior of the concrete-composite joint. In addition, the geometrical design of the laminate and anchors will also influence the mechanical behavior and consequently, the effectiveness of the reinforcement. Then, as a first step, whenever possible, and depending on the availability of testing equipment, preliminary studies of the adhesion parameters between the composite and concrete are required to determine the lengths of the joints for effective stress transfer needed to achieve the composite's strength capacity.

3. ENVIRONMENTAL EFFECTS ON THE CFRP-CONCRETE INTERFACE BOND STRENGTH

The interface at the concrete- CFRP has been recognized as the region where the efficiency of the load transfer from the structural element to the CFRP laminate takes place. As stated by Swamy RN et al (1987), the properties of the epoxy adhesive is of paramount importance as they varied considerably with the thickness of the test specimen and the rate of loading. Similarly, the fiber-matrix interphase is regarded as an important region of the composite laminate performance.

This matrix behavior at the concrete-CFRP is of particular interest in advanced composite materials, since its use in structural applications with exposure to the environment, requires that the material meets very strict performance, durability and safety standards. Moisture transport in polymeric systems is related to the availability of "free space" or "free volume" of molecular size in the structure of the polymer, as well as its affinity to water. [M. R. Vanlandingham, et al (1999)]. Such availability of "free spaces" depends on the microstructure, morphology and density of crosslinking, which are functions of the degree of curing, stoichiometry, stiffness of the molecular chains and the cohesive energy density of the polymer. The polymer-water affinity is related to the presence of hydrogen bond sites along the polymer chains that create sites of attractive forces between the water molecules and those of the polymer. Water molecules that are free to move through holes or free volume are known as adsorbed molecules. In the case of the epoxies it is also known that they have a significant free volume, particularly at temperatures 50-150 ° C below the Tg. The epoxy-water affinity is relatively strong because polar hydroxy groups (-OH) are created by the opening of the epoxy group by reaction with primary and secondary amines. [M. J. Adamson, 1736]. Then, in the case of these composites based on carbon fibers and epoxy matrix, those properties that are dominated by the matrix or fiber-matrix interface are degraded by the absorption of moisture while those dominated by fibers are not essentially affected. In particular, the interfacial shear strength, the interlaminar shear strength, and depending on the carbon fiber-epoxy resin laminae stacking sequence in the laminate, the edge effects also become points of possible failure initiation as well as the mode II fracture toughness and the interlaminar toughness. This degradation is attributed to the weakening of the fiber-matrix interphase and to swelling of the matrix and plasticization of the matrix [J. I. Cauich-Cupul, et al (2011) , E. Pérez-Pacheco, et al (2011), S. Wang et al, (2002), L.E. Asp, (1998), M. Todo, et al, (2000), R. Selzer et al, (1995),

M. J. Adamson, (1980), D. A. Bond, (2005), M. R. Vanlandingham, et al (1999)]. Moisture absorption can also cause a decrease of the residual stresses produced from the curing thermal gradients and thus, resulting in a decrease of fracture properties. The effects of humidity are considerably aggravated by the temperature and further complicated by the action of mechanical stresses imposed on the material. [J. B. Aguiar, et al (2008)].

Furthermore, these composite materials are exposed to different environmental conditions during their useful life, such as moisture, temperature and ultraviolet radiation and therefore to the possibility of synergistic effects on degradation mechanisms. Hence, there is always a concern for the long-term durability of these materials to be exposed to combined environmental conditions of humidity, temperature and ultraviolet radiation. [Springer, G.S. (ed.) (1984), Ranby, B. and Rabek J. F., (1975)]. Both, ultraviolet radiation and humidity have negative effects mainly on the mechanical properties of the epoxy resin and the fiber-matrix interface and thus affect the integrity of the composite [W. B. Liao, et al, 1998].

The subject of durability of the FRPC strengthening systems, as a whole, has been a major concern in structural rehabilitation applications. Behavior of FRPC strengthened beams subjected to freeze-thaw, wet-dry and temperature cycles or various aqueous solutions prior to loading have been studied by a limited number of researchers (Bank, et al, 1995, Gheorghiu C. et al, 2004, Grace N. F. et al 2005, Wang C. Y , et al, 2004, Xie M., 1995, Katz A., 1999). There has been a fundamental change in the approach to the subject. As opposed to subjecting a specific composite material to an environmental exposure for a specified time period and then performing mechanical tests to obtain “data” for design use, the more recent approach has been to try to develop an integrated chemical and mechanical set of tests that provide an understanding of the mechanisms of degradation within the composite material. These papers combine macromechanical test methods with investigations of changes in material composition together with a scanning electron microscopy to develop models that attempt to explain the change of mechanical properties in terms of the quantitative changes in the chemical nature of the materials and qualitative observation of the degradation phenomenon (Bank and Gentry, 1995).

Buyukozturk O, 1998 and Grace and Singh, 2005, and concluded that the long-term exposure to humidity is the most detrimental factor to the bond strength between CFRP plates and fabrics and RC beams. Beams strengthened with CFRP plates and exposed to 10,000 hours of 100% humidity (at 38 ± 2 °C) experienced an average of 33% reduction in their strength. The onset of delamination was the primary mode of failure for all of the test beams.

The durability of carbon fiber reinforced polymer (CFRP) pretensioned piles driven in tidal waters and an experimental study to assess the likely effect of diurnal/seasonal temperature change on twelve precracked CFRP pretensioned beams designed to fail by rupture of the prestressing rods were kept outdoors in two salt water tanks and simultaneously subjected to wet/dry cycles (simulating tides) and hot/cold cycles (simulating temperature variation), (Aiello, et al, 2001). Durability was assessed from flexure tests conducted periodically over the nearly 3-year exposure period. The results of the tests indicated that durability was largely unaffected, although both bond degradation and reductions in ultimate capacity were observed in some of the exposed specimens. Degradation appeared to be linked to the extent of precracking damage sustained prior to exposure. This suggests that when CFRP pretensioned piles are used, driving stresses should be carefully monitored to minimize damage.

Because of the change in behavior under varying environmental conditions, it can be said that a complete understanding of the effects these materials have on the performance of retrofit systems has not been achieved. In particular, various failure mechanisms that the retrofitted concrete beam can manifest, including the debonding and delamination mechanisms of FRP from the concrete beam, are not well known. More studies are needed to develop a better understanding of the shear capacity of retrofit sections, the effects in the anchorage regions of the FRP laminate, and failure

mechanisms of debonding and delamination. Topics of future study should also include effects of material compatibilities and their resistances to degradation through both environmental and load cycles, and the assessment of retrofitted system integrity through the use of nondestructive evaluation [Nakaba 2001].

Strictly speaking, the application of a fiber-reinforced composite laminate layer on the tensile side of the beam, either by bonding a laminate or by forming a composite material in situ, using the epoxy resin and fibers unidirectionally oriented in a textile, a manual lay-up procedure, will result in two interphase, the concrete-resin interphase and the fiber-matrix interphase, as shown in figure 4. Both interphases are susceptible to be affected by exposure to the environment. However, in the technical literature on the subject of RFPC beam retrofitting, there is only reference to the concrete-laminate interphase.

Karbhari and Engineer, 1996, investigated the degradation of the composite-concrete interface after exposure to environmental conditions that include moisture, sea water, freezing and freeze-thaw. In this investigation, the performance of plated beams was considered from aspects related to materials and durability. The effect of five different environmental conditions was studied and they showed that the selection of the appropriate resin system is critical to success and pointed out the dangers of selecting systems with low glass transition temperatures and drastic drops in instantaneous modulus as a function of temperature. Results indicated that degradation occurs primarily at the level of the resin in contact with the concrete, and that due care should be taken of changes in composite stiffness due to moisture exposure and the consequent resin plasticization, as well as due to stiffness increases under cold conditions (Aiello, et al, 2001, Plevris N, 1999, Soudki KA 2000, Wang CY 2004).

J. I. Cauich-Cupul et al, (2011) studied the effect of moisture uptake in the interphase in epoxy-single IM7-carbon fiber composites and showed a detrimental effect on the mechanical properties of the matrix, and this deterioration was attributed to a decrease of its glass transition temperature. Three levels of the IM7 carbon fiber-epoxy interface were studied. The first was the IM7 carbon fiber with the sizing removed, then, the fiber-matrix adhesion level was increased using a silane coupling agent to treat the IM7 fiber surface and third, the IM7 fibers were treated with nitric acid to produce more chemical reaction sites with the silane coupling agent.

The quality of the fiber-matrix interface was assessed using the single fiber fragmentation test and the fiber-fragment length, considered as an indicator of interfacial quality which indicated a continuous deteriorating effect of moisture uptake. That is, a short fiber-fragment length indicated a strong fiber-matrix interphase and a weak (or deteriorated) fiber-matrix interphase was indicated by a long fiber-fragment length (see figure 5). Furthermore, the role of swelling of the matrix because of moisture uptake on the residual stresses is considered to be important when considering the deterioration of interfacial shear properties. The contribution of the radial stresses was seen to decrease rapidly and the mechanical component of the fiber-matrix adhesion also decreased rapidly for higher moisture contents in the matrix and/or interface.

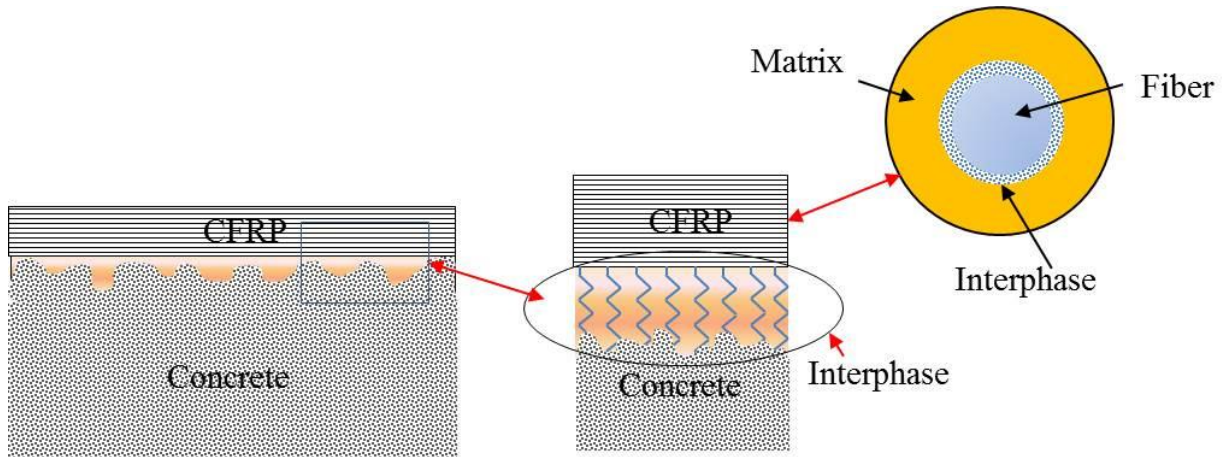


Figure 4. Schematic representation of the formation of dual interphases formed by the use of laminates or fabrics to retrofit steel reinforced concrete beams. One concrete-resin interphase and one fiber-matrix interphase.

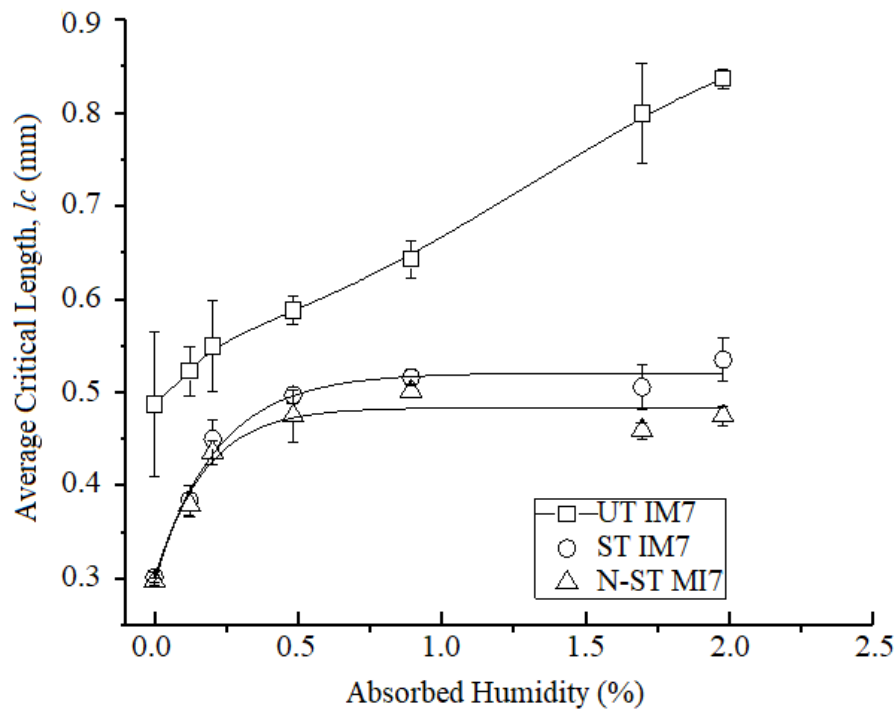


Figure 5. Fiber fragment length a function of matrix-interphase absorbed humidity in the composite, for untreated surface carbon fibers (UT IM7); silane coupling agent treated surface IM7 carbon fibers (ST IM7) and, nitric acid and silane coupling agent treated surface IM7 carbon fibers (N-ST IM7), (J. I. Cauich-Cupul et al, (2011))

Perez-Pacheco, *et al* (2013) concluded that the microstructure of the interphase played a significant role in the moisture diffusion process in a carbon fiber-epoxy laminate. Figure 6 shows the moisture absorption isotherms for a composite laminate subjected to several relative humidity environments. They also concluded that the effects of absorbed moisture on the interfacial region was detrimental to the interfacial strength between the fiber and the epoxy matrix and thus, to the performance of the composite. The use of 3-glycidoxypropyltrimethoxysilane as a fiber-matrix coupling agent enhanced the fiber-matrix adhesion. The plasticization, swelling stresses and any epoxy degradation because of hydrolysis may have contributed to the matrix failure mechanisms.

Plasticization of the epoxy matrix by moisture lead to the change in its glass-transition temperature (T_g) thus affecting the mechanical response of the composite. It was observed that the tensile strength of laminates made with the silane coupling agent showed a decrease but after a moisture uptake of approximately 0.45 %, the tensile strength remained constant. Then, the use of a proper silane coupling agent to enhance adhesion resulted in improved mechanical properties and reduced the dependence of the properties on humidity under tensile loading (see figures 7 and 8).

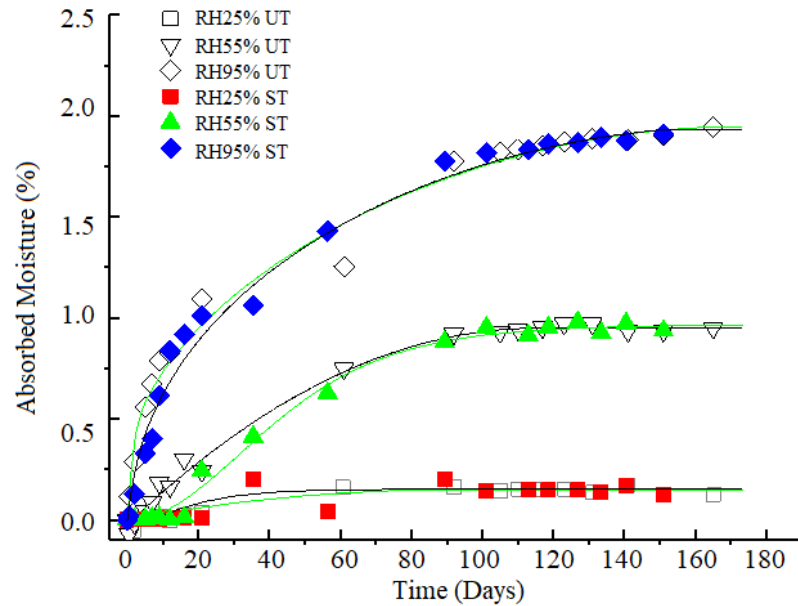


Figure 6. Absorption of moisture in the composite material laminate for different relative humidity environments. Without treatment: (UT) silane surface treatment (ST). RH25% UT, RH55% UT, and RH95% UT, and with silane surface treated fibers RH25% ST, RH55% ST and RH95% ST. (Perez-Pacheco, *et al* (2013))

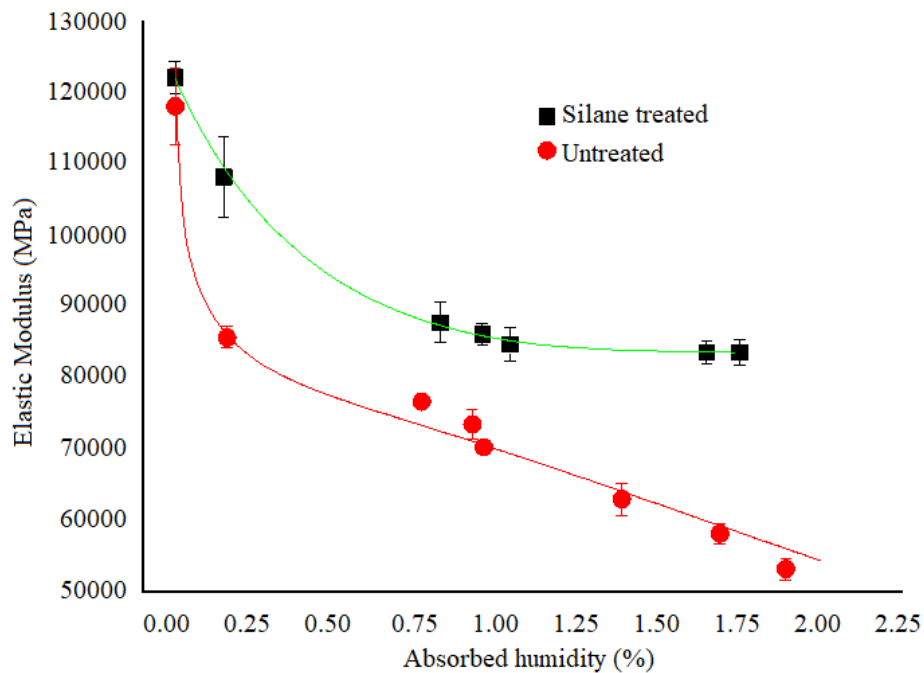


Figure 7. Behavior of the elastic modulus with respect to the moisture absorbed for the composite material with the treated and untreated fiber, respectively. (Perez-Pacheco, *et al* (2013))

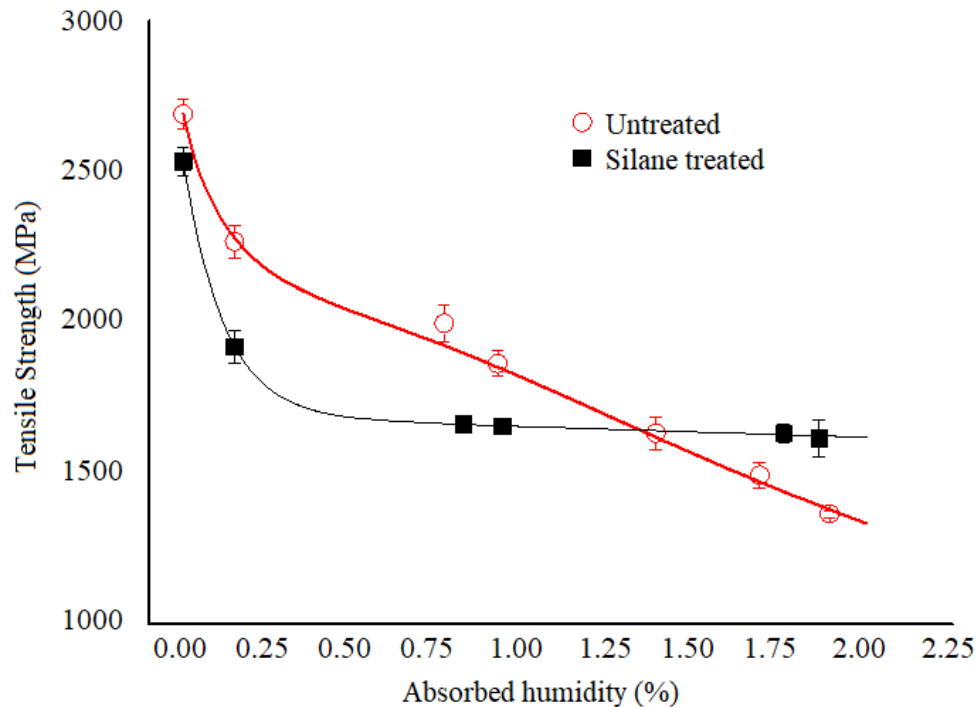


Figure 8. Tensile strength of a CFRP material made on the composite material after suffering hygroscopic degradation, for two different fiber-matrix interface conditions, that is, for treated and untreated fibers, respectively (Perez-Pacheco, *et al* (2013))

The behavior and potential of combining corrosion protection and FRP patching repair techniques to retrofit corrosion damaged RC beams has been demonstrated by Swamy RN et al, 1999 and Sebastian WM, 2001. They found that this type of arrangement can improve the load carrying capacity of cracked and corroded RC beams and provides the space for coating the corrosion protection materials. They also proposed that the equally spaced U-anchorage strips together with the longitudinal strips form an external reinforcing system for the corroded RC beam constrains the extension of the fiber in the longitudinal direction in the intersection area. Since the strain value is higher at this site, it enables the full usage of the fibrous composite material's strength. Hence any design that can reduce the stress concentration effect at the intersection area of the longitudinal and U-shaped anchorage strips may help the beam to escape from the premature failure mode of fiber breakage and reach its designed load carrying capacity.

As it can be seen, environmental issues are extremely important when designing a concrete-composite laminate joint for beams retrofitting. All the models described in numeral 2.1 of this paper consider the mechanical properties of the composite laminate, which as seen in figures 7 and 8, decrease as a function of absorbed humidity. Therefore, the composite laminate should be designed with dimensions such as thickness and width, appropriate to the stiffness and strength values, either those properties estimated after being degraded by the absorption of humidity or by including an appropriate safety factor to the composite mechanical properties before exposure to the environment. Another approach would be to provide a protective coating to prevent moisture absorption, especially at the laminate edges.

4. CONCLUSION

An effective method for strengthening existing concrete beams in bending consists on bonding fiber-reinforced composite laminates on the tension faces of the beams. However, it is often difficult to develop the full composite strength capacity because of premature failure due to delamination and peeling-off of the laminate. Conditions at the interface between the composite and concrete require a full understanding, and preliminary studies of the adhesion parameters between the composite and concrete are required to determine the effective stress transfer lengths needed to achieve the composite's strength capacity. A theoretical analysis for the behavior of such composite-to-concrete bonded joints has also been included in this review. The durability of the composite material-concrete interphase is also very important, especially when the structure is exposed to both thermal and moisture together. In the technical literature, no reference is made to the two interfacial issues, that is, the concrete-polymeric resin interphase and the fiber-matrix interphase in the composite itself. The durability of the composite laminate is shown to be affected by moisture absorption thus resulting in a reduction of both strength and stiffness higher than 30%.

5. ACKNOWLEDGEMENTS

The authors thank the School of Civil Engineering of Universidad Marista de Mérida for the kind support given to Mr. Poot Cauich and for providing materials for the experimental work.

6. REFERENCES

- Adamson, M. J. (1980), *Thermal expansion and swelling of cured epoxy resin used in graphite/epoxy composite materials*, Journal of Materials Science, Volume 15, I (7): 1736–1745, DOI: <https://doi.org/10.1007/BF00550593>
- Adhikary, B. B. and Mutsuyoshi, H., (2001). *Study on the bond between concrete and externally bonded CFRP sheet*, Proceedings of the 5th international symposium on fiber reinforced Concrete structures (FRPCRS-5), Thomas Telford Publishing, 371-378.
- Aguiar, J. B., Camoes, A. and Vaz, N. F. (2008), *Effect of temperature on RC elements strengthened with CFRP*. Materials and Structures 41:1133–1142, DOI: <https://doi.org/10.1617/s11527-007-9311-4>
- Aiello, M. A., Focacci, F., Nanni, A. (2001), *Effects of thermal loads on concrete cover of fiber-reinforced polymer reinforced elements: theoretical and experimental analysis*. ACI Materials Journal, 98(4):332–339.
- Bank, L. C., Gentry, T. R., Barkatt, A. (1995), *Accelerated test methods to determine the long-term behavior of FRP composite structures: environmental effects*. Journal of Reinforced Plastics and Composites, 14(6), 559–587, DOI: <https://doi.org/10.1177/073168449501400602>
- Bizindavyi, L., Neale, K. W. (1999), *Transfer lengths and bond strength for composites bonded to concrete*. ASCE, Journal of Composites for Construction, 3(4):153–160. DOI: [https://doi.org/10.1061/\(ASCE\)1090-0268\(1999\)3:4\(153\)](https://doi.org/10.1061/(ASCE)1090-0268(1999)3:4(153))
- Bond, D. A. (2005), *Moisture Diffusion in a Fiber-reinforced Composite: Part I – Non-Fickian Transport and the Effect of Fiber Spatial Distribution*, Journal of Composite Materials, Vol. 39(23): 2113-2141, <https://doi.org/10.1177/0021998305052030>
- Buyukozturk, O., Hearing, B. (1998), *Failure behavior of precracked concrete beams retrofitted with FRP*. ASCE, Journal of Composites for Construction; 2(3):138–144, DOI: [https://doi.org/10.1061/\(ASCE\)1090-0268\(1998\)2:3\(138\)](https://doi.org/10.1061/(ASCE)1090-0268(1998)2:3(138))

- Buyukozturk, O., Gunes, O., Karaca, E. (2004), *Progress on understanding debonding problems in reinforced concrete and steel members strengthened using FRP composites*. Construction and Building Materials, 18:9-19, DOI: [https://doi.org/10.1016/S0950-0618\(03\)00094-1](https://doi.org/10.1016/S0950-0618(03)00094-1)
- Camli, U. S. and Binici, B. (2007), *Strength of carbon fiber reinforced polymers bonded to concrete and masonry*. Construction and Building Materials, 21:1431-1446, DOI: <https://doi.org/10.1016/j.conbuildmat.2006.07.003>
- Cauich-Cupul, J. I, Pérez-Pacheco, E., Valadez-González, A., Herrera-Franco, P. J., (2011), *Effect of moisture absorption on the micromechanical behavior of carbon fiber/epoxy matrix composites*, Journal of Materials Science, 46:6664–6672, DOI: <https://doi.org/10.1007/s10853-011-5619-0>
- Chajes, M. J., Finch, W. W., Januszka, T. F., Thomson, T. A. (1996), *Bond and force transfer of composite materials plates bonded to concrete*. ACI Structural Journal, 93(2): 208–217.
- Chen, F. J., Teng, G, J. (2001), *Anchorage strength models for FRP and steel plates bonded to concrete*, Journal of Structural Engineering, 127(7): 784-791, DOI: [https://doi.org/10.1061/\(ASCE\)0733-9445\(2001\)127:7\(784\)](https://doi.org/10.1061/(ASCE)0733-9445(2001)127:7(784))
- Cho, J.-R., Park, S. Y., Cho, K., Kim, S. T., Kim, B.-S. (2012) *Pull-out test and discrete spring model of fibre-reinforced polymer perfobond rib shear connector*, Canadian Journal of Civil Engineering, 39(12): 1311-1320, DOI: <https://doi.org/10.1139/cjce-2011-0573>
- CNR—Italian Research Council, Advisory Committee on Technical Recommendations for Construction (2004), “*Guide for the Design and Construction of Externally Bonded FRP Systems for Strengthening Existing Structures. Materials, RC and PC Structures, Masonry Structures (CNR-DT 200/2004)*” Rome, Italy, 144 pp
- Dai, J. G., Ueda, T. and Sato, Y. (2006), *Unified analytical approaches for determining shear bond characteristics of FRP-concrete interfaces through pull-out tests*. Journal of Advanced Concrete Technology, 4:133-145, DOI: <https://doi.org/10.3151/jact.4.133>
- De Lorenzis, L., Miller, B., Nanni A. (2001), *Bond of fiber-reinforced polymer laminates to concrete*. ACI Materials Journal, 98(3): 256-264.
- Ferreira, M. P., Oliveira, M. H., Lima Neto, A. F., Tapajós, L. S., Nascimento, A., Freire, M. C. (2018), “*Influence of anchorage on flexural strength of beams strengthened with CFRP sheets*”, Revista ALCONPAT, 9 (1): 30 – 47, DOI: <http://dx.doi.org/10.21041/ra.v9i1.269>
- FIB (2001), *Externally bonded FRP reinforcement for RC structures*, FIB bulletin 14 Technical Report.
- Gheorghiu, C., Labossiere, P., Raiche, A. (2004), *Environmental fatigue and static behavior of RC beams strengthened with carbon-fiber reinforced polymer*. ASCE, Journal of Composites for Construction, 8(3):211–218, DOI: [https://doi.org/10.1061/\(ASCE\)1090-0268\(2004\)8:3\(211\)](https://doi.org/10.1061/(ASCE)1090-0268(2004)8:3(211))
- Grace, N. F., Sayed, G. A., Soliman, A. K., Saleh, K. R. (1999), *Strengthening reinforced concrete beams using fiber reinforced polymer (FRP) laminate*. ACI Structural Journal, 96(5):865–874.
- Grace N. F., Singh S. B. (2005), *Durability evaluation of carbon fiber-reinforced polymer strengthened concrete beams: experimental study and design*. ACI Structural Journal, 102(1):40–53.
- Hamoush, S. A., Ahmad, S. H. (1990), *Static strength tests of steel plate strengthened concrete beams*. Materials and Structures; 23:116–125, DOI: <https://doi.org/10.1007/BF02472571>
- Hamze-Ziabari, S. M. and Yasalovi, A. (2017), *Predicting bond strength between FRP plates and concrete substrate: Applications of GMDH and MNL approaches*, Journal of Advanced Concrete Technology 15: 644-661, DOI: <https://doi.org/10.3151/jact.15.644>
- Hawileh, R. A., Nawaz, W., Abdalla, J. A., Saqan, E. I. (2015), *Effect of flexural CFRP sheets on shear resistance of reinforced concrete beams*, Composite Structures 122: 468–476, DOI: <https://doi.org/10.1016/j.compstruct.2014.12.010>

- Japan Concrete Institute JCI. 2003. "Technical report of technical committee on retrofit technology." Proc., Int. Symp. on the Latest Achievement of Technology and Research on Retrofitting Concrete Structures, Sapporo, Japan
- Jeffries, J. M., (2004), *Bond behavior of fiber reinforced polymer laminates to concrete subjected to varied surface preparation*". Masters Theses. 2498.
- Karbhari, V. M., Engineer, M. (1996), *Effect of environmental exposure on the external strengthening of concrete with composite–short term bond durability*. Journal of Reinforced Plastics and Composites, 15:1194–1216., DOI: <https://doi.org/10.1177/073168449601501202>
- Karbhari, V. M., Shulley, S. B. (1995), *Use of composites for rehabilitation of steel structures – determination of bond durability*. ASCE, Journal of Materials in Civil Engineering, 7(4):239–245, DOI: [https://doi.org/10.1061/\(ASCE\)0899-1561\(1995\)7:4\(239\)](https://doi.org/10.1061/(ASCE)0899-1561(1995)7:4(239))
- Karbhari, V. M., Zhao, L. (1998), *Issues related to composite plating and environmental exposure effects on composite-concrete interface in external strengthening*. Composite Structures, 40(3-4):293–304, DOI: [https://doi.org/10.1016/S0263-8223\(98\)00031-2](https://doi.org/10.1016/S0263-8223(98)00031-2)
- Katz, A., Berman, N., Bank, L. C. (1999), *Effect of high temperatures on bond strength of FRP rebars*. ASCE Journal of Composites for Construction, 3(2):73–81, DOI: [https://doi.org/10.1061/\(ASCE\)1090-0268\(1999\)3:2\(73\)](https://doi.org/10.1061/(ASCE)1090-0268(1999)3:2(73))
- Khalifa, A., Gold, W. J., Nanni, A. and Aziz, A. (1998). *Contribution of externally bonded FRP to shear capacity of RC members*, Journal of Composites and Construction, ASCE, 2(4):195-203, DOI: [https://doi.org/10.1061/\(ASCE\)1090-0268\(1998\)2:4\(195\)](https://doi.org/10.1061/(ASCE)1090-0268(1998)2:4(195))
- Khan, A. R. and Shamsoun, F. (2014), *Behaviour of Reinforced Concrete Beams Strengthened by CFRP Wraps with and without End Anchorages*, Procedia Engineering 77: 123 – 130, <http://doi.org/10.1016/j.proeng.2014.07.011>
- Asp, L. E. (1998), *The effects of moisture and temperature on the interlaminar delamination toughness of a carbon/epoxy composite*. Composites Science and Technology, Vol. 58, (6): 967-977, DOI: [https://doi.org/10.1016/S0266-3538\(97\)00222-4](https://doi.org/10.1016/S0266-3538(97)00222-4)
- Leung, C. K. Y. (2001), *Delamination failure in concrete beams retrofitted with a bonded plate, Fracture Mechanics of Concrete Structures*, ASCE, Journal of Materials in Civil Engineering, Volume 13, Issue 2, DOI: [https://doi.org/10.1061/\(ASCE\)0899-1561\(2001\)13:2\(106\)](https://doi.org/10.1061/(ASCE)0899-1561(2001)13:2(106))
- Liau, W. B., Tseng, F. P. (1998), *The effect of long-term ultraviolet light irradiation on polymer matrix composites*, Polymer Composites, 19:440-445, DOI: <https://doi.org/10.1002/pc.10118>
- Lorenzis, L. D., Miller, B., Nanni, A. (2001), *Bond of fiber-reinforced polymer laminates to concrete*. ACI Materials Journal, 98(3):256–264.
- Lu, X. Z., Teng, J. G., Ye, L. P., Jiang, J. J. (2005), *Bond–slip models for FRP sheets/plates bonded to concrete*, Engineering Structures, 27: 920-937, DOI: <https://doi.org/10.1016/j.engstruct.2005.01.014>
- Lu, X. Z., Ye, L. P., Teng, J. G. and Jiang, J. J. (2005), *Meso-scale finite element model for FRP sheets/plates bonded to concrete*. Engineering Structures, 27(4): 564-575, DOI: <https://doi.org/10.1016/j.engstruct.2004.11.015>
- Vanlandingham, M. R., Eduljee, R. F., Gillespie Jr., J. W. (1999), *Moisture Diffusion in Epoxy Systems*, Journal of Applied Polymer Science, Vol. 71, 787-798, DOI: [https://doi.org/10.1002/\(SICI\)1097-4628\(19990131\)71:5<787::AID-APP12>3.0.CO;2-A](https://doi.org/10.1002/(SICI)1097-4628(19990131)71:5<787::AID-APP12>3.0.CO;2-A)
- Maeda, T., Asano, Y., Sato, Y. Ueda, T. and Kakuta, Y. (1997). *A study on bond mechanism of carbon fiber sheet*, in Proceedings of 3rd international symposium on nonmetallic (FRP) reinforcement for concrete structures, Sapporo, Japan Concrete Institute, 1:279-285
- Mander, J. B., Priestley, M. J. N., Park, R. (1998), *Theoretical stress–strain model for confined concrete*. ASCE, Journal of Structural Engineering, 114(8):1804–1826, DOI: [https://doi.org/10.1061/\(ASCE\)0733-9445\(1988\)114:8\(1804\)](https://doi.org/10.1061/(ASCE)0733-9445(1988)114:8(1804))

- Nakaba, K., Kanakubo, T., Furuta, T., Yoshizawa, H. (2001), *Bond behavior between fiber reinforced polymer laminates and concrete*. ACI Structural Journal, 98(3):359–367.
- Neubauer, U. and Rostasy, F. S. (1997), *Design aspects of concrete structures strengthened with externally bonded CFRP plates*. Proceedings of seventh international conference on structural faults and repairs, Edinburgh, ECS Publications, 1:109-118.
- Norris, T., Saadatmanesh, H., Ehsani, M. R. (1997), *Shear and flexural strengthening of R/C beams with carbon fiber sheets*. ASCE, Journal of Structural Engineering, 23(7):903–911, DOI: [https://doi.org/10.1061/\(ASCE\)0733-9445\(1997\)123:7\(903\)](https://doi.org/10.1061/(ASCE)0733-9445(1997)123:7(903))
- Pendhari, S. S., Kant, T., Desai, Y. M. (2008), *Application of polymer composites in civil construction: A general review*. Composite Structures 84:114–124, DOI: <https://doi.org/10.1016/j.compstruct.2007.06.007>
- Pérez-Pacheco, E., Cauich-Cupul, J. I., Valadez-González, A., Herrera-Franco, P. J. (2013), *Effect of moisture absorption on the mechanical behavior of carbon fiber/epoxy matrix composites*, Journal of Materials Science, 48:1873–1882, DOI: <https://doi.org/10.1007/s10853-012-6947-4>
- Pérez-Pacheco, E., Moreno-Chulim, M. V., Valadez-González, A., Rios-Soberanis, C. R. and Herrera-Franco, P. J., (2011), *Effect of the interphase microstructure on the behavior of carbon fiber/epoxy resin model composite in a thermal environment*, Journal of Materials Science, 46:4026–4033, DOI: <https://doi.org/10.1007/s10853-011-5331-0>
- Plevris, N., Triantafillou, T. C., (1994), *Time-dependent behavior of RC members strengthened with FRP laminates*. ASCE, Journal of Structural Engineering, 120(3):1016–1042, DOI: [https://doi.org/10.1061/\(ASCE\)0733-9445\(1994\)120:3\(1016\)](https://doi.org/10.1061/(ASCE)0733-9445(1994)120:3(1016))
- Selzer, R. and Friedrich, K. (1995), *Influence of water up-take on interlaminar fracture properties of carbon fibre-reinforced polymer composites*. Journal of Materials Science, Vol. 30, No. 2, 334, DOI: <https://doi.org/10.1007/BF00354392>
- Saadatmanesh, H., Tannous, F. E. (1999). *Long term behavior of aramid fiber reinforced plastic (AFRP) tendons*. ACI Materials Journal, 96(3):297–305.
- Sebastian, W. M. (2001), *Significance of midspan debonding failure in FRP-plated concrete beams*. ASCE, Journal of Structural Engineering, 127(7):792–798, DOI: [https://doi.org/10.1061/\(ASCE\)0733-9445\(2001\)127:7\(792\)](https://doi.org/10.1061/(ASCE)0733-9445(2001)127:7(792))
- Springer, G. S. (1984), *Environmental Effects on Composite Materials*, Vol. 1, Lancaster, Pennsylvania: Technomic Publishing Company, Inc.
- Swamy, R. N., Jones, R., Bloxham, J. W. (1987), *Structural behaviour of reinforced concrete beams strengthened by epoxy-bonded steel plates*. Structural Engineer, 65(2):59–68.
- Swamy, R. N., Mukhopadhyaya, P. (1999), *Debonding of carbon-fibre-reinforced polymer plate from concrete beams*. Proceedings of the Institution of Civil Engineers - Structures and Buildings, 134:301–317, DOI: <https://doi.org/10.1680/istbu.1999.31897>
- Täljsten, B. (1997), *Defining anchor lengths of steel and CFRP plates bonded to concrete*. International Journal of Adhesion and Adhesives, 17(4):319–327, DOI: [https://doi.org/10.1016/S0143-7496\(97\)00018-3](https://doi.org/10.1016/S0143-7496(97)00018-3)
- Tanaka, T., (1996), *Shear resisting mechanism of reinforced concrete beams with CFS as shear reinforcement*, Thesis (PhD). Hokkaido University.
- Lim, T.-Y., Paramasivam, P. and Lee, S.-L. (1987), *Behavior of Reinforced Steel-Fiber-Concrete Beams in Flexure*. Journal of Structural Engineering; 113-12:2439. [http://doi.org/10.1061/\(ASCE\)0733-9445\(1987\)113:12\(2439\)](http://doi.org/10.1061/(ASCE)0733-9445(1987)113:12(2439))
- Todo, M., Nakamura, T. and Takahashi, K. (2000), *Effects of moisture absorption on the dynamic interlaminar fracture toughness of carbon/epoxy composites*. Journal of Composite Materials, 34(8): 630–648, DOI: <https://doi.org/10.1177/002199830003400801>

- Van Gemert, D. (1980), *Force transfer in epoxy-bonded steel-concrete joints*, International Journal of Adhesion and Adhesives, 1, 67-72(1. 996), DOI: [https://doi.org/10.1016/0143-7496\(80\)90060-3](https://doi.org/10.1016/0143-7496(80)90060-3)
- Vanlandingham, M. R., Eduljee, R. F., Gillespie, J. W. Jr., (1999), *Relationships between Stoichiometry, Microstructure, and Properties for Amine-Cured Epoxies*, Journal of Applied Polymer Science; 71: 699–712, DOI: [https://doi.org/10.1002/\(SICI\)1097-4628\(19990131\)71:5<699::AID-APP4>3.0.CO;2-D](https://doi.org/10.1002/(SICI)1097-4628(19990131)71:5<699::AID-APP4>3.0.CO;2-D)
- Wang, C. Y., Shih, C. C., Hong, S. C., Hwang, W. C. (2004), *Rehabilitation of cracked and corroded reinforced concrete beams with fiber-reinforced plastic patches*. ASCE, Journal of Composites for Construction, 8(3):219–28, DOI: [https://doi.org/10.1061/\(ASCE\)1090-0268\(2004\)8:3\(219\)](https://doi.org/10.1061/(ASCE)1090-0268(2004)8:3(219))
- Wang, S. and Chung, D. D. L. (2002), *Effect of moisture on the interlaminar interface of a carbon fiber polymer-matrix composites, studied by contact electrical resistivity measurement*, Composite Interfaces, Vol. 9, No. 5: 453-458, DOI: <https://doi.org/10.1163/15685540260256546>
- Xie, M., Hoa, S. V., Xiao, X. R. (1995), *Bonding steel reinforced concrete with composites*. Journal of Reinforced Plastics and Composites, 14:949–63, DOI: <https://doi.org/10.1177/073168449501400903>
- Yuan, H., Wu, Z. and Yoshizawa, H. (2001), *Theoretical Solutions on Interfacial Stress Transfer of Externally Bonded Steel/Composite Laminates*. Doboku Gakkai Ronbunshu, J. Struct. Mech. Earthquake Eng., JSCE, 18 (675): 1-55, DOI: https://doi.org/10.2208/jscej.2001.675_27

Correlations between water absorption, electrical resistivity and compressive strength of concrete with different contents of pozzolan

R. A. Medeiros-Junior^{1*} , G. S. Munhoz¹ , M. H. F. Medeiros¹ 

*Contact author: medeirosjunior.ufpr@gmail.com

DOI: <http://dx.doi.org/10.21041/ra.v9i2.335>

Reception: 16/07/2018 | Acceptance: 27/02/2019 | Publication: 30/04/2019

ABSTRACT

This research confronts the following concrete properties: water absorptions (by immersion and capillarity), electrical resistivity and compressive strength. Concrete mixtures with two types of cement were tested. Results showed that concretes with higher content of pozzolan had higher resistivity and greater absorption by capillarity, for water/cement ratios lower than 0,60. This behavior is attributed to reduced pore diameters and microstructure densification. However, for water/cement ratio of 0,60, concrete with lower content of pozzolan presented higher absorption by capillarity. It was observed that the compressive strength and the electrical resistivity behaved inversely proportional to the water/cement ratio, and the absorption by immersion and capillarity are directly proportional to the water/cement ratio. Correlations with high determination coefficients were found between tests.

Keywords: durability; concrete; absorption; resistivity; compressive strength.

Cite as: Medeiros-Junior, R. A., Munhoz, G. S., Medeiros, M. H. F. (2019), “Correlations between water absorption, electrical resistivity and compressive strength of concrete with different contents of pozzolan”, Revista ALCONPAT, 9 (2), pp. 152 – 166, DOI: <http://dx.doi.org/10.21041/ra.v9i2.335>

¹ Department of Civil Construction, Federal University of Parana - UFPR, Curitiba, Brazil.

Legal Information

Revista ALCONPAT is a quarterly publication by the Asociación Latinoamericana de Control de Calidad, Patología y Recuperación de la Construcción, Internacional, A.C., Km. 6 antigua carretera a Progreso, Mérida, Yucatán, 97310, Tel.5219997385893, alconpat.int@gmail.com, Website: www.alconpat.org

Responsible editor: Pedro Castro Borges, Ph.D. Reservation of rights for exclusive use No.04-2013-011717330300-203, and ISSN 2007-6835, both granted by the Instituto Nacional de Derecho de Autor. Responsible for the last update of this issue, Informatics Unit ALCONPAT, Elizabeth Sabido Maldonado, Km. 6, antigua carretera a Progreso, Mérida, Yucatán, C.P. 97310.

The views of the authors do not necessarily reflect the position of the editor.

The total or partial reproduction of the contents and images of the publication is strictly prohibited without the previous authorization of ALCONPAT Internacional A.C.

Any dispute, including the replies of the authors, will be published in the (first issue of 2020 provided that the information is received before the closing of the third issue of 2019.

Correlações entre absorção de água, resistividade elétrica e resistência à compressão de concreto com diferentes teores de pozolana

RESUMO

Essa pesquisa confronta as seguintes propriedades do concreto: absorção de água (por imersão e capilaridade), resistividade elétrica e resistência à compressão. Concretos com dois tipos de cimento foram ensaiados. Os resultados mostraram que os concretos com maior teor de pozolana apresentam maior resistividade e absorção por capilaridade, para relação água/cimento menor que 0,60. Esse comportamento é atribuído à redução no diâmetro dos poros. No entanto, para relação água/cimento de 0,60, concretos com menor teor de pozolana apresentaram maior absorção por capilaridade. Ademais, a resistência à compressão e a resistividade elétrica são inversamente proporcionais a relação água-cimento, enquanto que a absorção por imersão e capilaridade são diretamente proporcionais a relação água/cimento. Correlações com elevados coeficientes de determinação foram encontradas entre os ensaios.

Palavras-chave: durabilidade; concreto; absorção; resistividade; resistência à compressão.

Correlación entre la absorción de agua, la resistividad eléctrica y la resistencia a la compresión del hormigón con diferentes contenidos de puzolana

RESUMEN

Esta investigación correlaciona las siguientes propiedades: absorción de agua (por inmersión y capilaridad), resistividad eléctrica y resistencia a compresión. Se ensayaron dos tipos de hormigones con cementos diferentes. Los resultados mostraron que los hormigones con mayor contenido de puzolanas y relación agua-cemento menor que 0,60, presentaron mayor resistividad y absorción por capilaridad. Ese comportamiento se atribuye a la reducción del diámetro de los poros. Por otro lado, en los hormigones con relación agua/cemento de 0,60, pero con menor contenido de puzolanas, también se observó un aumento de la absorción por capilaridad. Como esperado, la resistencia a compresión y la resistividad eléctrica fueron inversamente proporcionales a la relación agua/cemento, en cuanto que la absorción por inmersión y capilaridad se mostraron directamente proporcionales a la relación agua/cemento. Las correlaciones encontradas entre los ensayos tuvieron altos coeficientes de determinación.

Palabras clave: durabilidad; hormigón; absorción; resistividad; resistencia a la compresión.

1. INTRODUCTION

Durability of concrete structures have a direct impact in the economy of civil construction industry. Therefore, it is essential to understand the mechanisms that cause the degradation of concrete structures. Some of the main variables that control the degradation processes in the concretes are electrical resistivity, water absorption and concrete porosity. Electrical resistivity can be correlated with the corrosion rate and its deterioration level, while water absorptions (by immersion and capillarity) can be directly related to the diffusivity of aggressive ions into the concrete microstructure. Moreover, the porosity (pore size, connectivity and tortuosity) is, also, an important aspect that may influence all these properties, including the compressive strength (Hornbostel et al., 2013; Ye et al., 2017).

Ramezaniyanpour et al. (2011) studied the relation between concrete resistivity, water absorption, chloride penetration and compressive strength, in order to offer a better comprehension over these properties. The authors concluded that the resistivity, the water absorption and the chloride penetration could be correlated. However, contrary to the expected, the compressive strength could not express a clear correlation with the electrical resistivity, once both parameters held variables (such as the cement type) that were not accounted in their study. Therefore, this article tries to fill this gap with the study of cements with different levels of pozzolans.

Still in this perspective, Andrade and D'Andrea (2011), Silva et al. (2011) Ait-Mokhtar et al. (2013) and Sengul (2014) also studied extensively these correlations. According with their research, due to the existing relation between porosity, permeability, saturation level, mechanical strength, chloride penetration and diffusivity, the electrical resistivity can be very helpful to service life predictions of concrete elements.

The influence of different cement types and mineral admixtures in the physical-electrical properties of the concrete was investigated by several studies (López and Castro, 2010; Yildirim et al., 2011; Lubeck et al., 2012; Hoppe Filho et al., 2013; Medeiros-Junior and Lima, 2016). Some of them tested partial replacements of cement by blast furnace slag, silica fume and fly ash. In general, the authors concluded that higher electrical resistivity coefficients and lower water absorptions were found in concrete with partial replacements by mineral admixtures, due to the pore refinement that reduced its connectivity. However, the effects are not yet fully understood. For example, concrete curing can play an important role in these relations. Presuel-Moreno et al. (2013) and Sabbag and Uyanik (2018) concluded that the curing process influences the permeability of the concrete. This reflected in higher water absorption rates and electrical resistivity and lower compressive strengths. According to these authors, better results were found when specimens were cured immersed in water or, at least, stored in a moist chamber.

The aim of this research is to investigate the possible correlations between concrete water absorption (by immersion and capillarity), electrical resistivity and compressive strength, comparing two different cements with different fly ash contents (12.5% and 27.0%). Therefore, this study attempts to understand the intensity of the correlations between these variables through coefficients of determination and how these relations are affected by the different content of pozzolan.

Finally, the results obtained with this research are useful to better understand the relation between parameters related with the durability of concrete structures and its compressive strength, which is the main variable regarding quality control in building design and construction.

2. EXPERIMENTAL PROGRAM

2.1 Materials

In this study, two mixtures with different pozzolan contents were selected. Design Mix I is composed by IP pozzolan-modified Portland cement (12.5% of fly ash) and Design Mix II is composed by IP (MS) Portland-pozzolan cement (27.0% of fly ash). The chemical composition and physical properties of both cements are listed in Table 1. In addition, the main characteristics of the fine and coarse aggregates are shown in Table 2. Natural sand was used as fine aggregate from the Iguazu River, in Porto Amazonas.

Table 1. Mechanical, physical and chemical cement characteristics.

Properties and Characteristics	Units	Design Mix I: Pozzolan-modified Portland cement	Design Mix II: Portland pozzolan cement
Fly ash content	%	12.5	27.0
Al ₂ O ₃	%	6.22	9.77
SiO ₂	%	21.98	29.17
Fe ₂ O ₃	%	3.08	3.84
CaO	%	54.46	45.04
MgO	%	3.68	2.94
SO ₃	%	2.54	2.27
Loss on ignition	%	5.40	3.54
Free CaO	%	0.66	0.61
Insoluble residue	%	11.04	25.62
Alkaline content (Na ₂ O e K ₂ O)	%	0.85	1.15
Expansibility	mm	0.24	0.26
Initial setting time	h:min	4:20	4:26
Final setting time	h:min	5:06	5:11
Blaine	cm ² /g	3,560	4,193
# 200	%	1.83	0.49
# 325	%	8.33	2.78
Compressive strength (1 day)	MPa	11.8	13.0
Compressive strength (3 days)	MPa	25.3	25.9
Compressive strength (7 days)	MPa	32.1	32.9
Compressive strength (28 days)	MPa	41.0	45.4

Table 2. Characteristics of the aggregates used.

Characteristics of the aggregates	Units	Design Mix I		Design Mix II	
		Fine	Coarse	Fine	Coarse
Type	-	Natural sand	Basalt gravel	Natural sand	Granite gravel
Maximum aggregate size	mm	2.36	19	2.36	19
Specific gravity	g/cm ³	2.35	2.71	2.65	2.71
Water absorption	%	1.88	0.40	0.70	0.20

According to Bem et al. (2018), chemical admixtures might affect the electrical properties of the concrete. Therefore, no chemical admixtures were used. The proportioning in weight of the concrete mixtures was set as 1:1.4:2.1 (cement:fine aggregate:coarse aggregate). The content (kg/m³) of the ingredients used in each Design Mix is shown in Table 3.

Table 3. Concrete specimen mix design.

Codes	Design Mix I			Design Mix II			
	B0.40	B0.50	B0.60	G0.42	G0.48	G0.54	G0.60
Cement (kg/m³)	489.8	480.0	470.6	484.9	471.2	458.3	446.0
Fine aggregate (kg/m³)	685.7	672.0	658.8	678.9	659.7	641.5	624.4
Coarse aggregate (kg/m³)	1028.6	1008.0	988.2	1018.3	989.5	962.3	936.6
Water (kg/m³)	195.9	240.0	282.4	203.7	226.2	247.5	267.6
Water/cement ratio	0.40	0.50	0.60	0.42	0.48	0.54	0.60

The concrete specimens consisted in cylindrical samples, measuring $\varnothing 100$ mm x 200 mm of height. This geometry was chosen, due to the tabulated data of the form correction factor, which is necessary to determine the electrical resistivity. According with UNE 83988-2 (2014), for this geometry, the factor is 0.377.

Concretes were cast following the recommendations of the Brazilian standard NBR 5738 (2015). Thus, 24 hours after molding, the samples were demolded and cured in a moist chamber (relative humidity $\geq 95\%$, and temperature of $23^{\circ}\text{C} \pm 2^{\circ}\text{C}$) for, at least, 28 days. Finally, as three specimens were used for each test performed, the results discussed in this study are the mean of three replicates.

2.2 Methods

2.2.1 Electrical Resistivity

The non-destructive electrical resistivity test was performed according with the European code UNE 83988-2 (2014), which establishes the experiment setup for the four-point probe technique (Wenner's method). In this approach, four electrodes are placed over the specimen's surface. Then, the concrete is subjected to an electric current applied between the two external electrodes. This way, the resulting difference on the electric potential can be measured by the two internal electrodes. Nonetheless, for each test specimen, three measurements were required to be taken, with a 120° -angle-distance apart. The specimens were in a saturated-dry surface condition during the experiment.

2.2.2 Compressive Strength

The compressive strength test was performed in the same specimens used, firstly, to execute the electrical resistivity experiment. Moreover, the test procedures were followed as described in the Brazilian standard NBR 5739 (2018). In this context, samples were placed on a hydraulic machine, where they were compressive-loaded until failure. During this experiment, it was used an equipment with a loading-capacity of 1000 kN, with a loading rate of 0.45 ± 0.15 MPa/s.

2.2.3 Water absorption by immersion

The water absorption test by immersion, performed only for the Design Mix II specimens, complied with the prescriptions of the Brazilian code NBR 9778 (2009). The experiment started by having the samples dried in an oven ($T = 105^{\circ}\text{C}$), until mass variation was lower than 0.10 g. Then, the oven-dried mass of the concrete was registered. Thereon, the cylindrical specimens were immersed in water for 72 hours. The immersion was performed according to Brazilian standard: 1/3 of the samples' height immersed in the first 4 hours, 2/3 in the subsequent 4 hours, and finally, the total

concrete sample immersion, in the 64 hours remaining. Thus, the water absorption rate by immersion, in percentage, represents the difference between the mass of the specimen after immersion (72h) and its oven-dry mass.

2.2.4 Water absorption by capillarity

The aim of this procedure is to monitor the mass increase of the samples, due to the water absorption by capillarity. This way, the test is started by drying the samples in an oven ($T=105^{\circ}\text{C}$), until mass variation is lower than 0.10 g, according to NBR 9779 (2012). After that, specimens are placed in a (5 ± 1) mm water layer, with exposed bottoms, and their weights are measured after 3, 6, 24, 48 and 72 hours of exposure. These measurements were also used to determine the sorptivity (S), according with Eq.1.

$$S = \frac{V_{\text{water}}}{A \times \sqrt{t}} \quad (\text{Eq.1})$$

Where, V_{water} represents the volume of water absorbed by capillarity, in mm^3 ; A represents the area of the specimen in contact with the water, in mm^2 ; and t is the exposure period, in hours.

3. RESULTS AND DISCUSSION

3.1 Electrical resistivity and compressive strength

Table 4 shows the electrical resistivity and the compressive strength for each mixture and water/cement ratio at 28 days. According to Table 4, the greater the water/cement ratio, the lower is the electrical resistivity and the compressive strength. As the water/cement ratio increases, the internal porosity of the concrete microstructure and its connectivity increase as well. Therefore, the greater the permeability of the concrete, the lower is the mechanical strength, as well as the resistance against the electric current flow. This is not new and has already been reported by several studies (Mehta and Monteiro, 2006; Ait-Mokhtar et al., 2013; Olsson et al., 2013).

Table 4. Electrical resistivity and compressive strength.

Code	Design Mix I			Design Mix II			
	B0.40	B0.50	B0.60	G0.42	G0.48	G0.54	G0.60
Electrical resistivity ($\text{k}\Omega\cdot\text{cm}$)	8.3	5.5	4.3	14.9	11.5	9.7	8.7
Compressive strength (MPa)	45.2	33.2	21.4	49.3	41.0	32.0	27.9

Medeiros-Junior and Lima (2016) and Yu et al. (2017) also related the increase of the water/cement ratio with the increase of the porosity of the specimens. This way, the resistance to the electric current flow decreases when more water is present inside the concrete pores. To ensure this, it was performed the Mercury Intrusion Porosimetry (MIP) test, in the G0.42 and G0.54 samples. The results showed that the porosity was 23.6% and 36.3%, respectively. In addition, the mean pore diameters were 43.9 nm e 48.8 nm, for each concrete tested.

Design Mix II had the greatest resistivity and compressive strength values among the mixtures tested (Table 4). The greater amount of pozzolan in Design Mix II contributed with the pore refinement, restraining its connectivity. This effect directly contributed to the reduction in the permeability and increased the resistance against the electric current flow. Similar results were found by López and Castro (2010), Yildirim et al. (2011) and Medeiros-Junior et al. (2014). Also,

the partial replacement of cement by pozzolan resulted in the consumption of the calcium hydroxide – $\text{Ca}(\text{OH})_2$, in a chemical combination called Pozzolanic Reaction. This process hydrates the mixtures gradually and slowly, contributing to the increase of mechanical strength over time, as proven by Medeiros-Junior and Lima (2016).

Finally, in order to confirm the differences seen in the results obtained for each type of cement adopted, the values from Table 4 were submitted to a statistical treatment. The Analysis of Variance (ANOVA) with a single-factor and 5% significance proved that the electrical resistivity and the compressive strength were statistically different for each Design group.

That said, a graph with curves for each Design Mix was created, correlating the electrical resistivity versus the compressive strength (Figure 1). In addition, to describe the behavior of these variables, a logarithmical approach was chosen. This was the better data adjustment and it was also used by other studies (Andrade and D'Andrea, 2011; Wei and Xiao, 2014; Medeiros-Junior et al., 2014).

In Figure 1, both parameters are directly proportional, i.e., the greater the compressive strength, the greater the electrical resistivity. This behavior was also noted by Dinakar et al. (2007) and Lubeck et al. (2012), and it is related with the clear influence that the porosity has over both properties. Moreover, the good graphical correlation shown in Figure 1 (both R-Squared over 0.98) reaffirms this relation.

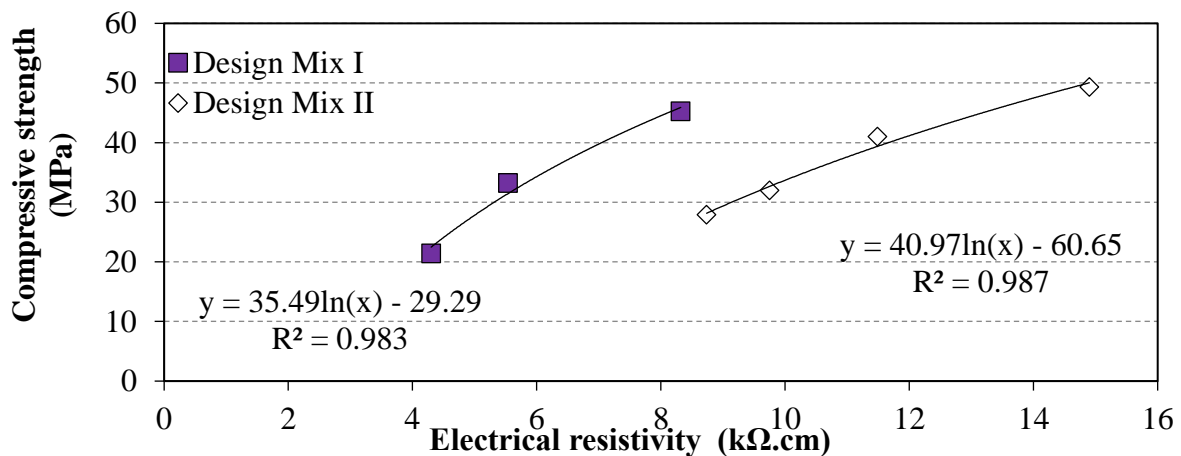


Figure 1. Correlation between electrical resistivity and compressive strength.

Furthermore, when both mixes are compared with the same range of compressive strength, it can also be observed that the correlation curve for Design Mix II has a smoother slope. This is due to the greater pozzolan content in Design Mix II, which created a denser microstructure with greater electrical resistivity.

3.2 Water absorption by immersion

Water absorptions by immersion were 3.67%, 4.32%, 5.69% and 6.36% for test specimens G0.42, G0.48, G0.54 and G0.60, respectively. Therefore, the water/cement ratio increased, and so did the absorption coefficients. This had already been observed by Zhang and Zong (2014), Castro and Ferreira (2016), Gans (2017) and Pinto et al. (2018), and it is mainly due to the porosity in the concrete microstructure and its permeability, given that both are parameters significantly influenced by the water/cement ratio.

In addition, according with the Comité Euro-International du Béton (CEB 192, 1989), the concrete may be qualitatively classified as good, average or poor, according to its absorption by immersion level. Figure 2 correlates the results obtained through the experiments with these levels. In Figure 2, while the higher water/cement ratios (0.60 and 0.54) are associated with poor quality concrete, the lower values of this parameter (0.42 and 0.48) classified the concrete with an average quality.

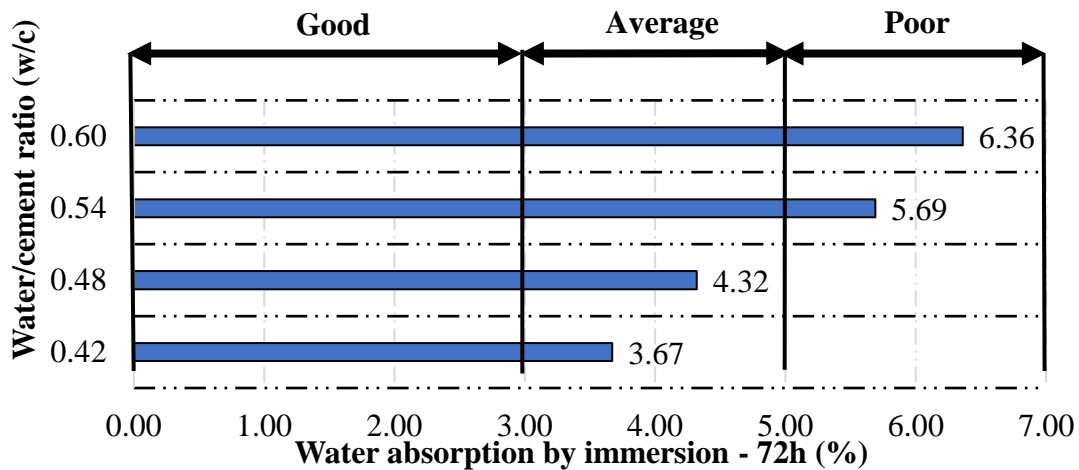


Figure 2. Water absorption by immersion and the concrete quality according with the criteria proposed by the CEB192 (1989).

Figure 3 shows the correlation between the water absorption by immersion and the electrical resistivity. Similarly to Figure 1, a logarithmical approach better described the behavior of both quantities.

The good correlation obtained in Figure 3 portrays the inversely behavior between the water absorption by immersion and the electrical resistivity. Thus, the water absorbed into the concrete microstructure enhances its electrical conductivity and, consequently, reduces its electrical resistivity. Figure 4 correlates the water absorption by immersion and the compressive strength, using a logarithmical approach.

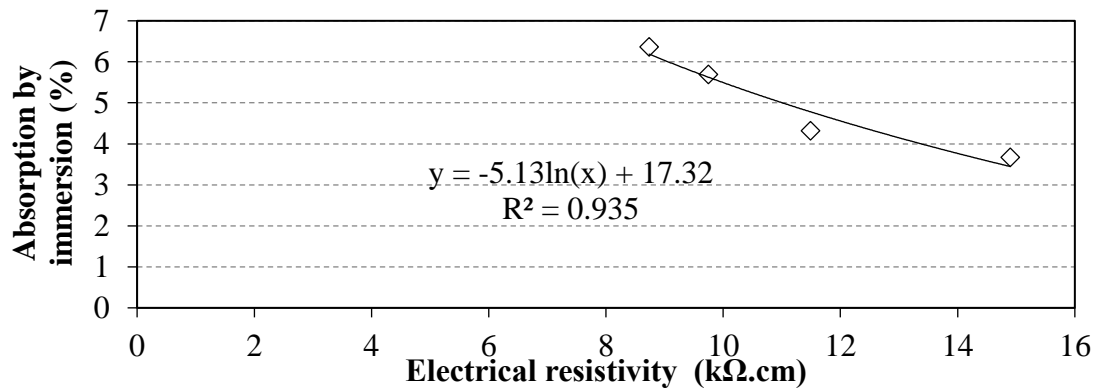


Figure 3. Correlation between electrical resistivity and absorption by immersion.

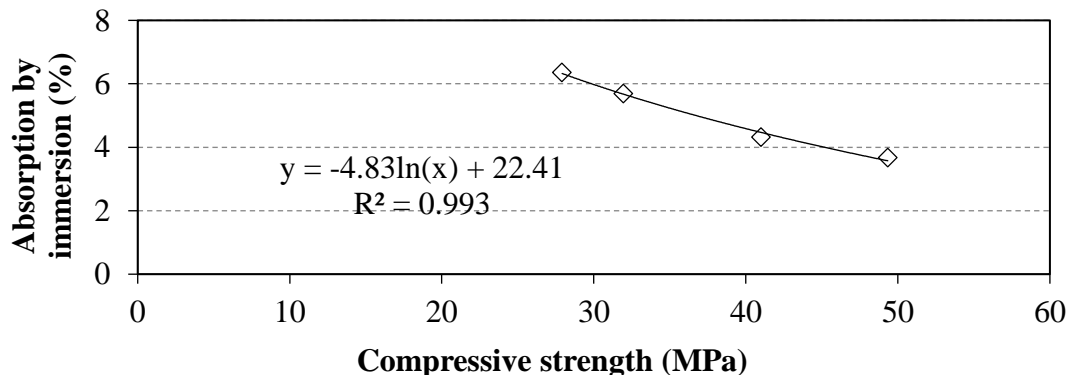


Figure 4. Correlation between compressive strength and absorption by immersion.

According to Figure 4, as the water absorption by immersion increases, the compressive strength decreases. The curves from Figure 3 and Figure 4 have the same behavior since the parameters that influence these tests are similar. Therefore, the greater the water/cement ratio, the greater is the porosity and its connectivity. This implies in reduced compressive strengths and electrical resistivity, while the water absorption by immersion is increased.

In summary, comparing the R-squared values from both graphs (Figures 3 and 4), it can be noted that the water absorption by immersion is better correlated with the compressive strength than with the electrical resistivity. This might be related with the dependence that the electrical resistivity has with the chemical composition of the solution present within the concrete pores (Ramezaniyanpour et al., 2011; Presuel-Moreno et al., 2013; Sabbag and Uyanik, 2018). Also, this behavior explains the low dispersion obtained in the regression curve shown in Figure 3, even though a high R-squared coefficient was found ($R^2 = 0.935$).

3.3 Water absorption by capillarity

Figures 5 and 6 show the variation of the water absorbed by capillarity over time for Design Mixes I and II, respectively. Water absorption by capillarity increased over the 72-hour exposure, in both mixtures. However, as the specimen approached its maximum absorption capacity, a stabilization tendency was identified. This behavior could be observed by different slopes in the curves over time. Usually, the increase in the absorption level was greater during the first 12 hours of the experiment.

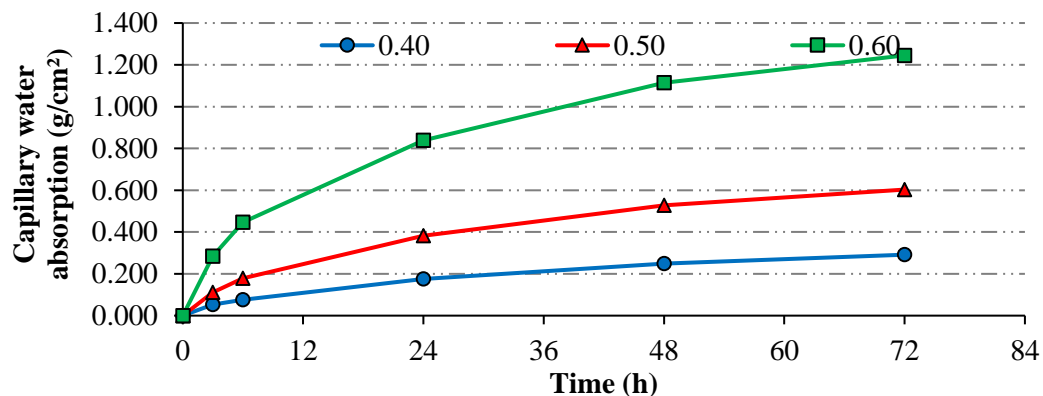


Figure 5. Absorption by capillarity over time - Design Mix I.

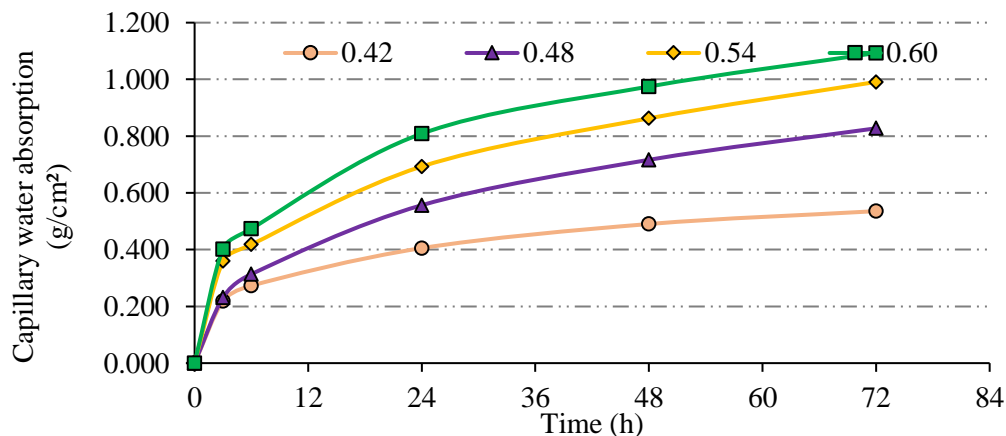


Figure 6. Absorption by capillarity over time - Design Mix II.

In addition, the water absorption by capillarity increased with the water/cement ratio. This way, as proven previously through the MIP test, a more porous concrete contributes directly to the water absorption and percolation.

Furthermore, in order to determine the sorptivity of the concrete, the results obtained with the absorption by capillarity experiment was used in Eq. (1). The sorptivity of the specimens ranged from 0.034 to 0.147 $\text{g}/(\text{cm}^2 \cdot \text{min}^{1/2})$. Figure 7 illustrates the correlation and the variation of this parameter according with the water/cement ratio.

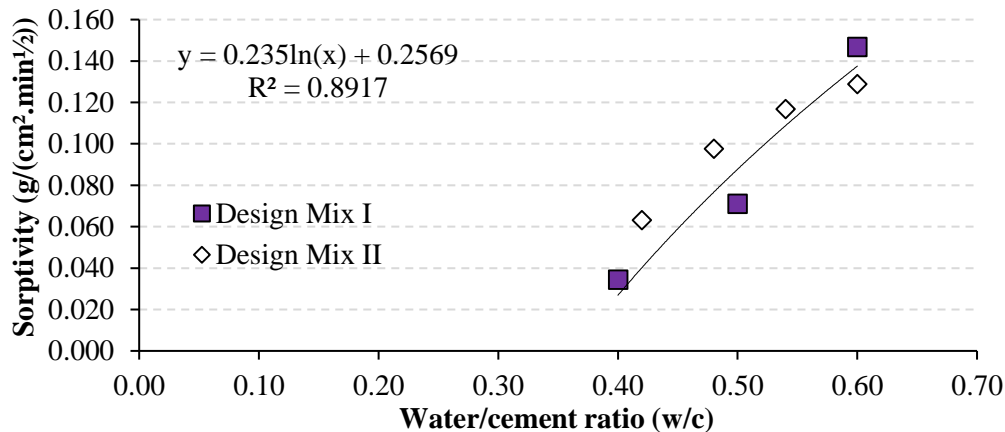


Figure 7. Sorptivity variation with different water/cement ratios.

As shown in Figure 7, greater water/cement ratios had greater sorptivity values. This was mainly due to the porosity increase. However, comparing both Design Mixes, it can be noted that Design Mix II (with larger amounts of pozzolan) had absorption by capillarity coefficients greater than in the first mix. This is observed visually at points above the trend line shown in Figure 7.

The main reason for greater coefficients in Design Mix II was the pore refinement and the reduction of its diameters. Consequently, in association with the surface tension of water, stronger capillary forces were experienced, and more water was absorbed (Mehta and Monteiro, 2006; Yildirim et al., 2011; Medeiros et al., 2017).

Similarly, Pinto et al. (2018) observed the same behavior, while analyzing the influence of carbonation in the absorption by capillarity. According to López and Castro (2010), Chen et al. (2014) and Leung et al. (2016), the greater the replacement of cement by pozzolan, the better the microstructure is rearranged, and therefore, less porous.

In contrast, comparing the results for the water/cement ratio equal to 0.60, it is observed that the sorptivity behavior was the opposite, with Design Mix I (with lower pozzolan content) developing greater coefficients. This was also seen by Olsson et al. (2013) and might be related to the pore tortuosity. In this case, larger amounts of pozzolan replacements have more tortuous pores, as observed by Medeiros-Junior and Lima (2016). Thus, even though its capillary forces are stronger, its absorption by capillarity coefficients are lower.

In summary, the effect of the reduced diameters of capillary pores linked to the surface tension of water was the main reason responsible for the growth of capillary absorption in lower water/cement ratios (sorptivity of Design Mix II > Design Mix I). On the other hand, for greater water/cement ratios, the tortuosity of the pores was the major factor that led to lower absorption coefficients in Design Mix II.

In addition, the water absorption by capillarity was correlated with other properties of the concrete. Figure 8 shows the capillary absorption after 72 hours and the electrical resistivity correlation. Figure 9 presents the behavior of the capillary absorption versus the compressive strength.

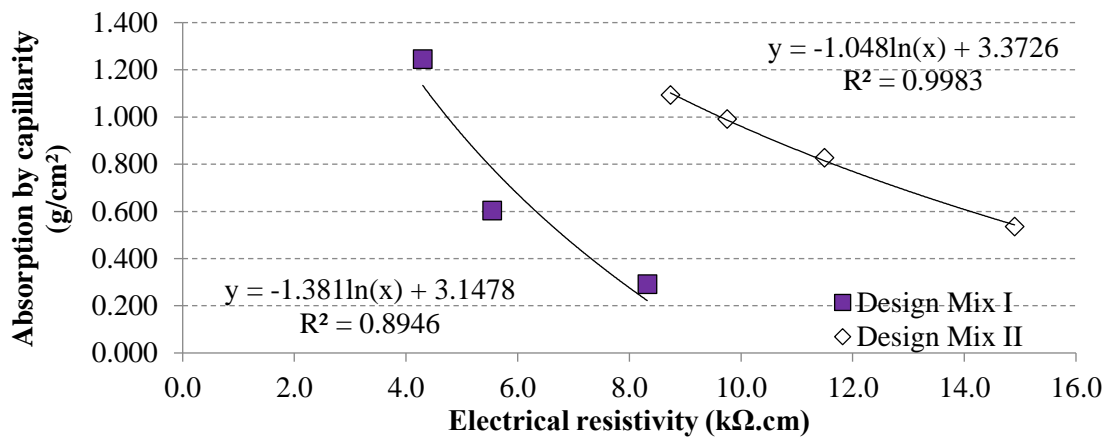


Figure 8. Correlation between electrical resistivity and water absorption by capillarity.

According to Figure 8, the water absorption by capillarity decreases as the electrical resistivity increases, for both design mixes. Similarly, according to Figure 9, the water absorption by capillarity and the compressive strength are inversely-related parameters. Also, good R-squared coefficients were found, which assures the dependence between both variables.

Furthermore, Figure 10 shows the correlation between the water absorption by immersion versus capillarity. Both absorption measurements are directly-related and according to Figure 10, a high dependence can be identified among them, consolidating the influence of both properties in the water absorption and percolation in the concrete microstructure.

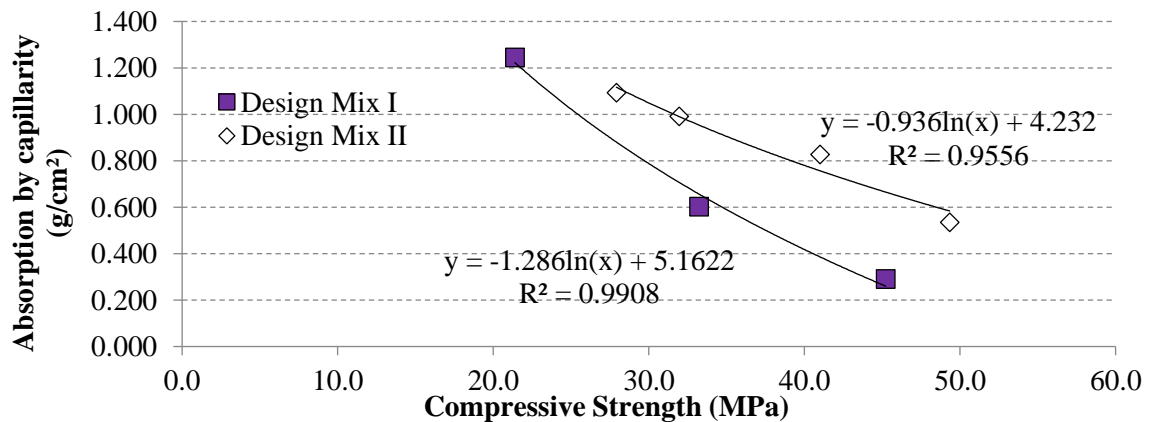


Figure 9. Correlation between the compressive strength and the water absorption by capillarity.



Figure 10. Correlation between water absorptions by immersion and by capillarity.

Finally, Table 5 summarizes all the logarithmical tendency equations obtained with the correlations. According to Table 5, most of the R-squared coefficients found were greater than 0.900. This is a consequence of the dependence between all the parameters studied (electrical resistivity, compressive strength, water absorption by immersion and water absorption by capillarity) and the porosity of the material, although this correlation was not exclusive. However, equations in Table 5 must be extrapolated cautiously, as they are solely valid for the materials and considerations adopted in this research. Nonetheless, the study of the validation of these equations, as well as other materials, is highly encouraged.

Table 5. Correlation equation of the parameters evaluated.

Parameters	Equation	Design Mix	R ²
Compressive strength (f_c) and Electrical resistivity (p)	$f_c = 35.49\ln(p)-29.29$	I	0.983
	$f_c = 40.97\ln(p)-60.65$	II	0.987
Absorption by immersion (A_i) and Electrical resistivity (p)	$A_i = -5.13\ln(p)+17.32$	II	0.935
Absorption by immersion (A_i) and Compressive strength (f_c)	$A_i = -4.83\ln(f_c)+22.41$	II	0.993
Absorption by capillarity (A_c) and Electrical resistivity (p)	$A_c = -1.38\ln(p)+3.15$	I	0.895
	$A_c = -1.05\ln(p)+3.38$	II	0.998
Absorption by capillarity (A_c) and Compressive strength (f_c)	$A_c = -1.29\ln(f_c)+5.16$	I	0.991
	$A_c = -0.94\ln(f_c)+4.23$	II	0.956
Absorption by capillarity (A_c) and Absorption by immersion (A_i)	$A_c = 0.94\ln(A_i)-0.63$	II	0.942

4. CONCLUSIONS

The following conclusions were drawn through the development of this study:

- There is a dependence relation between the compressive strength and the electrical resistivity, which was proved by the R-squared coefficient over 0.98, in both design mixes. Thus, the electrical resistivity and compressive strength of concrete tend to grow together, at least until the age investigated in this article.
- The water absorption by immersion was inversely proportional to the compressive strength and the electrical resistivity of the concrete. Moreover, the absorption by immersion was directly proportional to the water/cement ratio.
- The same behavior can be observed in the water absorption by capillarity. Correlation coefficients higher than 0.89 were observed in this case.
- Concretes with higher pozzolan content had higher resistivity and absorption by capillarity, for water/cement ratios lower than 0.60. This behavior is attributed to reduced pore diameters and microstructure densification. However, concrete with lower pozzolan content presented higher absorption by capillarity for water/cement ratio of 0.60 due to smaller tortuosity of the pores.
- It was proved that the correlation between the parameters should be used separately for each type of cement with different pozzolan contents, since the correlation curves were displaced for the two types of cement used in this article. The only exception was the correlation between the sorptivity and the water/cement ratio, which an adjustment between both mixes as a single group was possible (R-squared = 0.89).

5. ACKNOWLEDGEMENTS

The authors thank the Postgraduate Program in Civil Construction (PPGECC) of the Federal University of Parana (UFPR) for its infrastructure support for the development of this research.

6. REFERENCES

- Ait-Mokhtar, A., Belarbi, R., Benboudjema, F., Burlion, N., Capra, B., Carcasses, M., Colliat, J. B., Cussigh, F., Deby, F., Jacquemot, F., Larrard, T., Lataste, J. F., Bescop, P. L., Pierre, M., Poyet, S., Rougeau, P., Rougelot, T., Sellier, A., Yanez-Godoy, H. (2013), *Experimental investigation of the variability of concrete durability properties*. Cement and Concrete Research. 45:21-36. <https://doi.org/10.1016/j.cemconres.2012.11.002>
- Andrade, C., D'andrea, R. (2011), *La resistividad eléctrica como parámetro de control del hormigón y de su durabilidad*, Revista ALCONPAT, 1(2), 93-101. DOI: <http://dx.doi.org/10.21041/ra.v1i2.8>
- Asociación Española de Normalización (2014). *UNE 83988-2: Durabilidad del hormigón. Métodos de ensayo. Determinación de la resistividad eléctrica. Parte 2: Método de las cuatro puntas o de Wenner*. Madrid.
- Associação Brasileira de Normas Técnicas (2015). *NBR 5738: Concreto - Procedimento para moldagem e cura de corpos de prova*. Rio de Janeiro.
- Associação Brasileira de Normas Técnicas (2018). *NBR 5739: Concreto - Ensaio de compressão de corpos-de-prova cilíndricos*. Rio de Janeiro, 2018.
- Associação Brasileira de Normas Técnicas (2009). *NBR 9778: Argamassa/concreto endurecidos - Determinação da absorção de água, índice de vazios e massa específica*. Rio de Janeiro.
- Associação Brasileira de Normas Técnicas (2012). *NBR 9779: Argamassa e concreto endurecidos — Determinação da absorção de água por capilaridade*. Rio de Janeiro.
- Bem, D. H., Lima, D. P. B., Medeiros-Junior, R. A. (2018), *Effect of chemical admixtures on concrete's electrical resistivity*. International Journal of Building Pathology and Adaptation. 36(2):174-187. <https://doi.org/10.1108/IJBPA-11-2017-0058>
- Castro, A., Ferreira, F. (2016), *Effect of particle packing in the durability of high performance concretes*. Ingeniería de Construcción. 31(2):91-104. <http://dx.doi.org/10.4067/S0718-50732016000200003>
- Chen, C. T., Chang, J. J., Yeh, W. C. (2014), *The effects of specimen parameters on the resistivity of concrete*. Construction and Building Materials. 71:35-43. <https://doi.org/10.1016/j.conbuildmat.2014.08.009>
- Comité Euro-International du Béton. (1989). *CEB Bull 192: Diagnosis and assessment of concrete structures — state of the art report*. Lausanne.
- Dinakar, P., Babu, K. G., Santhanam, M. (2007), *Corrosion behaviour of blended cements in low and medium strength concretes*. Cement and Concrete Composites. 29(2):136-145. <https://doi.org/10.1016/j.cemconcomp.2006.10.005>
- Gans, P. S. (2017), *“Correlação entre a resistividade elétrica e a resistência à Compressão do concreto exposto a ciclos de molhagem e Secagem com cloretos e sulfatos”*, Dissertação de Mestrado em Engenharia de Construção Civil, Universidade Federal do Paraná, Curitiba.
- Hoppe Filho, J., Medeiros, M. H. F., Pereira, E., Helene, P., Isaia, G. C. (2013), *High-Volume Fly Ash Concrete with and without Hydrated Lime: Chloride Diffusion Coefficient from Accelerated Test*. Journal of Materials in Civil Engineering, 25(3):411-418. [https://doi.org/10.1061/\(ASCE\)MT.1943-5533.0000596](https://doi.org/10.1061/(ASCE)MT.1943-5533.0000596)

- Hornbostel, K., Larsen, C. K., Geiker, M. R. (2013), *Relationship between concrete resistivity and corrosion rate – A literature review*. Cement and Concrete Composites. 39:60-72. <https://doi.org/10.1016/j.cemconcomp.2013.03.019>
- Leung, H. Y., Kim, J., Nadeem, A., Jaganathan, J., Anwar, M. P. (2016), *Sorptivity of self-compacting concrete containing fly ash and silica fume*. Construction and Building Materials. 113:369-375. <https://doi.org/10.1016/j.conbuildmat.2016.03.071>
- López, M., Castro, J. T. (2010), *Efecto de las puzolanas naturales en la porosidad y conectividad de poros del hormigón con el tiempo*. Ingeniería de Construcción, 25(3):419-431. <http://dx.doi.org/10.4067/S0718-50732010000300006>
- Lubeck, A., Gastaldini, A. L. G., Barin, D. S., Siqueira, H. C. (2012), *Compressive strength and electrical properties of concrete with white Portland cement and blast-furnace slag*. Cement and Concrete Composites. 34(3):392-399. <https://doi.org/10.1016/j.cemconcomp.2011.11.017>
- Medeiros, M. H. F., Raisdorfer, J. W., Hoppe Filho, J., Medeiros-Junior, R. A. (2017), *Partial replacement and addition of fly ash in Portland cement: influences on carbonation and alkaline reserve*. Journal of Building Pathology and Rehabilitation. 2(4):1-9. <https://doi.org/10.1007/s41024-017-0023-z>
- Medeiros-Junior, R. A., Lima, M. G. (2016), *Electrical resistivity of unsaturated concrete using different types of cement*. Construction and Building Materials. 107:11-16. <https://doi.org/10.1016/j.conbuildmat.2015.12.168>
- Medeiros-Junior, R. A., Lima, M. G., Medeiros, M. H. F., Real, L. V. (2014), *Investigação da resistência à compressão e da resistividade elétrica de concretos com diferentes tipos de cimento*. Revista ALCONPAT, 4(2), 113-128. DOI: <http://dx.doi.org/10.21041/ra.v4i2.21>
- Mehta, P. K., Monteiro, P. J. M. (2006), *“Concrete – Microstructure, Properties and Materials”*. McGraw Hill, New York City, United States, cap. 5, pp. 121-198.
- Olsson, N., Baroghel-Bouny, V., Nilsson, L. O., Thiery, M. (2013), *Non-saturated ion diffusion in concrete – A new approach to evaluate conductivity measurements*. Cement and Concrete Composites. 40:40-47. <https://doi.org/10.1016/j.cemconcomp.2013.04.001>
- Pinto, S. R., Macedo, A. L. A., Medeiros-Junior, R. A. (2018), *Effect of preconditioning temperature on the water absorption of concrete*. Journal of Building Pathology and Rehabilitation. 3(3):1-10. <https://doi.org/10.1007/s41024-018-0032-6>
- Presuel-Moreno, F., Wu, Y. Y., Liu, Y. (2013), *Effect of curing regime on concrete resistivity and aging factor over time*. Construction and Building Materials. 48:874-882. <https://doi.org/10.1016/j.conbuildmat.2013.07.094>
- Ramezaniyanpour, A. A., Pilvar, A., Mahdikhani, M., Moodi, F. (2011), *Practical evaluation of relationship between concrete resistivity, water penetration, rapid chloride penetration and compressive strength*. Construction and Building Materials. 25(5):2472-2479. <https://doi.org/10.1016/j.conbuildmat.2010.11.069>
- Sabbag, N., Uyanik, O. (2018), *Determination of the reinforced concrete strength by electrical resistivity depending on the curing conditions*. Journal of Applied Geophysics. 155:13-25. <https://doi.org/10.1016/j.jappgeo.2018.03.007>
- Sengul, O. (2014), *Use of electrical resistivity as an indicator for durability*. Construction and Building Materials. 73:434-441. <https://doi.org/10.1016/j.conbuildmat.2014.09.077>
- Silva, P. C., Ferreira, R. M., Figueiras, H. (2011). *“Electrical Resistivity as a Means of Quality Control of Concrete – Influence of Test Procedure”* in: Freitas, V. P., Corvacho, H., Lacasse, M. (Eds.), XII International Conference on Durability of Building Materials and Components, FEUP Edições, Porto: Distrito de Porto (PT), 8 p.
- Wei, X., Xao, L. (2014), *Kinetics parameters of cement hydration by electrical resistivity measurement and calorimetry*. Advances in Cement Research. 26(4):187-193. <https://doi.org/10.1680/adcr.13.00034>

- Ye, H., Jin, N., Jin, X. (2017), *An Experimental Study on Relationship among Water Sorptivity, Pore Characteristics, and Salt Concentration in Concrete*. Periodica Polytechnica Civil Engineering. 61:530-540. <https://doi.org/10.3311/PPci.9621>
- Yildirim, H., Ilica, T., Sengul, O. (2011), *Effect of cement type on the resistance of concrete against chloride penetration*. Construction and Building Materials. 25(3):1282-1288. <https://doi.org/10.1016/j.conbuildmat.2010.09.023>
- Yu, B., Liu, J., Chen, Z. (2017), *Probabilistic evaluation method for corrosion risk of steel reinforcement based on concrete resistivity*. Construction and Building Materials. 138:101-113. <https://doi.org/10.1016/j.conbuildmat.2017.01.100>
- Zhang, S. P., Zong, L. (2014), *Evaluation of Relationship between Water Absorption and Durability of Concrete Materials*. Advances in Materials Science and Engineering. 2014:1-8. <http://dx.doi.org/10.1155/2014/650373>

Electrochemical behavior of dissimilar welded joints between ASTM A615 and AISI 304 with and without buttering using Inconel 182

J. C. I Ramirez –Soto^{1*} , J. T. Pérez-Quiroz² , J. M. Salgado-López³ , M. Martínez-Madrid² , T. Pérez-López¹ , M. Rendón-Belmonte² , E. Alvarez-Alfaro⁴ 

*Contact author: jcirs@hotmail.com

DOI: <http://dx.doi.org/10.21041/ra.v9i2.315>

Reception: 16/07/2019 | Acceptance: 04/03/2019 | Publication: 30/04/2019

Responsible Associate Editor: Dr. Pedro Garcés Terradillos

ABSTRACT

In this study, the corrosion performance of dissimilar welded joints between ASTM A615 and AISI 304 stainless steel with and without buttering using Inconel 182 was evaluated. In both cases, the filler metal was ER-309L and the base metals were prepared with a 45° single bevel. One half of the specimens were welded with “buttering” using Inconel 182. The electrochemical results showed that despite welding defects, the welded specimens formed a passive layer in alkaline environments. The specimens welded with buttering exhibited the best corrosion resistance and mechanical properties.

Keywords: corrosion; dissimilar welding; infrastructure.

Cite as: Ramirez –Soto, J. C. I., Pérez-Quiroz, J. T., Salgado-López, J. M., Martínez-Madrid, M., Pérez-López, T., Rendón-Belmonte, M., Alvarez-Alfaro, E. (2019), “*Electrochemical behavior of dissimilar welded joints between ASTM A615 and AISI 304 with and without buttering using Inconel 182*”, Revista ALCONPAT, 9 (2), pp. 167 – 184, DOI: <http://dx.doi.org/10.21041/ra.v9i2.334>

¹ Centro de Investigaciones en Corrosión, México.

² Instituto Mexicano del Transporte, México.

³ Tecnología de Materiales, México.

⁴ Tecnológico Nacional de México Instituto Tecnológico de Querétaro, México.

Legal Information

Revista ALCONPAT is a quarterly publication by the Asociación Latinoamericana de Control de Calidad, Patología y Recuperación de la Construcción, Internacional, A.C., Km. 6 antigua carretera a Progreso, Mérida, Yucatán, 97310, Tel.5219997385893, alconpat.int@gmail.com, Website: www.alconpat.org

Responsible editor: Pedro Castro Borges, Ph.D. Reservation of rights for exclusive use No.04-2013-011717330300-203, and ISSN 2007-6835, both granted by the Instituto Nacional de Derecho de Autor. Responsible for the last update of this issue, Informatics Unit ALCONPAT, Elizabeth Sabido Maldonado, Km. 6, antigua carretera a Progreso, Mérida, Yucatán, C.P. 97310.

The views of the authors do not necessarily reflect the position of the editor.

The total or partial reproduction of the contents and images of the publication is strictly prohibited without the previous authorization of ALCONPAT Internacional A.C.

Any dispute, including the replies of the authors, will be published in the first issue of 2020 provided that the information is received before the closing of the third issue of 2019.

Comportamiento electroquímico de uniones disimiles soldadas entre acero ASTM A615 y AISI 304 utilizando enmantequillado con Inconel 182 y sin enmantequillado

RESUMEN

Este trabajo evaluó el desempeño frente a la corrosión de uniones soldadas disimiles, utilizando como metales base acero al carbono ASTM A 615 y acero inoxidable austenítico AISI 304, y como metal de aporte electrodo ER-309L, se utilizó bisel simple a 45°. La mitad de los especímenes fueron sometidos a un proceso de “mantequillado” utilizando electrodo Inconel 182. Los resultados electroquímicos muestran que, a pesar de los defectos presentados en la unión soldada, estas tienden a pasivarse en medio alcalino, siendo las probetas con mantequillado las menos deterioradas por efecto de la corrosión y su resistencia mecánica no se ve minimizada.

Palabras clave: corrosión; soldadura disímil; infraestructura.

Estudo do comportamento eletroquímico da junta soldada em aço ASTM A 615 e aço inoxidável AISI 304 com manteiga de Inconel 182

RESUMO

Este trabalho avaliou o desempenho contra a corrosão de juntas soldadas dissimilares, utilizando aço carbono ASTM A 615 e aços inoxidáveis austeníticos AISI 304 como metais básicos, e como metal de enchimento eletrodo ER-309L, utilizando bisel único de 45 °. Metade dos corpos-de-prova foram submetidos a um processo de "manteiga" com eletrodo Inconel 182. Os resultados eletroquímicos mostram que, apesar dos defeitos apresentados na junta soldada, eles tendem a passivar em meio alcalino, sendo os corpos de prova com manteiga menos deteriorado pelo efeito da corrosão.

Palavras-chave: corrosão; soldagem dissimilar; infra-estrutura.

1. INTRODUCTION

The most common material in construction is reinforced concrete, whose mechanical and chemical properties are important for reliability. However, impairment of concrete structures, which is associated with corrosion in the reinforcement bars, has been reported in the literature (Pérez, 2009). Most bridges and piers in México have been built using concrete reinforced with carbon steel. An exception is the pier in Progreso, Yucatán, and some sections of the pier in Coatzacoalcos, Veracruz. The former uses stainless steel as reinforcement material and the latter galvanized steel. This information indicates that the resistance against aggressive environments is limited (especially in the case of environments with chloride ions and carbon dioxide). Traditionally, different types of methods are applied for counteracting the corrosion damage in concrete structures. Those methods can be classified into four categories based on the protection mechanism (Kepler, 2000):

- **Concrete matrix modification**
Water/ concrete ratio; Adding cementing materials
- **Barrier Methods**
Polymer coatings; Paintings; Metallic coatings
- **Electrochemical Methods**
Cathodic protection by impressed current (ICCP) or galvanic anodes (CPGA); Corrosion inhibitors; Electrochemical extraction of chlorine ions; Electrochemical re-alkalinization.

● **Rehabilitation of concrete structures with new materials.**

Composite materials, Stainless Steel.

The rehabilitation and refurbishing techniques are many and diverse; some are applied to the steel, others in the concrete, and others in both materials (Gonzalez 2010). The preservation of infrastructure is vital in both economic and social terms, because it provides security and supports social development. However, concrete structures corrode and must be repaired after 10, 20, or 30 years of service because the consequences affect not only the structural integrity but also human safety. Moreover, corrosion reduces the functionality and the value of a structure, leading to large financial expenditures needed to repair, refurbish, or replace the corroded infrastructure. Owing to these reasons, there is a need to develop processes for controlling and preventing corrosion in reinforcement steel bars embedded in concrete structures (Rougier, 2010; Terradillos, 2008). In this way, stainless steel reinforcement bars for concrete structures represent an attractive option that has been proposed for several years in order to increase the endurance of concrete in aggressive environments (BSSA, 2003; Medina, 2013).

Many researchers, for instance Brown (1976), Treadaway (1989), Sorensen (1990), Nurnberger (1996) McDonald (1998), Pedferri (1997), Bertolini (1998), and Baltazar (2007), have carried out studies to evaluate the behavior of stainless steel as reinforcement material for concrete structures. On the other hand, Lundin, (1982), Doddy, (1992), Ospina, (2007), García (2011), and Pérez-Quiroz (2016) have researched the metallurgy and mechanical properties of dissimilar welded joints, and their results demonstrated that the application of these joints is feasible for refurbishing concrete structures. Considering that stainless steel is more expensive than carbon steel, carbon and stainless-steel reinforcement bars can be joined by connectors or weld joints to improve the corrosion resistance of a concrete structure and reduce costs.

Perez Quiroz (2016) pointed out that to avoid carbon diffusion into the stainless steel and to minimize the damage risk due to corrosion during welding, buttering using Inconel 182 is a good option. Thus, it is desirable to investigate the metallurgy of dissimilar welded joints and the corrosion behavior of such welded unions. Today, there are few studies that evaluate the corrosion behavior of joints between carbon and stainless steel with and without buttering using Inconel. Therefore, in this work the corrosion resistance of welded joints between carbon and stainless-steel bars with and without buttering using Inconel 182 was tested to evaluate this methodology for refurbishing the concrete structures of maritime piers (Figure 1).

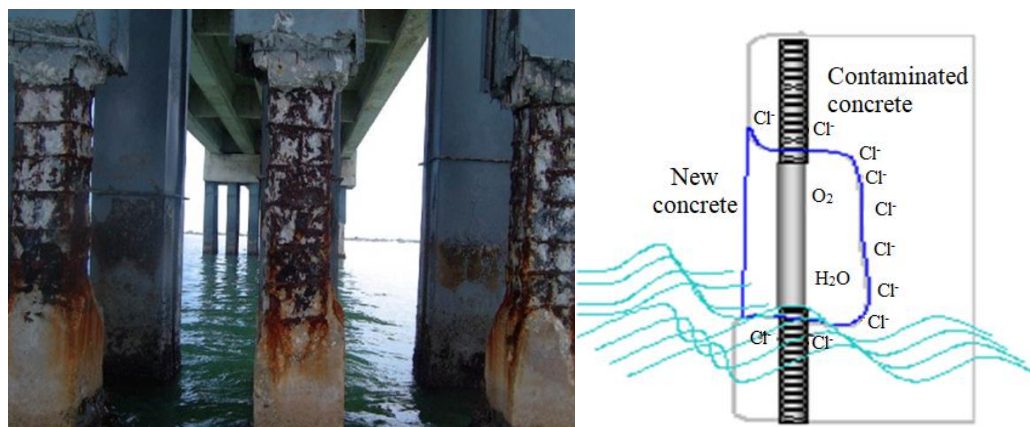


Figure 1. Repairing concrete structures using stainless steel proposed by Pérez Quiroz, (2009)

2. EXPERIMENTAL PROCEDURE.

The materials and processes applied in this project were selected under two criteria: cost of the joint(s) and feasibility for field application of the welding process and electrodes. Table 1 lists the materials, equipment, and chemicals that were used in this research, and Table 2 provides the chemical compositions of the base metals, 309L electrode, and Inconel filler metal.

Table 1. Materials, equipment, and chemical solutions.

Materials	Equipment	Chemical solutions
ASTM A615 reinforcement bars. AISI 304 reinforcement bars. ER 309L electrode Inconel 182 electrode	Saw cutting machine Automatic disc cutting machine Conventional lathe machine Conventional milling machine Castolin Eutectic, Master NT2000 AC/DC welding machine Electro discharge machine Grinding double disc machine Polishing double disc machine Magnetic heater Fluke multimeter Gamry interface1000 equipment Reference electrode Ag/AgCl	3.5 weight % Sodium chloride solution (NaCl) (sea water). Saturated solution calcium hydroxide (Ca (OH) ₂)

Table 2. Chemical compositions of base metals, 309L electrode and Inconel filler metal.

Steel	C	Si	Mn	P	S	Cr	Mo	Ni	Al	Co	Cu	Fe
ASTM A 615	0.24	0.18	0.77	0.03	0.03	0.08	0.04	0.07	0.01	0.01	0.23	98.3
AISI 304	0.01	0.33	1.39	0.07	0.03	18.1	0.27	8.61	0.01	0.18	0.38	74.1
Element	C		Mg		Si		Cr		Ni		Fe	
Composition 309L (%)	0.03		1.92		0.80		23.8		13.3		Balance	
Element	C	Si	Mn	P	S	Cr	Ni	Nb	Fe	Ti		
Composition Inconel (%)	<0.1	<1	5-9.5	<0.03	<0.015	13-17	>59	1-2.5	<10	<1		

The identification of the samples was made as indicated in Table 3.

Table 3. Designations of test samples.

Designation	Type of sample
A.C. SW	ASTM A615 carbon steel in NaCl 3.5% wt solution
A.I. SW	AISI 304 stainless steel in NaCl 3.5 % wt solution
A.C. HC	ASTM A615 carbon steel in calcium hydroxide
A.I. HC	AISI 304 stainless Steel in calcium hydroxide
Dissimilar welded joint BsAM1	Single bevel joint without buttering in NaCl 3.5 % wt solution
Dissimilar welded joint BcAM2	Single bevel with buttering in NaCl 3.5 % wt solution
Dissimilar welded joint BsHC1	Single bevel joint without buttering in calcium hydroxide
Dissimilar welded joint BcHC2	Single bevel joint with buttering in calcium hydroxide

The samples were carbon and stainless-steel bars with the following dimensions: 1.9 cm in diameter and 10 cm in length (Figure 2). The bevel of the joint was prepared at 45°, in accordance with NMX-H-121-1988 and ANSI/AWS D1.4-M 2005. The welding process for the joints was Shielded Metal Arc Welding (SMAW), because this process is the most commonly used in field welding of reinforcement bars.

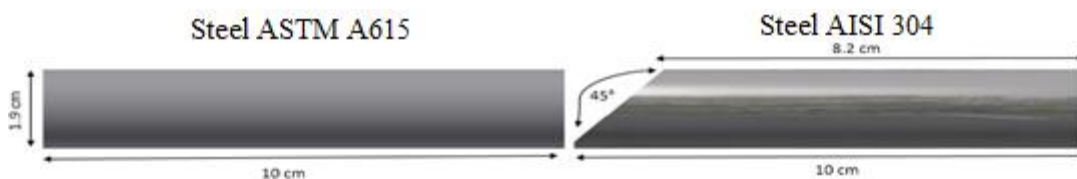


Figure 2. Diagram of a welded joint with a single bevel at 45°.

The applied filler metal for the welded joints was AISI 309L stainless steel. In the case of buttering welding, the electrode was Inconel 182. This step consisted of applying a 2 mm thick layer on the frontal surface of the AISI 304 bar. The welding machine was a Castolin Eutectic, Master NT2000 AC/DC and the welding parameters are given in Table 4.

Table 4. Welding parameters.

Diameter of the bar (mm)	19
Diameter of the electrode (mm)	3.2
Electric potential (V)	22
Welding intensity (A) DC-PI	90-95
Welding speed (mm/min)	45
Heat input (kJ/mm)	2.5

After welding, the samples were longitudinally and transversally cut with an ACTSPARK electrical discharge machine. The samples were mounted in epoxy and then prepared for metallography according to ASTM E 3. Before polishing, the stainless-steel base metal of each sample was drilled to introduce a copper wire to achieve the electrical contact necessary for

electrochemical testing. The corrosion behavior of the welded dissimilar joint was evaluated with a Gamry Interface 1000 potentiostat (Figure 3) by applying the following electrochemical techniques: measurement of corrosion potential according to ASTM C 876; linear polarization resistance test in accordance with ASTM G 59, and electrochemical noise measurement under ASTM G 199.

Linear Polarization Resistance (LPR)

This technique consists of measuring the relationship between the potential and the current density in steady state, exciting the system by application of direct-current signals. To perform the Rpl test, a three-electrode cell was used: the reference (Ag / AgCl), an auxiliary electrode (graphite), and the working electrode was an AC / SS specimen. The electrodes were placed in the cell and the Rpl test was performed using the Gamry interface1000 potentiostat with the following settings: scanning of +/- 20 mV with a scanning rate of 10 mV / min, in accordance with ASTM G 59.

Electrochemical Noise (EN)

Electrochemical noise is a technique that measures the spontaneous fluctuations of the potential and the current in electrochemical systems, which are of low frequency (<10 Hz) and amplitude. Electrochemical noise originates, in part, from natural variations in electrochemical kinetics during a corrosion process. Frequently, EN is considered and analyzed as a random (stochastic) phenomenon coupled to deterministic kinetics.

The EN technique was performed with the help of a Gamry Interface 1000 potentiostat. This equipment is capable of measuring in real time the oxide-reduction phenomena that occur in the electrodes. The number of readings per test piece was 2048, with stabilization time of 10 seconds; the test time was 45 min. This test requires three electrodes, two are identical steel electrodes, and a silver / silver chloride (Ag / AgCl), as reference electrode.

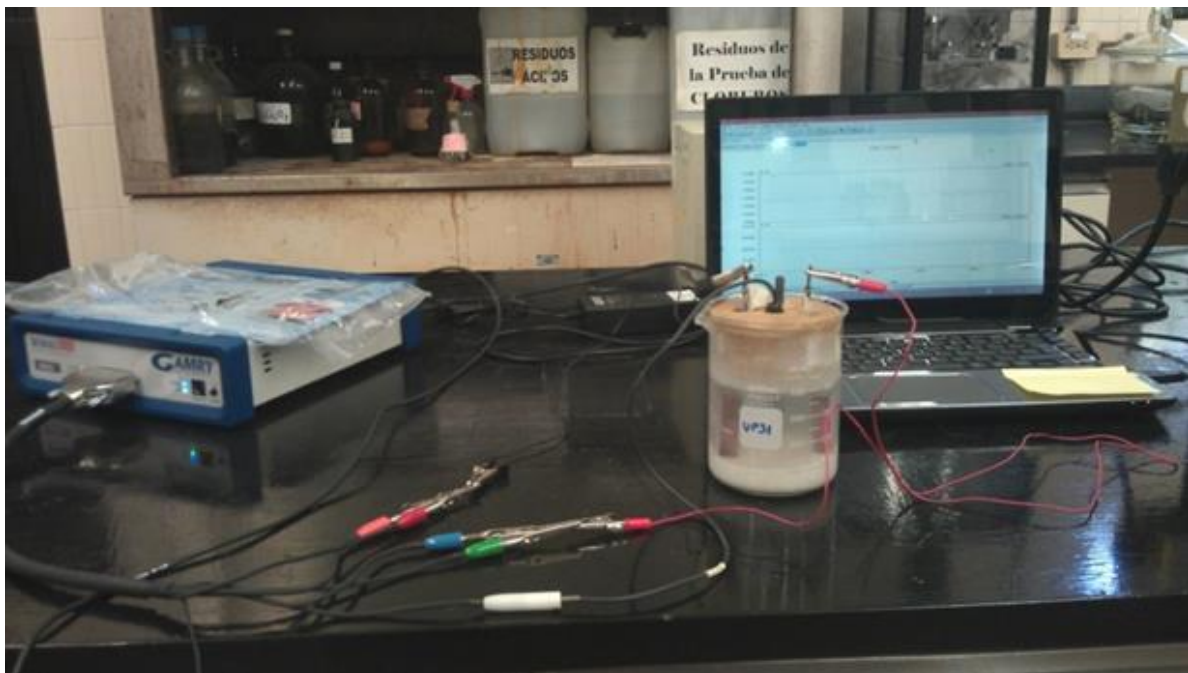


Figure 3. Electrochemical cell setup for corrosion tests.

3. RESULTS AND DISCUSSION.

Before electrochemical testing, the samples were observed using a stereoscopic microscope, and cracks were observed in the samples where buttering was carried out (Figure 4); those cracks (approximately 2 mm in length) are associated with hot cracking owing to the nickel content in the Inconel 182 used for buttering. Recall that buttering is applied to dissimilar welded joints in order to prevent carbon diffusion, phase segregation, and chromium carbides precipitation, as these phenomena influence corrosion behavior in stainless steel. The results match those of Evans (1962), who reported that nickel alloys welded to stainless steel are susceptible to hot cracking. The macrographs in Figure 4 show some lack of fusion near the carbon steel/filler metal/buttering interface. Such defects should not influence the corrosion behavior of the welded joint because they are in the interior of the metal, but if the electrolyte were to make contact with them, they would become an anode and would allow localized corrosion. On the other hand, they have a strong impact on the mechanical properties because they act as stress risers / concentrators.

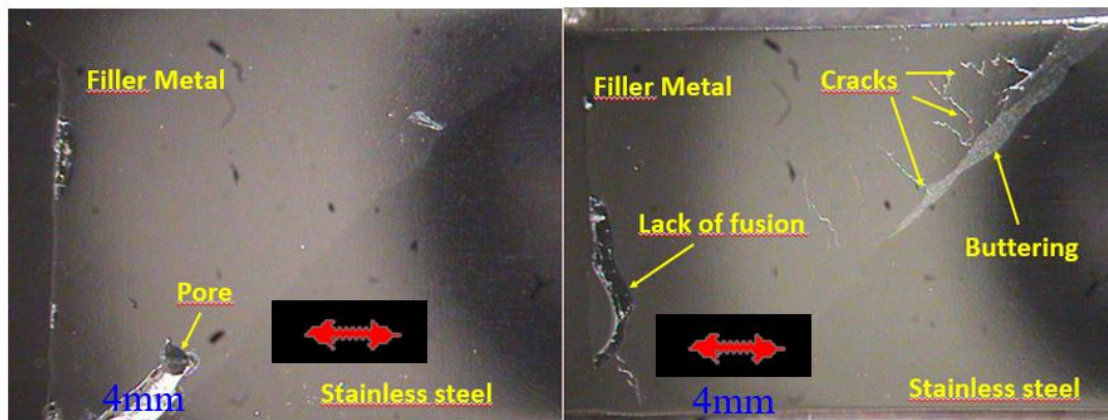


Figure 4. Samples at 7x magnification showing cracks and lack of fusion of the dissimilar welded joints.

3.1 Corrosion potential (E_{corr}).

In Figure 5, the results of the corrosion potential of the base metals are shown. Measurements were carried out over 14 days for samples immersed in NaCl and Ca(OH)₂. In Figure 5, the more negative values occur for carbon steel in salt solution (A.C.), which simulates sea water. Such results indicate a high probability of corrosion under ASTM C 876 (2015). Sistonen (2002) indicated that such values represent a severe risk of corrosion. In the case of the stainless steel (A.I.), the results of the corrosion potential are more positive than for carbon steel in the same solution and in accordance with ASTM C876 (2015), the results fall within the uncertainty zone. Such results can be explained by the passive layer of chromite on the stainless steel, which protects the material to some extent. Sistonen (2002) suggested that the corrosion potential should be interpreted based on the criteria shown in Table 5.

In the case of the Ca(OH)₂ solution, the corrosion potential results for both base materials are more positive than in sea water because of the alkalinity of the Ca(OH)₂ solution, per the ASTM C 876 (2015) standard. The same standard mentions that the probability for damage of carbon steel in such environments is minimal. Based on Sistonen's (2002) criteria, both steels are in the medium corrosion risk category.

Table 5. Criteria for corrosion potential of carbon steel and stainless steel (Sistonen, 2002).

Corrosion condition	Black Steel bar mV vs CSE	Stainless Steel bar mV vs CSE
Low corrosion risk around 10%	> - 200	> - 100
Medium corrosion risk	- 200 a - 350	- 100 a -250
High corrosion risk < 90%	- 350 a - 500	-250 a - 400
Severe corrosion risk	< - 500	< - 400

Figure 6 shows the relationship between corrosion potential and time for single bevel welded joints in 3.5 wt % NaCl solution. The values fall within the high probability corrosion range according to ASTM C 876 (2015), but in accordance with Sistonen (2002), they fall within the range of severe corrosion risk. Note that the variation of the corrosion potential of sample BsAM2 was caused by experimental error, although the trend follows the other samples, where the corrosion risk is high.

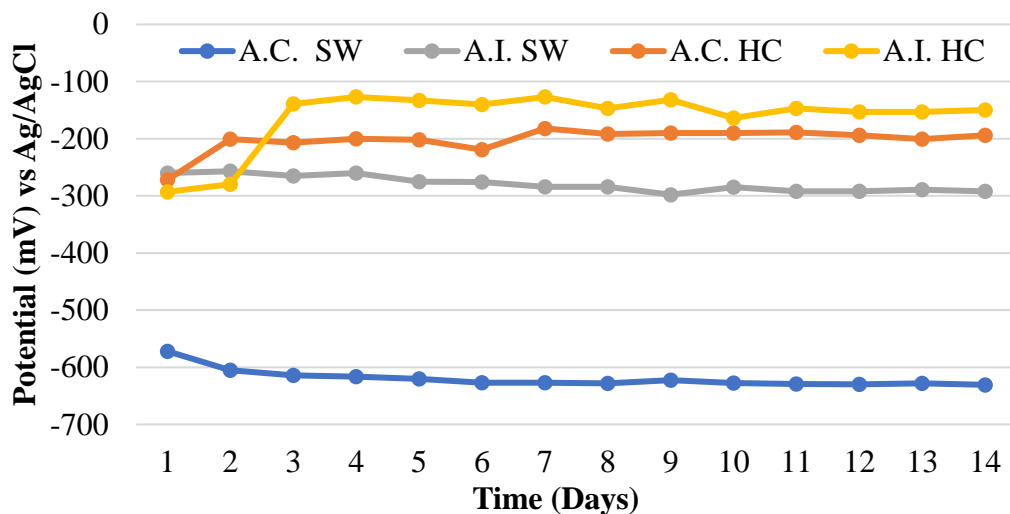


Figure 5. Corrosion potentials of the base metals in sea water and calcium hydroxide.

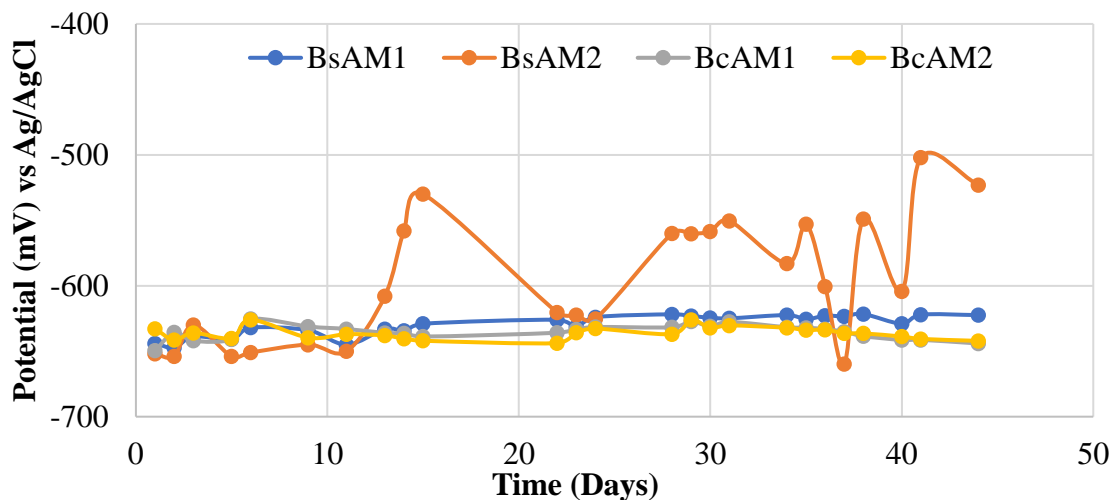


Figure 6. Corrosion potential vs time in single bevel welded joints in sea water.

By comparing Figure 5 to Figure 6, it is not easy to detect any effect of the buttering on corrosion potential. However, such comparison indicates that the corrosion potential of an entire joint dropped to more negative values, which are very similar to the values of carbon steel immersed in sea water. These results indicate higher corrosion susceptibility.

Regarding samples in the sodium chloride (NaCl) and calcium hydroxide (Ca(OH)₂) solutions, the trend of the corrosion potential values with respect to time is between -0.500 V to -0.670 V vs Ag/AgCl, because the more active metal is carbon steel (Figure 5) according to ASTM G 82. Because the corrosion potential of carbon steel is approximately -0.600 V vs the stainless-steel potential which is -0.300 V vs Ag/AgCl (Figure 5). The potential values shown in Figure 6 with respect to ASTM C876 indicate that there is a 90% probability of corrosion because they are more negative than -0.350 V vs Ag/AgCl. Figure 6 also shows that the value of the corrosion potential is in the range of -0.500 V to -0.650 V vs Ag/AgCl.

Samples with higher numbers of defects (pores, cracks, etc.) were selected for testing in calcium hydroxide to investigate if they generated a passive layer, which reduces the corrosion rate. Figure 7 shows the results, indicating that after 15 days, the values are in the probable corrosion range according to ASTM C 876 (2015) and Sistonen (2002). However, after 20 days the corrosion potentials changed to more positive values. These results indicate that the corrosion process occurred during the first 14 days, after which a compact, adherent passive layer was formed on the surface of the samples owing to the alkalinity of the environment, according to ASTM C 876 (2015) and Sistonen (2002). Thus, based on these criteria, further corrosion damage in carbon steel, stainless steel, and the welded joint should be minimal. Note that for this test, samples with a higher number of defects were selected (with and without buttering). Thus, the results suggest that alkaline conditions lead to minimal damage due to corrosion in the case of reinforcement bars for concrete.

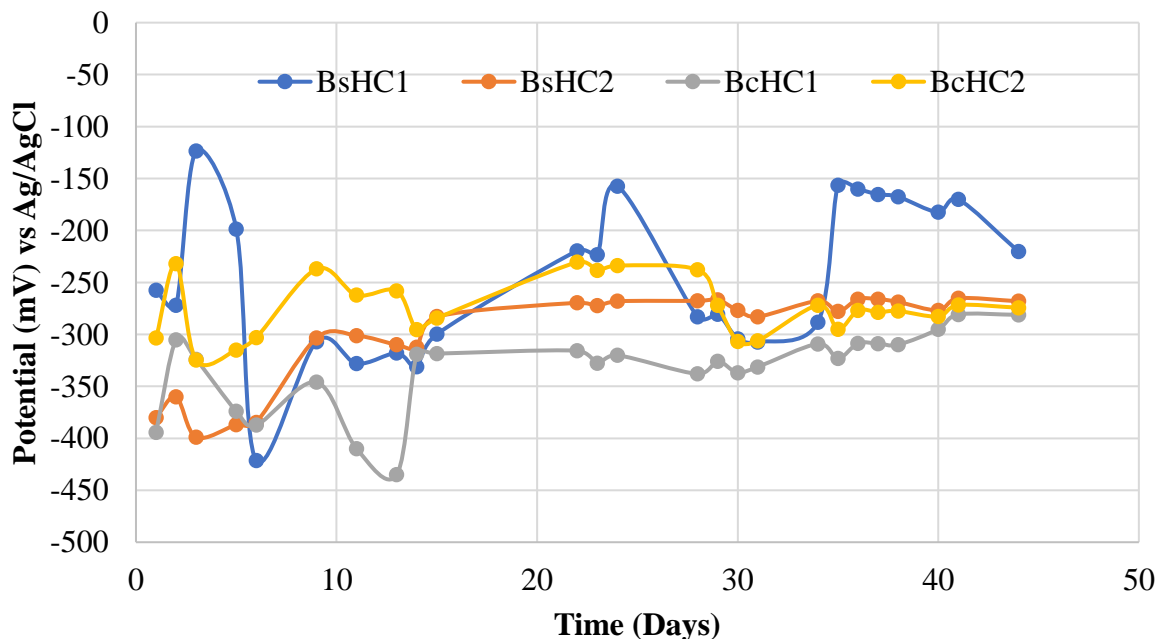


Figure 7. Potential vs time for single bevel welded joint in calcium hydroxide.

3.2 Measurements of corrosion rate based on polarization resistance.

Figure 8 shows the corrosion rates for the samples immersed in sea water, where all rates are in the range between 0.15 to 0.25 mm/y. The values are 10 times higher than the recommendations made by DURAR (1997). Thus, it can be stated that corrosion under these conditions is unavoidable for the base material and the filler metal. As mentioned previously, the electric

connection of sample BsAM2 was lost, indicating why the values of that sample are almost zero.

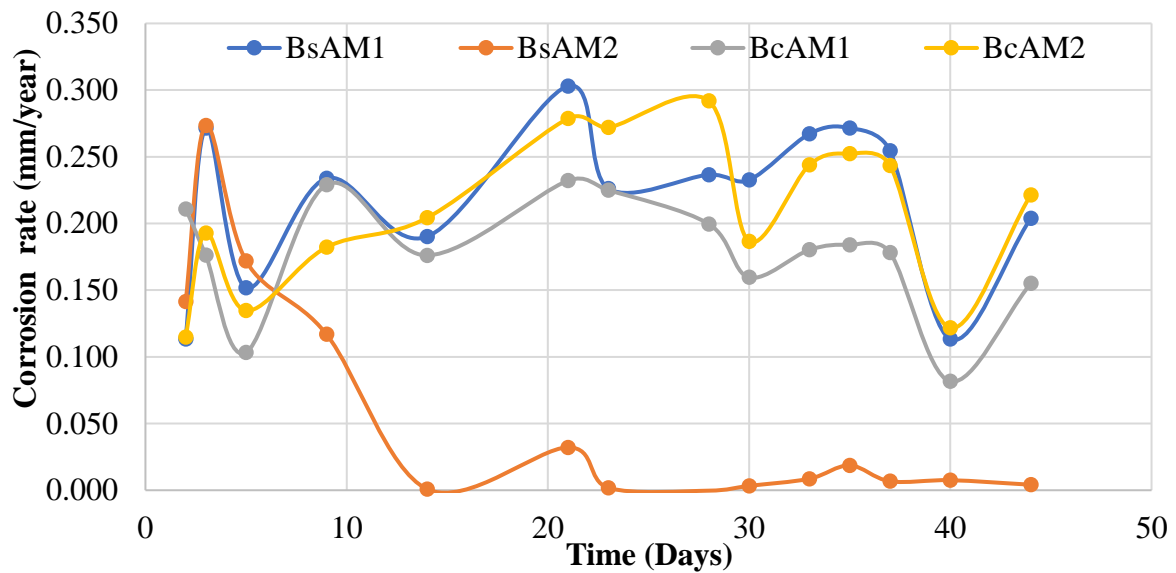


Figure 8. Corrosion rate of single bevel welded joints in sea water.

Figure 9 displays changes in corrosion rate for calcium hydroxide, which are related to the beginning of the corrosion process and the possible passivation of the sample surfaces because of the alkaline medium in which the samples were tested.

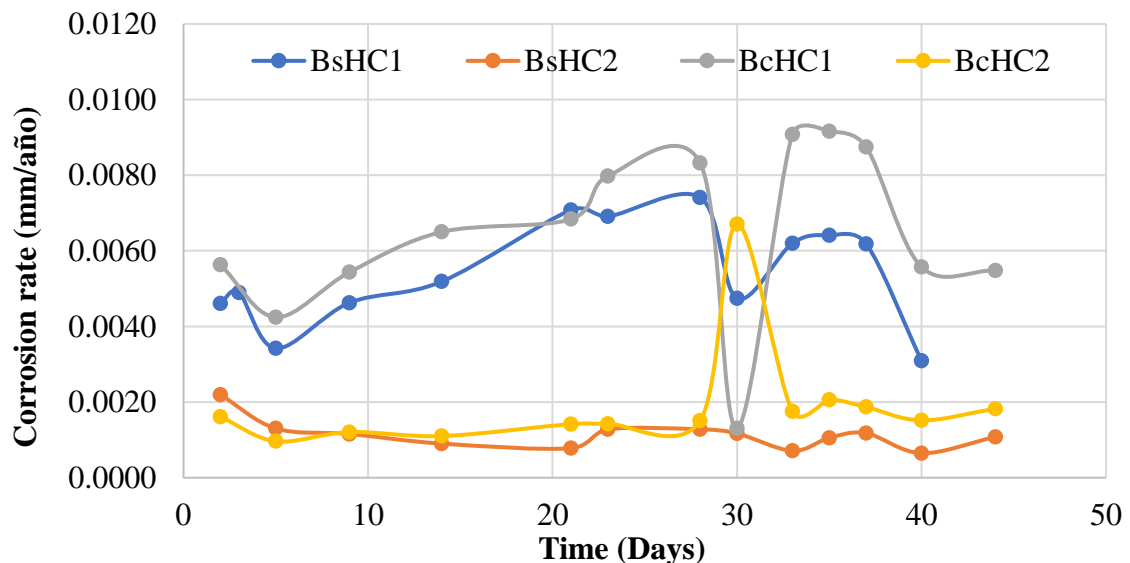


Figure 9. Corrosion rates of single bevel welded joints in calcium hydroxide.

Figure 9 shows the corrosion rates of the welded joints immersed in a calcium hydroxide solution, which are many orders of magnitude lower than the corrosion rates in sea water (see Figure 8). As mentioned previously, this can be explained by the formation of the passive layer due to the alkaline environment of the solution, even with the welding defects shown in Figure 4. These facts support the argument that stainless steel is a good option for partly substituting carbon steel in reinforcement bars in concrete structures, as those shown in Figure 1. Moreover, assuming that stainless steel bars were embedded in new concrete, the material would already be passivated and severe corrosion damage would not occur quickly. The previous statement is

justified by the Pourbaix (1966) diagram of iron, which indicates that in the alkaline ranges, it is protected by passivation.

Researchers such as Medina (2012), Bastidas (2014), Velasco (2013), Sanchez (2013), Bautista (2013), Acosta (2013), Landmann (2013), Andrade (1993), and González (1984) have reported good performance of stainless steel even in saline environments, because the dangerous corrosion rate level for concrete structures (100–125 $\mu\text{m}/\text{y}$) is higher than the results they obtained for stainless steel. Figure 8 verifies that the corrosion rates of the samples are higher than the recommended range of rates, while Figure 9 indicates corrosion rates are substantially lower than those ranges. Thus, repairs using stainless steel would meet the specification for an alkaline environment.

3.3 Measurements of corrosion rate by electrochemical noise.

The metallurgical effect of corrosion behavior on welded joints was evaluated using electrochemical noise. This technique consists of setting two electrodes in an electrolyte as described in Chapter 2 of ASTM C 199 and is shown in Figure 3. The results of this technique are shown in Figures 10–13. Two variables characterize the corrosion behavior of the samples: noise resistance (R_n), which is equivalent to polarization resistance; and the second variable is the localization index (I_L), which points out the corrosion form of the samples. The following criteria apply: uniform corrosion (0.001 to 0.01), mix between uniform and localized corrosion (0.01 to 0.1), and finally localized corrosion (0.1 to 1). Those criteria have been previously considered by Eden (1987), Kelly (1996), Mansfeld (1999), and Balán (2017).

Figure 10 shows that the values of I_L of the BsAM samples are in the localized corrosion range. Recall that those samples had no buttering layer and were immersed in sea water. Therefore, corrosion is expected in those samples. Figure 11 shows that the corrosion products are on specific spots of the sample surfaces, as predicted by ASTM G 199.

Although the values of I_L of the BcAM samples are in the localized corrosion range, the corrosion products are uniformly distributed on the sample surfaces, which agree more closely with the mixed corrosion criterion. This suggests that buttering leads to more uniform corrosion. The general scientific consensus is that uniform corrosion is less aggressive than pitting and crevice corrosion, because the latter types of corrosion cause structural damage and can lead to catastrophic failure.

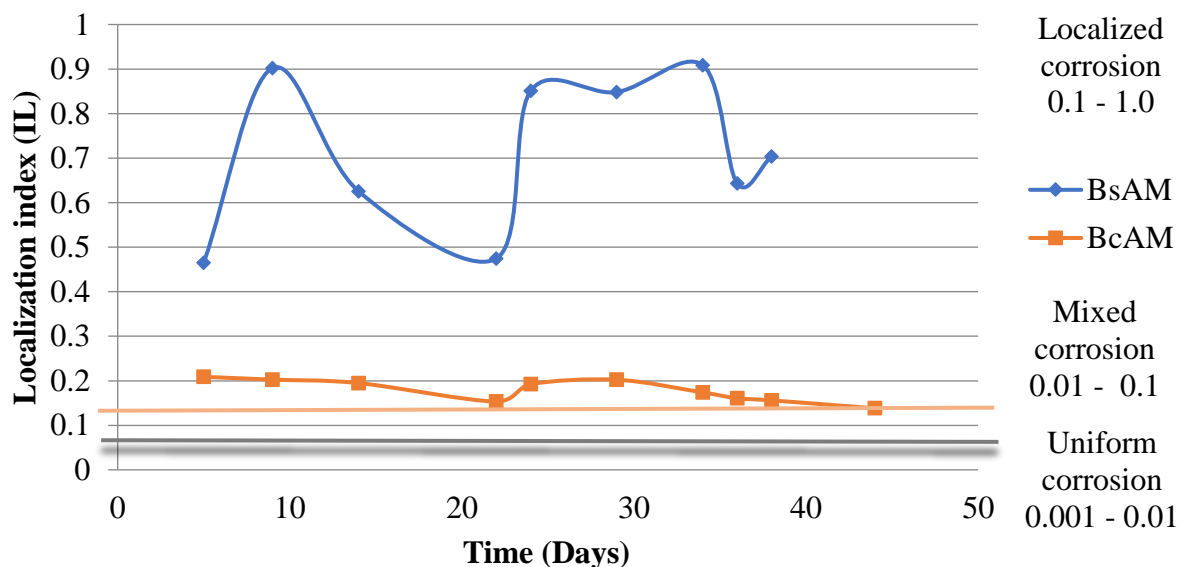


Figure 10. Results of electrochemical noise testing of BsAM and BcAM samples in seawater.

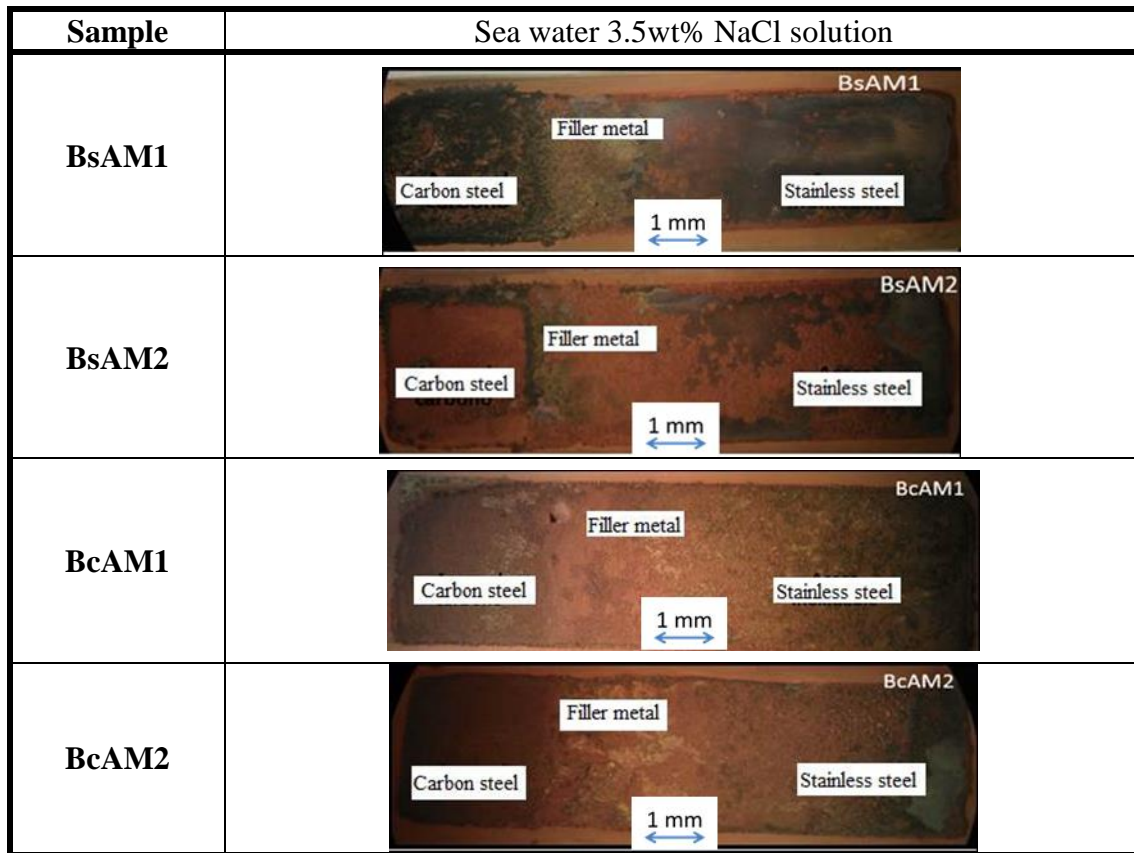


Figure 11. Stereographic images of BsAM and BcAM tested in sea water (3.5wt % NaCl solution). (Ramírez 2016)

Figure 12 shows the results of the samples tested in calcium hydroxide. Those results indicate localized corrosion occurs in the defects of the welded joint (as can be observed in Figure 13), where such corrosion occurs by the formation of differential aeration corrosion cells. Sample BsHC, which did not contain welding defects, exhibited a white layer on the surface of the welded joint (Figure 13), which inhibited corrosion. Therefore, the only places susceptible to localized corrosion were the welding defects.

In this case, the behavior of sample BsCH is related to the graph of Figure 12. This sample shows a corrosion tendency like BcCH because the results of both samples are in the localized corrosion range. However, in the case of BcHC it is considered that corrosion is associated with welding defects as well as with localized dissolution of the nickel layer. As explained by Pourbaix (1966), nickel corrodes slightly in alkaline solutions before forming a passive layer. The behavior of the BcHc sample agrees with this statement and explains the differences in the results between the two samples.

Figure 13 shows stereographic images of samples tested in calcium hydroxide, which were covered with a white color layer (calcareous deposit), which forms a passive layer on the samples' surfaces.

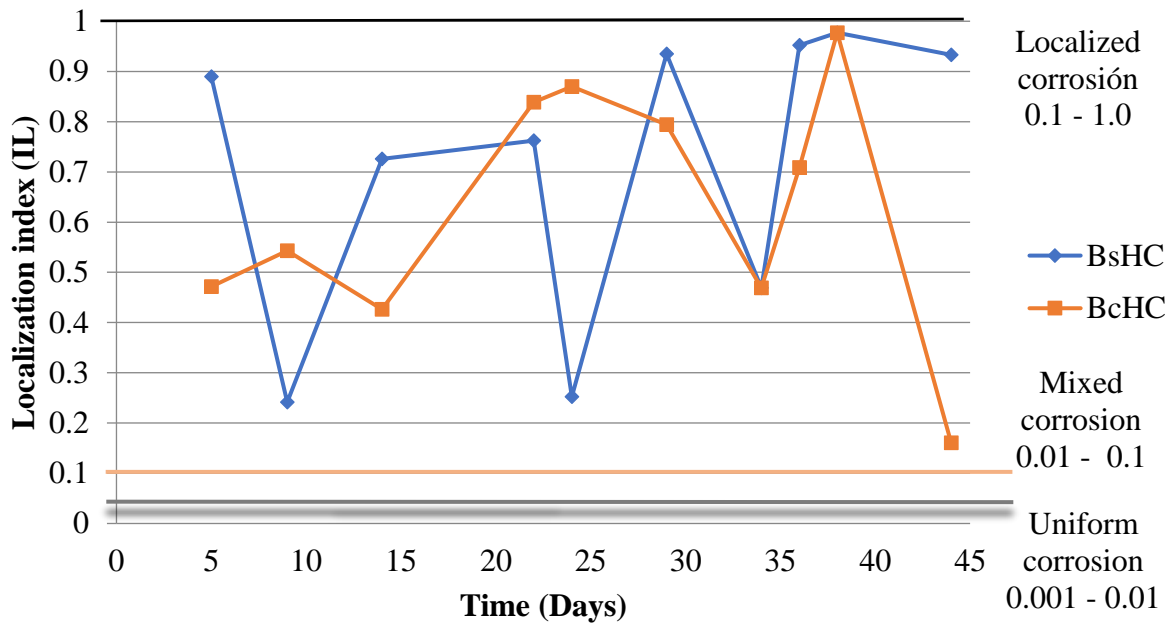


Figure 12. Graph of I_L values for samples BsHC and BcHC tested in calcium hydroxide.

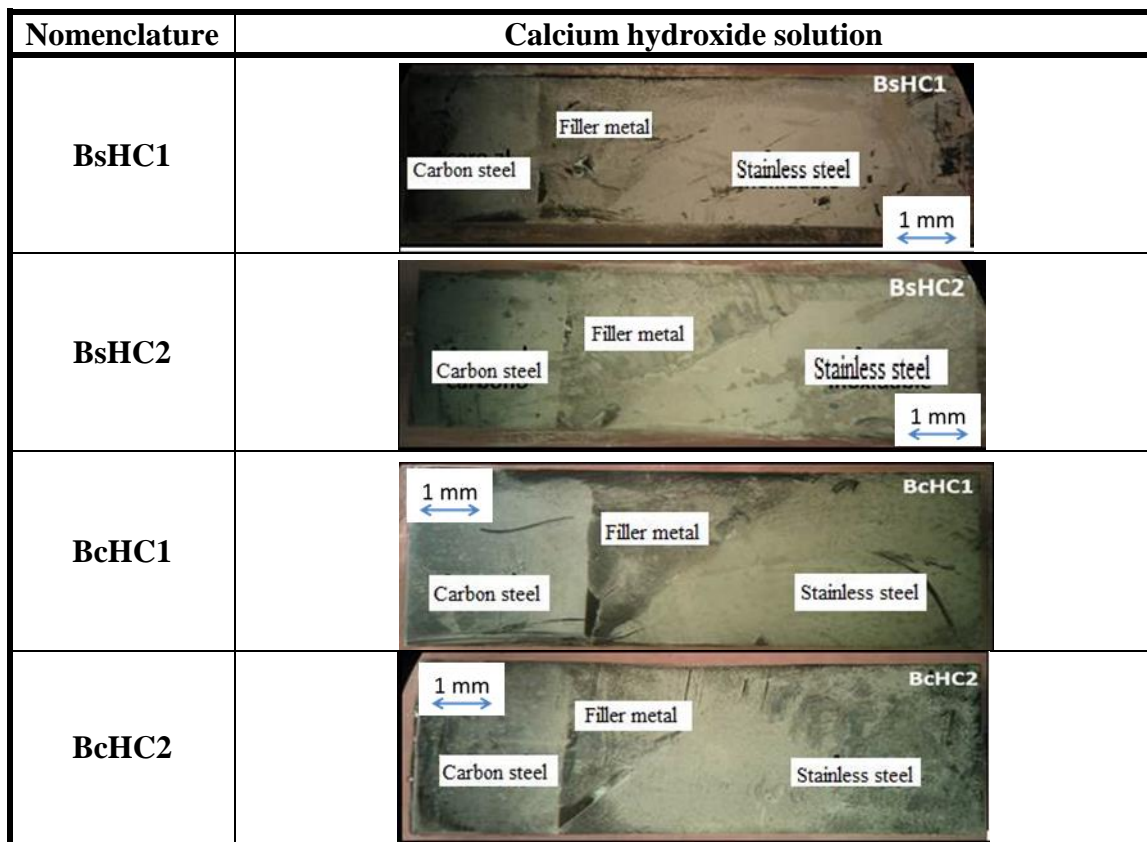


Figure 13. Surfaces of BsHC and BcHC samples after testing in calcium hydroxide. (Ramírez 2016)

Resistance noise (R_n) is a very powerful tool to assess the low corrosion rate of the BsHC and BcHC samples immersed in calcium hydroxide and is similar to polarization resistance. Therefore, this technique was applied to those samples and the results are shown in Figures 14 and 15. ASTM G 102 (2015) specifies the relationship between R_p and i_{corr} , which is inversely

proportional. In other words, the higher the values of noise resistance, the lower the corrosion current density, indicating a lower corrosion rate. Samples in sea water (NaCl 3.5wt% solution) exhibited lower noise resistance values than the samples in the Ca(OH)₂ solution, thus had a higher corrosion current density, indicating higher corrosion rates. Figures 14 and 15 highlight these results. The results agree with the results reported by Kelly (1996) and Garcia (2014).

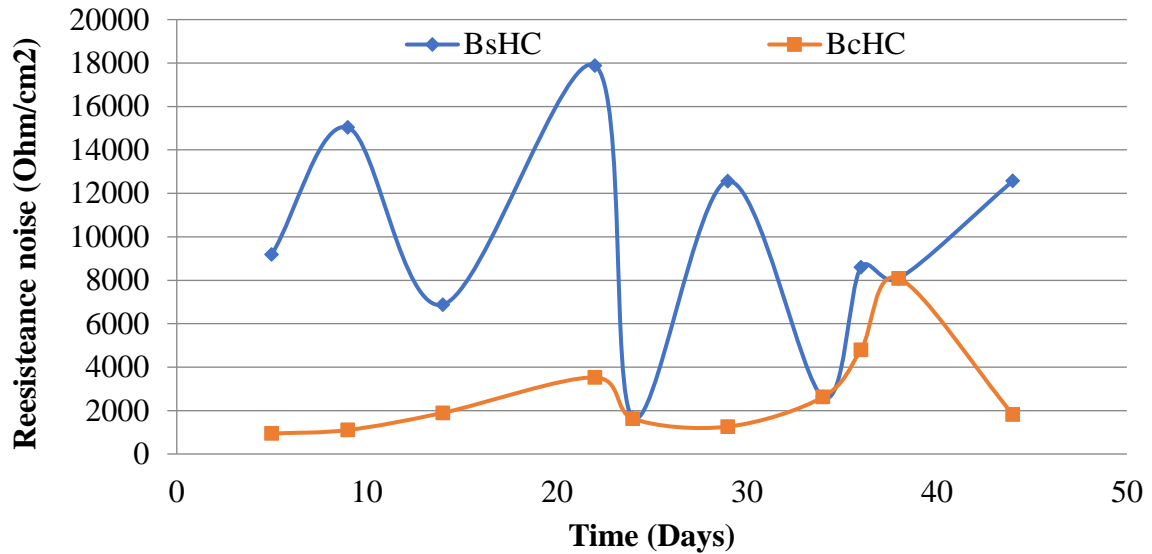


Figure 14. Resistance in noise (Rn) of the BsHC and BcHC samples tested in saline solution.

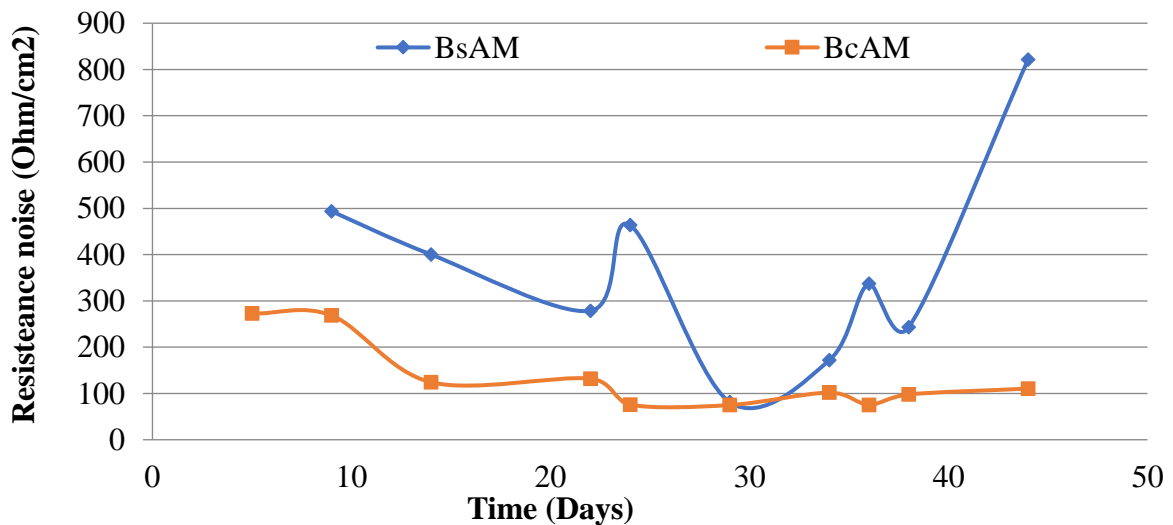


Figure 15. Values of Rn for BsHC and BcHC tested in calcium hydroxide.

4. CONCLUSIONS

The results of this work indicate that refurbishing of concrete structures using stainless steel is feasible, particularly if the steel is passivated. The construction or repair of a concrete structure must be carried out following the applicable standards in order to verify that the repaired area undergoes passivation to reduce future corrosion.

Measurements of corrosion potential were useful to determine the corrosion behavior in two different environments for bars made of carbon steel, stainless steel, and a dissimilar metal welded joint between the two materials buttered with Inconel 182 and without buttering. It was found that carbon steel in sea water is susceptible to corrode with 90% probability, while stainless steel is in the range of uncertainty. However, essentially opposite results were obtained for an alkaline environment ($\text{Ca}(\text{OH})_2$ solution), where the probability of corrosion was 10%. Both dissimilar welding joints with and without buttering resulted in a 90% probability of corrosion in sea water, while in the alkaline media the probability of corrosion for either joint decreased to 10%. This was explained by a passive layer found on the sample surfaces. The corrosion rate of the welded joint with buttering was lower in an alkaline environment ($\text{Ca}(\text{OH})_2$ solution) than in sea water (NaCl 3.5 wt% solution). These results were also explained by formation of a passive layer on the surface defects of the samples in the alkaline environment. The results of electrochemical noise were used to describe electrochemical behavior in the alkaline solution and in sea water of welded joints with and without buttering. The results indicated that the corrosion type on such samples was mixed corrosion, and they match the results obtained by polarization resistance and corrosion potential measurements.

5. REFERENCES

- Acosta, P., Matres, V., Pachón, A., Sánchez, J., Fulla, J., Picón, J. M. (2013). “*Armaduras de acero inoxidable expuestas en ambiente marino. Caracterización in-situ de la corrosión*”. DM Bastidas, E. Medina Sánchez, CEDINOX (Eds.), *Armaduras Acero Inoxidable*, CEDINOX, Madrid (España), 115-128.
- American National Standards - American Welding Society (2005) *ANSI/AWS D1.4-M Structural Welding Code - Reinforcing Steel*.
- ASTM International. (2014). *ASTM G59-97(2014) Standard Test Method for Conducting Potentiodynamic Polarization Resistance Measurements*. Retrieved from <https://doi.org/10.1520/G0059-97R14>
- ASTM International. (2014). *ASTM G199-09(2014) Standard Guide for Electrochemical Noise Measurement*. Retrieved from <https://doi.org/10.1520/G0199-09R14>
- ASTM International. (2015). *ASTM C876-15 Standard Test Method for Corrosion Potentials of Uncoated Reinforcing Steel in Concrete*. Retrieved from <https://doi.org/10.1520/C0876-15>
- ASTM International. (2015). *ASTM G102-89(2015)e1 Standard Practice for Calculation of Corrosion Rates and Related Information from Electrochemical Measurements*. Retrieved from <https://doi.org/10.1520/G0102-89R15E01>
- ASTM International. (2017). *ASTM E3-11(2017) Standard Guide for Preparation of Metallographic Specimens*. Retrieved from <https://doi.org/10.1520/E0003-11R17>
- Balán-Ortiz, C. A., Luna Brito, M., Pérez López, T.; Camacho-Chab, R.J. (2017) “*Análisis estadístico de los registros de ruido electroquímico obtenidos del proceso de corrosión del acero de refuerzo embebido en concreto*”, *Revista Mexicana de Ingeniería Química* 2017, 16 (1). ISSN 1665-2738, Disponible en: <https://www.redalyc.org/articulo.oa?id=62049878028>
- Baltazar, M., & Almeraya, F., Nieves, D., & Borunda, A., Maldonado, E., Ortiz, A. (2007). “*Corrosión del acero inoxidable 304 como refuerzo en concreto expuesto a cloruros y sulfatos*”. *Scientia Et Technica*, 13 (36), 353- 357. Disponible en: <https://www.redalyc.org/html/849/84903663/>
- Bastidas, D. M., Zapico, C. (2014). “*Comportamiento frente a la corrosión de armaduras de acero inoxidable dúplex en solución simulada de poros de hormigón con elevado contenido de cloruros*”. *Industria química*, ISSN 2340-2113, N°. 17, 2014, págs. 68-74

- Bautista, A., Paredes, E. C., Velasco, F. (2013). “*Influencia del corrugado en la durabilidad de las barras austeníticas en medios sin carbonatar y con cloruros*”. Armaduras de Acero Inoxidable, ISBN 978-84-695-8183-4, págs. 105-114
- Bertolini, L., Gastaldi, M., Pastore, T., Pedferri, M. P., Pedferri, P. (1998). *Effects of galvanic coupling between carbon steel and stainless steel reinforcement in concrete*. International Conference on “Corrosion and Rehabilitation of Reinforced Concrete Structures”, Federal Highway Administration, Orlando. December 7–11.
- Brown, B. L., Harrop, D., Treadaway, K.W.J. (1976) “*Corrosion Testing of Steels for Reinforced Concrete Corrosion Testing and Monitoring*”, Reprint.
- British Stainless Steel Association (BSSA) (2003) “*The Use of Stainless Steel Reinforcement in Bridges*”, Special BSSA Report - April 2003, Disponible en: <https://www.bssa.org.uk/cms/File/REBar%20report.pdf>
- Doddy, T. (1992), “*Intermediate mixed zones in dissimilar metal welds for sour service*”, Welding Journal, 71 (3), pp. 55-60.
- DURAR (1997). *Manual de inspección, evaluación y diagnóstico de corrosión en estructuras de hormigón armado*. CYTED, Programa Iberoamericano de Ciencia y Tecnología para el Desarrollo, Subprograma XV Corrosión/Impacto Ambiental sobre Materiales Maracaibo, Venezuela, ISBN 980-296-541-3.
- Dirección General de Normas Mexicanas (1988). *NMX-H-121: Procedimiento de soldadura estructural acero de refuerzo*”.
- Eden, D. A., John, D. G., Dawson, J. L. (1987), *Corrosion monitoring. International Patent WO 87/07022*. World Intellectual Property Organization, 19.
- Evans, R. M. (1962). “*Joining of Nickel-Base Alloys*”, (No.181). DMIC Report 181, Battelle Memorial Institute, Columbus 1, Ohio
- García Fuentes, A., Centeno, L., Salas García, R., Velazquez Del Rosario, A. (2011). *Metalurgia de uniones soldadas de aceros disímiles (ASTM A240–A537) y comportamiento mecánico ante cargas monotónica y cíclica*, Revista Latinoamericana De Metalurgia Y Materiales, 2012, 32(1). Recuperado de <http://www.rlmm.org/ojs/index.php/rlmm/article/view/113>
- García, I. L. (2014). “*Caracterización electroquímica del acero al carbono e inoxidable en soluciones concentradas con extracto de cemento*”; Tesis que para obtener el Grado de: Maestría en Ciencias de Materiales.
- González Díaz, F. (2010). “*Recalcalinización electroquímica del concreto reforzado carbonatado: una opción de prevención contra la corrosión*”. Doctoral dissertation, Universidad Autónoma de Nuevo León.
- González, J. A., Andrade, C., Escudero, M. L., (1984), “*Corrosión de las armaduras por carbonatación del hormigón*”. Rev. Iberoamericana de corrosión y protección 15 (4), 11-19.
- Kelly, R. G; M. E. Inman, J. L. Hudson, (1996) “*Analysis of Electrochemical Noise for Type 410 Stainless Steel in Chloride Solutions (STP 1277)*”, STP 1277 Electrochemical Noise Measurement for Corrosion Applications (ASTM International), pp. 101-113 DOI: <https://doi.org/10.1520/STP37954S>
- Kepler, J. L., Darwin, D., Locke Jr, C. E. (2000). *Evaluation of corrosion protection methods for reinforced concrete highway structures* (No. K-TRAN: KU-99-6,). Kansas Department of Transportation
- Landmann, M. S., Fuentes, J. R., Bonaste, V., & Martínez, A. S. (2013). “*Rehabilitación con armaduras de acero inoxidable*”. In Armaduras de acero inoxidable (pp. 167-190). ISBN 978-84-695-8183-4
- Lundin, C. D. (1982). *Dissimilar metal welds-transition joints literature review*. Welding Journal, 61(2), 58-63. URL: http://files.aws.org/wj/supplement/WJ_1982_02_s58.pdf

- Mansfeld, F., Sun, Z. (1999), *Technical Note: Localization Index Obtained from Electrochemical Noise Analysis*. Corrosion Science, 55 (10) pp. 915-918 DOI: <https://doi.org/10.5006/1.3283926>
- McDonald, D. B., Pfeifer, D. W., Sherman, M. R. (1998), *Corrosion evaluation of epoxy-coated, metallic-clad, and solid metallic reinforcing bars in concrete*, Report No. FHWA-RD-98-153, Federal Highway Administration, McLean, VA, December, 137 pp. URL: <https://trid.trb.org/view/496237>
- Medina, E., Cobo, A., Bastidas, D. M. (2012). “Evaluación del comportamiento estructural y de resistencia a la corrosión de armaduras de acero inoxidable austenítico AISI 304 y dúplex AISI 2304 embebidas en morteros de cemento Portland”. Revista de Metalurgia, 48(6), 445-458. DOI: <https://doi.org/10.3989/revmetalm.1203>
- Medina, E. D. B. (2013). “Introducción a las Armaduras de acero inoxidable”, 1-22. URL: <http://hdl.handle.net/10261/85075>
- Molina, F.J., Alonso, C., Andrade, C. (1993), “Cover cracking as a function of rebar corrosion: Part 2—Numerical model”, Materials and Structures 26, 532. DOI: <https://doi.org/10.1007/BF02472864>
- Nurnberger, U. (1996), “Stainless steel in concrete”. European Federation of Corrosion publications, No. 18. London, Institute of Materials.
- Ospina Lopez, R., Aguirre Corrales, H., Parra, H. (2007). “Soldabilidad en aceros inoxidables y aceros disimiles”. Scientia et technica, 13(34). Disponible en: <https://www.redalyc.org/articulo.oa?id=84934046>
- Pedefferri, P., Bertolini, L., Bolzoni, Pastore, F. T. (1997), “Behavior of Stainless Steels in Concrete,” Proceedings of the International Seminar: The state of the art of the repair and rehabilitation of reinforced concrete structures Eds. W.F. Silva-Araya, O.T. DE RINCÓN, and L. P. O’Neill, (Reston, VA: ASCE, 1997): p.192.
- Pérez, L.T. (2002). “Aplicación de la Técnica de Espectroscopia de Impedancia Electroquímica en el Estudio de la Corrosión del Acero de Refuerzo Embebido en Concreto”. Programa de Corrosión del Golfo de México.
- Pérez-Quiroz, J. T., Alonso-Guzmán, E. M., Martínez-Molina, W., Chávez-García, H. L., Rendón Belmonte, M., Martínez-Madrid, M. (2014), “Electrochemical Behavior of the Welded Joint Between Carbon Steel and Stainless Steel by Means of Electrochemical Noise”, International Journal of Electrochemical Science, pp. 6734 – 6750.
- Pérez Quiroz, J. T. (2009), “Evaluación de acero inoxidable para la rehabilitación de estructuras de concreto reforzado”. Tesis para obtener el grado de Doctor en Ingeniería Química.
- Pourbaix, M. (1966), *Atlas of electrochemical equilibria in aqueous solutions*. Pergamon Press, New York.
- Ramírez-Soto, J. C. I., Salgado-López, J. M., Pérez-Quiroz, J. T., Pérez-López, T., Terán-Guillén, J., & Martínez-Madrid, M. (2016). “Effect of buttering in mechanical properties of dissimilar metal weld joints for reinforcement bars in concrete structures”. Revista ALCONPAT, 6(3), 248-261.
- Schierloh, M., Rougier, V., Souchetti, R. (2010). “Vigas de hormigón armado afectadas por corrosión y reparadas con materiales de matriz polimérica reforzados con fibras (PRFS)”. IX Jornada “Técnicas de restauración y conservación del patrimonio”.
- Sánchez, E. M., Llorente, I., Fajardo, S., Bastidas, D. M. (2013), “Comportamiento frente a la corrosión por cloruros de una nueva armadura de acero inoxidable dúplex de bajo contenido en níquel”, Armaduras de acero inoxidable, ISBN 978-84-695-8183-4, págs. 91-103, Editores: CEDINOX, Centro para la investigación y desarrollo del acero inoxidable.
- Sistonen, E., Tukiainen, P., Peltola, S., Skriko, S., Lastala, M., Huovinen, S. (1998-2000), *Improving the durability of reinforced outdoor concrete structures by restricting cracks and protecting reinforcement*, part I & II. Project 1998–2002

- Soerensen, B., Jensen, P. B., Maahn, E. (1990), *The corrosion properties of stainless-steel reinforcement*. Corrosion of Reinforcement in Concrete. Ed. by C. L. Page, K. W. J. Treaday, P. B. Bamforth. Papers Presented at the Third International Symposium on "Corrosion of Reinforcement in Concrete Construction", Belfry Hotel, Wishaw, Warwickshire, May 21-24, 1990
- Terradillos, P. G., Llorca, M. Á. C., Gómez, E. Z. (2008). “*Corrosión de Armaduras en estructuras de Hormigón Armado*”. Editorial Club Universitario. ISBN: 978-84-8454-685-6, Sapin.
- Treadaway, K. W. J., Cox, R. N., Brown, B. L. (1989), *Durability of corrosion resisting steels in concrete*. Proceedings Institution Civil Engineers, 86, pp.13–27.
- Velasco Lopez, F. J., Alvarez Arboleda, S. M., Bautista Arija, M. A. (2013), *Comportamiento frente a la corrosión de corrugados dúplex de baja aleación en disoluciones simuladas de poros de hormigón*. In: Armaduras de acero inoxidable, pp. 81-90, ISBN: 978-84-695-8183-4

Evaluation of the aggregates used in the metropolitan region of Salvador regarding the occurrence of alkali-aggregate reactions (AAR)

D. V. Ribeiro^{1*} , R. O. Rey¹ 

*Contact author: verasribeiro@hotmail.com

DOI: <http://dx.doi.org/10.21041/ra.v9i2.326>

Reception: 19/06/2018 | Acceptance: 19/02/2019 | Publication: 30/04/2019

ABSTRACT

In the present work the AAR of the aggregates used in the metropolitan region of Salvador and the use of mineral additions in order to mitigate this reaction was evaluated. The accelerated test method using mortar bars, recommended by NBR 15577-4: 2008, was used. The results indicate that the sands of the metropolitan area of Salvador have low reactivity, however, the gravels presented high reactivity and that mineral additions with pozzolanic characteristics can mitigate the AAR. This study, although limited to the conditions used, is unprecedented in the State of Bahia and presents a high index of originality, since it uses higher contents of mineral additions than conventional use. It was concluded that microsilica, if used at very high contents, can even accelerate the AAR.

Keywords: AAR; aggregates; mineral additions; mitigation.

Cite as: Ribeiro, D. V., Rey, R. O. (2019), "Evaluation of the aggregates used in the metropolitan region of Salvador regarding the occurrence of alkali-aggregate reactions (AAR)", Revista ALCONPAT, 9 (2), pp. 185-199, DOI: <http://dx.doi.org/10.21041/ra.v9i2.326>

¹ Federal University of Bahia, Brazil.

Legal Information

Revista ALCONPAT is a quarterly publication by the Asociación Latinoamericana de Control de Calidad, Patología y Recuperación de la Construcción, Internacional, A.C., Km. 6 antigua carretera a Progreso, Mérida, Yucatán, 97310, Tel.5219997385893, alconpat.int@gmail.com, Website: www.alconpat.org

Responsible editor: Pedro Castro Borges, Ph.D. Reservation of rights for exclusive use No.04-2013-011717330300-203, and ISSN 2007-6835, both granted by the Instituto Nacional de Derecho de Autor. Responsible for the last update of this issue, Informatics Unit ALCONPAT, Elizabeth Sabido Maldonado, Km. 6, antigua carretera a Progreso, Mérida, Yucatán, C.P. 97310.

The views of the authors do not necessarily reflect the position of the editor.

The total or partial reproduction of the contents and images of the publication is strictly prohibited without the previous authorization of ALCONPAT Internacional A.C.

Any dispute, including the replies of the authors, will be published in the first issue of 2020 provided that the information is received before the closing of the third issue of 2019.

Avaliação dos agregados utilizados na região metropolitana de Salvador quanto à ocorrência de Reatividade Álcalis-Agregado (RAA)

RESUMO

O presente artigo avaliou a RAA dos agregados utilizados na região metropolitana de Salvador e o uso de adições minerais, a fim de mitigar essa reação. Empregou-se o método acelerado de barras de argamassa, preconizado pela NBR 15577-4: 2008. Os resultados indicam que os agregados miúdos da região metropolitana de Salvador apresentam baixa reatividade, entretanto, os agregados graúdos apresentaram elevada reatividade e que adições minerais com características pozolânicas podem mitigar a RAA. Este estudo, apesar de se limitar às condições utilizadas, é inédito no Estado da Bahia e apresenta elevado índice de originalidade por utilizar teores de adições superiores às convencionais. Concluiu-se neste estudo que a microssílica, se utilizada em teores muito elevados, pode, inclusive, acelerar a reação.

Palavras-chave: RAA; agregados; adições minerais; mitigação

Evaluación de los agregados utilizados en la región metropolitana de Salvador en cuanto a la ocurrencia de Reacción Alkali-Agregado (RAA)

RESUMEN

En el presente trabajo se evaluó la RAA de los agregados utilizados en la región metropolitana de Salvador y el uso de adiciones minerales, a fin de mitigar esa reacción. Se utilizó el método acelerado de barras de mortero, preconizado por la NBR 15577-4: 2008. Los resultados indican que las arenas de la región metropolitana de Salvador presentan baja reactividad, sin embargo, las gravas presentaron alta reactividad y que adiciones minerales con características pozolánicas pueden mitigar la RAA. Este estudio, a pesar de limitarse a las condiciones utilizadas, es inédito en el Estado de Bahía y presenta un elevado índice de originalidad por utilizar contenidos de adiciones superiores a las convencionales. Se concluyó en este estudio que la microssílica, si se utiliza en niveles muy elevados, puede, incluso, acelerar la reacción.

Palabras clave: RAA; agregados; adiciones minerales; mitigación

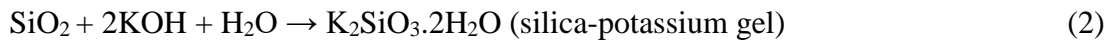
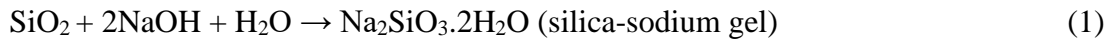
1. INTRODUCTION

Alkali-aggregate reactions (AAR) are chemical reactions that occur between reactive mineralogical constituents of aggregates, alkaline ions and hydroxyl present in the interstitial solution of cement paste. The reaction product is an expansive gel that in the presence of water expands, causing an increase in the internal structural forces, generating deformations and cracks in the concrete surface. These can have a highly detrimental effect on the cement, compromising even the lifespan of the structure (Thomas, 2011).

Currently, three types of deleterious reaction are considered, depending on the mineralogical composition of the aggregates and the mechanisms involved: alkali-silica reaction, alkali-silicate reaction and alkali-carbonate reaction. The alkali-carbonate reaction is not discussed in greater detail in this paper because it was not part of our research. The term alkali-aggregate reaction (AAR) when mentioned in the text refers to the alkali-silica or alkali-silicate reactions.

The first stage of the alkali-silica reaction (ASR) is the reaction between the hydroxyl ions (OH⁻) present in the pore solution, and the reactive silica of the aggregate. Initially the alkalis increase the concentration of hydroxyl ions in the solution, and the expansive gel production (Thomas, 2011;

Beyene et al., 2013). ASR can be represented in a simplified form by equations (1) and (2) (West, 1996 apud Campos, 2015).



For AAR to occur, three conditions are necessary: i) presence of reactive phases in the aggregate (ii) enough moisture, and iii) high alkali hydroxides concentration in the concrete pore's solution, enough to react with the reactive phases of the aggregates (Giordano, 2007).

The raw materials used in the manufacture of Portland cement are generally responsible for the alkalis present in the cement, ranging from 0.2% to 1.5% Na_2O equivalent ($\text{Na}_2\text{O} + 0.658\text{K}_2\text{O}$). Because of cement hydration, there is an interstitial solution in the concrete containing essentially sodium, calcium and potassium hydroxide. Normally, depending on the amount of alkalis, the pH in the pore solution ranges from 12.5 to 13.5. This pH represents a strongly alkaline liquid in which some acid rocks (aggregates composed of silica and siliceous minerals) do not remain stable (Giordano, 2007). In other words, the presence of alkalis influences the reactivity of the aggregate because the more alkalis available, the higher the concentration of OH^- in the solution of the pores and, consequently, the more silica will dissolve (Beyene et al., 2013).

If the expansive gel is formed, there is no way to reverse the process, only minimizing its damage. Recent studies (Thomas, 2011; Beyene et al., 2013) showed that AAR expansion is reduced when a pozzolanic cement or pozzolanic mineral additions are used. Therefore the use of pozzolanic mineral additions, such as silica fume and metakaolin, in the concrete mixture is recommended. These studies evaluate the effects of mineral additions on the alkali-aggregate reaction and note that the use of a sufficient amount of a suitable mineral addition is one of the most efficient measures for the AAR prevention, by controlling expansion when a reactive aggregate is used in the production of concrete (Thomas, 2011).

2. MATERIALS AND METHODS

2.1. Materials

In the present work, a special cement produced by the Brazilian Association of Portland Cement (ABCP), containing high alkali contents and indicated for accelerated AAR tests was used. Additionally, an ordinary Portland cement CP V ARI-RS (equivalent to type V cement, high sulfate resistance, according to ASTM C150), composed of clinker and calcium sulphate, non-mitigating of the alkali-aggregate reaction, was used so as to evaluate the effect of the additions (metakaolin and silica fume).

Portland cement CP V ARI, metakaolin, silica fume, sand and gravel commercialized in the city of Salvador, BA, Brazil, water from the public supply system and a water-based superplasticizer chemical additive were used.

2.2. Methods

2.2.1 Materials characterization

Characterization of the materials included the physical parameters, such as the specific surface area (estimated by BET, using a Micromeritics Gemini 2370V1.02 surface area analyzer) and specific gravity (Micromeritics Accupyc 1330V2.01 helium pycnometer) for the cement, metakaolin and silica fume. Sieving was done according to Brazilian standard NBR 9776 ("Aggregates - Determination of the specific mass of small aggregates by Chapman flask"), for the sand. The chemical composition of the cement was determined by X-ray diffraction (XRD).

2.2.2 Mortar molding

The mortar mix proportions were 1.0 : 3.0 (Portland cement : sand) and the water/binder ratio was 0.6 (by weight), with the mineral additives and superplasticizer additive present in varying contents according to Table 1.

Table 1. Material consumption needed to produce 1m³ of mortar with silica fume or metakaolin.

Content	Cement (kg)	Sand (kg)	Water (kg)	Additive (kg)	Silica Fume or Metakaolin (kg)	Water/binder ratio	Water/cement ratio
REF	485.45	1456.35	291.27	1.37	0.00	0.60	0.60
10%	436.90	1456.35	291.27	3.55	48.55	0.60	0.67
15%	412.63	1456.35	291.27	7.10	72.82	0.60	0.71
20%	388.36	1456.35	291.27	14.20	97.09	0.60	0.75

In order to relate the physical properties of the mortars to their behavior according to the alkali-aggregate reaction and to analyze the influence of mineral additions, some tests were performed on the mortars used. The experimental study involved mechanical strength tests (ABNT, 2005), water capillarity and apparent density tests using the Archimedes principle.

The AAR expansion was measured using prismatic specimens (25×25×285 mm³) into which steel bars were inserted during molding, according to NBR 15577/2008 Parts 4 and 5 (ABNT 2004a; ABNT 2004b). These tests were carried out to verify the aggregates reactivity in relation to the alkali-aggregate reaction and the capacity of the mineral additions to mitigate this reaction.

A minimum of 4 samples were tested for each mixture.

2.2.3 Mortar performance analysis

a) Mechanical resistance

For mechanical strength performance analysis, axial compression and flexural tensile strength tests were performed at 3, 7 and 28 days, according to NBR 13279 (ABNT, 2005).

The axial compression strength (R_C) is given by the ratio between the maximum load (P) supported by the specimens and the specimens original section area (A), according to equation (3).

$$R_C = \frac{P}{A} \quad (3)$$

The flexural tensile strength (R_{TF}) is determined by equation (4).

$$R_{TF} = \frac{PL}{B.D^2} \quad (4)$$

Where P = maximum load applied, in N; L = distance between support blades, in mm; B = specimen width in the section of rupture, in mm; D = specimen height in the breaking section, in mm.

b) Apparent Density and Porosity

For the determination of the apparent density and porosity of the concretes, the Archimedes principle was used. The technique consists of comparing the masses of the test specimens, 28 days during, before and after immersion in water. The samples are weighed still dry (M_s) and then immersed in water for 24 hours. After this period, the immersed mass (M_i) and the wet mass (M_u) are determined. With these values, the apparent porosity (P_a) and the apparent density (D_a) are calculated using Equations 5 and 6.

$$\% Pa = 100 \cdot \frac{Mu - Ms}{Mu - Mi} \quad (5)$$

$$Da = \rho \cdot \frac{Ms}{Mu - Mi} \quad (6)$$

In which ρ is the density of the liquid used (in this case, the water, ρ equals 1.0 g/cm³).

c) Sorptivity

The sorptivity is defined as a measure of the capacity of the matrices to absorb or desorb liquid by capillarity. High sorptivity is an indicator of a greater diffusion of elements and solutions in the cementitious matrix, increasing the chances of AAR occurrence.

Capillary water absorption (sorptivity) was determined from specimens measuring 40 mm x 40 mm x 160 mm. The specimens were demolded 24 hours after being cast and were cured for 28 days in a humid chamber (>95% RH). During the test, the saturated mass of the specimens with time intervals standardized by the NBR 9779:2012 ("Mortar and hardened concrete - Determination of water absorption by capillarity") is determined. The capillary absorption coefficient (or absorptivity, S), which represents the mass of water absorbed per square meter of the mortar in contact with water, can be calculated as a function of the square root of the time elapsed until reaching this point of absorption.

2.2.4 Alkali-Aggregate Reactivity (AAR) determination

To evaluate the reactivity of the Salvador metropolitan region aggregates to AAR, the Brazilian standard NBR 15577-4 (ABNT, 2008a) was used. This method consists of evaluating the dimensional mortar bars expansion subjected to a sodium hydroxide alkaline solution at 80°C.

For the mortar preparation, the gravels must be obtained with minimum crushing in order to produce a product classified according to the standard. Bars (25 mm x 25 mm x 285 mm) were molded with weight ratios of cement: aggregate 1: 2.25 and with ratio water/cement fixed and equal to 0.47, using a special cement produced by ABCP, suitable for conducting this type test and meeting the ABNT NBR 5732 (ABNT, 1991) requirements.

2.2.5 Efficiency evaluation of the active additions in mitigating the occurrence of AAR

The method defined by NBR 15577-5 (ABNT, 2008b), using the same principle as the ABNT method NBR 15577-4 (ABNT, 2008a) is recommended to evaluate the efficiency of pozzolanic materials to mitigate expansion due to AAR.

In this method mixtures are made with additions and without additions. Three mortar bars with dimensions 25 mm x 25 mm x 285 mm were made for each. Portland cement CPV ARI-RS (equivalent to type V cement, according to ASTM C150) was used, which proved to be non-mitigating to the AAR and the reactive aggregate available in the region.

The expansion measures are done in a similar way to NBR 15577-4 (ABNT, 2008a), and after 30 days the comparative expansion analysis in the reference mortar bars (without additions) and the mortar bars with addition of metakaolin and silica fume, in the contents of 10%, 15% and 20% are carried out. As a result, it is possible to see whether or not the material contributed to the reduction of expansion caused by the AAR.

3. RESULTS AND DISCUSSIONS

3.1. Materials characterization

The chemical composition of the cement and the physical characteristics of the materials used in the study are shown in Tables 2 and 3.

Table 2. Cement chemical composition, determined by XRD.

SiO ₂	Al ₂ O ₃	Fe ₂ O ₃	CaO	MgO	Alkali Content		
					Na ₂ O	K ₂ O	Na ₂ O _{eq} *
19.10	4.84	3.19	61.12	2.73	0.24	0.70	0.70

$$* \text{Na}_2\text{O}_{\text{eq}} = \text{Na}_2\text{O} + 0,658\text{K}_2\text{O}$$

Table 3. Physical Characteristics of the Materials

Properties	CPV ARI RS	Metakaolin	Silica fume	Sand
Specific gravity (g/cm ³)	3.08	2.68	2.35	2.66
Specific surface area BET (m ² /g)	0.33	16.85	9.78	-
Sieve 75 μm (%)	2.39	-	-	-

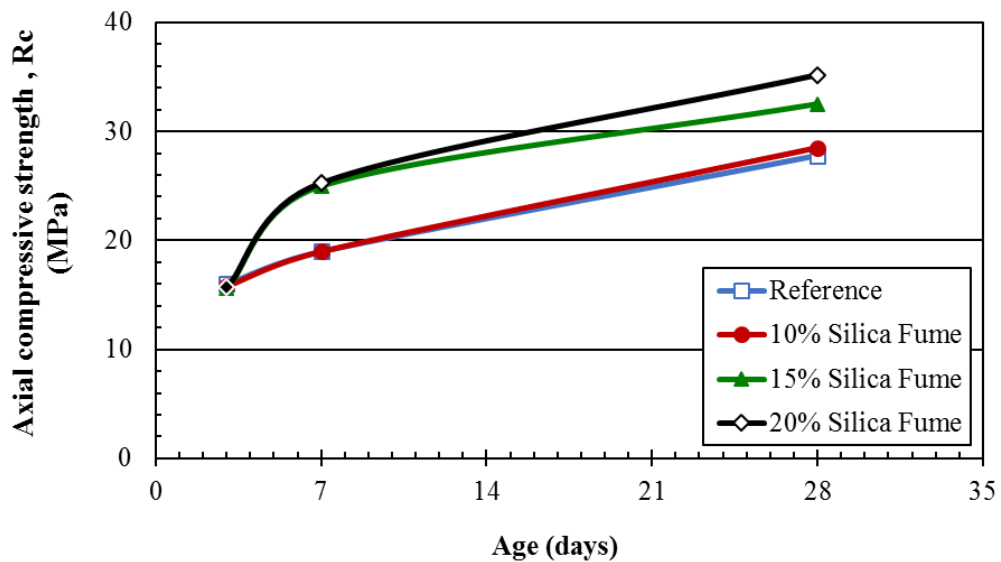
3.2 Mortar performance analysis

Figures 1 and 2 present the compressive strength and flexural tensile strength results, at 3, 7 and 28 days, of the mortars with partial cement replacement with silica fume and metakaolin, respectively. The traces used were 1: 3, with water / binder ratio (cement + addition) equal to 0.6, according to Table 1. A super plasticizing additive was also used in order to ensure the workability of the mixture.

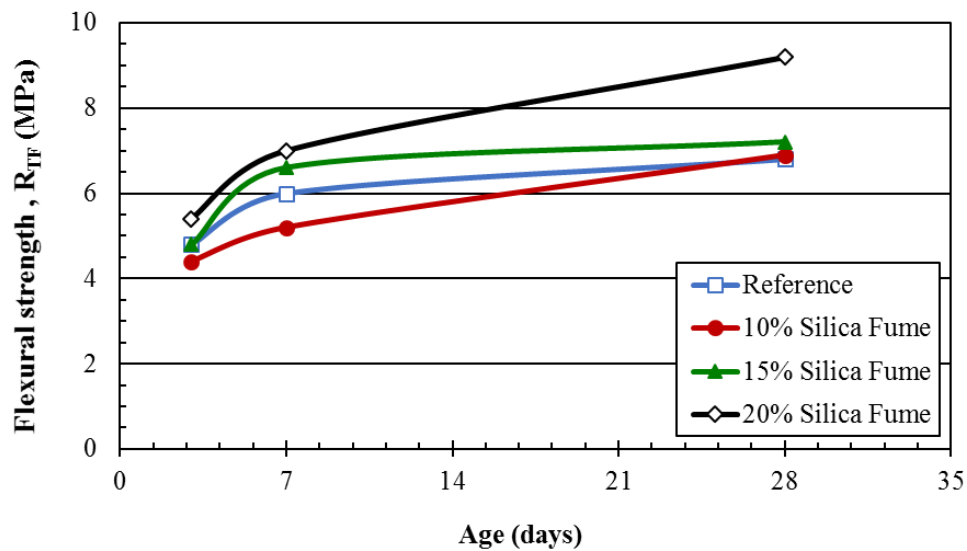
It can be observed that as the silica fume content increases, there is an increase in the mechanical strength of the mortar, reaching axial compression values of 35.2 MPa with 20% silica fume, while the reference mortar presented a resistance of 27.8 MPa (a 27% increase). Similar behavior is observed for the flexural tensile results, however, for silica fume contents of less than 20%, at 28 days, the specimens showed a resistance close to the reference for the mortar specimens.

The increase in strength is also observed with 15% metakaolin (Figure 2), where the axial compression reached 32.5 MPa, while the reference mortar presented a resistance of 27.8 MPa (a 17% increase). Although the mortars of 10% showed less resistance than the reference mortars, the results are in very close error ranges, and it was concluded that there was no considerable resistance variation with a 10% addition of material.

In the flexural tensile results, no significant resistance increase was observed in the mortar with the addition. This behavior was also observed by Beltrão (2010) when testing concrete specimens with added metakaolin contents of 6%, 10% and 14%.



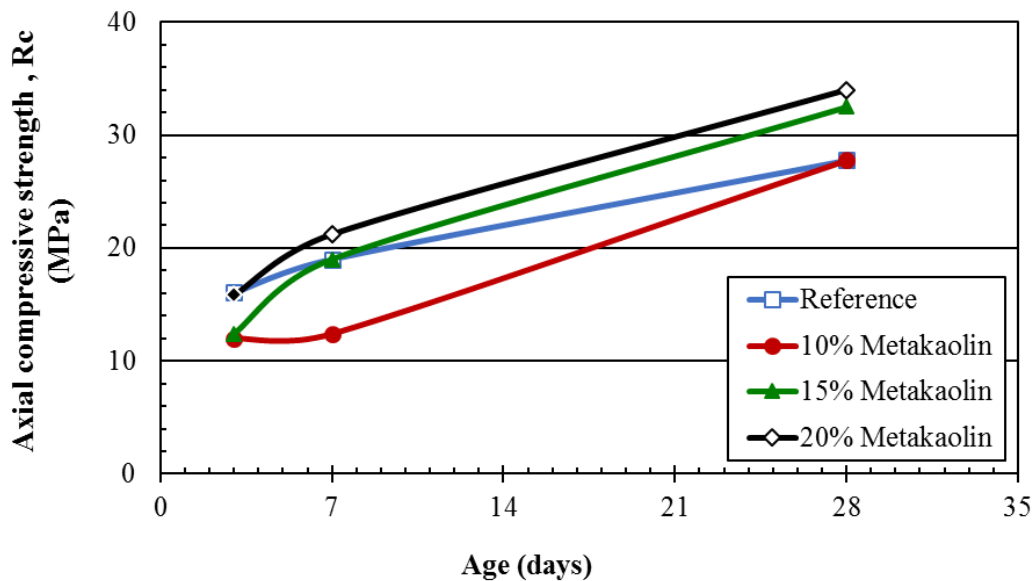
(A)



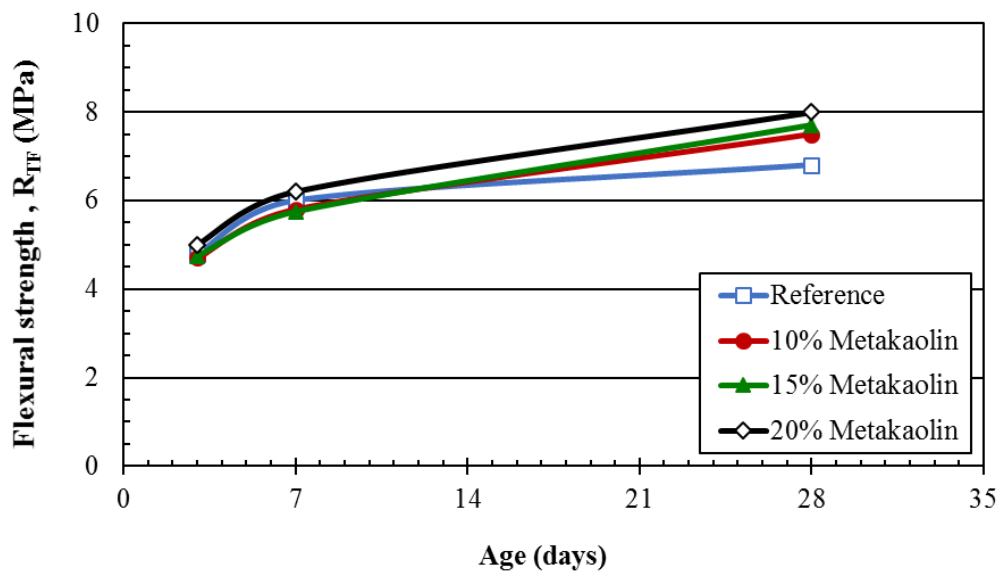
(B)

Figure 1. (A) Axial compressive and (B) flexural tensile strength of mortars containing silica fume, partially replacing Portland cement, as a function of days of curing.

According to Hassan et al. (2012) the compressive strength results at 28 days show that the addition of any metakaolin content increases the compressive strength of the concrete. However, there is no "linearity" in the relationship between the content used and the increase in resistance because concrete with 8% metakaolin showed better results than with 11%. Munhoz (2007) also observed a decrease in compressive strength when comparing the results of specimens with active additions of 5% and 10%, the result was 10% lower when compared with contents of 5% up to 20%. In addition, an improvement of only 7% in the compressive strength was observed with the 8% of metakaolin addition, when using contents up to 25% (Munhoz, 2007). It is possible that "mortar saturation" occurred because the available addition amount was much greater than the calcium hydroxide amount (cement hydration product). With this "disproportional" relationship, the pozzolanic reaction will occur more slowly, delaying the formation of C-S-H and resulting in a smaller increase in the resistance with high addition contents (Beltrão, 2010) as a result.



(A)



(B)

Figure 2. (A) Axial compressive and (B) flexural tensile strength of mortars containing metakaolin, partially replacing Portland cement, as a function of days of curing.

The increase in the mortar resistance with the addition of silica fume and metakaolin occurs because pozzolana, together with calcium hydroxide, generates binding products, like the phases resulting from the direct hydration of the clinker grains. Consequently, the structure is more compact, chemically and mechanically stronger than that of ordinary Portland cement. Thus, the presence of pozzolanic cements contributes to greater compactness and compressive strength after 28 days curing and greater impermeability to water (Giordano, 2007).

The use of silica and metakaolin in cement produces a less permeable mortar as expected and also observed in studies by Gomez-Zamorano et al. (2015). From the characterization results (Table 3), it is possible to observe that silica and metakaolin are finer than cement and thus they have a larger surface area. The finer particles of these materials tend to decrease the relative amount of capillary pores, reflecting a reduction in water absorption by capillarity, as seen in Figure 3.

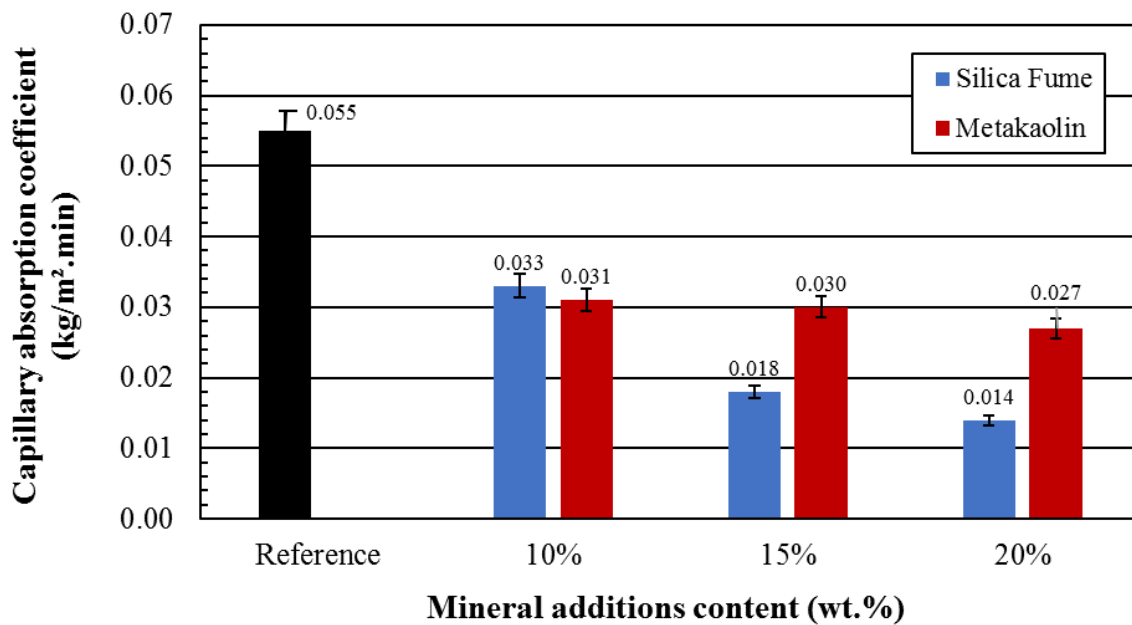


Figure 3. Capillary absorption coefficient of mortars containing silica fume and metakaolin partially replacing the Portland cement after curing for 28 days.

Figures 4 and 5 presents the apparent density and porosity results for the reference mortars (without addition) and those containing silica fume and metakaolin in partial replacement of the Portland cement. It can be observed that there is no significant variation in mortar density when partially replacing Portland cement with pozzolanic materials, however, a significant increase in porosity is observed when using silica and a reduction in porosity is observed when using metakaolin.

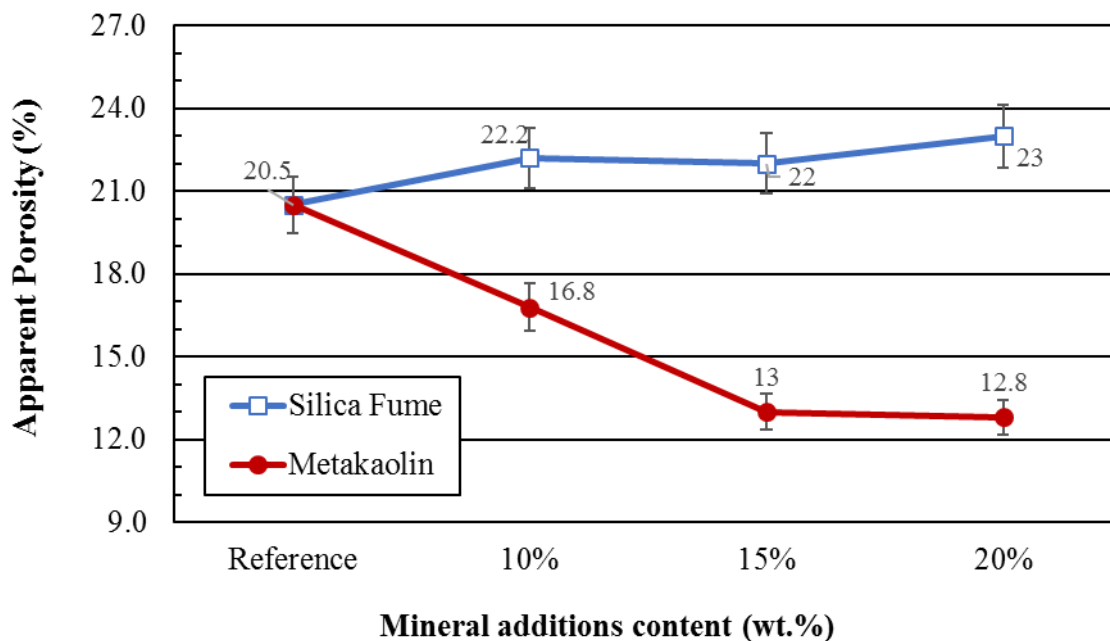


Figure 4. Apparent porosity of mortars containing silica fume and metakaolin partially replacing the Portland cement after curing for 28 days

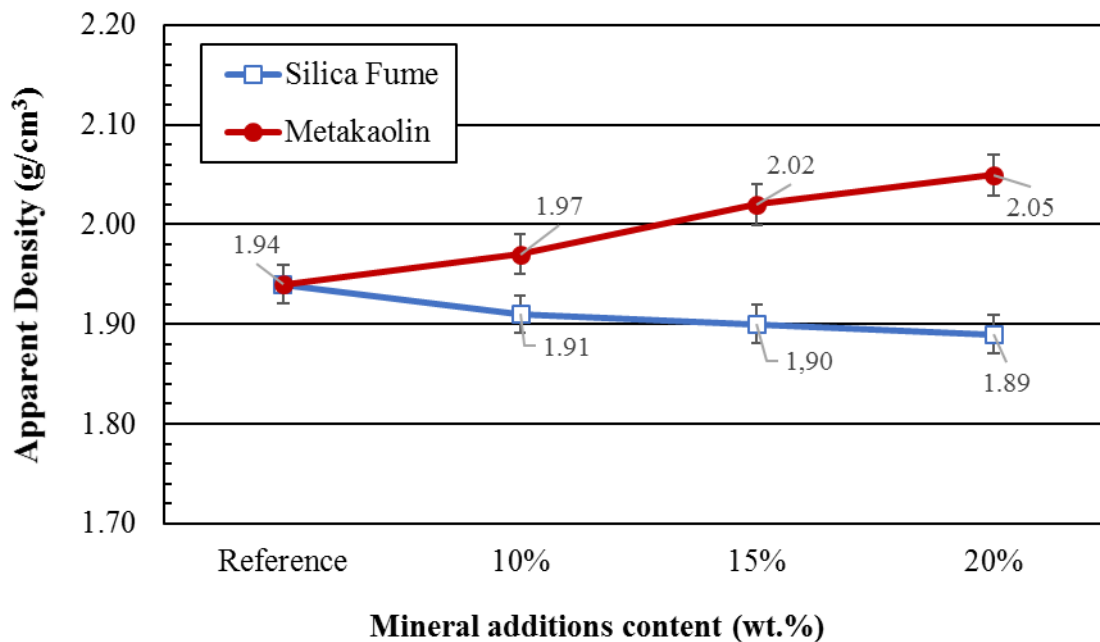


Figure 5. Density of mortars containing silica fume and metakaolin partially replacing the Portland cement after curing for 28 days

Since metakaolin and silica fume are finer than cement, it is expected that there will be pore filling, as well as its refinement and, consequently, porosity reduction.

The results reported by Siddique (2011) indicate that the use of silica fume reduces the porosity of the cement unlike what was observed in this work. It is believed that the use of the additive without partial water reduction influenced this behavior. This is because despite the water / binder ratio being constant, the w/c ratio varied, as shown in Table 1. For higher silica contents, a higher a/c ratio and, consequently, a higher water amount in the mixture is observed. The additional water, which is not consumed in the hydration of the cement, remains free in the system and, upon evaporation, gives rise to the increase in the porosity of the mortar.

3.3 Aggregates reactivity determination of the Salvador metropolitan region

Some sands and gravels from deposits located in the metropolitan region of Salvador (SMR) and Feira de Santana were analyzed. Figure 6 presents the results of the mortar bars expansion, submitted to the AAR test, as a test time function, for several gravels. According to the NBR 15577: 2008, for AAR tests for the evaluation of gravels, they must be ground in order to obtain a desired granulation similar to sand.

Figure 7 shows the results of the mortar bar expansions, submitted to the AAR test, as a test time function, for sands marketed in SMR and in Feira de Santana.

Analyzing the results obtained with the aggregates used, it can be observed that, in general, the gravels are reactive regarding AAR, whereas the sands are potentially innocuous. Therefore, there are restrictions on the use of gravels in SMR. Depending on the moisture conditions and the selected cement, it will be necessary to use active additions in the cement to mitigate the AAR.

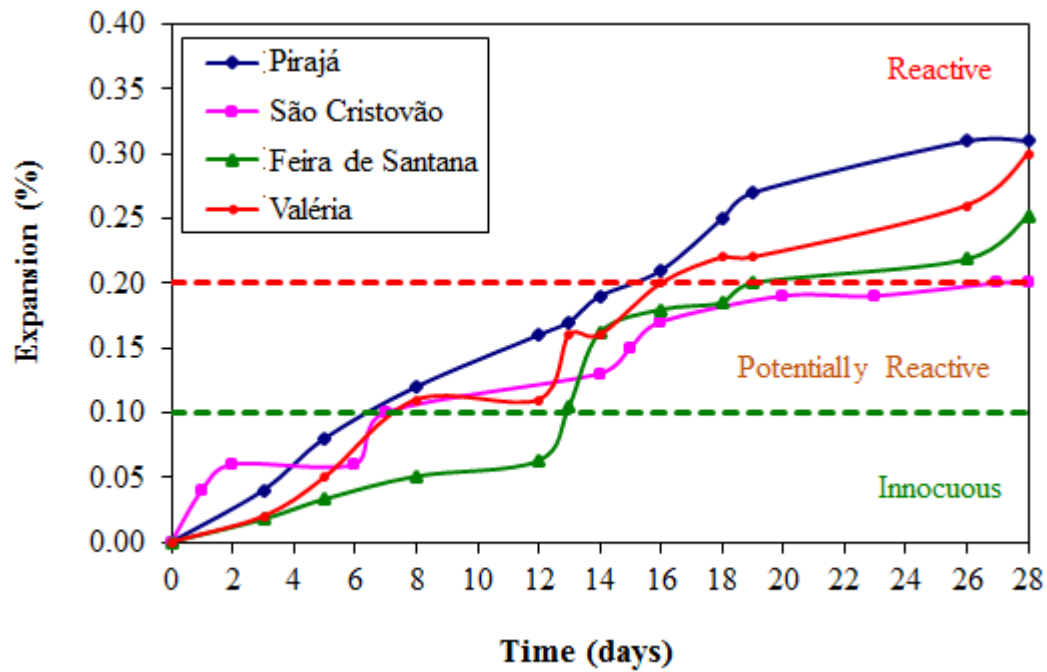


Figure 6. Expansion, due to AAR, in mortars containing gravels used in Salvador, Bahia, Brazil.

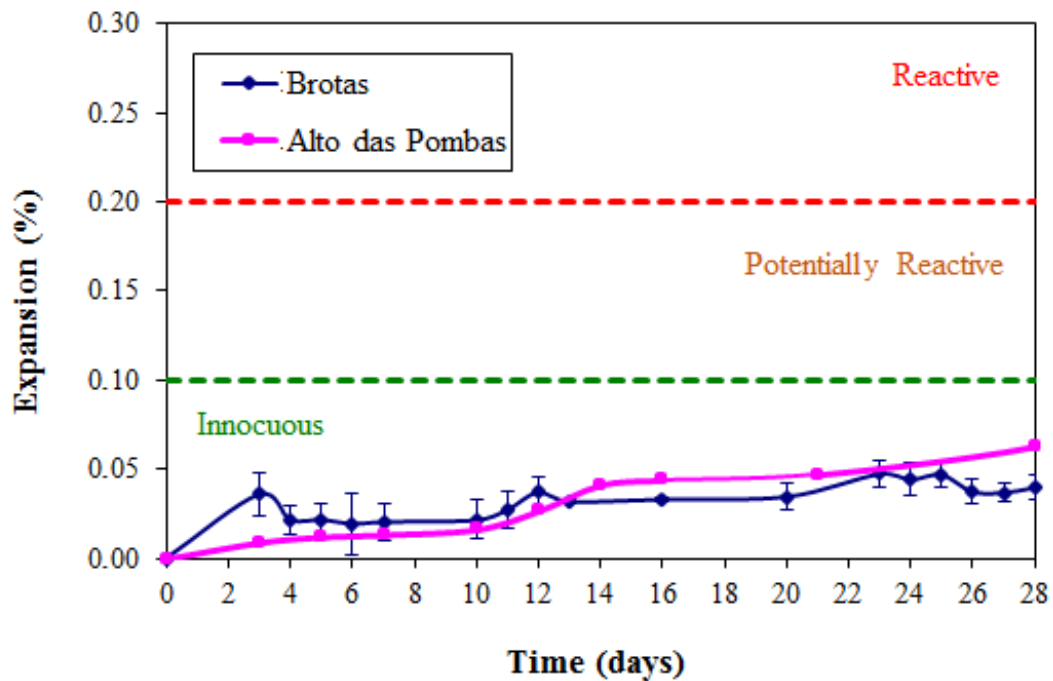


Figure 7. Expansion due to AAR in mortars containing sands used in Salvador, Bahia, Brazil.

3.4 Efficiency evaluation of the mineral additions in AAR mitigation

The results of the investigations of the expansions carried out using the accelerated method in the presence of silica fume and metakaolin are presented in Figures 8 and 9, respectively.

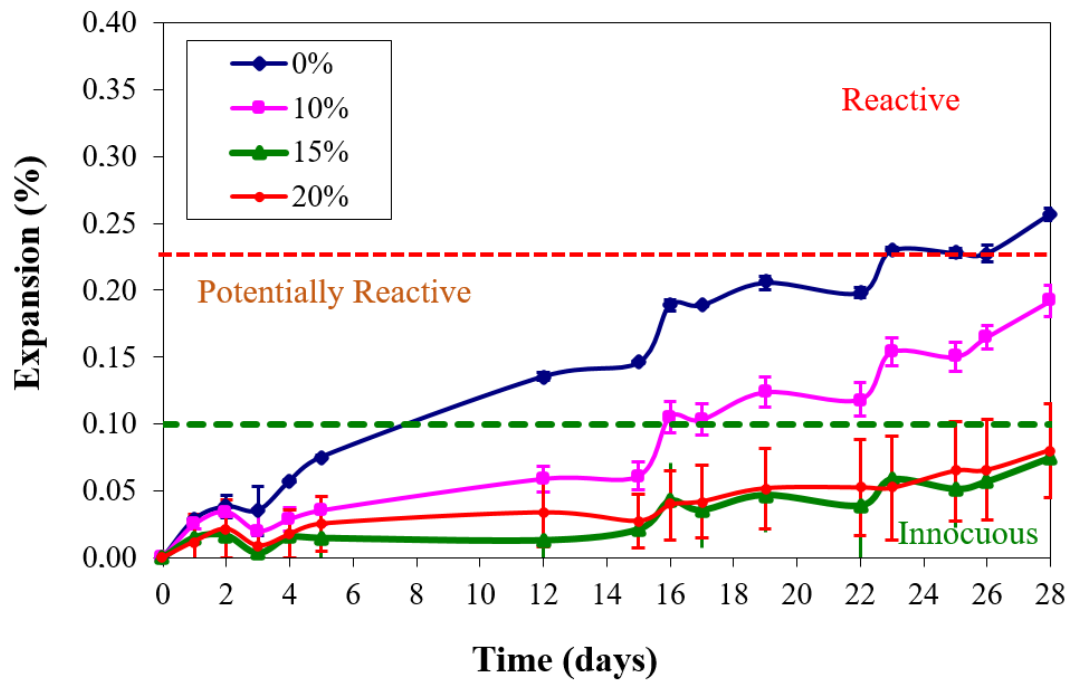


Figure 8. Expansion due to AAR in mortars with varying silica fume contents added.

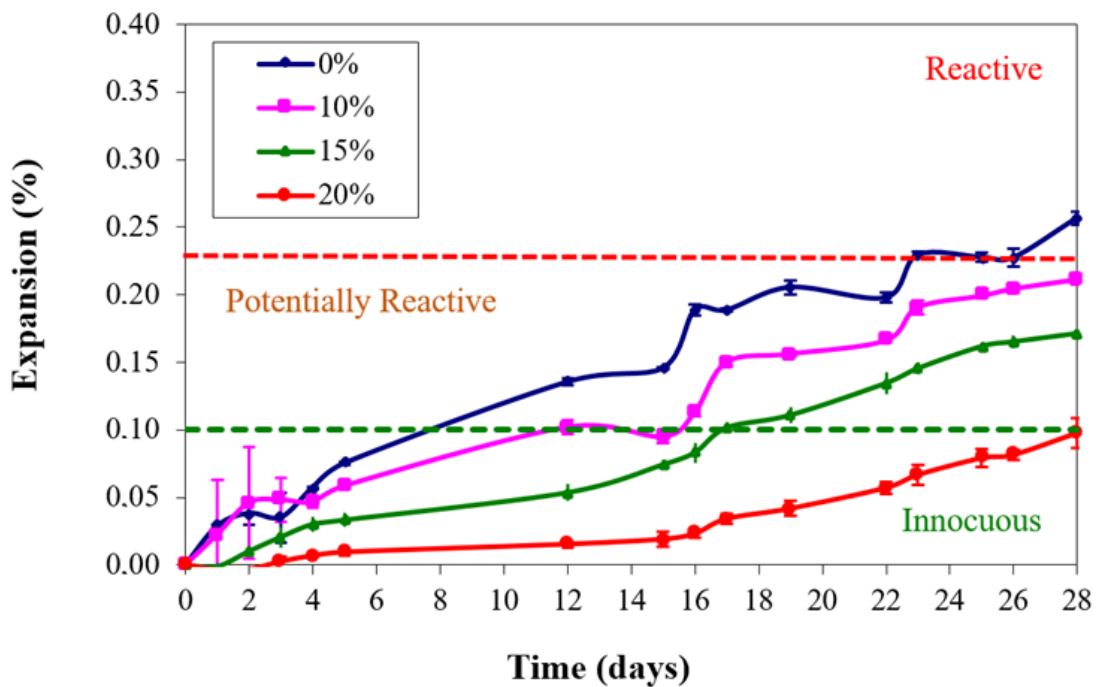


Figure 9. Expansion, due to AAR in mortars with varying metakaolin contents added.

The behavior of the mortar specimens with the addition of silica fume (Figure 8) was similar to that observed by several authors (Thomaz, 2011; Hasparyk and Farias, 2013; Lindgard et al., 2012), who found that this contributes to the reaction mitigation due to the pozzolanic properties of the material.

The works cited used maximum levels of silica fume between 12% and 15%, however, in the present research, higher levels were added in order to verify if the indiscriminate use of this material

interferes in the AAR. It was found that when the content reached 15%, there was a stagnation in the mitigation capacity of this additive. Thus, when using higher amounts than this no improvement in the material behavior is expected, and it may even result in an inverse behavior, that is, an AAR increase. This is because the silica fume is amorphous silica and therefore reactive, therefore it is thought that if used in excess, a "saturation" of this material can occur in the interstitial pores of the cementitious matrix. Part of the silica fume will react with $\text{Ca}(\text{OH})_2$ as a pozzolanic material, and the excess will be available to react with the alkalis which have not been incorporated into the C-S-H structure.

The behavior of the specimen with the addition of metakaolin (Figure 9) was similar to that observed by other authors (Munhoz, 2007; Hasparyk and Farias, 2013). The increase in the metakaolin content contributed to the mitigation of the reaction due to the pozzolanic properties of this material. An increasing reduction in reactivity was observed when higher contents of metakaolin was added. The Brazilian standard determines that the reaction mitigation proof is obtained when the accelerated test result in mortar bars is less than 0.10% at 16 days (França et al, 2016). From the results obtained, it is possible to predict that by using metakaolin contents higher than 15%, there will be a greater reduction in expansion and it will be possible to mitigate the AAR. However, these results were only effective when adding 20% of this material.

When comparing the performance of the mineral additions, it can be observed that the silica fume was more effective in mitigating the occurrence of AAR.

4. CONCLUSIONS

From the results of the present study, we conclude that:

- All the gravels commercially available in the metropolitan region of Salvador and Feira de Santana, studied in the present research, can be classified as reactive aggregates regarding AAR
- The small aggregates marketed in the metropolitan region of Salvador, from deposits in the Camaçari region, are classified as potentially innocuous aggregates in relation to the AAR
- The mortar performance analysis confirmed that the silica fume and metakaolin improves the properties of the cementitious matrix, resulting in mortars that are more resistant to compression and tensile in flexion and have lower permeability
- The silica fume proved to mitigate the expansions caused by AAR, reaching saturation point at 15% addition
- When used in excess, occur a silica fume "saturation" in the interstitial solution of pores in the cementitious matrix leading to parts that will not react with the excess $\text{Ca}(\text{OH})_2$ to be available to react with the alkalis that were not incorporated into the CSH structure
- The metakaolin showed an increased capacity to mitigate the expansions caused by the AAR when applied at levels of 10%, 15% and 20%
- The silica fume was more effective in AAR mitigation than metakaolin.

5. ACKNOWLEDGMENTS

The authors thank LC Lacrose, Metacaulim do Brasil, Companhia de Ferro Ligas da Bahia (Ferbasa), Vedacit and Mizu Cimentos, who donated the materials used in the research. We also thank the National Council for Scientific and Technological Development (CNPq) and the Foundation for Research Support of the State of Bahia (FAPESB) for financial support.

6. REFERENCES

- Associação Brasileira de Normas Técnicas (1991). *NBR 5732: Cimento Portland comum*. Rio de Janeiro.
- Associação Brasileira de Normas Técnicas (1998). *NBR NM 76: Cimento Portland – Determinação da finura pelo método de permeabilidade ao ar - Método de Blaine*. Rio de Janeiro.
- Associação Brasileira de Normas Técnicas (2005). *NBR 13279: Argamassa para assentamento e revestimento de paredes e tetos - Determinação da resistência à tração na flexão e à compressão*. Rio de Janeiro
- Associação Brasileira de Normas Técnicas (2005). *NBR 13279: Argamassa para assentamento e revestimento de paredes e tetos - Determinação da resistência à tração na flexão e à compressão*. Rio de Janeiro
- Associação Brasileira de Normas Técnicas (2008a). *NBR 15577: Agregados – Reatividade álcali-agregado. Parte 4: Determinação da expansão em barras de argamassa pelo método acelerado*. Rio de Janeiro
- Associação Brasileira de Normas Técnicas (2008b). *NBR 15577: Agregados – Reatividade álcali-agregado. Parte 5: Determinação da mitigação da expansão em barras de argamassa pelo método acelerado*. Rio de Janeiro
- Associação Brasileira de Normas Técnicas (2012). *NBR 9779: Argamassa e concreto endurecidos - Determinação da absorção de água por capilaridade*. Rio de Janeiro
- Beltrão, F. C. M. (2010), “*A influência do metacaulim nas propriedades do concreto*”, Trabalho de conclusão de curso. Universidade da Amazônia, Belém, p.44.
- Beyene, M., Snyder, A., Lee, R. J., Blaskiewicz, M. (2013), *Alkali Silica Reaction (ASR) as a root cause of distress in a concrete made from Alkali Carbonate Reaction (ACR) potentially susceptible aggregates*. Cement and Concrete Research. 51(9). 85-95. DOI: <https://doi.org/10.1016/j.cemconres.2013.04.014>
- Campos, R. N. (2015) “*Durabilidade em concretos contendo cinza de biomassa contendo elevado teor de álcalis*”, Dissertação de Mestrado. Universidade Estadual de Feira de Santana, Feira de Santana, p. 89.
- França, D. F. S., Rey, R. O., Ferreira, L. R. C., Ribeiro, D. V. (2016) *Avaliação da reologia, da RAA e das propriedades de argamassas no estado fresco utilizando cinza de eucalipto como substituição parcial ao cimento Portland*. Ambiente Construído, 16 (3), 153-166, DOI: <http://dx.doi.org/10.1590/s1678-86212016000300098>
- Gamino, A. L. (2003), “*Reações álcali-agregado: análise da potencialidade de ocorrência em agregados utilizados no laboratório de engenharia civil da FEI/UNESP*”. In: V Simpósio EPUSP sobre Estruturas de Concreto, pp. 42-54.
- Giordano, B. L. (2007), “*Estudo da reação álcali-agregado dos agregados da região metropolitana de Belém*”. Trabalho de conclusão de curso. Universidade da Amazônia, Belém, p. 47.
- Gomez-Zamorano, L. Y., Iniguez-Sanchez, C. A. E., Lothenbach, B. (2015), *Microestructura y propiedades mecánicas de cementos compuestos: Efecto de la reactividad de adiciones puzolánicas e hidráulicas*. Revista ALCONPAT, 5 (1), 18-30. DOI: <http://dx.doi.org/10.21041/ra.v5i1.74>
- Hasparyk, N. P., Farias, L. A. (2013), “*Comportamento de adições e aditivos na expansão da reação álcali-agregado – Um estudo envolvendo reologia*”. In: 55º Congresso Brasileiro de Concreto, pp. 1-12.
- Hassan, A. A. A., Lachemi, M., Hossain, K. M. A. (2012), *Effect of metakaolin and silica fume on the durability of self-consolidating concrete*. Cement and Concrete Composites, 34(6), 801– 807. DOI: <https://doi.org/10.1016/j.cemconcomp.2012.02.013>

- Lindgard, J., Andiç-Çakir, O., Fernandes, I., Ronning, T. F., Thomas, M. D. A. (2012). *Alkali-silica reactions (ASR): Literature review on parameters influencing laboratory performance testing*. Cement and Concrete Research, 42(2), 223-243. DOI: <https://doi.org/10.1016/j.cemconres.2011.10.004>
- Munhoz, F. A. C. (2007), “*Efeito de adições ativas na mitigação das reações álcali-sílica e álcali-silicato*”. Dissertação de Mestrado. Universidade de São Paulo, São Paulo, 108 p.
- Siddique, R. (2011), *Utilization of silica fume in concrete: Review of hardened properties*, Resources, Conservation and Recycling, 55 (11) 923–932. DOI: <https://doi.org/10.1016/j.resconrec.2011.06.012>
- Thomas, M. (2011), *The effect of supplementary cementing materials on alkali-silica reaction: A review*. Cement and Concrete Research, 41(12), 1224–1231. DOI: <https://doi.org/10.1016/j.cemconres.2010.11.003>

Durability of concrete mixtures with different contents of activated fly ash

M. Rendón Belmonte¹ , M. Martínez Madrid¹ , R. V. Martínez Pérez¹ , J. T. Pérez Quiroz¹ 

*Contact author: marielarb17@hotmail.com

DOI: <http://dx.doi.org/10.21041/ra.v9i2.313>

Reception: 20/06/2018 | Acceptance: 28/02/2019 | Publication: 30/04/2019

Responsible Associate Editor: Dr. Pedro Garcés Terradillos

ABSTRACT

This article describes properties related to the durability of five different mixtures of concrete with different contents of activated fly ash (AFA) and Portland cement (CPC 40). The measurements carried out were apparent speed of ultrasonic pulse, electrical resistivity, fast ion permeability of chloride and mechanical resistance to compression. The performance of all mixtures proved to be durable, and the development of the electrical resistivity and the decrease in the level of the chloride ion permeability were enhanced by the contents of AFA, although the resistance to compression at higher contents of AFA was minor. The maximum percentage of AFA to comply with the current criteria of durability was 65%.

Keywords: activated fly ash; durability; ecological concrete.

Cite as: Rendón Belmonte, M., Martínez Madrid, M., Martínez Pérez, R. V., Pérez Quiroz, J. T. (2019), "Study of the durability of concrete mixtures with different contents of activated fly ash", Revista ALCONPAT, 9 (2), pp. 200 – 214, DOI: <http://dx.doi.org/10.21041/ra.v9i2.313>

¹ Instituto Mexicano del Transporte, México.

Legal Information

Revista ALCONPAT is a quarterly publication by the Asociación Latinoamericana de Control de Calidad, Patología y Recuperación de la Construcción, Internacional, A.C., Km. 6 antigua carretera a Progreso, Mérida, Yucatán, 97310, Tel.5219997385893, alconpat.int@gmail.com, Website: www.alconpat.org

Responsible editor: Pedro Castro Borges, Ph.D. Reservation of rights for exclusive use No.04-2013-011717330300-203, and ISSN 2007-6835, both granted by the Instituto Nacional de Derecho de Autor. Responsible for the last update of this issue, Informatics Unit ALCONPAT, Elizabeth Sabido Maldonado, Km. 6, antigua carretera a Progreso, Mérida, Yucatán, C.P. 97310.

The views of the authors do not necessarily reflect the position of the editor.

The total or partial reproduction of the contents and images of the publication is strictly prohibited without the previous authorization of ALCONPAT Internacional A.C.

Any dispute, including the replies of the authors, will be published in the first issue of 2020 provided that the information is received before the closing of the third issue of 2019.

Durabilidad de mezclas de concreto con diferentes contenidos de ceniza volante activada

RESUMEN

Este artículo describe propiedades referentes a la durabilidad de cinco mezclas de concreto con distintos contenidos de ceniza volante activada (CVA) y cemento portland tipo CPC 40. Los ensayos realizados fueron: velocidad de pulso ultrasónico, resistividad eléctrica aparente, permeabilidad rápida al ión cloruro y resistencia mecánica a la compresión. Los resultados indicaron que la calidad de todas las mezclas resultó durable, el desarrollo de la resistividad eléctrica y disminución del nivel de permeabilidad al ión cloruro fue favorecido por el contenido de CVA. En cuanto a las resistencias a la compresión, se notó que a mayor contenido de CVA estas resultaron menores. El porcentaje máximo de sustitución de CVA para cumplir con los criterios de durabilidad actuales resultó del 65%.

Palabras clave: ceniza volante activada; durabilidad; concretos ecológicos.

Durabilidade de misturas de concreto com diferentes teores de cinzas volantes ativadas

RESUMO

Este artigo descreve propriedades relativas à durabilidade de cinco misturas de concreto com diferentes teores de cinzas volantes ativadas (CVA) e cimento portland tipo CPC 40. Os ensaios realizados foram: velocidade de pulso ultrassônico, resistividade elétrica aparente, permeabilidade rápida ao íon cloreto e resistência mecânica à compressão. A qualidade de todas as misturas foi duradoura, o desenvolvimento da resistividade elétrica e a diminuição do nível de permeabilidade ao íon cloreto foi favorecido pelo conteúdo de CVA, embora a resistência à compressão em maior conteúdo de CVA tenha sido menor. O percentual máximo de substituição do CVA para atender aos critérios atuais de durabilidade foi de 65%.

Palavras chave: cinza volante ativada; durabilidade; concreto ecológico.

1. INTRODUCTION

Nowadays, concrete is the modern world's most widely used building material. Estimates indicate that, by the year 2050, the consumption of Portland cement could increase up to 225% with respect to the current values, mainly due to the high demand of this binder from emerging countries, such as China, India, Brazil and Mexico (Garcés et al., 2012). According to the CANACEM (National Chamber of cement), in 2016, cement production was 40.6 million tons and the consumption was 40.1 million tons.

It is known that the world production of cement produces approximately 7% of the generation of carbon dioxide in the atmosphere (Mehta, 2001; Nath et al., 2011). Also, structures built with cement in corrosive environments begin to deteriorate after 20 to 30 years, although they have been designed for more than 50 years of useful life (Chandra et al., 2015). With the purpose of reducing the use of natural resources, energy and emissions of carbon dioxide, the development of ecological concretes is being researched that besides from being friendly to the environment, provide sustainability and durability for the long service life of structures (Madhavi et al., 2014; Mishra, 2017).

One of the options that is being considered to achieve this is the partial replacement of Portland cement (CP), in particular with materials such as natural pozzolans, silica fume, slag and fly ash (FA) (Al-Amoudi et al., 1996; Malhotra, 1990; Mehta, 2002; Garcés et al., 2012; Moffatt et al., 2017; Mishra, 2017; Saha, 2018).

FA is an industrial byproduct generated in large quantities around the world, almost 800 million tons per year (Heidrich et al., 2013; International Energy Agency Coal Industry Advisory Board, 2014), but a significant amount of this material (around 50%) is deposited in landfills, causing a serious environmental risk and decreasing the reactivity of the FA due to weathering conditions (Mishra, 2017).

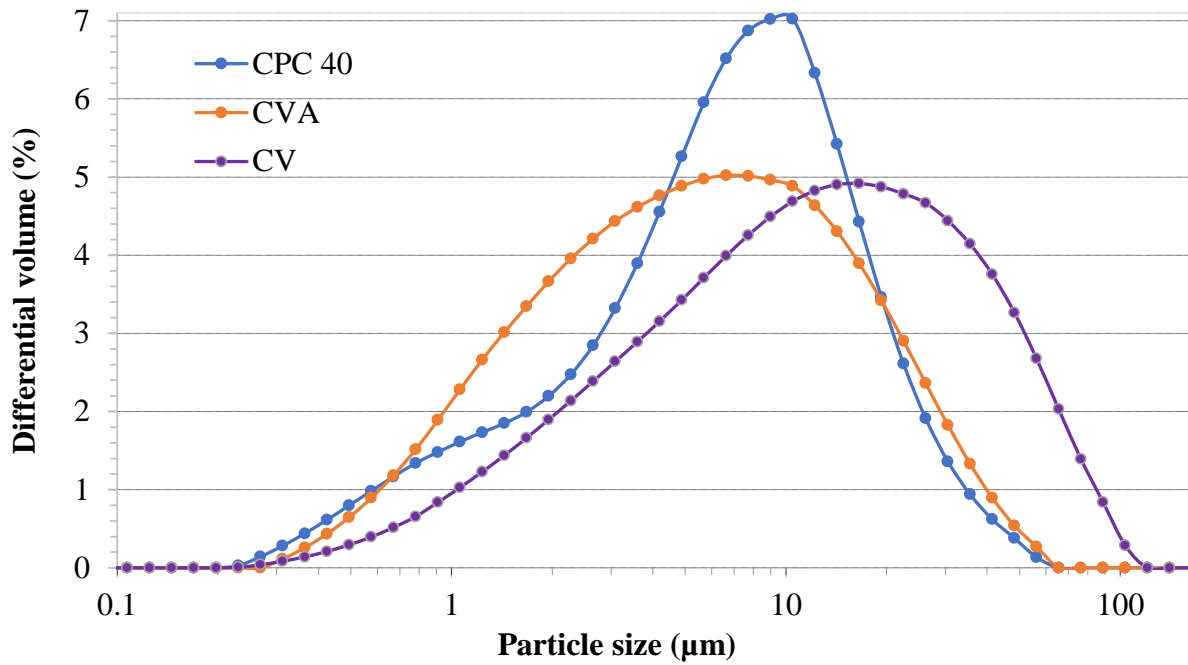
Even though FA has been used as an additive in concrete for a while and there is extensive research based on its use as a cement replacement material in concrete, the level of replacement according to the available literature is still limited to a maximum of 35% of cement mass. The latter is based on the argument that higher replacement percentages of FA do not improve the strength characteristics in its natural form (Hemalatha et al., 2017). To improve properties, increasing the percentage of FA replacement, different approaches were explored. These were: reduction of the water/cementitious material ratio, replacement of Portland cement of high initial strength by ordinary Portland cement, replacement of a portion of FA by a more reactive pozzolan, such as silica fume or rice husk ash, incorporation of nanomaterials and accelerated curing (Yu et al., 2017). Chemical, mechanical and thermal methods, or a combination of these methods, have also been used with the aim of improving the reactivity of this disposal (Mucsi, 2016; Sahoo, 2016). Alkaline activation consists of a chemical process that allows the transformation of a material with a partially or fully amorphous structure into compact cementing compounds (Palomo et al., 1999). Mechanical activation is defined as activation using a grinding process or using sieving and separation by air, and thermal activation refers to slow or fast cooling producing changes in the vitreous and crystalline relationships (Hela et al., 2013; Mucsi, 2016). In addition to these methods, there is electrometagenesis, which consists of the activation of FA from the entry of ions in an alkaline solution by the application of an electric field through the hardened concrete. (Lizarazo et al., 2015). Up until now, the use of FA is considered an effective solution (Zobal et al., 2017).

Considering the background use of FA, positive effects on concrete properties, low cost and current availability of FA in Mexico (stored), this article focuses on determining durability properties, which were: quality concrete through ultrasonic pulse velocity (UPV), apparent electrical resistivity (ρ), rapid chloride permeability, mechanical resistance to compression and mixtures with FA with different contents of Portland cement (CPC). The tested cement widely used in construction in Mexico, and the Mexican FA subjected to a chemical activation process using chemicals in the dust and a grinding method (with the aim of improving its reactivity). Due to the existence of a confidentiality contract, the characterization of the evaluated mixtures cannot be disclosed yet.

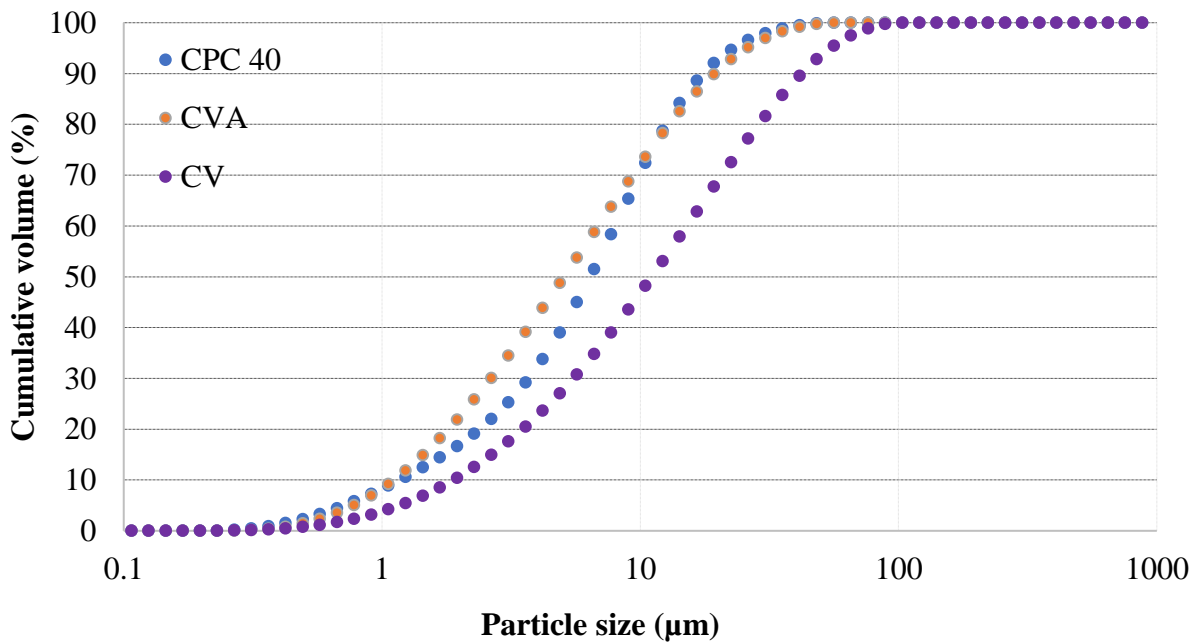
2. EXPERIMENTAL PROCEDURE

2.1. Materials

The raw materials used in this investigation were FA activated by the addition of chemicals from dust and grinding in a ball mill, limestone rock, and tap water. The Fraunhofer laser diffraction sizing distribution of the raw materials is shown in Figure 1. The suspension of particles was prepared in ethanol, used as a means of dispersing bath, and stirred ultrasonically for 5 mins. Portland cement (CPC) was used as received and FA was ground in a ring mill. As seen, 90% of CPC and activated fly ash (AFA) particles are less than 20 μm in size, whereas FA has a larger particle size when first received



(a)



(b)

Figure 1. Granulometry distribution by laser ray diffraction: a) particle distribution and b) particle size.

Table 1 shows characteristics of the aggregates used. These values were obtained according to the standards ASTM C127 and ASTM C128.

Table 1. Characteristics of the materials used for the manufacture of the mixtures.

Material	Density (kg/l)	Absorption (%)
Gravel 5-20 mm	2.67	0.9
Sand 0-5 mm	2.40	2.40

2.2. Preparation of test specimens

Five mixtures with different percentages of substitution of AFA (0, 30, 50, 65 and 75%) with respect to the weight of cement were prepared. The mixtures named, M1, M2, M3, M4, and M5, respectively, had a water/cement material ratio of 0.35. Additive thinning and water reducer were used to achieve this relationship. The proportions of the mixtures are presented in Table 2.

Table 2. Mixture design.

Material	Units	M1	M2	M3	M4	M5
Cement CPC 40	kg/m ³	450	315	225	157.5	112.5
CVA	kg/m ³	0	135	225	292.5	337.5
Gravel	kg/m ³	1006	1006	1006	1006	1006
Sand	kg/m ³	710	710	710	710	710
Curing condition	°C	Curing room	Curing room	Curing room	Curing room	Curing room
w/cm		0.35	0.35	0.35	0.35	0.35

*cm: cement material (FA+CPC or CPC)

The five mixtures cast into 10 cm × 20 cm cylindrical molds, were manufactured according to the standard procedure NMX-C-159-16, hydrated with tap water and cured following the standard NMX-C-148-10. After the curing period (28 days), all samples were kept at room temperature and in a wet condition. This was achieved by spraying the samples with water daily and keeping them in plastic containers.

2.3. Durability tests

The measurements carried out were ultrasonic pulse velocity (UPV) (ASTM C-597-02), apparent electrical resistivity (ρ) (NMX-C514-16), rapid chloride permeability (ASTM C1202-10) and compressive strength (NMX C-083-02) at different ages over 122 days. It is necessary to mention that, in each of the age tests of UPV and electrical resistivity, fifteen cylinders of each mixture along with three cylinders were evaluated and tested for compressive strength and rapid chloride permeability testing (two samples required).

3. RESULTS

Below, the results of each performed test are described.

3.1 UPV

Figure 2 presents the behavior of the ultrasonic pulse rate.

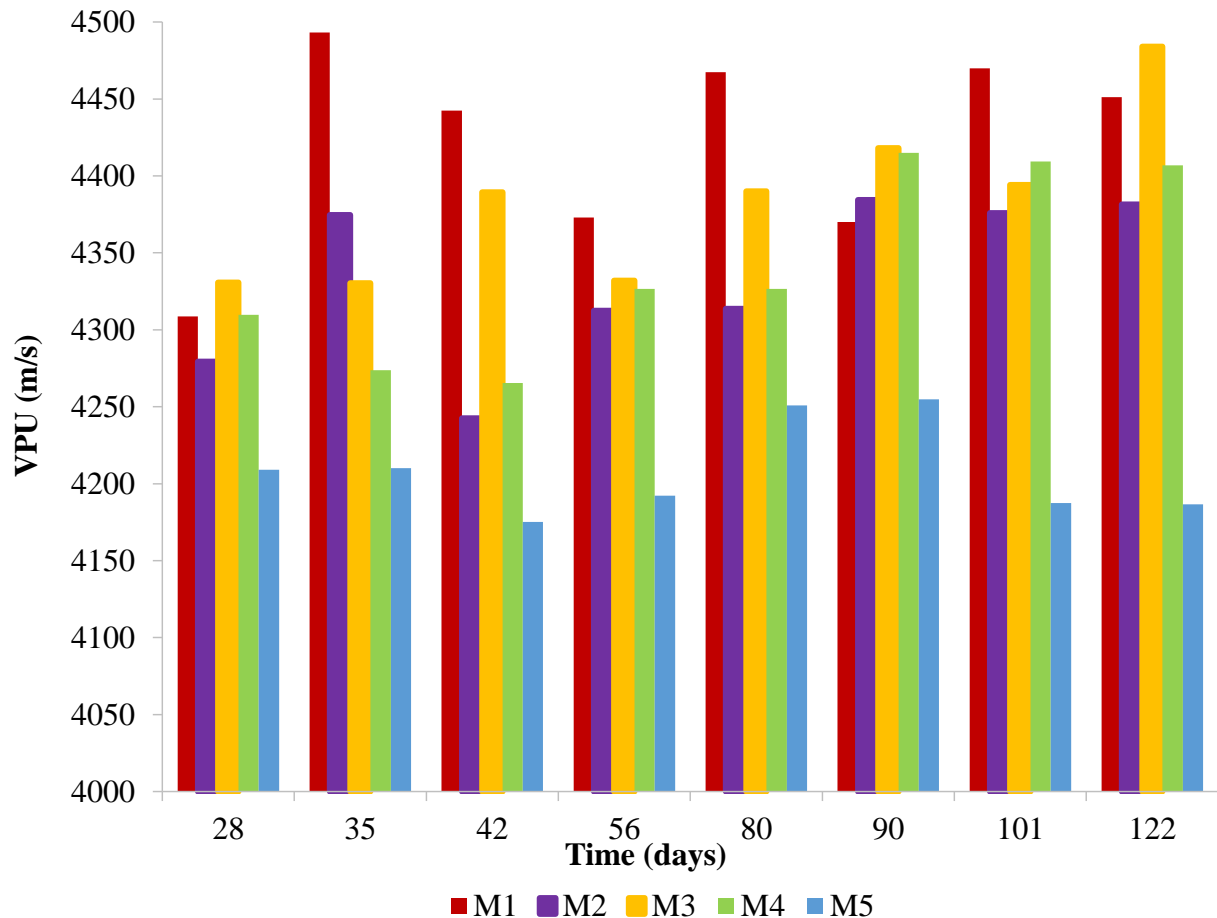


Figure 2. UPV at different ages of mixtures for M1, M2, M3, M4 and M5.

UPV values obtained in the five mixtures and for different age tests are reported in Figure 2. They were all above 4000 m/s, indicating that the quality in all cases was durable. However, in the mix with a higher content of AFA (M5), the values are lower compared to the rest of the mixtures. This behavior may be due to the lack of calcium hydroxide content in the mixture provided by the Portland cement.

The UPV results obtained in this research with AFA are like the results reported by Al-Amoudi who evaluated mixtures of concrete with and without FA (up to a 40%). The values are in the same order ~4000 m/s (Al-Amoudi et al., 1996).

3.2 Apparent electrical resistivity (ρ)

Figure 3 shows the apparent electrical resistivity of five mixtures with respect to time. Standard NMX-C-514 defines the apparent electrical resistivity as: “the resistivity measured on concrete not saturated with water”.

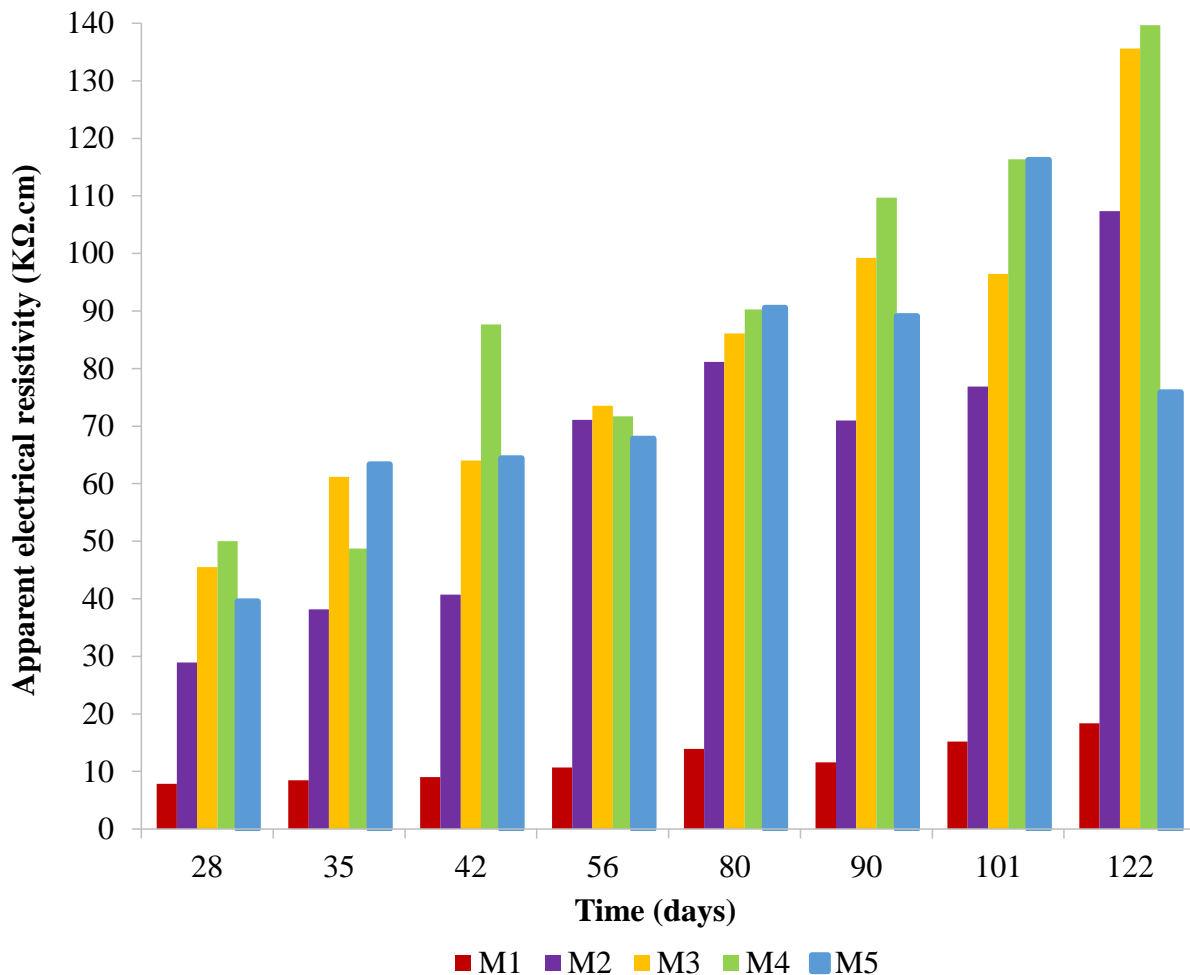


Figure 3. Apparent electrical resistivity at different ages for mixtures M1, M2, M3, M4 and M5.

According to Figure 3, the mixtures with AFA content showed apparent electrical resistivity values higher than the mixture without AFA (M1), which reached a maximum of 18 kΩ.cm. After 122 days, M2 reached 110 kΩ.cm, while M3 and M4 reached values close to 140 kΩ.cm. In the case of M5, there was a decay of the resistivity measurement at day 122; it decreased from 116 kΩ.cm to 76 kΩ.cm. An increase in the chloride ion permeability value was observed on this date as shown in Figure 3. This behavior is thought to be due to two possible causes: 1) at this age the AFA reaction is more sensitive to the moisture content in the concrete matrix, slowing down its reaction or 2) the ash content in the mixture is excessive to maintain a constant reaction of the AFA. However, even with the decrease seen in M5, the electrical resistivity values of the AFA mixtures exceeded those achieved with the M1 mixture (0% FA). From the criteria established in the Mexican standard NMX C-514-16 and Figure 3 values, the mixture M1 showed a considerable interconnected porosity, while the mixtures M2, M3 and M4 indicated extremely low interconnected porosity and M5 had low interconnected porosity.

3.3 Rapid chloride permeability

Figure 4 shows the results of the rapid chloride permeability test for the five mixtures. The reported values correspond to ages of 28, 56, 90 and 122 days.

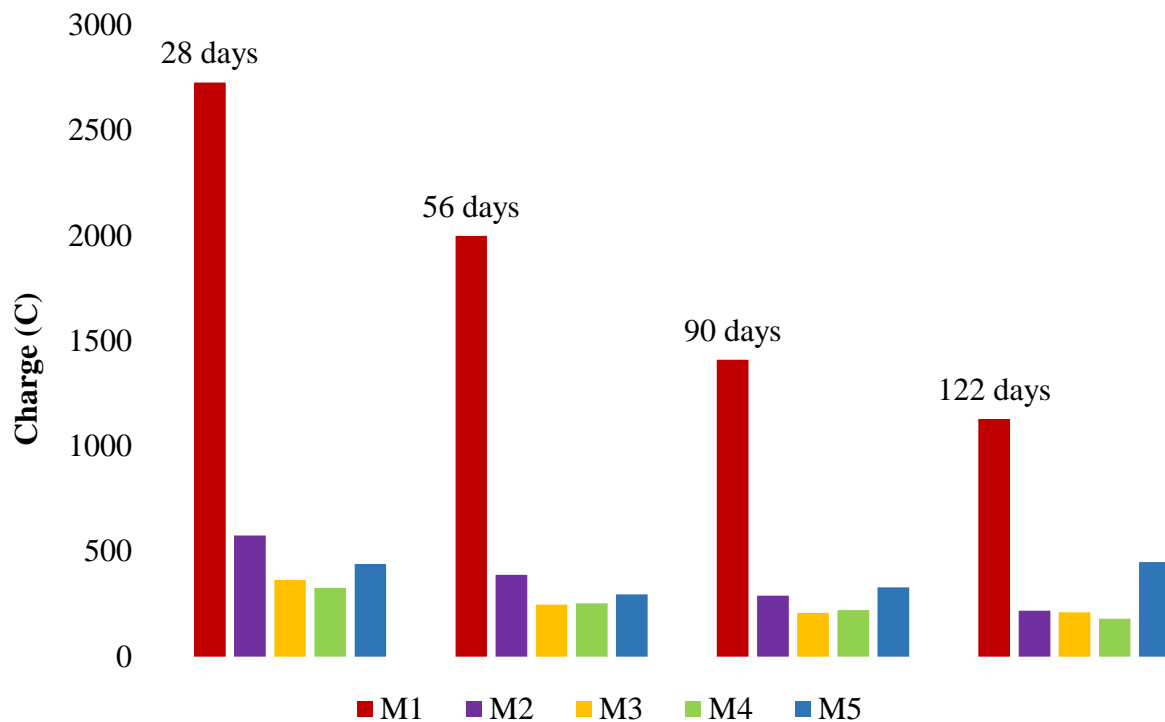


Figure 4. Rapid chloride permeability at different ages for mixtures M1, M2, M3, M4 and M5.

Considering the values of Figure 4 and the criteria established in standard ASTM C-1202-12, the results of the mixture without AFA (M1) initially showed values higher than 2500 C, but as the time increased it decreased to 1100 C after 122 days. With these values this mixture reached a level of penetrability of the chloride ion that was first moderate and then later low.

For mixtures with AFA content, the amount of charge that passed at all ages of evaluation was less than 500 C, which is a very low level of penetrability. The tendency of permeability with respect to time of M2, M3 and M4 was decreasing. The behavior was variable only in the case of M5, but it exceeded 500 C at no time.

Mixtures with AFA content showed lower chloride permeability compared to the mixture without AFA, these results coincide with investigations that report that the presence of FA promotes a low level of permeability to this ion (Malhotra, 1990; Nath et al., 2011; Saha, 2018; Mittal).

3.4 Compressive strength

Figure 5 shows the compressive strength and the standard deviation (σ in MPa) obtained from three tests of the mixtures at ages of 3, 7, 14, 28, 56 and 90 days, according to standard NMX-C-083-14.

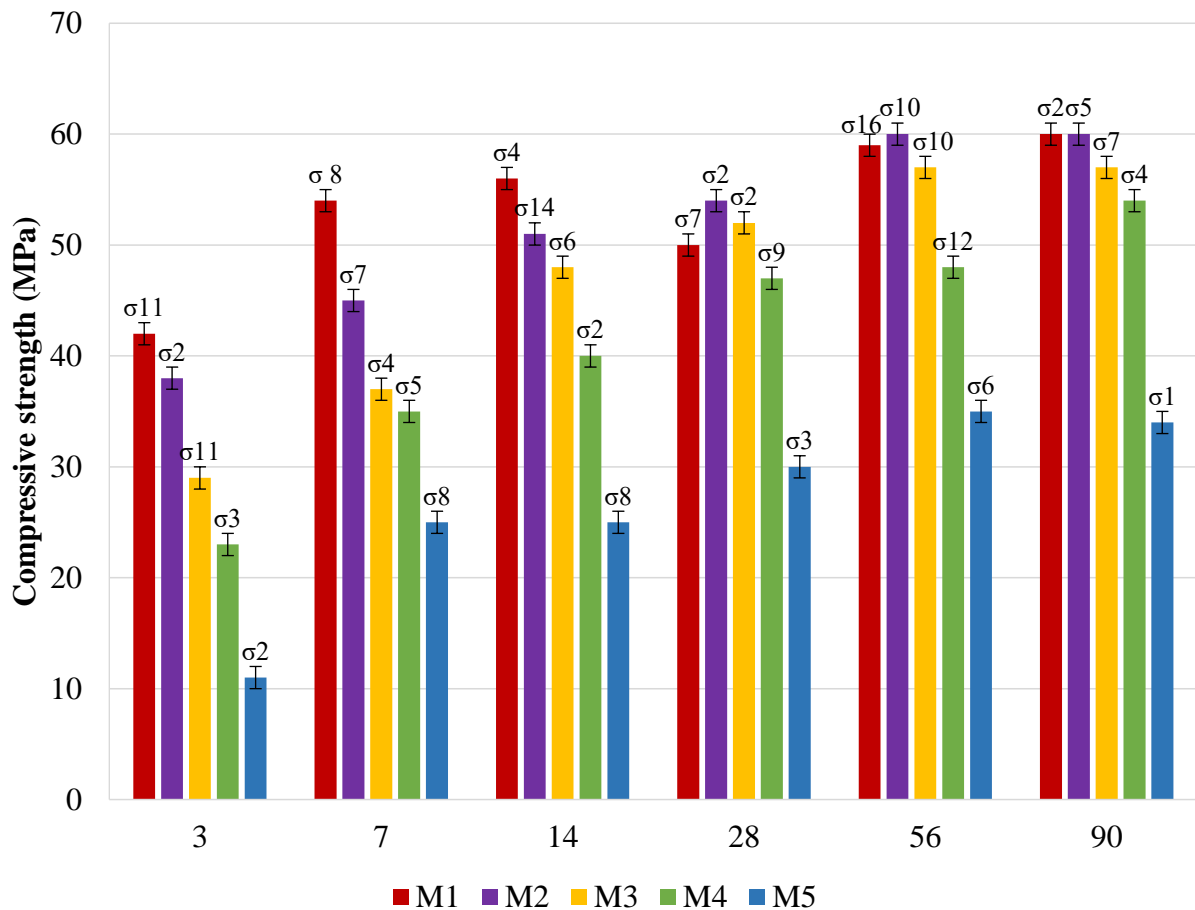


Figure 5. Compressive strength of mixtures M1, M2, M3, M4 and M5.

According to Figure 5, the compressive strength at early ages (3 and 7 days) of the samples with AFA content was lower compared to the control samples (0% AFA). However, with the passage of time, a gradually increasing trend can be seen that is associated with the slow ash pozzolanic reaction (Nath and Sarker, 2011, Mishra, 2017, Saha, 2018).

The compressive strength values of M1 were developed after 56 days with a value of 60 MPa. For M2 and M3 after 14 days they had a compressive strength greater than 45 MPa, while M4 achieved this after 28 days. M5 showed increasing resistance values with time, however, at all ages, the compressive strength was lower than the other mixtures. It achieved a maximum value of 35 MPa. This result is mainly attributed to the lack of calcium hydroxide in the mixture (Saha, 2018), mainly contributed by the Portland cement, as in this case the content in the M5 mix was 25% with respect to the total weight of the cementitious material.

The compressive strength values were lower with higher AFA content in the mixture; however, at the age of 28 days, the M2, M3 and M4 mixtures exceeded 45 MPa, which is the compressive strength considered necessary for concrete to have high resistance according to the Manual of the DURAR network.

3.5 Apparent electrical resistivity vs. compressive strength

Figure 6 shows the electrical resistivity vs. the compressive strength for the five mixtures after 7, 14, 28, 56 and 90 days.

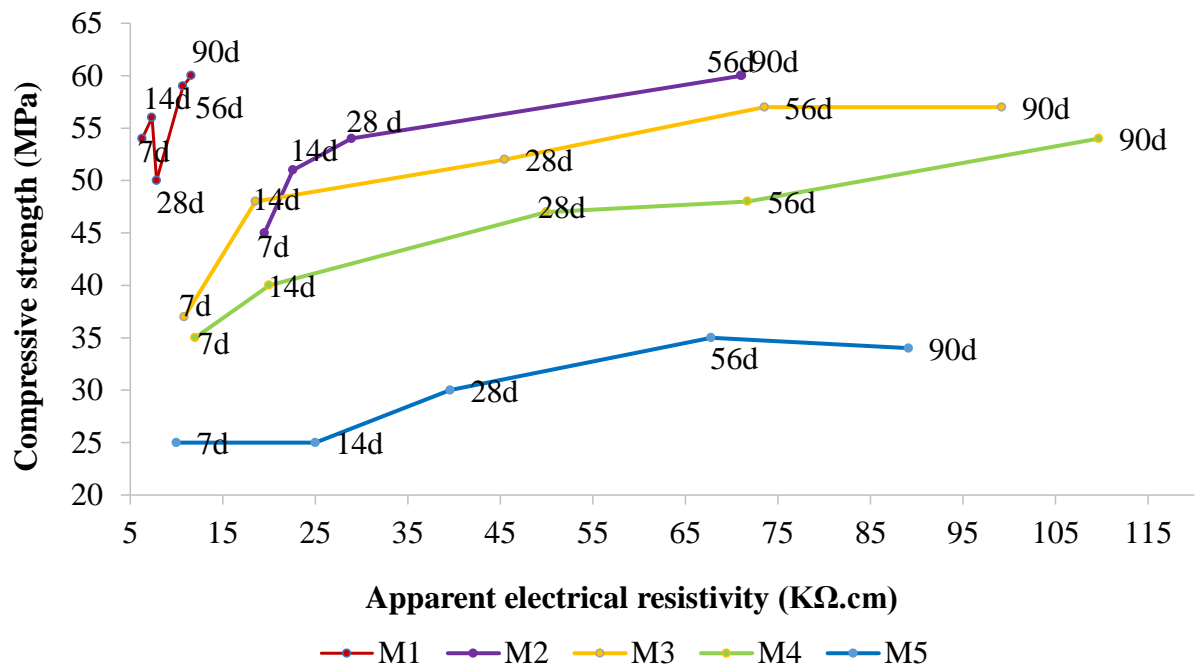


Figure 6. Apparent electrical resistivity vs. compressive strength for mixtures M1, M2, M3, M4 and M5 obtained at 7, 14, 28, 56 and 90 days.

According to Figure 6, M1 showed an upward trend for the apparent electrical resistivity with respect to time. The initial value (7 days) was 6 k Ω .cm and the end value (90 days) was 12 k Ω .cm. In terms of compressive strength, the initial value was 54 MPa and the final value was 60 MPa. In this case, even though there was an increase in both parameters with respect to time, it was not as considerable as that observed in the mixtures with AFA content (M2, M3, M4 and M5), where it was evident that the apparent electrical resistivity and the compressive strength increased. This progressive behavior, with mixtures containing FA, is attributed to the benefit provided by FA in the compactness of the concrete with respect to time.

In all of the mixtures, it was determined that the evolution of the resistivity is parallel to that of the resistance. This behavior was also reported by Andrade (Andrade and D'Andrea, 2011).

Considering that the compressive strength and electrical resistivity required for a durable concrete must be at least 45 MPa and 50 k Ω .cm, respectively, the percentages of AFA that met this requirement were 30%, 50% and 65%.

3.6 UPV vs. compressive strength

Figure 7 shows the compactness of concrete (UPV) vs. the compressive strength for the five mixtures after 7, 14, 28, 56 and 90 days.

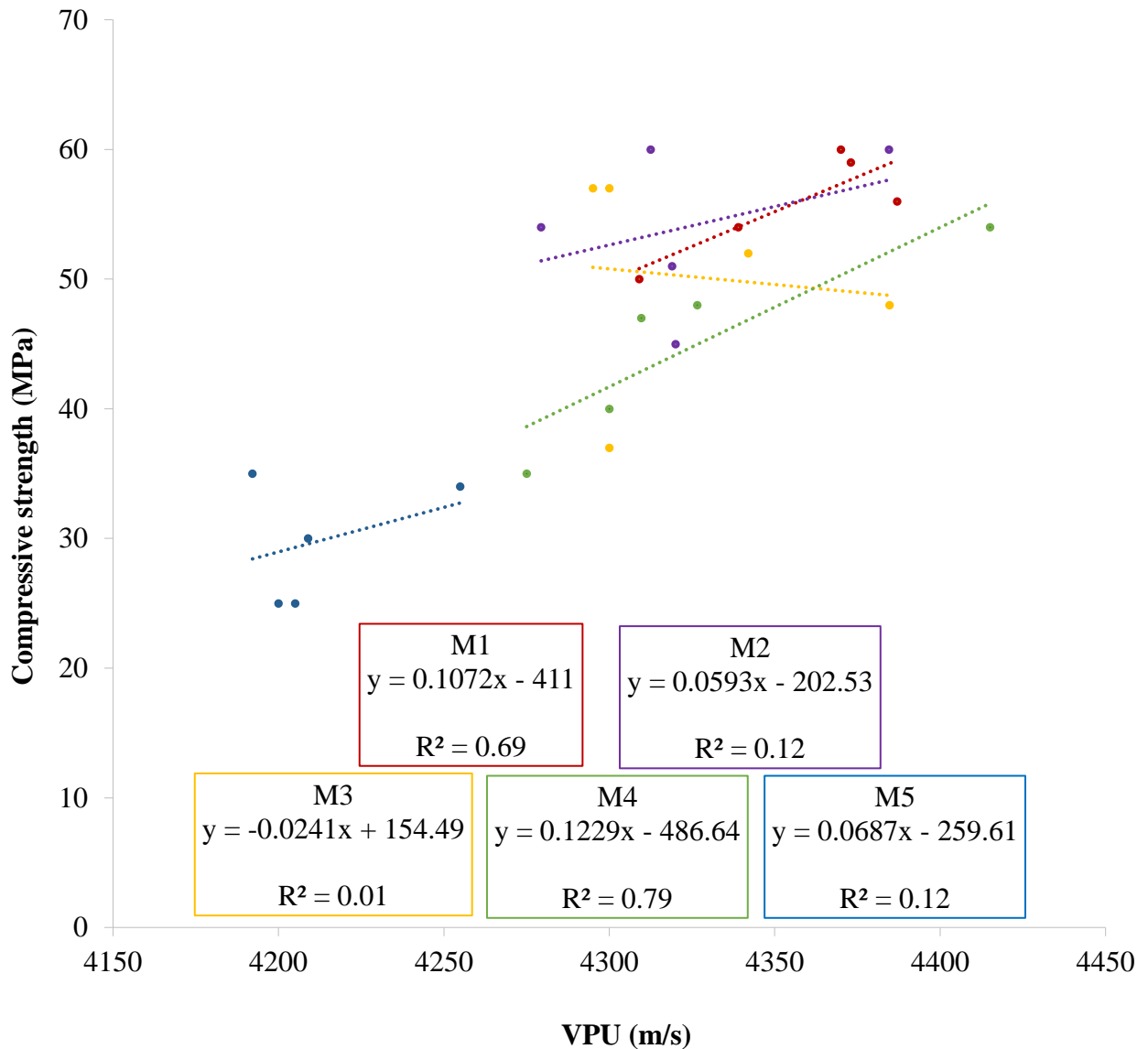


Figure 7. UPV vs compressive strength for mixtures M1, M2, M3, M4 and M5 obtained at 7, 14, 28, 56 and 90 days.

According to Figure 7, it can be observed that M1 and M2 are higher than 4275 m/s and 45 MPa at all ages and evaluated values. For the cases of M3 and M4, at all ages, the UPV values were higher than 4275 m/s, but the compressive strength at 7 days was lower than 45 MPa. This value increased with time. Only for M5 the values of compressive strength and UPV were lower than those of the other mixtures. This behavior is attributed to the high content of FA (75%) and low content of calcium hydroxide (25% in CPC 40). From these results it is observed that for UPV values less than 4250 m/s the compressive strength values obtained were less than 35 MPa (M5), and when the UPV values exceeded 4250 m/s the compressive strength values were greater than 35 MPa. However, the R^2 values indicate that the UPV and compressive strength are not proportional, and therefore, it is necessary to evaluate each parameter independently.

3.7 Apparent electrical resistivity vs. rapid chloride permeability

Figure 8 shows that the apparent electrical resistivity has a correlation with rapid chloride permeability. It was noted that greater electrical resistivity permeability level was lower. Mixtures with AFA content exceeded the values of electrical resistivity obtained with M1 (no AFA content) and as a result the level of permeability was lower. Concrete resistivity increases with time due to refinement of the pore structure (Andrade et al., 2009). The presence of FA favors a pore structure causing lower permeability.

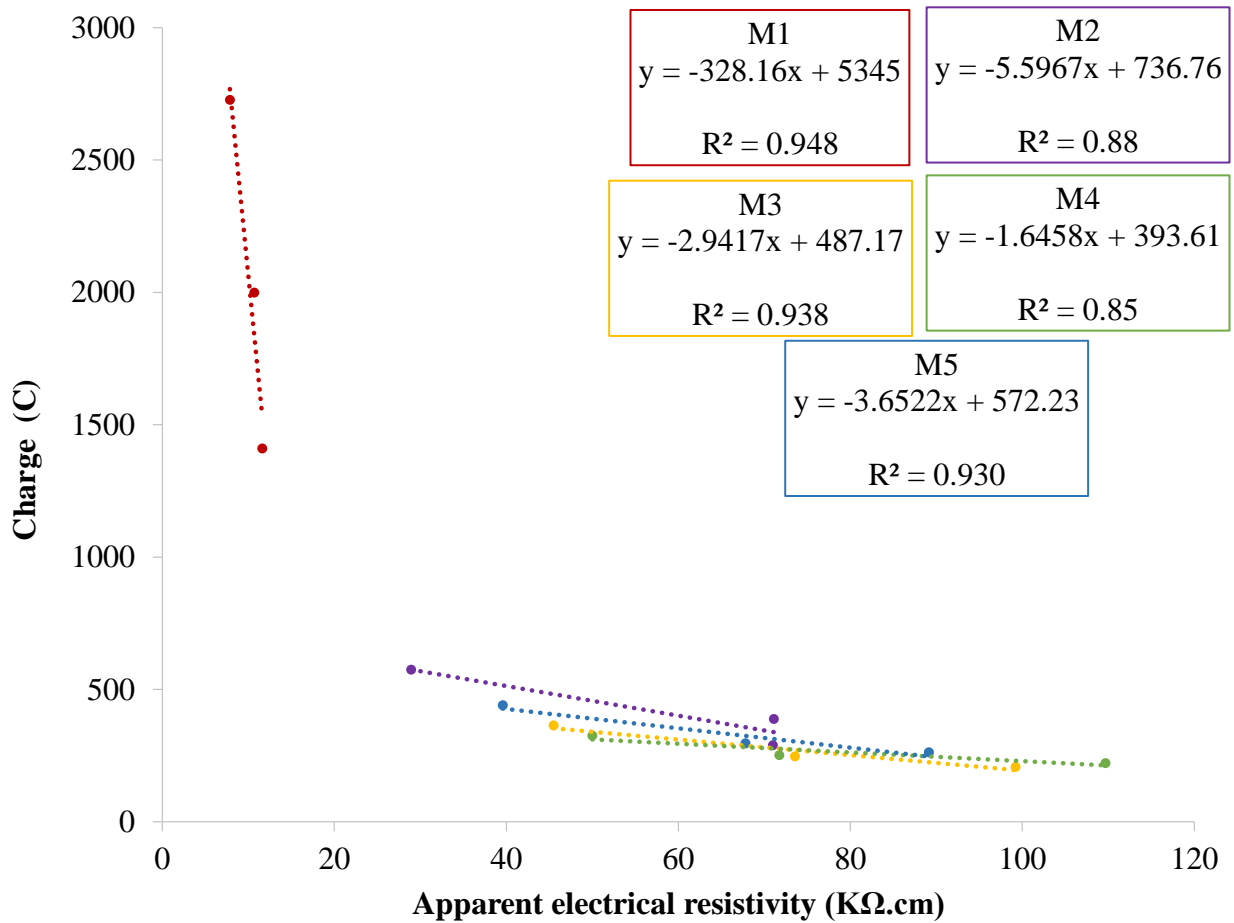


Figure 8. Apparent electrical resistivity vs. rapid chloride permeability for M1, M2, M3, M4 and M5 at 28, 56 and 90 days.

4. CONCLUSIONS

1. The use of AFA as a replacement material for Portland cement (CPC 40) in concrete mixtures improves apparent electrical resistivity, and therefore, the transport of aggressive agents is much lower than that in mixtures without AFA.
2. The level of chloride permeability in the concrete mixtures with AFA contents was very low. This means that when the FA is subjected to a chemical and mechanical treatment it is favorable to reach materials that are not very permeable to this ion, which benefits its durability.
3. The behavior of the compressive strength of the mixtures with 30%, 50% and 65% AFA after 28 days was greater than 45 MPa. This points to the possibility of sustainably manufacturing

- concretes for the construction sector that do not require high resistance at an early age.
4. The electrochemical behavior of the steel reinforcement embedded in the above mixtures, the resistance to sulfates and the characterization of the reaction products are currently being studied. The results will be reported in a future publication.

5. REFERENCES

- Al-Amoudi, O., Maslehuddin, M., Asi, I. (1996), "*Performance and Correlation of the Properties of Fly Ash Cement Concrete*," Cement, Concrete and Aggregates, Vol. 18, No. 2, pp. 71-77, DOI: <https://doi.org/10.1520/CCA10153J>. ISSN 0149-6123
- Andrade, C., D'Andrea, R. (2011), "*La resistividad eléctrica como parámetro de control del hormigón y de su durabilidad*", Revista ALCONPAT, V.1, No.2, pp. 93-101. DOI: <http://dx.doi.org/10.21041/ra.v1i2.8>
- Andrade, C., d'Andréa, R., Castillo, A., Castellote, M. (2009), *The use of electrical resistivity as NDT method for specification the durability of reinforced concrete*, NDTCE'09, Non-Destructive Testing in Civil Engineering, Nantes, France, June 30th – July 3rd
- ASTM International. (2002). *ASTM C597-02 Standard Test Method for Pulse Velocity Through Concrete*. Retrieved from <https://doi.org/10.1520/C0597-02>
- ASTM International. (2012). *ASTM C1202-12 Standard Test Method for Electrical Indication of Concrete's Ability to Resist Chloride Ion Penetration*. Retrieved from <https://doi.org/10.1520/C1202-12>
- ASTM International. (2013). *ASTM C642-13 Standard Test Method for Density, Absorption, and Voids in Hardened Concrete*. Retrieved from <https://doi.org/10.1520/C0642-13>
- ASTM International. (2015). *ASTM C127-15 Standard Test Method for Relative Density (Specific Gravity) and Absorption of Coarse Aggregate*. Retrieved from <https://doi.org/10.1520/C0127-15>
- ASTM International. (2015). *ASTM C128-15 Standard Test Method for Relative Density (Specific Gravity) and Absorption of Fine Aggregate*. Retrieved from <https://doi.org/10.1520/C0128-15>
- Chandra Debanath, O., Saiful Islam, Md., Moinul Islam, Md. (2015), "*Use of Geopolymer Concrete as Green Construction Material- A Review*", Proceedings of the International Conference on Mechanical Engineering and Renewable Energy 2015 (ICMERE 2015) 26 – 29 November, 2015, Chittagong, Bangladesh
- DURAR (1998), "*Manual de Inspección, Evaluación y Diagnostico de Corrosión en Estructuras de Hormigón Armado*", Programa iberoamericano de ciencia y tecnología para el desarrollo (CYTED), subprograma XV "corrosión/impacto ambiental sobre materiales". Red temática Durabilidad de la armadura. 2a Edición
- Garcés, P., Zornoza, E., Baeza, F., Galao, O., Payá, J. (2012), "*¿Es compatible la durabilidad con la sostenibilidad en la industria de la construcción?*", Revista ALCONPAT, V.2, No.2, pp. 57-71. DOI: <http://dx.doi.org/10.21041/ra.v2 i2.27>
- Hela R., Orsáková, D. (2013), "*The Mechanical Activation of Fly Ash*", Procedia Engineering V.65, pp. 87 – 93. DOI: <https://doi.org/10.1016/j.proeng.2013.09.016>
- Heidrich, C., Joachim Feuerborn, H., Weir, A. (2013), "*Carbon combustion products: a global perspective*". World Conference of Coal Ashes, pp. 22-25. URL: <http://www.flyash.info/2013/171-Heidrich-Plenary-2013.pdf>
- Hemalatha, T., Ramaswamy, A. (2017), "*A review on fly ash characteristics – Towards promoting high volume utilization in developing sustainable concrete*", Journal of Cleaner Production, V.147, pp. 546-559. DOI: <https://doi.org/10.1016/j.jclepro.2017.01.114>
- International Energy Agency (2014), "*The Impact of Global Coal Supply on Worldwide Electricity Prices*". Report by the IEA Coal Industry Advisory Board, pp. 55, URL:

- https://www.iea.org/publications/insights/insightpublications/ImpactGlobalCoalSupply_WorldwideElectricityPrices_FINAL.pdf
- Lizarazo Marriaga, J., García, F., Higuera Flórez, C. (2015), “*Activación de las propiedades cementicias de la ceniza volante mediante electromutagénesis química*”, Revista Latinoamericana de Metalurgia y Materiales, V. 35, No.2, pp. 305-314. eISSN: 2244-7113
- Madhavi, T. Ch., Swamy Raju, L., Mathur, D. (2014) “*Durability and Strength Properties of High Volume Fly Ash Concrete*”, Journal of Civil Engineering Research, V. 4, pp. 7-11. URL: <http://article.sapub.org/10.5923.c.jce.201401.02.html>
- Malhotra, V. M. (1990), “*Durability of concrete incorporating high-volume of low-calcium (ASTM Class F) fly ash*”, Cement and Concrete Composites, Volume 12, Issue 4, Pages 271-277, DOI: [https://doi.org/10.1016/0958-9465\(90\)90006-J](https://doi.org/10.1016/0958-9465(90)90006-J)
- Malhotra, V. M. (1985), “*Métodos no destructivos para evaluar concreto*”. Department of Energy, Mines and Resources, Ottawa, Canada.
- Moffatt, E., Thomas, M., Fahim, A. (2017), “*Performance of high-volume fly ash concrete in marine environment*”, Cement and Concrete Research, V.102, pp. 127-135. DOI: <https://doi.org/10.1016/j.cemconres.2017.09.008>
- Mehta, K. (2001), “*Reducing the environmental impact of concrete*”, Concrete International, pp. 61-66. URL: <http://maquinamole.net/EcoSmartconcrete.com/docs/trmehta01.pdf>
- Mehta, K. (2002), “*Greening of the concrete industry for sustainable development*”, Concrete international, 24 (7) pp. 23-28.
- Mishra, D. K., Yu, J., Leung, C. K. Y. (2017), “*Very high volume fly ash green concrete for applications in India*”, Global Waste Management, International Society of Waste Management, Air and Water. pp. 480-487.
- Mittal, A., Kaisare, M. B., Shetti, R. “*Experimental Study on use of fly ash in concrete*”, Tarapur Atomic Power Project 3 & 4, Nuclear Power Corporation of India Limited URL: https://www.sefindia.org/forum/files/experimental_study_on_use_of_fly_ash_in_concrete_by_mr_amit_mittal_136.pdf
- Mucsi, G. (2016), “*Mechanical activation of power station fly ash by grinding – A review*”, Journal of Silicate Based and Composite Materials, V. 68, No. 2, pp. 56-61. DOI: <http://dx.doi.org/10.14382/epitoanyag-jsbcm.2016.10>
- Nath, P., Sarker, P. (2011) “*Effect of Fly Ash on the Durability Properties of High Strength Concrete*”, Procedia Engineering V.14, pp. 1149-1156. DOI: <https://doi.org/10.1016/j.proeng.2011.07.144>
- Organismo Nacional de Normalización y Certificación de la Construcción y Edificación, S.C. (ONNCCE) (2010), *NMX-C-105-ONNCCE-2010: Industria de la Construcción-Cementos hidráulicos Gabinetes y cuartos húmedos y tanques de almacenamiento para el curado de especímenes de mortero y concreto de cementantes hidráulicos*”.
- Organismo Nacional de Normalización y Certificación de la Construcción y Edificación, S.C. (ONNCCE) (2014), “*NMX-C-083-ONNCCE-2014: Industria de la Construcción Concreto Determinación de la Resistencia a la Compresión de Especímenes Método de Ensayo*”.
- Organismo Nacional de Normalización y Certificación de la Construcción y Edificación, S.C. (ONNCCE) (2016), “*NMX-C-159-ONNCCE-2016: Concreto, elaboración y curado de especímenes en el laboratorio*”.
- Organismo Nacional de Normalización y Certificación de la Construcción y Edificación, S.C. (ONNCCE) (2016), “*NMX-C-413-ONNCCE-2016: Industria de la Construcción Resistividad Eléctrica del Concreto Hidráulico Especificaciones y Métodos de Ensayo*”.
- Palomo, A., Grutzeck, M., Blanco, M. (1999), “*Alkali-activated fly ashes: A cement for the future*”, Cement and Concrete Research, Volume 29, Issue 8, August, Pages 1323-1329, DOI: [https://doi.org/10.1016/S0008-8846\(98\)00243-9](https://doi.org/10.1016/S0008-8846(98)00243-9)

- Saha, K. A. (2018), “*Effect of class F fly ash on the durability properties of concrete*”, Sustainable Environment Research, Volume 28, Issue 1, January, Pages 25-31. DOI: <https://doi.org/10.1016/j.serj.2017.09.001>
- Sahoo, S., (2016), “*A Review of Activation Methods in Fly Ash and the Comparison in Context of Concrete Strength*”, Journal of Basic and Applied Engineering Research, Volume 3, Issue 10; July-September 2016, pp. 883-887. e-ISSN: 2350-0255, <http://www.krishisanskriti.org/Publication.html>
- Yu, J., Lu, C., Leung, C. K. Y., Li, G. (2017). *Mechanical properties of green structural concrete with ultrahigh-volume fly ash*. Construction and building materials, 147, pp. 510-518. [Online] Disponible en: <https://doi.org/10.1016/j.conbuildmat.2017.04.188>
- Zobal, O., Reiterman P., Plachý, T., Bittnar, Z. (2017), “*Durability of Concrete with Fly Ash from the Dam Orlik after 55 Years*”, Advanced Materials Research, V.1144, pp. 81-87. DOI: <https://doi.org/10.4028/www.scientific.net/AMR.1144.81>

Effluent reuse in the manufacture of concrete blocks for sealing masonry

A. Plaza Meurer¹ , R. Alves Amorim¹ , L. Carvalho Quintanilha¹ , D. Cardoso Parente^{*1,2} 

*Contact author: denisparente@yahoo.com.br

DOI: <http://dx.doi.org/10.21041/ra.v9i2.278>

Reception: 26/10/2017 | Acceptance: 29/05/2018 | Publication: 30/04/2019

Responsible Associate Editor: Dr. Paulo Helene

ABSTRACT

This work seeks to assess the use of reuse water from sewage treatment stations in the manufacture of simple concrete hollow blocks. The use of these blocks has been adopted as a rationalization option in the composition of the sealing and structural masonry, providing a reduction in the losses of materials and layers of coating. Made from the mixture of agglomerate, aggregate and water, around 60 m³ of concrete, required for the production of 12,350 blocks (14 x 19 x 39 cm), would consume 4, 500 l of water. The study includes the analysis of the physical and mechanical properties of effluent dosed blocks. Consequently, the results show that these properties remain unchanged, which can make the effluent use viable.

Keywords: recycled water; concrete block; treated effluent.

Cite as: Plaza Meurer, A., Alves Amorim, R., Carvalho Quintanilha, L., Cardoso Parente, D. (2019), "Effluent reuse in the manufacture of concrete blocks for sealing masonry", Revista ALCONPAT, 9 (2), pp. 215 – 227, DOI: <http://dx.doi.org/10.21041/ra.v9i2.278>

¹ Universidad Federal do Tocantins - UFT, Brasil.

² Centro Universitário Luterano de Palmas - CEULP/ULBRA, Brasil.

Legal Information

Revista ALCONPAT is a quarterly publication by the Asociación Latinoamericana de Control de Calidad, Patología y Recuperación de la Construcción, Internacional, A.C., Km. 6 antigua carretera a Progreso, Mérida, Yucatán, 97310, Tel.5219997385893, alconpat.int@gmail.com, Website: www.alconpat.org

Responsible editor: Pedro Castro Borges, Ph.D. Reservation of rights for exclusive use No.04-2013-011717330300-203, and ISSN 2007-6835, both granted by the Instituto Nacional de Derecho de Autor. Responsible for the last update of this issue, Informatics Unit ALCONPAT, Elizabeth Sabido Maldonado, Km. 6, antigua carretera a Progreso, Mérida, Yucatán, C.P. 97310.

The views of the authors do not necessarily reflect the position of the editor.

The total or partial reproduction of the contents and images of the publication is strictly prohibited without the previous authorization of ALCONPAT Internacional A.C.

Any dispute, including the replies of the authors, will be published in the first issue of 2020 provided that the information is received before the closing of the third issue of 2019.

Reuso de efluentes na fabricação de blocos de concreto para alvenaria de vedação

RESUMO

Este trabalho busca avaliar a utilização da água de reuso proveniente de estações de tratamento de esgoto na fabricação de blocos vazados de concreto simples. O uso desses blocos tem sido adotado como opção de racionalização na composição da alvenaria de vedação e estrutural, por permitir redução nas perdas de materiais e camadas de revestimento. Fabricados a partir da mistura de aglomerante, agregado e água, em média 60 m³ de concreto, necessários para produção de 12.350 blocos (14 x 19 x 39 cm), consumiria 4.500 l de água. O estudo compreende a análise das propriedades físicas e mecânicas dos blocos dosados com efluente e os resultados mostram que essas propriedades permanecem inalteradas, o que pode viabilizar a utilização do efluente.

Palavras chave: água de reuso; bloco de concreto; efluente tratado.

Reutilización de efluentes en la fabricación de bloques de concreto para albañilería

RESUMEN

En este trabajo se evalúa la utilización del agua de reutilización proveniente de estaciones de tratamiento de aguas residuales en la fabricación de bloques huecos de concreto simple. El uso de esos bloques ha sido adoptado como opción de racionalización de la composición de la albañilería para mampostería tradicional y estructural, por permitir reducción de pérdidas de materiales y capas de revestimiento. Fabricados a partir de la mezcla de aglomerante, agregado y agua, en promedio 60 m³ de concreto, necesarios para la producción de 12.350 bloques (14 x 19 x 39 cm), consumiría 4.500 l de agua. El estudio comprende el análisis de las propiedades físicas y mecánicas de los bloques dosificados con el efluente y los resultados muestran que esas propiedades permanecen inalteradas, lo que puede viabilizar la utilización del efluente.

Palabras clave: reutilización del agua; bloque de concreto; aguas residuales tratadas.

1. INTRODUCTION

According to Visvanathan and Asano (2001), uncontrolled industrial development caused the depletion and pollution of water resources, and it was necessary to make ever stricter regulations that would force industries to reduce drinking water. The author still states that technological advances enable the treatment of wastewater for a diversity of industrial reuse.

Another relevant point is the reuse of water, which presents itself as one of the solutions for the face of the water crisis. According to data from the World Bank (2015), approximately 90% of the wastewater from developing countries has its disposition in the environment without any treatment. The World Bank also points out that in Latin America about three-quarters of water contaminated with fecal coliform, return to the water body, causing serious public health and environmental problems.

In this context, the general objective of this work is to evaluate and compare the physical-mechanical properties of concrete blocks made with drinking water and blocks manufactured using domestic effluent treated by Waste Water Treatment Station (WWTS) Vila Uniao, located in Palmas – TO.

2. CAST CONCRETE BLOCK

The Brazilian Association of Technical Standards (ABNT) defines concrete hollow blocks as a “component for the execution of masonry, with or without structural function, leaked in the upper and lower faces, whose net area is equal to or less than 75% of the raw area” (ABNT NBR 6136:2014, p. 1)

In the production of concrete blocks is used the dry concrete, also known as concrete without rebate (MARCHIONI, 2012). This concrete differs from conventional concrete (plastic) in certain properties such as: cement consumption, granulometry of mixtures and workability. The resistance of dry concretes does not follow the law of Abram, applied to plastic concretes. (FRASSON JR. and PRUDENCIO JR., 2002)

There are advantages of using hollow blocks: the lower consumption of mortar in the execution of the masonry; the possibility of being filled with steel bars and grout reaching capacity to support structural loads; and the use of its cavities for the passage of electrical and plumbing installations, which avoids the cutting in the masonry, which contributes in the reduction of solids waste and increase productivity.

Because they have very small dimensional tolerances, they generate a sharp reduction in the coating application in relation to the ceramic block (SANTOS, 2016). The concrete block for submitting greater adhesion, in relation to the ceramic block, requires less coating. Another advantage is in relation to the loss of material, taking advantage that the concrete blocks do not break as much as the ceramics (HOMETEKA, 2016)

3. PROCEDURE

For the development of this research blocks of concrete with treated effluent, collected in the month of July 2016, from WWTS Vila Uniao, located in Palmas - Tocantins were manufactured

3.1. Collection of treated effluent

The effluent collection for chemical analysis was carried out in the WWTS Vila Union, where the treatment is performed by ascending flow reactors (UASB), activated sludge lakes and decanters. The collection of the manual was made on the flow rate meter device of the treated effluent of the station.

The procedure for sampling in surface water and manual collection was carried out according to the specifications of NBR 9898:1987 and the National Guide to Collection and Preservation of Samples (2011) CETESB.

3.2. Treatment effluent analysis

The essays to evaluate recycled water were divided into the following stages: preliminary evaluation, chemical analysis, paste setting time and resistance to mortar compression.

The preliminary evaluation step included the completion of the following trials specified in Table 1, held at the General Chemistry Laboratory of the Federal University of Tocantins – UFT.

Table 1. Preliminary evaluation

Parameter	Norm
Oils and Fat	ABNT NBR 15900-3
Detergents	
Color	
Solid Material	
Odor	
Acid	
Organic Matter	

Chemical analyses were performed by the MICROLAB Environmental Laboratory of Goiânia – GO and contemplated the trials and standards specified in Table 2

Table 2. Chemical analysis

Test	Standard
Chloride	ABNT NBR 15900-6
Sulfates	ABNT NBR 15900-7
Alkali	ABNT NBR 15900-9
Phosphates	ABNT NBR 15900-8
Nitrates	ABNT NBR 15900-10
Lead	ABNT NBR 15900-5
Zinc	ABNT NBR 15900-4

According to the procedures of the NBR NM 45 and NBR NM 65, tests were carried out for determining the initial and final setting time for the cement paste with treated effluent. The water standard for concrete kneading (NBR 15900) says that the paste initial and final setting time, in samples prepared with the water in study, must not differ more than 25% of the initial and final setting time obtained with samples prepared with distilled water.

The compressive strength assays were performed at 7 and 28 days of curing of the mortar specimens, according to the procedures of NBR 7215. According to NBR 15900, the average resistance for the two ages must reach at least 90% of the average compressive strength of specimens prepared with drinking water.

3.3. Blocks Manufacturing

The next step was the manufacture of the concrete hollow blocks for sealing masonry using treated effluent and drinking water. Table 3 shows the trace used in the manufacture of the blocks.

Table 3. Trace of concrete for building blocks

Mass Trace (cem.: pebble dust: water)	Material	Unit	Quantity
1 : 9,250 : 0,325	Cement	Kg	40
	Pebble Dust	Kg	370
	Water	L	13

For the manufacture of the blocks, the cement CP II Z 32, manufacturer CIPLAN, originated from the local market (Palmas-TO). The materials used in the mixture of the concrete with

drinking water resulted in a volume of 0.17 m³ of concrete and the production of approximately 35 blocks. The same volume of concrete with treated effluent was produced, resulting in approximately 35 blocks

3.4. Essay for blocks

The tests for dimensional analysis, absorption and liquid area were carried out in the Civil Engineering Laboratory of the Federal University of Tocantins. And the test of resistance to compression of blocks and prisms in the Laboratory of Civil Engineering of the University Center Lutheran of Palmas (CEULP/ULBRA – TO). The procedures followed the NBR 6136 and NBR 12118 standards.

The test of resistance to the compression of prisms was carried out according to the procedures of the NBR 15961 standard. As with the mentioned procedure, two blocks prisms as one of the elements that can be used to estimate the compression resistance of structural masonry walls were adopted. Although the blocks were for sealing masonry, the two-block prism-compression resistance test was performed to obtain a better understanding of the transmission of loads from one block to another.

Table 4 shows the trace in volume and the water/cement ratio of the mortar used to seat the blocks in the assembly of the prism.

Table 4. Trace in the volume of mortar

Trace in volume (cem.: sand)	water/cement ratio
1 : 0,5	1,4

4. RESULTS AND DISCUSSIONS

4.1. Preliminary Evaluation of Effluent

After collecting the effluent, preliminary evaluation of the effluent was carried out in relation to the parameters: oils, fats, detergents, color, solid material, odor, acids and organic matter, according to the normative recommendations of NBR 15900-1:2009. In this evaluation, the tests were made from qualitative analyses, with the exception of the test of solid material whose present content was quantified in the sample. The obtained results are displayed in time Table 5.

Table 5. Results of the effluent's preliminary evaluation

Parameter	Result	Requirements
Oils and Fats	No Visible Traces	No more than visible traces
Detergents	Foam Presence	Any foam must disappear in 2 min
Color	Light Yellow	The color must be qualitatively compared to drinking water, and it must be light yellow and odorless
Solid Material	391 mg/L	Max of 50.000 mg/L
Odor	Odorless and without the odor of hydrogen sulfide after the addition of hydrochloric acid	Water should be odorless and without odor hydrogen sulfide, after the addition of hydrochloric acid
Acid	pH 8	pH ≥ 5
Organic Matter	Clearer sample solution than the standard solution	The watercolor must be lighter or equal to the standard solution, after the addition of NaOH

Although the recycled water from the WWTS does not meet parameter “missing foam”, it is permitted to use the treated effluent as kneading water, as long as it meets the criteria about setting time and compression resistance presented in item 4.4 from NBR 15900-1:2009.

Still, on the results presented in Table 5, the pH of the treated effluent presented results within the permitted and had a light-yellow color. In addition, the effluent in the odor test presented odorless and odor-free hydrogen sulfide odor after the addition of hydrochloric acid.

In relation to the parameter “oils and fats”, the value of the area is not visible. Also, through visual analysis, in the parameter “organic matter”, the sample solution was clearer than the standard solution. The solid material content was lower than the maximum content.

4.2. Chemical analysis of effluent

Chemically tested according to the standard recommendations presented in Table 6 in order to identify the presence of deleterious substances to the concrete, the content of chlorides, sulfates, alkali, phosphates, nitrates, lead, and zinc are quantified

Table 6. Results of chemical analysis

Substance	Content(mg /L)	Max Content (mg/L)	Final use	Method
Chlorides	75	500	Prestressed Concrete or grout	ABNT NBR 15900-6
		1.000	Reinforced concrete	
		4.500	Simple Concrete (Unreinforced)	
Sulphates	64	2.000	-	ABNT NBR 15900-7
Alkalis	295	1.500		ABNT NBR 15900-9
Phosphates	6,036	100		ABNT NBR 15900-8
Nitrates	0,02	500		ABNT NBR 15900-10
Lead	<0.01	100		ABNT NBR 15900-5
Zinc	0,081	100		ABNT NBR 15900-4

Source: Autor, 2016

Some substances, considered by Battagin (2010) like changes of the resistance to compression and of the setting time, were found at minimum levels in the effluent sample. For the author nitrate zinc, lead and manganese slow the handle, while chrome nitrates promote its acceleration. On the other hand, phosphates and borates of lead and zinc reduce the hydration rate, prolong the setting time and shorten the evolution of the initial resistance.

4.3. Setting Time

Still, in the provided essays for kneading water, it was carried out the setting time essay, following the NBR 15900-1:2009 standard. According to the criteria of the standard, it was assessed the approval or not of the recycled water as an input in the manufacture of the blocks. In Figure 1, the initial and final setting time of the paste with distilled water and treated effluent are displayed.

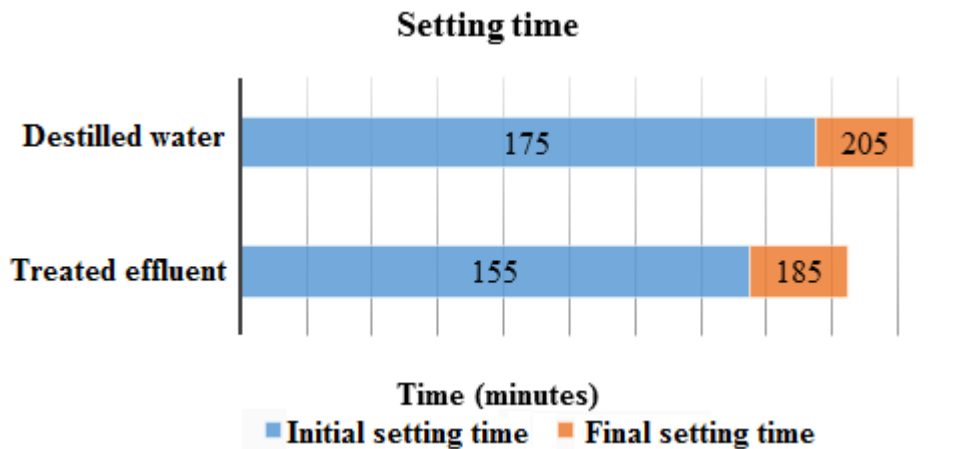


Figure 1. Results referring to the initial and final setting time

It is noticed that the initial and final setting times of the samples prepared with treated wastewater, did not diverge more than 25% from the ones prepared with distilled water, obeying the demanded from NBR 15900-1:2009. The effluent diverged 11,43% for initial setting time, and 9.76% for final setting time.

4.4. Resistance to compression

In the axial compressive strength test of the mortar, 4 specimens of each sample were used at 7 and 28 days of age, in a total of 16 test specimens tested. The results are shown in table 7

Table 7. Resistance to compression of the specimen.

Resistance to Compression (MPa)				
Concrete Specimen	Distilled Water		Treated Effluent	
	7 Days	28 Days	7 Days	28 Days
1	18,90	24,69	16,68	24,04
2	15,65	21,82	19,87	19,49
3	19,00	24,69	17,00	22,20
4	19,17	26,26	16,79	22,74
Average	18,18	24,37	17,59	22,12
S.D	1,69	1,85	1,53	1,91
C.V. (%)	9,30%	7,60%	8,70%	8,66%

The average resistance to compression strength of the mortar test specimens with treated effluent at 7 and 28 days, reached more than 90% of the resistance to the average compression of the specimens prepared with distilled water, meeting the requirement of NBR 15900-1:2009. At 7 days it had a reach of 96.75%, and with 28 days the reach was 90.77%

Using Student's "t" hypothesis test, it was verified that the average resistance of the mortar with distilled water and the mortar with treated effluent had significantly similar values, for a confidence level of 95%

4.5. Absorption and liquid area of the blocks

Three blocks were used for each sample (block A and B). The result of the determination of the absorption and net area of the conventional blocks can be visualized in table 8

Table 8. Determination of absorption and liquid area of the conventional blocks

Concrete Specimen	Absorption		Liquid Area	
	Individual (%)	Average (%)	Individual (mm ²)	Average (mm ²)
1	10,71%	10,50%	25.000,00	25.000,00
2	10,26%		24.736,84	
3	10,53%		25.263,16	

Table 9 shows the results of determination of absorption and net area of the blocks with treated effluent

Table 9. Determination of the absorption and liquid area of the blocks with treated wastewater

Concrete Specimen	Absorption		Liquid area	
	Individual	Average	Individual (mm ²)	Average(mm ²)
1	10,48%	10,66%	26.052,63	25.789,47
2	10,68%		25.789,47	
3	10,84%		25.526,32	

Source: Autor, 2016

The requirement of NBR 6136:2014 for the block absorption essay, with the use of normal aggregate, is individual absorption less or equal to 12% and average absorption less or equal to 10%. The results show that both block samples presented average absorption above the maximum limit at 28 days of curing. For Fernandes (2012), a block produced with an insufficient amount of water for perfect compaction or produced with very coarse granulometric composition usually presents a porous surface, subject to absorb water with ease. Since the granulometric distribution used to make the blocks allows a good surface for the pieces, it is believed that probably the amount of water added in the mixture was not enough to produce parts with little porosity, through the degree of compaction used. The high content of pulverulent materials may have increased water consumption due to the high specific surface of fines.

4.6. Block compression resistance test

For axial compression resistance test, 6 blocks of each sample (conventional and treated effluent) were used at 14 and 28 days old, in a total of 24 packs. The results are presented in Table 10 and show a comparison between the average resistance of the samples

Table 10. Result of compression resistance

Compression Resistance (MPa)				
Block	Conventional		Efluente Tratado Treated Effluent	
	14 Days	28 Days	14 Days	28 Days
1	2,28	3,16	3,61	3,58
2	1,87	3,43	3,04	5,03
3	2,03	3,26	3,11	4,20
4	2,53	3,17	3,00	3,53
5	2,43	3,09	4,96	3,54
6	2,40	3,09	2,05	4,80
Average	2,26	3,20	3,29	4,11
S.D.	0,26	0,13	0,96	0,67
C.V. (%)	11,30%	4,05%	29,19%	16,40%

Source: Autor, 2016

The average resistance to compression of the mortar specimen with treated effluent, at 7 days and 28 days, reached more than 90% of the average compression resistance of the concrete specimen prepared with distilled water, given the NBR 15900-1:2009 requirement. At 7 days the range of resistance was 96.75%, and with 28 days of 90.77%, presenting significantly similar values to a 95% confidence level

For classifying the blocks according to their due class, it is necessary to take as reference the estimated compression resistance ($F_{bk,est}$). The values of the $F_{bk,est}$ of the conventional block and of the treated effluent block are presented in Tables 11 and 12 respectively.

Table 11. Result of the compression resistance of conventional blocks

Concrete Specimen	Maximum break load (Kgf)	Compression Resistance (MPa)		$F_{bk,est}^a$	F_{bk}^b
		Individual	Average		
1	17.584	3,16	3,20	3,03	3,03
2	19.122	3,43			
3	18.154	3,26			
4	17.640	3,17			
5	17.222	3,09			
6	17.224	3,09			

^a Compression Resistance of estimate characteristic sample expressed in MPa
^b Characteristic resistance to compression expressed in MPa ($F_{bk,est} \geq \Psi \cdot F_{b1}$)

Source: Autor, 2016

Table 12. Result of the compression resistance of the blocks with treated effluent

Concrete specimen	Maximum break load (Kgf)	Compression Resistance (MPa)		$F_{bk,est}^a$	F_{bk}^b
		Individual	Average		
1	19.937	3,58	4,11	3,49	3,49
2	27.994	5,03			
3	23.406	4,20			
4	19.646	3,53			
5	19.709	3,54			
6	26.745	4,80			

^a Compression Resistance for estimated characteristic sample, expressed in MPa
^b Characteristic Resistance for compression, expressed in MPa ($F_{bk,est} \geq \Psi \cdot F_{b1}$)

Source: Autor, 2016

Both block samples have met the resistance specifications for Class C, F_{bk} , or 3 MPa blocks specified in item 6.5 of NBR 6136:2014.

The blocks made with treated effluent presented medium resistance and characteristic resistance larger than the blocks produced with drinking water, with gain resistance to compression to a confidence level of 95%

Considering that the manufacturing process, the trace, and the cure were the same for the two samples, then it is believed that this increase of resistance was given due to some problem in the molding of the blocks (carried out in the factory), to be seen that in the assay resistance test of the mortar the result was different

The effluent blocks showed greater compacity (particle packaging) and greater resistance. In Table 13, it can be verified that the sample of blocks with treated effluent showed greater density than the blocks of the other sample

Table 13. Density of the blocks

Mass (kg)	Volume (m ³)	m ³	Average Density (Kg/m ³)
Conventional Blocks			
9,80	0,00480	2041,67	2017,36
9,75		2031,25	
9,50		1979,17	
Blocks with treated effluent			
10,50	0,00480	2187,50	2149,31
10,30		2145,83	
10,15		2114,58	

Fonte Source: Autor, 2016

Fernandes (2014) states that, for better technological control, it is recommended to establish the desired piece and to obtain its weight by adopting it as standard in a range of no more than 5%. The establishment of the standard weight for the parts and the weight control immediately after extrusion is more efficient and practiced for controlling the standard deviation of the resistance in different batches, between cycles of the same mixture or even between parts of the same trays.

4.7 Resistance to prism compression

The resistance test to simple compression performed with 3-block prisms of each sample with 28 days, totaling 6 non-grouted prisms presented compression-resistance values and detailed prism/block efficiency factor values in Table 14

Table 14. Resistance to prisms simple compression

Maximum break load (Kgf)	Resistance (MPa)	Average (MPa)	S.D. (MPa)	C.V. (%)	Efficiency (f _{pm} /f _{bm})
Conventional Prism					
11.687	2,10	2,30	0,37	16,01%	71,97%
11.600	2,08				
15.199	2,73				
Prism with treated effluent					
16.012	2,88	3,15	0,25	7,94%	76,47%
17.779	3,19				
18.755	3,37				

It was observed in all prisms that the rupture occurred by traction in the block causing vertical cracking, initiated and intensified in the longitudinal walls and sometimes in the transverse walls. The red lines shown in Figure 3 demarcate the cracks in prisms



Image 3. Typical prisms rupture

The efficiency is conventionally defined as the relationship between the resistance of an element, e.g. a prism, and the resistance of the block that composes it. According to Ramalho and Corrêa (2003), the efficiency factor f_{pm}/f_{bm} ranges from 0.50 to 0.90. For the two samples were found values above 0.70 of prism/block efficiency, statistically similar via Student's "t" hypothesis test, for a 95% confidence level

5. CONCLUSIONS

The results of the recycled water analysis and the data of resistance to compression, initial and final setting time can confirm the non-interference of the effluent use in the composition of the blocks. All results have met the criteria of 'setting time' and compression resistance for concrete kneading water established by NBR 15900-1:2009

As for the dimensional checks of the molded blocks, it was verified that the average liquid areas of the two block samples presented a percentage of around 45% of the gross area of the block, meeting the requirements of values less than 75%, required by NBR 6136:2014. Both samples presented dimensions statistically similar, not interfering the effluent, in the dimensional stability of the parts

Regards the absorption of the blocks, the average results obtained for the two samples were above the maximum limit presented by the standard. The high content of pulverate materials must have increased the consumption of water, causing an insufficient amount of water to mix and consequently forming a porous concrete.

6. REFERENCES

- ABNT - Associação Brasileira de Normas Técnicas (1996), *NBR 7215: 1996, Cimento Portland – Determinação da resistência à compressão*. Rio de Janeiro.
- ABNT - Associação Brasileira de Normas Técnicas (1987), *NBR 9898: 1987, Preservação e técnicas de amostragem de afluente líquidos e corpos receptores – Procedimento*. Rio de Janeiro.
- ABNT - Associação Brasileira de Normas Técnicas (2006), *NBR NM 45:2006, Agregados – Determinação da massa unitária e do volume de vazios*. Rio de Janeiro.
- ABNT - Associação Brasileira de Normas Técnicas (2009), *NBR 15900-1:2009, Água de amassamento do concreto – Parte 1: requisitos*. Rio de Janeiro.
- ABNT - Associação Brasileira de Normas Técnicas (2009), *NBR 15900-2:2009, Água de amassamento do concreto – Parte 2: coleta de amostras para ensaios*. Rio de Janeiro.
- ABNT - Associação Brasileira de Normas Técnicas (2009), *NBR 15900-3:2009, Água de amassamento do concreto – Parte 3: avaliação preliminar*. Rio de Janeiro.
- ABNT - Associação Brasileira de Normas Técnicas (2009), *NBR 15900-4:2009, Água de amassamento do concreto – Parte 4: análise química – Determinação de zinco solúvel em água*. Rio de Janeiro.
- ABNT - Associação Brasileira de Normas Técnicas (2009), *NBR 15900-5:2009, Água de amassamento do concreto – Parte 5: análise química – Determinação de chumbo solúvel em água*. Rio de Janeiro.
- ABNT - Associação Brasileira de Normas Técnicas (2009), *NBR 15900-6:2009, Água de amassamento do concreto – Parte 6: análise química – Determinação de cloreto solúvel em água*. Rio de Janeiro.
- ABNT - Associação Brasileira de Normas Técnicas (2009), *NBR 15900-7:2009, Água de amassamento do concreto – Parte 7: análise química – Determinação de sulfato solúvel em água*. Rio de Janeiro.
- ABNT - Associação Brasileira de Normas Técnicas (2009), *NBR 15900-8:2009, Água de amassamento do concreto – Parte 8: análise química – Determinação de fosfato solúvel em água*. Rio de Janeiro.
- ABNT - Associação Brasileira de Normas Técnicas (2009), *NBR 15900-9:2009, Água de amassamento do concreto – Parte 9: análise química – Determinação de álcalis solúveis em água*. Rio de Janeiro.
- ABNT - Associação Brasileira de Normas Técnicas (2009), *NBR 15900-10:2009, Água de amassamento do concreto – Parte 10: análise química – Determinação de nitrato solúvel em água*. Rio de Janeiro.
- ABNT - Associação Brasileira de Normas Técnicas (2009), *NBR 15900-11:2009, Água de amassamento do concreto – Parte 11: análise química – Determinação de açúcar solúvel em água*. Rio de Janeiro.
- ABNT - Associação Brasileira de Normas Técnicas (2011), *NBR 15961-1:2011, Alvenaria estrutural — Blocos de concreto – Parte 1: projeto*. Rio de Janeiro.

- ABNT - Associação Brasileira de Normas Técnicas (2011), *NBR 15961-2:2011, Alvenaria estrutural — Blocos de concreto – Parte 2: execução e controle de obras*. Rio de Janeiro.
- ABNT - Associação Brasileira de Normas Técnicas (2012), *NBR 6136:2014, Blocos vazados de concreto simples para alvenaria – Requisitos*. Rio de Janeiro.
- ABNT - Associação Brasileira de Normas Técnicas (2013), *NBR 12118:2013, Blocos vazados de concreto simples para alvenaria – Métodos de ensaio*. Rio de Janeiro.
- AMN - Asociación Mercosur de Normalización (2002), *NM 65:2002, Cimento Portland – Determinação do tempo de pega*. Rio de Janeiro.
- Frasson Jr, A.; Oliveira, A. L.; Prudêncio Jr., L. R. (2002), *Influência do processo produtivo nas resistências dos blocos de concreto*. IX Encontro Nacional de Tecnologia do Ambiente Construído, Foz do Iguaçu, PR, maio, 8 p.
- CETESB - ANA (2011), *Guia nacional de coleta e preservação de amostras: água, sedimento, comunidades aquáticas e efluentes líquidos*, Companhia Ambiental do Estado de São Paulo, Agência Nacional de Águas, Organizadores: Carlos Jesus Brandão [et al.], Autores: Adriana Castilho R. de Deus [et al.], São Paulo; Brasília.
- Hometeka, *Bloco de concreto x bloco cerâmico na alvenaria estrutural*. Disponível em: <http://goo.gl/zqavdD>. Acesso em: 01 set. 2016.
- Marchioni, M. L. (2012), “*Desenvolvimento de técnicas para caracterização de concreto seco para peças de concreto para pavimentação intertravada*”, 111 p. Dissertação (Mestrado) – Escola Politécnica, Universidade de São Paulo. São Paulo, 2012.
- da Silva Battagin, I. L. (2010), “*A Norma Brasileira de água de amassamento do concreto: uma contribuição para a sustentabilidade*”, *Concreto & Construção*, São Paulo, v. 58, p.37-45, abr.-jun. 2010. Disponível em: <http://goo.gl/F4xWZb>, Acesso em: 01 set. 2016.
- Ramalho, M. A.; Corrêa, M. R. S. (2003), “*Projeto de edifícios de alvenaria estrutural*”, 1 ed. São Paulo: PINI.
- SANTOS, A. (2011), *Bloco de concreto começa a virar o jogo*. Disponível em: <http://goo.gl/d9LP02>, Acesso em: 01 set. 2016.
- Visvanathan, C., Asano, T. (2001), *The Potential for Industrial Wastewater Reuse*. Encyclopedia of Life Support Systems. UNESCO Publication. Disponível em: <http://goo.gl/HDq4TH>, Acesso em: 01 set. 2016.
- World Bank (2015), *Brasil, Colômbia e Peru lideram lista de países com mais água no mundo*. Disponível em: <http://goo.gl/F3j1AC>, Acesso em: 01 abr. 2016.

An approach to the convent of Santa Clara de Asís in Havana. Study of its conservation status and intervention proposals

J. L. Guevara^{1*} , Y. A. Toirac¹ , C. M. C. Marisy¹ 

*Contact author: jlopezg@civil.cujae.edu.cu

DOI: <http://dx.doi.org/10.21041/ra.v9i2.354>

Reception: 04/09/2018 | Acceptance: 18/02/2019 | Publication: 30/04/2019

ABSTRACT

Santa Clara de Asis Convent High Choir timber truss has been victim of humidity and attack of abiotic and biotic agents which have caused its gradual degradation. For the identification of pathological processes associated with these agents and because of its patrimonial character, a diagnosis study based on an organoleptic inspection and superficial tests was carried out with the available instruments, which allowed identifying the causes. By modeling the structure with SAP 2000 program, we obtained the results that were used to calculate the solutions proposed for the identified pathologies, mainly for the loss of connection between the wall plate and the tie rod beam.

Keywords: pathological processes; patrimonial character; organoleptic inspection; superficial tests; modeling.

Cite as: Guevara, J. L., Toirac, Y. A., Marisy, C. M. C. (2019), “An approach to the convent of Santa Clara de Asís in Havana. Study of its conservation status and intervention proposals”, Revista ALCONPAT, 9 (2), pp. 228 – 246, DOI: <http://dx.doi.org/10.21041/ra.v9i2.354>

¹ Facultad de Ingeniería Civil, Universidad Tecnológica de La Habana José Antonio Echevarría, La Habana, Cuba

Legal Information

Revista ALCONPAT is a quarterly publication by the Asociación Latinoamericana de Control de Calidad, Patología y Recuperación de la Construcción, Internacional, A.C., Km. 6 antigua carretera a Progreso, Mérida, Yucatán, 97310, Tel.5219997385893, alconpat.int@gmail.com, Website: www.alconpat.org

Responsible editor: Pedro Castro Borges, Ph.D. Reservation of rights for exclusive use No.04-2013-011717330300-203, and ISSN 2007-6835, both granted by the Instituto Nacional de Derecho de Autor. Responsible for the last update of this issue, Informatics Unit ALCONPAT, Elizabeth Sabido Maldonado, Km. 6, antigua carretera a Progreso, Mérida, Yucatán, C.P. 97310.

The views of the authors do not necessarily reflect the position of the editor.

The total or partial reproduction of the contents and images of the publication is strictly prohibited without the previous authorization of ALCONPAT Internacional A.C.

Any dispute, including the replies of the authors, will be published in the (irst issue of 2020 provided that the information is received before the closing of the third issue of 2019.

Un acercamiento al convento de Santa Clara de Asís de La Habana. Estudio de su estado de conservación y propuestas de intervención

RESUMEN

La armadura del Coro alto del Convento de Santa Clara de Asís ha sido víctima de la humedad, y del ataque de agentes bióticos y abióticos que han provocado su paulatina degradación. Para la identificación de los procesos patológicos asociados a estos agentes y por su carácter patrimonial se realizó un estudio de diagnóstico basado en una inspección organoléptica y en ensayos superficiales con el instrumental disponible, que permitieron identificar las causas. Mediante la modelación de la estructura en el programa SAP 2000 se obtuvieron las solicitaciones a las que se encuentran sometidos los elementos a intervenir y con el resultado se calcularon las soluciones propuestas para las patologías identificadas, fundamentalmente para la pérdida del vínculo entre la solera y el tirante.

Palabras clave: procesos patológicos; carácter patrimonial; inspección organoléptica; ensayos superficiales; modelación.

Inspeção ao convento de Santa Clara de Asís em Havana. Estudo do seu estado de conservação e propostas de intervenção

RESUMO

As treliças do Coro alto do Convento de Santa Clara de Assis têm sido vítimas da umidade, do ataque de agentes bióticos e abióticos que causaram sua degradação gradual. Para a identificação dos processos patológicos associados a esses agentes e pelo seu caráter patrimonial, foi realizado um estudo diagnóstico baseado em inspeção organoléptica e ensaios superficiais com os instrumentos disponíveis, que permitiram identificar o problema e fazer um diagnóstico. Modelando a estrutura no programa SAP 2000, foram encontradas as solicitações as quais os elementos estruturais estão submetidos. Com isso foi proposta a solução dos problemas patológicos, principalmente a intervenção para corrigir a perda do vínculo entre a viga e o tirante.

Palavras-chave: processos patológicos; caráter patrimonial; inspeção organoléptica; ensaios superficiais; modelar.

1. INTRODUCTION

A project to recover the Santa Clara de Asis Convent in La Habana Vieja has begun with the purpose of rescuing this ancient building to preserve its past, its present and its future, through a process of renovation, preservation and restoration of the heritage inherited by mankind so that it becomes part of contemporary life.

The convent, which is located in the old part of the capital of Cuba, Havana, with its High Choir as shown in “Figure 1” was, according to Pedro Herrera, “the first non-army structure on a monumental scale built in Havana; that is why the urban scene of the old villa experimented a definite transformation”. (López, 2006).



Figure 1. High Choir in Santa Clara Convent Church

Santa Clara Convent timber truss of the first cloister is considered the oldest timber truss preserved in La Habana Vieja. This type of roof is the best exponent because of its dissimilar solution. This composition of the structure has been exposed to the attack of external agents, both biotic and abiotic, which act in an aggressive way causing its degradation.

A study on this topic was carried out as part of the research to determine the state of deterioration of the timber truss High Choir Convent at present. This study resulted in the proposals of intervention techniques, both traditional and current ones. The techniques were aimed at recovering and improving the structural capacity of the timber truss at Santa Clara de Asís Convent, which was built in the 17th century and is considered a World Cultural Heritage with a protection 1 level, granted by the urban regulations in La Habana Vieja. The building constructive system represents a valuable heritage, so to preserve it means to rescue the cultural identity of the nation.

2. SANTA CLARA DE ASIS CONVENT: THE OLDEST TIMBER TRUSS EXPONENT PRESERVED IN LA HABANA VIEJA

The famous architect Felicia Chateloin, in her article called “Timber Truss in La Habana Vieja. The Privilege of its Preservation” stated that “Santa Clara Convent can be considered the most important example of a construction in Havana where timber truss has been used. The study of the convent is important not only because of its ancient construction, quality and variety of its roofs but also because of the number of elements that make up the roofs which is the same in any other construction” (Santiesteban, 2007).

“The coffered wood ceilings cover most of the premises on the top floor of the first cloister and are distinguished by their elegance as well as the size of the main elements, the ones in the church nave and its choir” (Espiniella, 2001; Arduengo and Cruz, 2012).

In Cuba, most of the sloping wooden roofs from the colonial times are descendant from Mudejar timber truss. For a long time, authors like Joaquin Weiss (Weiss, 1978) referred to this type of timber truss as carved ceiling, but Felicia Chateloin makes emphasis on the error in using this term in the timber truss, “today we recognize that this term must be restricted to decorated flat ceilings. They should be correctly called ‘timber trusses’ for their structural system. The timber truss, not the carved ceiling, was the one which characterized the roofs and ceilings of colonial Havana in the 17th and 18th centuries” (Santiesteban, 2007).

2.1 Structural and constructive characterization of the church High Choir timber truss

The High Choir ceiling is made up of rafters or angle rafter, see “Figure 2”, in twos, which start from the fastening, which is the perimetric frame of the structure, reaching the ridge beam or ridgepole to form four gables. According to Santiesteban, 2007, in spaces with a design span of

more than 10 m long, the rafters will have an approximate section of 14 x 17 cm. The angle braces are connected horizontally, two-thirds from the height, by the collar beams, which determine the ceiling central part, so that the interior perimeter is a trapezoid. Considering the characteristic mentioned, timber truss can be classified as a rafter and a collar beam truss and as a structural set, that works under compression. “On these roofs, the ridgepole is not visible and can or cannot be supported on hips. The collar beam has a section of equal dimensions or very similar to the ones of the rafters of its timber truss” (Santiesteban, 2007).



Figure 2. Structural elements of the Convent High Choir timber truss.

The rafters are supported by the walls by means of the fastening, which is a structural frame of the system. In religious temples, the section can be of 35 x 30 cm or more; the fastenings are the one which receives the horizontal thrust that the rafters transmit (Santiesteban, 2007). For stiffening the structure, the fastening is fastened by transverse beams or tie rod beams which work by traction and form a triangle together with the rafters. These section beams are 15 x 20 cm approximately and are joined by short pieces called links, thus forming what is called tie rod beams. See “Figure 3”, in the space between the links and halfway of the design span, there is a starred polygon with a decorative function. The objective of the tie rod beams is generally to join the wall plates which are made up by sections.



Figure 3. Tie rod beams on corbels.

It is noted that in the space angles, “Figure 4”, the ‘angle braces’ are assembled to the fastening. They have a stiffening action and like the tie rod beam, they work by traction (Santiesteban, 2007). The angle braces are placed at 45° supported by corbels in skew (Matauco, 2000). The corbels on which the angle braces are supported and parallel to the contiguous walls, thus making the front parts more visible.



Figure 4. Angle brace, skewed corbels and corner corbel.

3. METHODOLOGICAL APPROACH FOR THE DIAGNOSIS.

The methodology used for the analysis of the pathologies on the timber truss was done by studying the methodologies proposed by different authors (Álvarez et al., 2005); (Basterra et al., 2005); (Garófalo, 2000); (Otaño, 2002); (Rodríguez, 2006). “A comprehensive analysis of the problem will always take the study of the environment next to the building, the lesions and their strainal signs and their casuistic effects. The preservation or necessary protection goes from the building to the city and vice versa, like every process that works like a system” (Otaño, 2002).

The diagnosis methodology which the above authors define, has three fundamental stages, first, characterization of the object of study; second, organoleptic inspection and third, superficial examinations. In the first stage, a search and a bibliographic inspection to gather information about the history of the building unit as well as a description of the characteristics of the system and its components were carried out. The second stage consists of the inspection of the building and its environment, based on a rigorous and detailed organoleptic inspection which allows establishing the general state of conservation of the structure. The inspection will include a sketch where coordinate axis was drawn with the objective of better delimiting the areas of the space and facilitate the future description and representation of the identified pathologies. This will also be accompanied by a photographic documentation to provide evidence of the pathology referred to. In the third stage, the techniques and instruments used for carrying out non-destructive tests which allow doing a more detailed analysis of the pathological processes taking place on the structure are defined. In this stage, the environment parameters that can have an influence on the observed pathologies are assessed by applying tests in situ to check the temperature and the amount of environmental and superficial humidity of the elements. The anatomical identification of the species and xylophagous organisms is carried out in the laboratory. This final diagnosis has the purpose of confirming or rejecting the hypothesis developed in the second stage.

In diagnosing, the sketches which appear in “Figure 5”, the numbers of the elements which make up the structure of the High Choir are shown. The enumeration of the rafters was made in an independent way in each gable, whereas the components of the planking were defined according to the right joint in each case and they were numbered starting up from the timber truss on the walls in the direction of the ridgepole. The corbels, the angle braces, the hips and the tie rod beams (elements which can be seen in “Figure 6”) were numbered in a consecutive way, starting from the elements located at the intersection of the axes B'-1, and in a clockwise direction, see “Figure 5”.

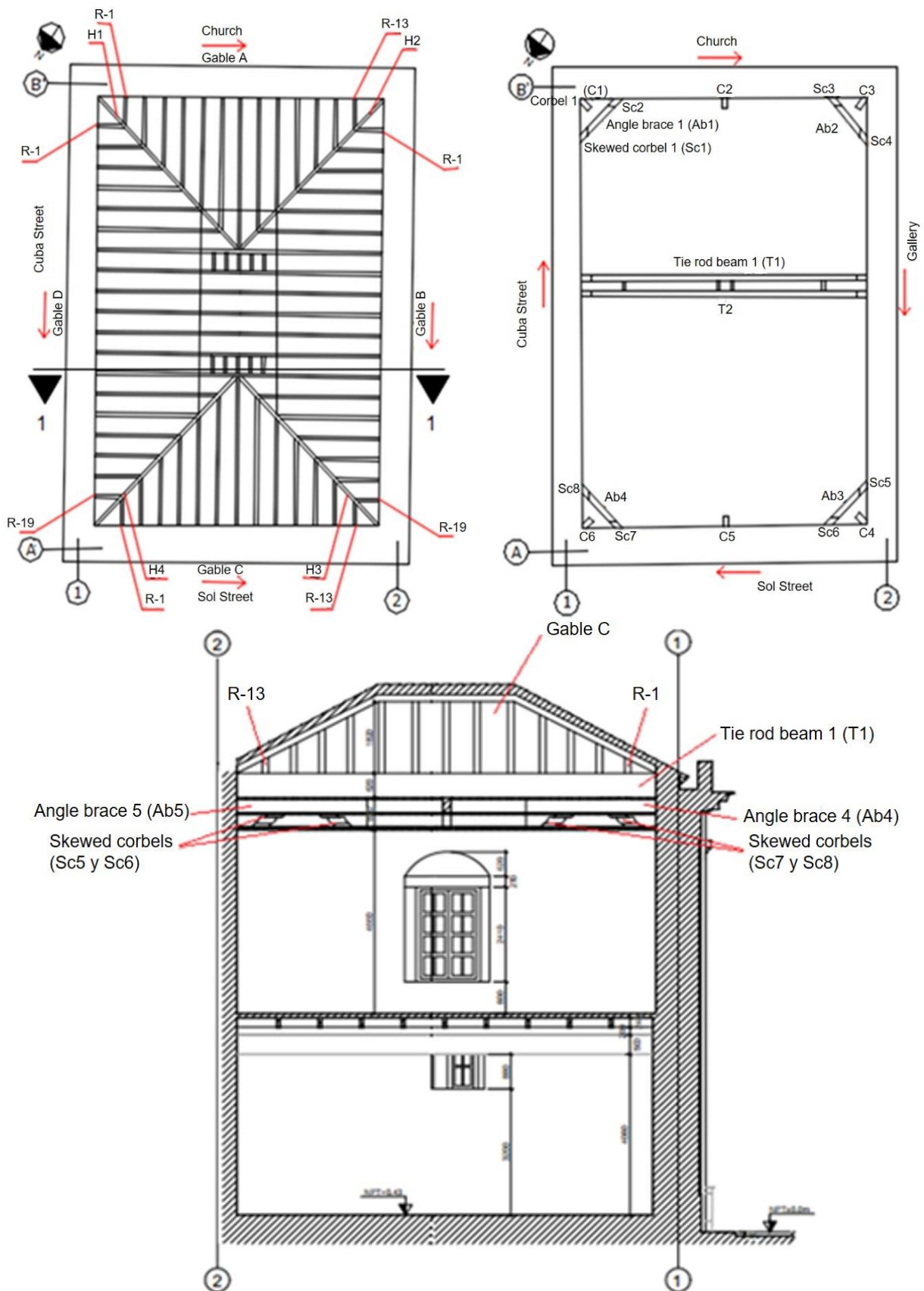


Figure 5. Nomenclature and numbering of the elements at the High Choir in an architectonic plan and in a cross section 1-1.

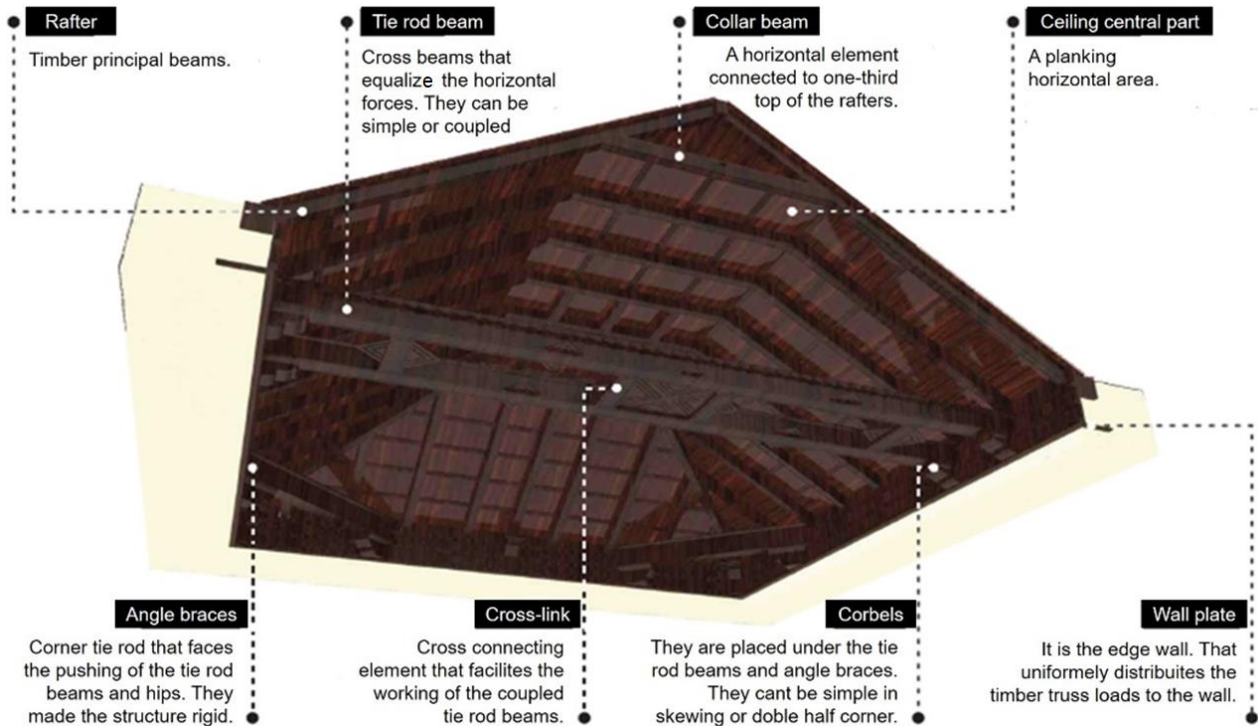


Figure 6. High Choir elements forming the timber truss. (Authors: Dayana Espinosa Ruiz, Arch; Lillian Potts Rodriguez, Arch. and Linnet Valdés Rivero, Arch.)

3.1 Visual inspection of the High Choir.

The first approach to the structure showed the evident state of abandoning and the level of deterioration due to the lack of maintenance. Dirtiness is visible on the walls as a result of the accumulation of dust, soot and organic matter because of the nearness to the Harbor Avenue and the passing of vehicles along the neighboring streets.

A high environmental humidity can be perceived in the place. On the other hand, the building has been exposed to an excess of water for long periods of time, as there are a lot of seepages coming from the roof, which are evident for the green patinas and rain wash patches on the walls, see “Figures 7-10”. These seepages can cause severe damages in the wood, accelerating the process of rottenness, as well as on the mud walls; these types of constructions tend to retain much humidity.



Figures 7 and 8. Patinas on gallery wall to axis 2 of the Choir.



Figure 9. Wall with rain wash in axis A



Figure 10. Top wall green patinas in axis 2.

Because of the proliferation of feeder plants on the roof, there are visible developed systems of roots which penetrate the mud walls, see “Figure 11”, and can cause fissures in the wall.



Figure 11. Roots in axis A from the feeder plants on the roof.

The groups of bats in the roof of the building (see “Figure 12”) have contributed with their excrements and remains of food to the dirtiness of the walls and the deterioration of the building in general, see “Figure 13”. Although in some situations, these chiropterans are beneficial to man, like in the maintenance and regeneration of forests in the dispersion of seeds. However, they can become a plague when they install in places that do not constitute their normal habitat.

The bats' stools contain acids, which cause problems of an esthetics nature in the walls due to the accumulation of black excrements. They can also affect people's health, by creating a propitious environment for the development of an ecological succession of microorganisms, starting with the growing of bacteria, fungi and finally the proliferation of xylophagous insects.



Figure 12. Presence of bats.



Figure 13. Dirtiness on the walls and in the building because of bat excrement and food remains.

Fissures and vertical cracks, which range between 1-2 cm thick and 3-4 cm deep, mainly in the joints of the walls, see “Figure 14”. These cracks can be the result of an inclination, caused by the thrust of the timber truss, since there are also horizontal cracks in the lower part of the wall, see “Figure 15”.



Figure 14. Crack 1-2 cm thick at the intersection of axes A-1.



Figure 15. Horizontal cracks in the lower part of the wall (axis 1).

As the ceiling is made of an organic material, the wood is exposed to the attack of different agents, both biotic and abiotic, which contribute to its degradation, and loss of its resistance in most cases. The abiotic agents are of chemical or physical type and are caused by meteorological or climatic phenomena like solar radiation, environmental humidity, the rain, the wind, among others (Group of authors, 1998).

According to the Wood Chilean Corporation (CORMA, its abbreviation in Spanish), certain conditions are needed for the growth and subsistence of biological agents like the existence of a source of food material to take nourishment, an interval of ideal temperature for their growth (between 3° and 50°C), being optimum about 37°C. Wood becomes sensitive to the attack of fungi, when humidity ranges between 20% and 140%, since below 20%, the fungus cannot grow, and above 140% humidity, there is not enough oxygen to be able to live. With the conditions mentioned above, the wood is exposed to the biological attack, thus creating alterations of great importance in the wood mechanical resistance or on its external aspect.

The joint between the tie rod beam and the wall plate is the most critical point, since its malfunction brings about problems to the roof and the inflow of water (Garófalo, 2000; Rodríguez, 2003). At the same time, the thrust on the wall are created by the detached tie rod beam, causing horizontal cracks which come up at a certain height, more visible on the internal face, accompanied by a displacement outward of the highest course. “Figures 16-19” show the drop of the corbels on which

the tie rod beams and angle braces are supported. The cause of this deterioration can be associated with the presence of humidity which is caused by the putrefaction of the supporting elements in the interior of the wall, that is why the elements stopped working like they used to do it and started to give way. In the case of the corbels on which the tie rod beams lean, they are associated to the force exerted by the tie rod beams.



Figure 16. Dropping of corbel under tie rod beam 2 (T2), on axis 2.



Figure 17. Dropping of corbels under tie rod beams 1 and 2 (T1 and T2), on axis 1.



Figures 18 and 19. Dropping of skewed corbels (Sc7 and Sc8) under angle brace 4 (Ab4).

3.2 Superficial examination of the High Choir timber truss.

We had the support of the Historian Office Diagnosis Group for carrying out the tests, levels I and II (Rodríguez, 2006) which complemented the organoleptic study done and it allowed a closer approach to the real state of preservation of the structure. As part of this study, the following tests were done: measurement of dimensions of the elements which form the ceiling (level I), measurement of superficial humidity, environmental humidity and temperature (level I), punching of the wooden elements (level I), identification of plants (level I) and anatomical identification of wood (level II, in the laboratory).

Dimensions of the elements.

For determining the squaring of the rafters that form the timber truss and the spacing between them, since we do not have the original plans, a metallic tape was used as a measuring element. The measurements were taken on the lower and lateral face of the elements. The spacing measurement was taken internally from face to face of the rafters. The sketch of measurements taken to these elements is shown in “Figure 20”.

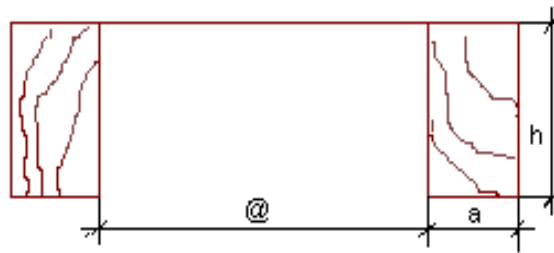


Figure 20. Rafters form of measurement.

Table 1 shows all the elements contained in the timber truss, as well as the dimensions of transverse sections according to the type of piece and its spacing.

Table 1. Dimensions of the elements of the High Choir timber truss.

Element	Quantity	Sections		(@) Spacing	
		Width (a)	Depth of beam (h)		
Hips	4	17 cm	20-22 cm	-	
Rafters	64	17 cm	20-22 cm	45-58 cm	
Angle braces	4	23-24 cm	30-31 cm	-	
Corbels	10	-	-	-	
Skewed corbels	8	-	-	-	
Simple tie rod beams	2	T1	24.5 cm	31.5 cm	80 cm
		T2	22.5 cm	31.5 cm	

Relative humidity and environmental temperature.

The levels of humidity were measured with the thermo-hygrometer, see “Figure 21”; they were measured in different points of the building and were controlled during three months (March-May of 2018), so that we could get the possible variations in the readings done as the evidence in atmospheric differences inside the same building. The levels measured in every case are higher than 65% and the thermohygrometric conditions are convenient, that is, inside the building, there are temperatures ranging between 20°C and 30°C, which help to the development of biodegradation agents and contribute to accelerate the vital cycles of a number of microorganisms and xylophagous insects which degrade the wood.

Superficial humidity.

The test of superficial humidity allows knowing the content of humidity kept on the fibers of the material, since its value has an influence on the physical properties of it. The instrument used to carry out the test was the Hygrometer *Protimeter Surveymaster SM*, see “Figures 22 and 23”.



Figure 21. Thermo-hygrometer.



Figure 22. Hygrometer Protimeter Surveymaster SM.



Figure 23. Measurement of superficial humidity on elements.

The instrument has two ways of measuring: by the color of the bar LED and by the reading of the percentage (%) of humidity kept in wood. According to the color of the bar, it is green when it is in a safe state of drying in the air, yellow represents the boundary line, and red when the wood is in an unfavorable condition. The classification of the levels of saturation established by the manufacturer is shown in Table 2.

Table 2. Levels of saturation established by the manufacturer.

Color	Level of saturation of superficial humidity.	Range of values (%)
Green (G)	Semi-dry	6-8-10
Yellow (Y)	Admissible humidity	12-14
Red (R)	Humid	16-18-20
	Saturated	= 20

The measurements were made on the rafters, in the areas close to the support and on the elements, which were more exposed to humidity. Five settings were registered in each measurement. To execute them, the equipment is pressed to a nominal depth of 5-15 mm on the element studied and this gives relative settings of humidity kept inside the material.

Values higher than 18% were detected in specific areas. This confirms the presence of humidity due to seepages in the roof which is one of the main causes of damage. Humidity ranging from 18 to 20% and higher than this value creates a favorable environment for the proliferation of fungi from rotteness and other xylophagous organisms which can affect the mechanical properties of wood.

In the case of the elements where damages have been found and are not above this range, we can infer that there are stages where there is a considerable increase of humidity, thus allowing the appearance of wood-degrading agents.

Research done with punch in wooden elements.

The objective of this test is to determine the state of conservation of the rafters in the area close to the supports, according to the measure obtained from the penetration of a graduated punch, see “Figure 24”. The value depends on the characteristics and the specific hardness of the wooden element being analyzed. When the punch does not penetrate or is superficial, it means that the studied element is in good shape. However, higher values of penetration (from 2-5 cm) are obtained when the elements are rotten and shredded. The result of this test reveals that the commonest identified damages are: shredding in the area of the rafters and angle braces head in the lower part and sides of 70% of the rafters which make up the ceiling gable, as well as other damages like

cracks, putrefaction, splintering and damp patches.



Figure 24. Investigation in wooden elements with graduated punch.

“Figure 25” summarizes the damages detected in the High Choir, placing them in an architectural plan.

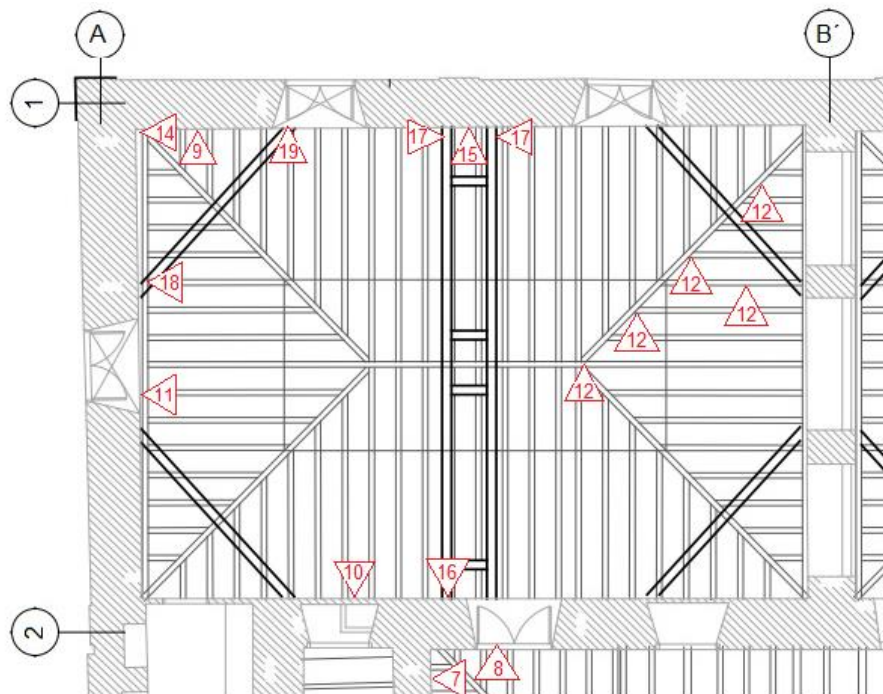


Figure 25. High Choir architectural plan showing the location and association of damages Figures 7-12 and 14-19.

Identification of feeder plants.

Photographs of parasite plants growing in the roof were taken; see “Figures 26 and 27”. The identification of superior plants was carried out by comparing them with specimens present in the herbarium of the Biology laboratory at the Havana Historian Office Diagnosis Group. There, the botanical family, the scientific and vernacular name (Group of authors, 1999); (Roig, 2014) and the biological aspect (Pérez and Rodríguez, 2007); (Pérez, 2010) were obtained.



Figure 26 and Figure 27. Invading plants on roof of the High Choir.

The plants identified are of herbaceous and arborous aspects, the latter has roots which can penetrate the walls and produce cracks which continue developing, widening and creating new internal tensions in the walls (Pérez, 2010).

Although the mechanical action of plants of herbaceous aspect are of less effect than the ones of arboreal aspect, they also play a role in developing damages, contributing to the chemical deterioration of the substratum in which they grow and the retention of humidity; thus, facilitating the growing of other more potential plants. So, it is necessary to know the species or group which the biological agent belongs to, from which are drawn up the strategies for the conservation of the deteriorated substratum.

Identification of timber species.

In order to carry out this test, random samples of the wooden elements for their identification were taken to obtain histological sections in the transverse, tangential and radial directions. The observation of the anatomical characters was taken with the use of the light optical microscope.

The samples were identified by using the compared anatomy method, which is based on the comparison of the macroscopic characters of the samples with pattern woods, previously identified and classified at the Xylotheque biology laboratory of the Historian Office. The characters were assessed are the color, texture, grain, luster, smell (on those that could be measured) and the presence of growth rings (Carreras and Dechamps, 1995). The samples were taken from the angle brace 4, from the wooden frieze, from the skewed corbel 4 and from the frieze from gable D. The results show that the skewed corbel 4, the wooden frieze and the frieze from gable D belong to the *Cedrela odorata* species, see “Figure 28” and angle brace 4 belongs to the *Tectona grandis* species, see “Figure 29”.

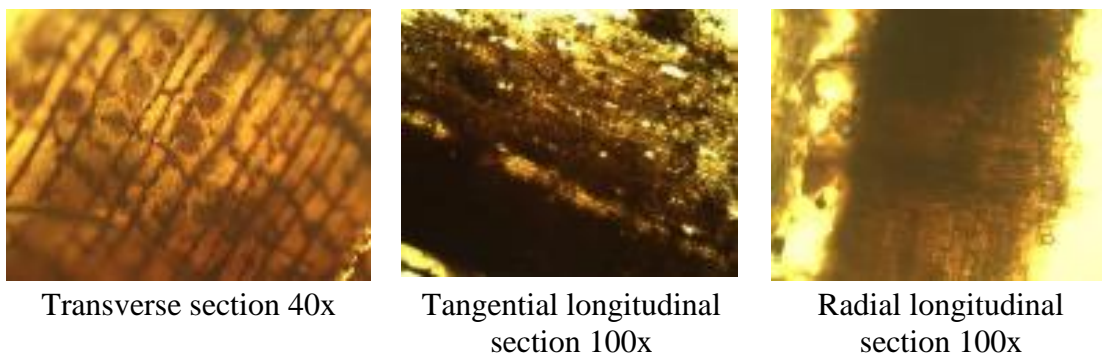
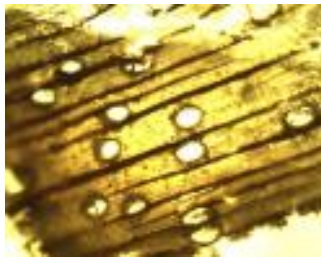
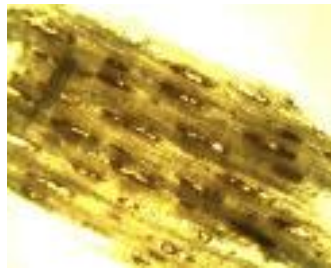


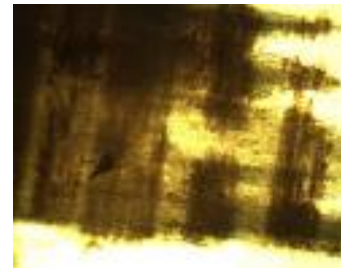
Figure 28. Anatomical sections of Cedar.



Transverse section 40x



Tangential longitudinal section 40x



Radial longitudinal section 40x

Figure 29. Teak anatomical sections.

The histological sections of the transverse, tangential-longitudinal, and radial-longitudinal samples were taken (“Figures 28 and 29”), which allow corroborating by the microscope a better observation of the radial parenchyma, making possible to determine that timber species are cedar and teak, according to the parenchyma model of the transverse section.

Once the species have been identified, Table 3 shows their physic mechanical properties, from the information given by the Cuban Institute of Agro forest Researches, which will be used in the structural modeling of the timber truss with the SAP 2000 program and the reinforcement calculations.

Table 3. Main mechanical and physical characteristics of identified woods.

Scientific name	Common name	Density g/cm ³	Elasticity modulus (kg/cm ² x1000)	Tensile Strength (kg/cm ²)	Flexural Strength (kg/cm ²)	Compressive Strength (kg/cm ²)		Shear Strength (kg/cm ²)
						Perpendicular to the fibers	Parallel to the fibers	
<i>Cedrela odorata</i>	Cedar	0,37-0,75	78.10	690	667	-	302	40
<i>Tectona grandis</i>	Teak	0,61-0,74	110	850	1160-1450	-	513-685	63.2

4. VERIFICATION OF ACTING LOADS ON THE BEAMS

The structure was modeled with the SAP 2000 program, see “Figure 30”, taking the weight of the materials (NC 283: 2003), the roof use load (NC 284: 2003) and the load of wind (NC 285: 2006) for the analysis of the loads combinations according to NC 450: 2006.

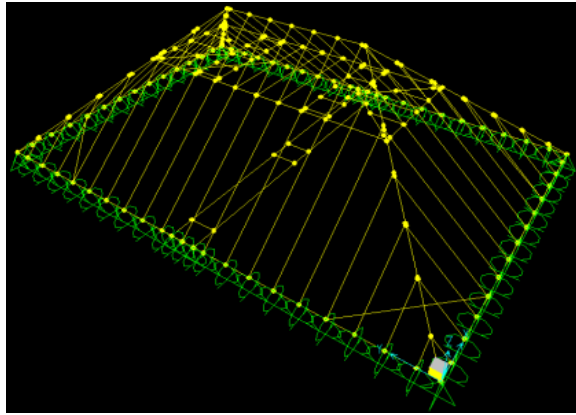


Figure 30. Modeling the structure with the SAP 2000 program.

Results of axial stress modeling in the tie rod beam 1: $NT1=60,15\text{kN}$ and in the tie rod beam 2: $NT2=52,49\text{kN}$, obtained from the less favorable combination.

5. INTERVENTION PROPOSALS.

5.1 Solution to tie rod beams with prosthesis.

It involves substituting the retired part of wood by inserting bars (steel ones or FRP- Fiber Reinforced Polymers ones) in drillings done in the wood and gluing the bars so that they adhere well. For the design, it was considered the greater axial solicitation, for both tie rod beams, of less favorable combination obtained from the modeling made with the SAP 2000 program. The diameters of the drillings must be broadening enough to leave a width of 3 to 6 mm around the bar, which will be filled with epoxy.

Process of execution: cut off the degraded part of the head with chain saw or handsaw; drill holes in the original tie rod beam and installation of the bars; selection and conformation of the new wood to be inserted, by mortising to carry out the joint with the wall plate. The holes are drilled in the new insertion and the epoxy resin is applied on the bars. Finally, the new wood to be inserted is placed, which must fulfill the requirements of durability for wood of structural use like the restriction of knots, drying cracks, and control of humidity of hygroscopic balance, among others. This solution can be applied to products from the Italian company of “Material aids for construction and industry” (MAPEI, its abbreviation in Italian). It consists in applying the epoxy resin first to the wood and holes for the bars. The Mapewood Primer 100 product, which is an epoxy impregnant of fluid consistency is left to be dried and then to apply it later on the bars and wood. The Mapewood Paste 140 product which is an epoxy adhesive of thixotropic consistency is very effective in the restauration of wood structural elements.

5.2 Reinforcement with carbon fibers.

It is a current technique for reinforcing structural elements, which has been used not only for recovering timber structures, but also concrete and masonry ones. It consists in fixing with epoxy resins platens of synthetic material with carbon fiber (approximately 1, 2 mm to 1, 4 mm thick and 60 mm width) to the element to be reinforced. Its use is generally aimed at absorbing the tensile stress, in this case is of 60,15 kN which was obtained as an axial stress less favorable in the modeling carried out, which generate tensile stress because of its high resistance. The fibers have high structural resistance compared to its practically inconsiderable weight and are resistant to corrosion (Morocho, 2014). The disadvantage in applying this method is its high cost.

5.3 Replacement of wall plate by a one made of wooden.

The wall plate is replaced by a mud sill with the same scantling as the original one with these dimensions (30x35cm); in order to execute the joints in the corners, they will be carried out with a rabbet joint and according to the length of the piece; this will be done every 5 m by means of a key joint. The wood to be used is the Manilkara valenzuelana (a hard-reddish wood, which grows in the island of Cuba) which is a harder wood than the cedar.

Design of the joint along the element.

The joint along the element is based on the key joint, which consists in transmitting the tensile stress (Nd) from one piece to another by means of parallel compression to the fiber applied on the front with a $b \cdot t$ surface, see “Figure 31”. Besides, the stress generated in the complete section through a longitudinal shear from shearing stress on the $b \cdot l$ surface section, see “Figure 31” (Martitegui et al., 2009).

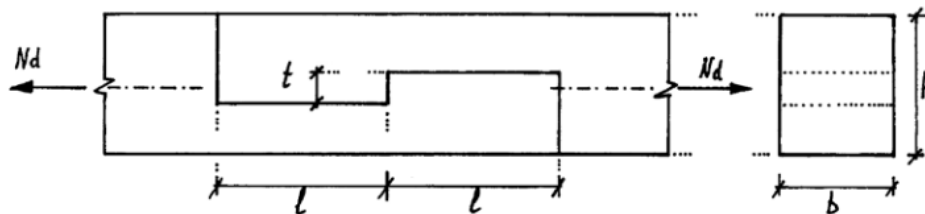


Figure 31. Key joint. Source: (Martitegui et al., 2009)

Joint design on the corner.

The joining of the corners will be done by rabbet joint “Figure 32”, which is reinforced with coach-screws as shown in “Figure 33”, and have a shank made up of a threaded area on the tip (thread) and a flat area (shank).

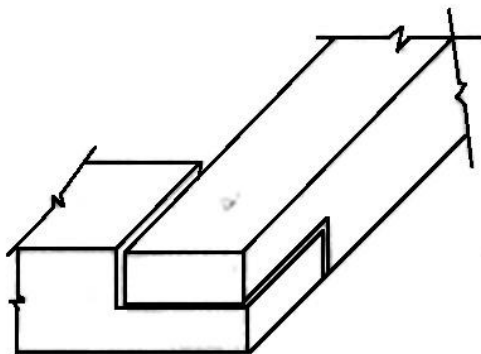


Figure 32. Rabbet joint. Source: (Martitegui et al., 2009).

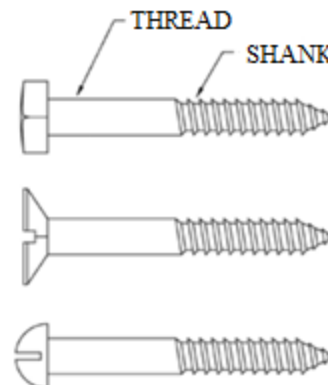


Figure 33. Coach-screws with hexagonal, countersunk, and round heads (up to down). Source: (Martitegui et al., 2009).

5.4 Replacement of tie rod beams with steel tensors.

It consists in placing the steel tensors which will take the stress of the original tie rod beams and will go through the wall plate that is fixed with two nuts and a metal sheet to avoid the crushing of the wood. Thus, using the axial stress obtained from the modeling of the elements with the SAP 2000 program.

The design was done by using bars as members under tension; they can be fixed with threads and

nuts (McCormac, 2002). The nominal stress under tension on threaded little bars when the thread is included in the cutting plane, according to Table J3.2 from Loading and Resistance Factors Designs (LRFD) is equal to $0.75F_u$. The failure possibility of these elements is because of fractures due to the area reduction caused by the threads.

The design involved A-36 steel bars with creep stress of $F_y=250\text{MPa}$ and last stress of $F_u=400\text{MPa}$. Nominal tensor stresses were analyzed for the most loaded tensor, although two tensors were placed in the same position as the tie rod beams.

It is convenient to limit the minimum diameter of the tensors (McCormac 2002) to 5/8 inches, since tensors with the smallest diameters get damaged frequently during the constructive process. Besides, some designers use diameters not less than 1/500 of the length of tensors, in order to obtain certain rigidity even when the stress calculations allow smaller diameters.

6. CONCLUSIONS

The most probable causes from the pathologies identified are associated with the excess of humidity due to seepages coming from the roof, which have created a favorable atmosphere for the proliferation of xylophagous organisms. The damage which is affecting most the behavior of the structural group is the disjoining or lack of link between the wall plate and the tie rod beam, originated by the putrefaction of these elements in the area of the support on the wall. This causes the thrust of the facade wall and its future collapse which is clearly seen in the vertical cracks at the intersection of axes and horizontal cracks on the wall of axis 1 of the High Choir. Overall, the structure is in a regular state.

The solution suggested to solve the main injury was the replacement of the wall plate by other wood and the tie rod beams by the steel tensors. The last ones will be covered in wood in order to affect as little as possible the esthetic of the building due to its patrimonial value.

7. ACKNOWLEDGEMENTS

The authors are very grateful to the specialists of the Havana Historian Office: the RESTAURA Projects Enterprise, the Diagnosis Department and the Investment Management Office for all their collaboration and the availability offered and for trusting our service to make this work possible. We also thank the collaboration of these architects: Dayana, Lillian and Linnet.

8. REFERENCES

Álvarez, L., Basterra, A., Casado-Sanz, M., y Acuña-Rello, L. (2005), “Aplicación del resistógrafo al diagnóstico de elementos singulares en estructura de madera” en I jornadas de investigación en construcción (2-4 de junio de 2005. Madrid, España). Madrid, España: Instituto de Ciencias de la Construcción Eduardo Torroja – CSIC. 165-181.





Arduengo García, D. A., Cruz Pérez, A. (2012), *Una nueva lectura del antiguo convento de Santa Clara de Asís desde la arqueología y la historiografía*. Arquitectura y Urbanismo, 33(1), 77-90. http://scielo.sld.cu/scielo.php?script=sci_arttext&pid=S1815-58982012000100006&lng=es&tlng=es.

Basterra, L. A., Casado, M., Acuña, L., Ramón-Cueto, G., López, G., Barranco, I., Relea, E. (2005). *Avance de propuestas metodológicas para el diagnóstico y análisis de estructuras de maderas históricas*. In Actas del Cuarto Congreso Nacional de Historia de la Construcción: Cádiz (pp. 27-29).

Carreras, R., Dechamps, R. (1995). *Anatomía de la madera de 157 especies forestales que crecen en Cuba y sus usos tecnológicos, históricos y culturales*. v. 1: El texto, v. 2: Las láminas.

- DCTA-UPM (1998), "*Tratado de rehabilitación: Patología y técnicas de intervención. Elementos estructurales*". Tomo 3, Ed. Munilla-Leria.
- Espiniella, D. T. (2001). *Del barroco colonial cubano. Su expresión en la arquitectura religiosa de La Habana*. In Actas III Congreso Internacional del barroco americano: Territorio, Arte, Espacio y Sociedad: Universidad Pablo de Olavide, Sevilla, 8 al 12 de octubre de 2001 (p. 71).
- Instituto de Ecología y Sistemas de Cuba (1999), *Cuba y sus árboles*. Editorial Academia La Habana. ISBN: 959-02-0252-7
- López, P. A. H. (2006). *El Convento de Santa Clara de La Habana Vieja* (R. y. M. C. Centro Nacional de Conservación Ed.). La Habana Vieja. Cuba: Consejo Nacional de Patrimonio Cultural.
- Martitegui, F. A., González, G. Í., Herrero, M. E., Álvarez, R. A., Cabo, J. L. F. (2009). *Diseño y cálculo de uniones en estructuras de madera*. Documento de aplicación del Código Técnico de la Edificación (CTE) Documento Técnico 03: MADERIA. Sociedad Española de la Madera.
- Matauco, E. N. (2000). *La carpintería de armar española*. (Munilla-Lería Ed.). Ministerio de Cultura, Instituto de Conservación y Restauración de bienes culturales. España.
- McCormac, J. C. (2002). *Diseño de estructuras de acero. Método LRFD* (S. A. d. C.V. Alfaomega Grupo Editor Ed. 2ª edición ed.).
- Morocho, D. E. E. (2014). *Reforzamiento estructural para forjados de madera en edificaciones patrimoniales y contemporáneas*. (Bachelor's thesis), Universidad de Cuenca, Cuenca-Ecuador.
- Norma Cubana (2003), *NC 283: 2003 Densidad de materiales naturales, artificiales y de elementos de construcción como carga de diseño*.
- Norma Cubana (2003), *NC 284: 2003 Edificaciones. Cargas de uso*.
- Norma Cubana (2006), *NC 285: 2006 Carga de viento. Método de cálculo*.
- Norma Cubana (2006), *NC 450: 2006 Edificaciones. Factores de carga o ponderación. Combinaciones*.
- Otaño, I. M. G. (2002). *Métodos Organolépticos de Evaluación y Dictámen. Paper presented at the Conferencia. II: Evaluación Organoléptica y Diagnóstico en Edificaciones*. Instituto Superior Politécnico José Antonio Echevarría. Facultad de Arquitectura.
- Pérez, A. C., Rodríguez, R. (2007). *Plantas epilíticas del Castillo de La Fuerza en el Centro Histórico de La Habana Vieja, mecanismos de dispersión y distribución*. Revista del Jardín Botánico Nacional. Universidad de La Habana, 61-64.
- Pérez, A. C. (2010). *Plantas epilíticas deteriorantes de la Fortaleza San Carlos de la Cabaña*. Revista del Jardín Botánico Nacional. Universidad de La Habana, 219-222.
- Rodríguez, O. A. (2003). *Patología, diagnóstico y rehabilitación de edificaciones*. Monografía. Instituto de Ensayos y Materiales. Universidad Mayor de San Andrés. La Paz. Bolivia.
- Rodríguez, O. Á. (2006). *Metodología para realizar el estudio de diagnóstico para la rehabilitación estructural de forjados planos de madera en edificaciones ubicadas en el Centro Histórico de La Habana*, (Doctorado), CUJAE.
- Roig, J. T. (2014). *Diccionario botánico de nombres vulgares cubanos* (E. Científico Técnica Ed. Cuarta edición ed.). La Habana.
- Santiesteban, F. C. (2007). *Las armaduras de pares en La Habana Vieja. El privilegio de su conservación*. Gabinete de Arqueología, 6, 49-60.
- Tejera Garófalo, P. (2000). *Patología de las Edificaciones en conservación y rehabilitación de edificaciones*. Folleto Maestría.
- Weiss, J. E. (1978). *Techos coloniales cubanos* (E. A. y. Literatura Ed.). La Habana: Editorial Arte y Literatura.

Analysis of pathological manifestations of concrete in urban overpasses

H. J. N. Lima¹ * , R. S. Ribeiro² , R. A. Palhares³ , G. S. S. A. Melo¹ 

*Contact author: hjnery@gmail.com

DOI: <http://dx.doi.org/10.21041/ra.v9i2.308>

Reception: 14/06/2018 | Acceptance: 14/11/2018 | Publication: 30/04/2019

ABSTRACT

The paper presents the case study of pathological manifestations in concrete structures, located in the Northern Road Hub of Brasília, using the GDE / UnB methodology, which qualifies and quantifies the degradation of structural damages. The general state of the structure was characterized in order to serve as a subsidy for decision making regarding routine interventions, in order to extend the useful life of the structure. The methodological routine consists of conducting field inspections, catalog of structural pathologies with photographic survey, characterization of pathologies and classification according to the weighting factors and damage intensity factors of the structure according to the GDE / UnB methodology for special works of art, calculation and overall classification of the structure damage.

Keywords: pathologies; concrete structure; overpass.

Cite as: Lima, H. J. N., Palhares, R. A., Ribeiro, R. S., Melo, G. S. S. A. (2019), “*Analysis of pathological manifestations of concrete in urban overpasses*”, Revista ALCONPAT, 9 (2), pp. 247 – 259, DOI: <http://dx.doi.org/10.21041/ra.v9i2.308>

¹ Programa de Pós-Graduação em Estruturas e Construção Civil – Universidade de Brasília, Brasília, Brasil

² Departamento de Engenharia Civil, Centro Universitário do Distrito Federal – UDF, Brasília, Brasil

³ Departamento de Estruturas, Faculdade de Engenharia – UFJF, Juiz de Fora, Brasil

Legal Information

Revista ALCONPAT is a quarterly publication by the Asociación Latinoamericana de Control de Calidad, Patología y Recuperación de la Construcción, Internacional, A.C., Km. 6 antigua carretera a Progreso, Mérida, Yucatán, 97310, Tel.5219997385893, alconpat.int@gmail.com, Website: www.alconpat.org

Responsible editor: Pedro Castro Borges, Ph.D. Reservation of rights for exclusive use No.04-2013-011717330300-203, and ISSN 2007-6835, both granted by the Instituto Nacional de Derecho de Autor. Responsible for the last update of this issue, Informatics Unit ALCONPAT, Elizabeth Sabido Maldonado, Km. 6, antigua carretera a Progreso, Mérida, Yucatán, C.P. 97310.

The views of the authors do not necessarily reflect the position of the editor.

The total or partial reproduction of the contents and images of the publication is strictly prohibited without the previous authorization of ALCONPAT Internacional A.C.

Any dispute, including the replies of the authors, will be published in the (first issue of 2020 provided that the information is received before the closing of the third issue of 2019.

Análise de manifestações patológicas do concreto em viadutos urbanos

RESUMEN

O trabalho apresenta o estudo de caso de manifestações patológicas em estruturas de concreto, localizadas no Eixo Rodoviário Norte de Brasília, por meio da metodologia GDE/UnB, que qualifica e quantifica a degradação de danos estruturais. Foi realizada a caracterização do estado geral da estrutura com a finalidade de servir de subsídio para tomadas de decisões quanto a intervenções rotineiras, de forma a ampliar a vida útil da estrutura. A rotina metodológica consiste na realização de inspeções em campo, catálogo das manifestações patológicas estruturais com levantamento fotográfico, caracterização dos fenômenos patológicos e classificação segundo os fatores de ponderação e fatores de intensidade de danos da estrutura conforme a metodologia GDE/UnB para obras de arte especiais, cálculo e classificação global dos danos da estrutura.

Palabras clave: manifestações patológicas; estrutura de concreto; viadutos.

Análisis de manifestaciones patológicas del concreto en viaductos urbanos

RESUMEN

El trabajo presenta el estudio de casos de manifestaciones patológicas en estructuras de hormigón, ubicadas en el Eje Rodoviario Norte de Brasilia, por medio de la metodología GDE / UnB, que califica y cuantifica la degradación de daños estructurales. Se realizó la caracterización del estado general de la estructura con la finalidad de servir de subsidio para tomas de decisiones en cuanto a intervenciones rutinarias, para ampliar la vida útil de la estructura. La rutina metodológica consiste en la realización de inspecciones en campo, catálogo de las manifestaciones patológicas estructurales con levantamiento fotográfico, caracterización de las manifestaciones patológicas y clasificación según los factores de ponderación y factores de intensidad de daños de la estructura conforme a la metodología GDE / UnB para obras de arte especiales, calculo y clasificación global de los daños de la estructura.

Palabras clave: manifestaciones patológicas; estructura de hormigón; viaductos.

1. INTRODUCTION

The correct identification of the beginning of the pathological problems allows the researcher to establish in which moment of the management of the construction they occurred. Thus, it is possible to know if they were originated in the project phase, in the specification of the material, because of unskilled workers in the execution stage of the construction, lack of supervision, or yet if the failures were due to improper operation and poor maintenance.

This analysis of identification and proposal to attack the pathological manifestations is appropriate and it is confirmed when they are compared with the cost of late changes when the manifestations have already occurred, as defined in the management of works by Mattos (2010) and PMBOK (2014). In this approach, when evaluating the cost of avoiding a pathological problem in different phases of construction, it is observed that the later the possibility of problems or pathological manifestations due to lack of planning is identified, the greater is the cost of the repair and the possibility of structural collapse.

According to Helene (1997), the intervention costs increase exponentially the later the intervention occurs, and, in summary, they can be avoided in the following phases:

- a. Project phase - represents the reference cost among the measures that can be verified to avoid future problems. Some mitigating measures can be highlighted as follows:

- Additives and additions to improve concrete durability and decrease permeability;
 - Increase the thickness of the concrete cover as a measure of protection against corrosion;
 - Reduce the water–cement (w/c) ratios of the concrete in order to reduce the porosity of the concrete and consequently decrease the permeability;
 - Increased characteristic strength of the concrete.
- b. Execution phase - its delayed intervention implies a cost five (5) times higher than the cost of an intervention if the project phase is taken as the reference.
- c. Preventive maintenance phase - can cost up to 25 times more than correct measurements taken in the structural design phase. Usual measures that could avoid cost increases:
- Periodic paints;
 - Waterproofing.
- d. Corrective maintenance phase - corresponds to the repair of structures that already have visible pathological manifestations. These activities can be associated with a cost 125 times higher than the cost of the measures that could and should have been taken in the design phase. It should be noted that the high cost is not only associated with labor costs and costs of the materials for the maintenance itself, but also with the indirect costs related to its intervention, such as the time and disturbances of the interdiction of the structure during the repair period.

2. LITERATURE REVIEW

2.1 Pathological manifestations found in reinforced concrete

According to Metha (2008) and Ribeiro (2014), the pathological causes in reinforced concrete can be divided into three groups: physical, chemical and biological.

The physical causes of the reinforced concrete deterioration can be subdivided into two categories: surface wear (or loss of mass) due to abrasion, erosion, and cavitation; cracking due to temperature and humidity normal gradients, salt crystallization pressures in the pores, structural loading and exposure to extremes temperatures such as freezing or fire.

The chemical causes of concrete deterioration are usually due to the presence of chemical substances, which can occur due to: hydrolysis and leaching of the cement paste components by pure water; ionic exchanges between the aggressive fluids and the cement paste; causative reactions of expandable products such as sulfate expansion, alkali-aggregate reaction and corrosion of the reinforcement in the concrete.

The biological causes are mainly related to the presence of microorganisms, which provide aggressive corrosive environments to concrete and steel, by means of sulfur or sulfide-oxidizing bacteria, which accelerate the deterioration of these structures.

2.2 Non-destructive testing

Often, in addition to the visual analysis, it is necessary to perform experiments to provide information related to the conditions of strength and rupture of components of the surveyed structure, as well as to obtain greater knowledge about the foundation soil.

The decision to whether carry out additional tests on visual inspection shall be taken by the engineer responsible for drawing up the technical report. The most well-known tests on concrete and masonry structures are classified as non-destructive and destructive tests according to Table 1.

Table 1. Destructive and non-destructive tests

Non destructive	Destructive
Sclerometry; Carbonation; Control of the expansion joint cracks with plaster or glass seals; Ultrasonography; Gammagraphy; Load test; Measurements of deformations and settlements.	Axial compression strength in specimens removed from the structure; Tensile strength in specimens removed from the structure; Modulus of deformation of concrete and mortars; Reconstitution of concrete and mortar trace; Specific mass, permeability and water absorption; Chloride content; Determination of tensile flow in reinforcement samples taken from the structure; Determination of the corrosion potential of reinforcement samples taken from the structure; Compressive strength of individual bricks and blocks; Compressive strength of brick and block prisms.

3. STATE OF THE ART OF THE GDE/UNB METHODOLOGY

The use of the GDE/UnB methodology is pertinent for the analysis of pathological manifestations since it makes possible to compare, in a fast and objective way, the degree of deterioration of different concrete structures through data collected in field visual inspections.

Several authors developed the methodology and adapted it over time for different applications.

Klein et.al. (1991) was the pioneer of the improved methodology at the University of Brasília. The objective of this study was to create and implement a systematic survey of concrete structures with the aim of prioritizing actions to repair structures in the city of Porto Alegre. The methodology classifies the structures according to the variety and severity of the presented problems, through the definition of a degree of risk. The study resulted from an agreement signed between the Federal University of Rio Grande do Sul and the City Hall of Porto Alegre where eleven constructions were classified according to the degree of deterioration of the damages imposed by the pathological manifestations.

Castro et al. (1995) developed a systemic methodology based on the observations made by Klein et.al. (1991). The Castro's methodology, also called the GDE/UnB methodology, aims to adjust the specific evaluations of bridges and overpasses to any conventional concrete structure. For the model, optimized formulations of the Tuutti's (1982) model of concrete reinforcement corrosion evolution were implemented. By analogy, the author was able to quantify the degree of deterioration in the structures for other degradation processes. Subsequently, it was implemented in the methodology the Inspection Book, which was an essential document of data collection, which contained the concept of the highest incidence damages and references to the values of Intensity of damage factors.

Lopes (1998), used the methodology to develop the study of improvement of the building maintenance system of a commercial edifice. Through the quantification of physical degradation, it was possible to reliably predict the best time for preventive maintenance interventions in buildings. In this study, the degree of deterioration of the individual structure was analyzed, associating it with the other components, which allowed, as a result, a unique degradation index for the building. However, there was a need to make some changes in the methodology proposed by Castro et al. (1995) in order to improve its applicability. In this study, the following changes were made in the element families, in the damage relationship, in the definition of new damage weighting factors and in the calculation of the deterioration degree of an element (G_{de}). The

research was carried out in six 'Banco do Brasil' buildings and, in general, proved to be effective for use in building applications.

Boldo (2002) reports the results of evaluations performed in forty buildings of concrete structures of the Brazilian Army, regarding the application of the methodology, which allowed quantify the degree of deterioration of concrete structures, using parameters that evaluate the manifestations of damages and their evolution. With the efficiency of the GDE/UnB methodology for use in buildings proven, it has enabled the establishment of systematic and more effective maintenance programs at Army facilities.

Fonseca (2007) applied the GDE/UnB methodology in building structures at the UnB Central Institute of Sciences - ICC and proposed changes in the formulation to calculate the degree of deterioration of a family (G_{df}) and degree of damage (D).

Euqeres (2011) carried out a study with eleven inspections in bridge structures in order to validate proposals for a reformulation of the methodology to calculate the structure deterioration according to the GDE/UnB methodology. As a basis for the decisions regarding the rehabilitation of the inspected work, visual inspections were carried out in all structures. The author emphasized the sampling of incidences of relevant pathological manifestations in the structures, among which we can report the corrosion of the reinforcement, cracks by crushing, crushing of the support apparatus, efflorescence with the formation of stalactites, concreting mistakes, and stains of moisture.

Medeiros (2015) evaluated the durability conditions of the Carmo River Bridge in a region of aggressive environmental. In the study, the following tests were performed: sclerometry non-destructive tests, ultrasound, carbonation depth, and the presence of chlorides. The pathological manifestations were estimated using the methodologies of inspections: standard DNIT 010/2004 and GDE/UnB. According to Medeiros, by the analysis of the results, comparatively the GDE/UnB methodology, they lead to a greater accuracy due to the richness of details in its analysis.

Verly (2015), as well as Medeiros (2015), studied two methodologies for inspecting structures regarding the evaluation of the following special engineering structures: National Department of Transport Infrastructure (DNIT) and the GDE/UnB methodology. Verly carried out visual inspections in 22 overpasses located in Brasília/DF. Initially, changes were proposed in the formulation of the GDE/UnB methodology for a better application to special engineering structures. Due to the incidence of different damages in the inspected structures, it is again possible to conclude that the GDE/UnB methodology presented results with a better scale of values that simplified the arranging of the structures regarding decision making for interventions.

3.1 GDE/Unb Methodology

A series of inspections are carried out on the element to be analyzed. Sequentially, a photographic report of the pathological manifestations presented is carried out which are compared with the reference frame for the assignment of damage values. With this data, it is possible to develop the routines of the GDE/UNB methodology.

Figure 2 shows the block diagram. It presents the analysis sequence of the element deterioration identification model and the other parameters used in the methodology.

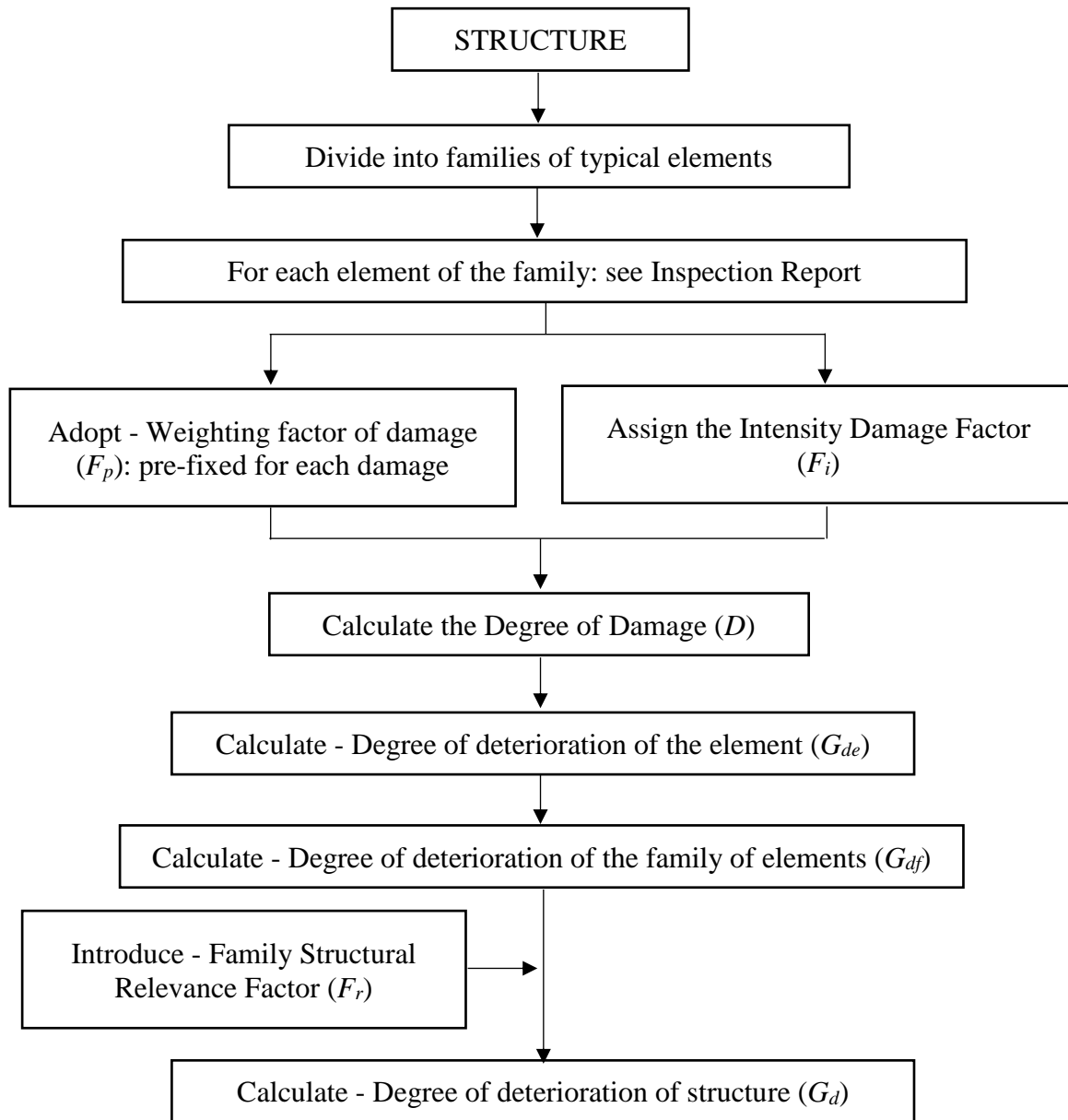


Figure 2. Structure of the GDE/UNB Methodology.

Initially, the conceptualization of damages and typical degradations is performed. With the help of the Reference tables, the values of the damage weighting factors (F_p) according to the family of elements and the damage intensity factors (F_i) of the elements are assigned. Then, with the use of the formulations, the calculation is performed to determine the degree of damage in each element, the element families, and the degree of overall deterioration of the structure.

It is worth mentioning that the Brazilian Standard regarding the inspection of special engineering structures is ABNT NBT 9452 (2016) - Inspection of bridges, overpasses and concrete footbridges - Procedure.

4. ANALYSIS OF RESULTS

For the analysis of the methodology and results, inspections were carried out on 03 overpasses. They are located on Avenida Eixo L, Eixo W, and Eixão Norte. The 03 are positioned perpendicular to the avenues, between the superquadras 103/104 and 203/204 North, as it is shown in Figure 3.



Figure 3. Location of the 03 overpasses of superquadras 103/104 and 203/204 North.

Only the visible structural elements of the overpasses were analyzed. In addition, they are composed of curtains, slab, bodyguard and bearing track. Since the span length of the overpass is relatively short, no structure had intermediate columns. The methodology was applied and used to quantify the structural damages. Thus, it served as a subsidy for decision making for interventions. Since several maintenances have been made on the bearing track over the years, it was not possible to check the state of the expansion joints.

The data collected from each analyzed structure are presented below.

4.1 Overpass 01

The overpass 01 is in Eixo L near to the superquadras 103/104 North.

Stains were identified in the structural elements of reinforced concrete in the soil as presented in Figure 4. They can be caused mainly by the infiltration of rainwater from the soil adjacent to the structure, and by infiltration of water from the flexible pavement of the bearing track to the slab. This situation could be mitigated if there was a drip tray on the side of the support floor of the bodyguard that is on the slab. Another measure that should be adopted is the waterproofing of the concrete layer on the slab before the layer of H.M.A. of the pavement. These poor waterproofing phenomena were also seen in the curtains.

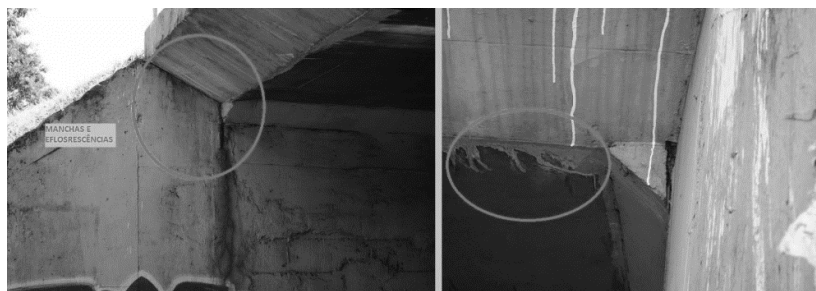


Figura 4. Manchas na estrutura da Laje

By the analysis of Figure 5, it was observed, in the slab region, large areas with insufficient concrete cover to protect the steel reinforcement. As a result of this insufficient cover, there is a high level of deterioration on the rebars. Because it was exposed to moisture, a reduction of steel section was observed. Thus, the durability of the reinforcement was significantly affected.



Figura 5. Cobrimento insuficiente e deterioração da Armadura

Failures were observed in the concreting at the surface of the slab as well as segregation of the aggregate, due to a bad concrete launching and vibration. It was also possible to observe the phenomenon of deterioration of the rebars; mainly on some longitudinal reinforcements.

Another damaging factor was verified and it is the impact of vehicles on the structure. Although it interferes in the integrity of the structure, it is not included in the GDE/UnB Methodology. In this specific case, the large number of trailing marks, due to hit from the top of load trucks, can be observed in the slab.

The bearing track, regarding the methodology, presented very good maintenance and conservation results. Apparently, it did not show excessive surface wear and the presence of cracks and holes.

4.1.1 Analysis of the Degree of Deterioration of the Structure (GD)

From the inspection, the Degree of Deterioration of the Structure was calculated. The final result of the global deterioration of the structure is defined as the weighted average of the degrees of deterioration of the elements families (G_{df}), taking as their weights the respective relevance factors (F_r) from Table 2. Considering the degree of deterioration for the curtain 7.8, for the bodyguard 6.0, for the slab deck 34, 67.

$$G_d = \left(\frac{\sum_{i=1}^n F_{ri} \cdot G_{df}}{\sum_{i=1}^n F_{ri}} \right) \quad (01)$$

$$G_d = \left[\frac{(7,8 \cdot 3) + (6,0 \cdot 1) + (34,67 \cdot 4)}{3 + 1 + 4} \right] = \frac{168,08}{8} = 21,01 \quad (02)$$

Degree of deterioration of the structure (G_d) of the Overpass 01 = 21.01

Table 2. Structural Relevance Factor of the Element Families (F_r)

Family	F_r
Barriers, bodyguard, wheel guard, bearing track	1
Expansion joints	2
Transversal, curtains, wings	3
Slabs, foundations, secondary beams, supports	4
Main beams and columns	5

The structure obtained a final G_d of 21.01 which according to the level of deterioration is considered average for values in the range of 15-50. Hence, for Overpass 01, it is recommended to define the term and nature of new inspection and to plan a long-term intervention at a maximum of 2 years.

It is worth noting that this inspection/intervention period is in accordance to the method of analysis adopted. For other authors, for example, they consider that the interventions should be immediate and the inspections should be periodic.

4.2 Overpass 02

The overpass 02 is located at the Eixão between the superquadras 103/104 and 203/204 North. It presented a great number of stains in several parts of the structure; most of them in the part that is exposed to rain without a concrete cover as seen in Figure 6.



Figure 6. Stains scattered on the structure

Different types of damage to the bodyguard such as failure on the concreting, displacement of the concrete covering on the columns that resulted in the exposure of the rebars to the rains, and corrosive agents in the reinforcement can be observed in Figure 7.

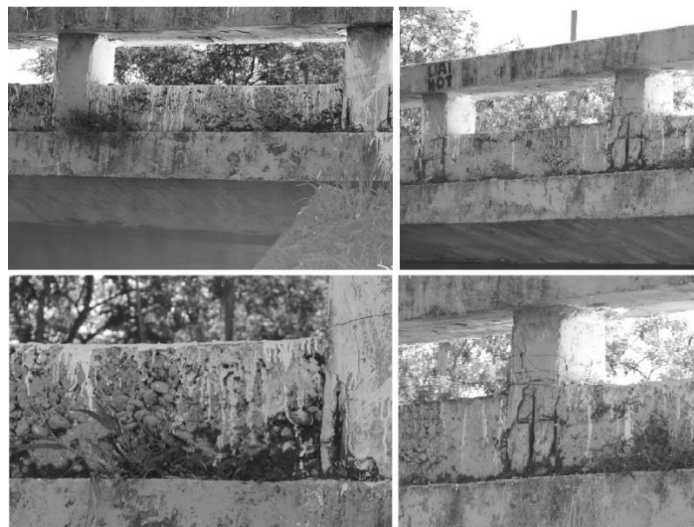


Figure 7. Failure in concreting, displacement of concrete, and pathological manifestations on the rebars (Bodyguard)

In the slabs deck, several damages were also observed: concrete failure due to lack of vibration after the launch, pathological manifestations of the reinforcement and, in some parts, it is possible to notice a deficient concrete covering by the visualization of exposed stretches of the rebars in small extensions. In the edges of the slab, where is the most susceptible part to the action of the rain, it can be perceived strong stains of great extension. Also, it can be verified that this phenomenon has compromised the reinforcement by the deterioration of the steel. In addition, in some parts it is possible to clearly notice the loss of section.

Damage was observed such as insufficient concrete covering, failure on the concreting, staining and attacking to the reinforcement. In the lower part of the bodyguard beam, it was seen signs of concrete failure, cracking, concrete displacing and pathological manifestations of reinforcement in its exposed regions.

In Figure 8, it is possible to visualize a vertical crack and wooden formwork left in the region of the curtain. In addition, the condition of the flexible pavement was analyzed. On the slab of the overpass, by the figure, it is noticeable the presence of a small hole and a crack perpendicular to the flow. Analyzing the crack, there is evidence that it has caused by the wear of the expansion joint material of the deck.

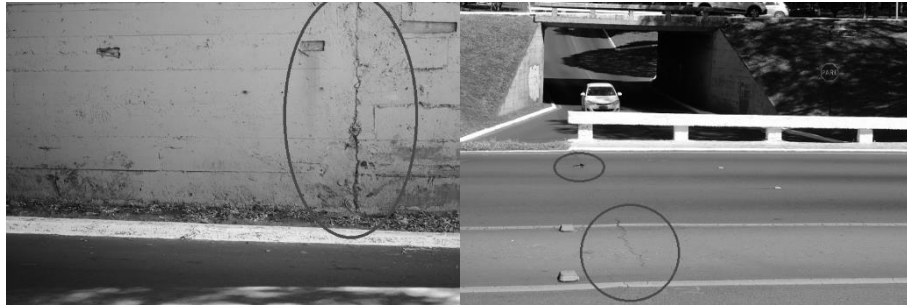


Figure 8. Crack in the curtain and pathological incidences in the bearing track.

4.2.1 Analysis of the Degree of Deterioration of the Structure (GD)

The final result of the global deterioration of the structure (G_{df}), weighted by the respective relevance factors (F_r), was 37.25. This result, according to the level of deterioration, is considered average for values in the range of 15-50. Hence, for the Overpass 01, it is recommended to define the term and nature of new inspection and to plan a long-term intervention at a maximum of 2 years. It is worth noting that this inspection/intervention period is in accordance to the method of analysis adopted. There are authors who consider that the interventions should be immediate, and the inspections should be periodic.

4.3 Overpass 03

Overpass 03 is located at Eixo W near the superquadras 203/204 North.

Figure 9 shows two types of frequent damage caused by the impact of vehicles on this type of overpasses. They are both related to the impact of a vehicle on the bodyguard and the dragging of the truck body that travels in the track with a higher height to the height of the overpass. Those impacts cause damage to the concrete covering of the slab and, in some occasions, to the own reinforcement of the structure.



Figure 9. Damage to the bodyguard structure and overview - Damage to the slab due to vehicle tallest than the height of the overpass.

4.3.1 Analysis of the Degree of Deterioration of the Structure (GD)

Applying the methodology, it was found a final G_d of 19.48. According to the level of deterioration, it is considered average for values in the range of 15-50. Hence, for Overpass 03, it is recommended to define the term and nature of new inspection and to plan a long-term intervention of no more than 2 years. It is worth observing that this inspection/intervention period is in accordance to the method of analysis adopted. There are other authors who consider that the interventions should be immediate, and the inspections should be periodic.

5. CONCLUSIONS

From the information obtained in the technical literature, field inspections, and the use of the GDE/UNB methodology, the following conclusions are presented. They have the purpose of serving as a subsidy for decision-making regarding the prioritization of routine interventions, so the lifetime of the elements and of the overall structure may be extended.

- In overpass 01, the element that presented the highest degree of deterioration was the slab with the value of 34.67. It is recommended for it to define the term and nature of new inspection and to plan a long-term intervention at a maximum of 2 years due to their degree of average damage.
- In overpass 01, the G_d presented a final value of 21.01 which according to the level of deterioration is considered average. Hence, it is recommended to define the term and nature of new inspection and to plan a long-term intervention at a maximum of 2 years.
- In overpass 02, the element that presented the highest degree of deterioration was the slab with the value of 62.46. This result is considered high, being recommended to define a term for specialized inspection and to plan a medium-term intervention in a period of maximum 1 year.
- In overpass 02, the G_d presented a final value of 37.25, which according to the level of deterioration is considered average. Hence, it is recommended to define the term and nature of new inspection and to plan a long-term intervention at a maximum of 2 years.
- In Overpass 03, the element that presented the highest degree of deterioration was the bodyguard with a value of 84.53, which is considered a poor level. Therefore, it is recommended to define a period for rigorous specialized inspection and to plan a short-term intervention at a maximum of 6 months.
- In Viaduct 03, the G_d presented a final value of 19.48 which according to the level of deterioration is considered average. Hence, it is recommended to define the term and nature of new inspection and to plan a long-term intervention at a maximum of 2 years.
- Therefore, Overpass 02 presented the highest deterioration value of 37.25. Since all the three overpasses are very close to each other, a plausible justification for this difference of values would be the flow of vehicle that in this overpass is much more intense than in the other two, causing its durability to decrease and the structure life as well.
- The elements that also suffered the highest incidence of damages were the slabs. Both can be verified visually by the field photographic records and by the results of the methodology.

In view of the above, it is considered that the methodology meets its assumptions of assisting the responsible engineer to make a fast decision on inspections of overpasses and other special engineering structures. It is suggested that inspections should be made periodically, and the maintenance should also be periodic, in order to ensure the structural safety and durability of the elements analyzed.

The repair and reinforcement of the elements that need intervention must come from projects elaborated by expert professionals and executed by companies with the technical capacity to act in recovery and reinforcement of bridges structure. One point to be considered is that a management system should be in place to manage constructions, inspections, monitoring, and interventions. Traffic is constantly increasing, evidencing the need to control the road system.

6. ACKNOWLEDGMENTS

The authors would like to acknowledge CNPq, CAPES and FAP-DF for financial support in all stages of this research. They also thank the University Center of the Federal District - UDF for their support.

7. REFERENCES

- ABNT - Associação Brasileira de Normas Técnicas (2014), *ABNT NBR 6118:2014 - Projeto de estruturas de concreto — Procedimento*, Rio de Janeiro.
- ABNT - Associação Brasileira de Normas Técnicas (2016), *ABNT NBR 9452:2016 - Inspeção de pontes, viadutos e passarelas de concreto – Procedimento*. Rio de Janeiro.
- Boldo, P. (2002), *Avaliação quantitativa de estruturas de concreto armado de edificações no âmbito do Exército Brasileiro*. Dissertação de Mestrado, Departamento de Engenharia Civil e Ambiental, Universidade de Brasília, Brasília, DF. 295p.
- Castro, E. K. (1994), *Desenvolvimento de metodologia para manutenção de estruturas de concreto armado*, Dissertação de Mestrado, Departamento de Engenharia Civil, Universidade de Brasília, Brasília, DF. 185 p.
- Castro, E. K., Clímaco, J. C. T. S., Nepomuceno, A. A. (1995), “*Desenvolvimento de uma metodologia de manutenção de estruturas de concreto armado*”, 37º. Congresso Brasileiro do Concreto, Instituto Brasileiro do Concreto - Ibracon, Anais, v.1, pp. 293-307, Goiânia.
- Euqueres, P. (2011), *Metodologia de inspeção em estruturas de pontes de concreto armado*. Dissertação (Mestrado), Universidade Federal de Goiás, Goiânia, 168 p.
- Fonseca, R. P. (2007), *A estrutura do Instituto Central de Ciências: Aspectos históricos, científicos e tecnológicos de projeto, execução, intervenções e propostas de manutenção*. Dissertação de Mestrado em Estruturas e Construção Civil, Departamento de Engenharia Civil e Ambiental, Universidade de Brasília, Brasília, DF. 213 p.
- Helene, P. R. L. (1997), *Introdução da durabilidade no projeto das estruturas de concreto*. In: WORKSHOP DURABILIDADE DAS CONSTRUÇÕES. São Leopoldo. Anais, São Leopoldo: ANTAC, 1997. p. 31-42.
- Klein, D. L., Gastal, F. P. S. L., Campagnolo, J. L. (1998), *Critérios adotados na vistoria e avaliação de obras de arte*. In: XXV Jornadas Sul-Americanas de Engenharia Estrutural, 1991, Porto Alegre. Anais... Porto Alegre: UFRGS, 1991, p. 185-197
- Lopes, B. A. R. (1998), “*Sistema de manutenção predial para grades estoques de edifícios: Estudo para inclusão do componente “Estrutura de Concreto”*”. Dissertação de Mestrado, Departamento de Engenharia Civil, Universidade de Brasília, Brasília, DF, 1998. 308 p.
- Mattos, Aldo Dórea (2010), *Planejamento e controle de obras*. Pini.
- Medeiros, A. G. (2015), *Análise de durabilidade da ponte do Rio do Carmo utilizando ensaios não destrutivos, norma DNIT e a metodologia GDE/UNB*. 165 f. Dissertação (Mestrado em Engenharia Civil) – Programa de Pós-Graduação em Engenharia Civil. Universidade Federal do Rio Grande do Norte. URI: <http://repositorio.ufrn.br/handle/123456789/20496>
- Mehta, P. K; Monteiro, P. J. M. (2008), *Concreto: microestrutura, propriedades e materiais*. 3º ed., IBRACON, São Paulo, p. 674.

- Ribeiro, D. V. et al. (2014), *Corrosão em estruturas de concreto armado: teoria, controle e métodos de análise*. 1º ed., Campus / Elsevier, Rio de Janeiro, 2014. p. 272. ISBN:978-85-352-7547-6
- Tuutti, K. (1982). *Corrosion of steel in concrete*. Stockholm - Swedish Cement and Concrete Research Institute.
- Verly, R. C. (2015), *Avaliação de metodologias de inspeção como instrumento de priorização de intervenções em obras de arte especiais*. Dissertação (Mestrado em Estruturas e Construção Civil)—Universidade de Brasília, Brasília.